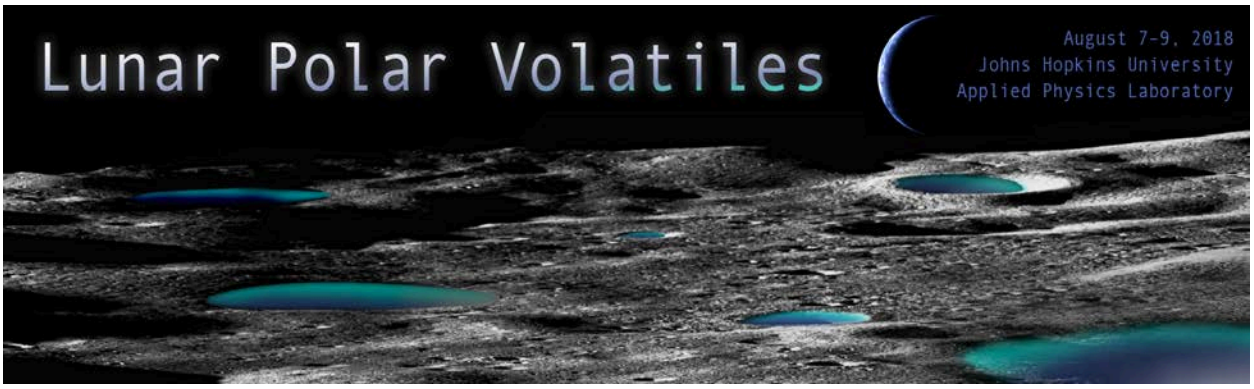

Program and Abstracts

LPI

USRA

Lunar Polar Volatiles

August 7–9, 2018 • Laurel, Maryland

Organizers

Lunar and Planetary Institute
Universities Space Research Association
Johns Hopkins University, Applied Physics Laboratory

Convener

Kathleen Mandt
John Hopkins University, Applied Physics Laboratory

Science Organizing Committee

Kathleen Mandt
Johns Hopkins University, Applied Physics Laboratory

William Farrell
NASA Goddard Space Flight Center

Elizabeth Fisher
Brown University

Andrew Jordan
University of New Hampshire

Rachel Klima
Johns Hopkins University, Applied Physics Laboratory

Paul Lucey
University of Hawaii

Lunar and Planetary Institute 3600 Bay Area Boulevard Houston TX 77058-1113

Abstracts for this meeting are available via the meeting website at

https://www.hou.usra.edu/meetings/lunarvolatiles2018/

Abstracts can be cited as

Author A. B. and Author C. D. (2018) Title of abstract. In *Lunar Polar Volatiles,* Abstract #XXXX. LPI Contribution No. 2087, Lunar and Planetary Institute, Houston.

Guide to Sessions

Tuesday, August 7, 2018

9:00 a.m.	Bldg. 200, Room E-100	Lunar Polar Volatiles: Current Understanding, Recent Discoveries, and Future Exploration
10:45 a.m.	Bldg. 200, Room E-100	Volatile Sources for the Lunar Poles: I
1:30 p.m.	Bldg. 200, Room E-100	Volatile Sources for the Lunar Poles: II
3:00 p.m.	Bldg. 200, Room E-100	Panel Discussion on Volatile Sources
4:00 p.m.	Bldg. 200, Room E-100	Distribution Differences Between the Surface and Deeper Volatiles: I
5:00 p.m.	Bldg. 200, Lobby	Welcome Reception

Wednesday, August 8, 2018

9:00 a.m.	Bldg. 200, Room E-100	Distribution Differences Between the Surface and Deeper Volatiles: II
10:30 a.m.	Bldg. 200, Room E-100	Panel Discussion on Distribution of Volatiles
1:00 p.m.	Bldg. 200, Room E-100	Transport of Volatiles at the Poles and Processes that Influence Distribution: I
3:50 p.m.	Bldg. 200, Room E-100	Panel Discussion on Transport and Processes: I
5:30 p.m.	Bldg. 200, Room E-100	Poster Session: Lunar Polar Volatiles Workshop

Thursday, August 9, 2018

9:00 a.m.	Bldg. 200, Room E-100	Transport of Volatiles at the Poles and Processes that Influence Distribution: II
10:15 a.m.	Bldg. 200, Room E-100	Panel Discussion on Transport and Processes: II
10:45 a.m.	Bldg. 200, Room E-100	Composition of Lunar Polar Volatiles: It's More Than Just Water!
11:45 a.m.	Bldg. 200, Room E-100	Panel Discussion for Composition of Lunar Polar Volatiles: It's More Than Just Water!
1:20 p.m.	Bldg. 200, Room E-100	Future Steps
4:00 p.m.	Bldg. 200, Room E-100	Panel Discussion on Future Steps

Program

Tuesday, August 7, 2018
LUNAR POLAR VOLATILES: CURRENT UNDERSTANDING, RECENT DISCOVERIES, AND FUTURE EXPLORATION
9:00 a.m. Bldg. 200, Room E-100

Chair: Kathleen Mandt

9:00 a.m. Mandt K. *
Welcome and Logistics

9:15 a.m. Hayne P. O. *
Lunar Polar Volatiles: Current Understanding, Recent Discoveries, and Future Exploration **[#5017]**
Recent observations and models have provided new insights into the nature and origins of lunar polar volatiles. I will provide a summary of current understanding of lunar volatiles and possible future directions for addressing outstanding questions.

10:15 a.m. *Coffee Break*

VOLATILE SOURCES FOR THE LUNAR POLES: I
10:45 a.m. Bldg. 200, Room E-100

Chair: David Blewett

10:45 a.m. Lucey P. G. * Hurley D. Farrell W. Petro N. E. Cable M. Dyar D. Orlando T. McCanta M. Fisher E. Hibbitts K. Prem P. Benna M. Hayne P. Green R. Pieters C. M. Mandt K. Horyani M. Haleakas J. Li S.
The Lunar Volatile System in Space and Time: Supplies to the Lunar Poles **[#5015]**
Volatile sources for the poles vary in space and time. Now, meteorites and solar wind dominate the inputs; in the past volcanic eruptions and impacts overwhelmed the current sources. Major gaps in understanding persist regarding all epochs.

11:05 a.m. Needham D. H. * Kring D. A.
A Volcanic Source for Lunar Polar Volatiles **[#5009]**
Ancient eruptions of lunar mare basalts released significant masses of volatiles around the Moon. These internally sourced volatiles may have migrated to the lunar poles, forming a substantial component of currently observed polar volatile deposits.

11:25 a.m. Tucker O. J. * Killen R. M. Saxena P. Johnson R. E. Prem P.
Lifetime of a Transient Atmosphere Produced by Lunar Volcanism **[#5039]**
We estimate the thermal escape lifetime of a volcanically produced early Moon atmosphere for comparison to the Needham and Kring (2017), Earth and Planet. Sci., study.

11:45 a.m. Orlando T. M. * Jones B. M. Alexandrov A. B. Hibbitts C. A. Dyar M. D.
A Solar Wind Source of Water in the Polar Regions of the Moon? **[#5008]**
We address formation of water via thermally activated recombinative desorption of hydroxyls in proton irradiated regolith. This temperature dependent process can lead to limited water build-up at the poles or in permanently shadowed regions.

12:05 p.m. *Lunch*

Tuesday, August 7, 2018
VOLATILE SOURCES FOR THE LUNAR POLES: II
1:30 p.m. Bldg. 200, Room E-100

Chair: David Blewett

1:30 p.m. Mandt K. E. * Luspay-Kuti A.
Comets and Meteorites as Sources of Lunar Polar Volatiles **[#5041]**
Volatiles stored in the lunar polar region could provide a time-line of volatile delivery to the Moon. We will review composition tracers for comets and meteorites that can be used to evaluate the history of volatile delivery to the Moon.

1:50 p.m. Schorghofer N. *
Transport in the Lunar Water Exosphere **[#5004]**
A surface-bounded exosphere has a non-exponential vertical density distribution. Delivery of water to the polar cold traps is dramatically more efficient on the Moon than on Mercury and Ceres. Uncertainties lie with the surface interaction.

2:10 p.m. Taylor G. J. * Kring D. A. Needham D. H.
The Lunar Interior as a Source of Polar Water **[#5007]**
Water released from the lunar crust by moonquakes and impacts each account for between 100 and 10,000 kg of water per year, at least three orders of magnitude less than contributed by solar wind or impact of water-bearing projectiles.

2:30 p.m. *Coffee Break*

PANEL DISCUSSION ON VOLATILE SOURCES
3:00 p.m. Bldg. 200, Room E-100

Moderator: Adrienn Luspay-Kuti

Panel Members: Kathleen Mandt
Jeff Taylor
Debra Needham
O. J. Tucker

Tuesday, August 7, 2018
DISTRIBUTION DIFFERENCES BETWEEN THE SURFACE AND DEEPER VOLATILES: I
4:00 p.m. Bldg. 200, Room E-100

Chair: John Gruener

4:00 p.m. Siegler M. A. * Keane J. T. Paige D. A.
Subsurface Ice Stability on the Moon **[#5038]**
The Moon has about 26,000 km^2 of surface area in the large shadowed regions near the poles where ice could be stable. However, over 240,000 km^2 of area in the upper meter alone that could hide subsurface ice. Much of the lunar ice may be at depth.

4:20 p.m. Jordan A. P. * Wilson J. K. Schwadron N. A. Spence H. E. Petro N. E.
A Framework to Determine the History of the Moon's Polar Ice **[#5003]**
We describe a framework for interpreting the large-scale distribution of water ice in the polar regions of the Moon, and we show how this framework can help constrain the history of the ice as a function of depth.

4:40 p.m. McClanahan T. P. * Mitrofanov I. G. Boynton W. V. Chin G. Livengood T. A. Sanin A. Litvak M. Parsons A. Hamara D. Harshman K. Starr R. Su J. J.
Lunar Regolith Geochemistry Variation May Explain the Polar Wander Observations **[#5012]**
We examine recently recalibrated Lunar Exploration Neutron Detector (LEND) polar observations and the observation of polar wander. Preliminary studies suggest that regolith geochemistry variation could explain the polar wander observation.

Wednesday, August 8, 2018
DISTRIBUTION DIFFERENCES BETWEEN THE SURFACE AND DEEPER VOLATILES: II
9:00 a.m. Bldg. 200, Room E-100

Chair: Susan Klem

9:00 a.m. Fisher E. A. * Lucey P. G. Lemelin M. Greenhagen B. T. Siegler M. A. Mazarico E. Aharonson O. Williams J. Hayne P. O. Neumann G. A. Paige D. A. Smith D. E. Zuber M. T.
Evidence for Surface Water Ice in the Lunar Polar Regions Using Reflectance Measurements from the Lunar Orbiter Laser Altimeter and Temperature Measurements from the Diviner Lunar Radiometer Experiment **[#5011]**
We study LOLA derived normal albedo as a function of Diviner maximum temperature, to see if lunar permanently shadowed regions cold enough (<110K) to preserve surface water frost over geologic timescales show increased reflectance.

9:20 a.m. Li S. * Lucey P. G. Milliken R. E. Hayne P. O. Fisher E. Williams J. P. Hurley D. Elphic R. C.
Direct Detections of Surface Exposed Water Ice in the Lunar Polar Regions **[#5010]**
IR absorptions of ice near 1.3, 1.5, and 2.0-µm were detected using the M^3 data near the lunar polar regions, which is the first direct evidence for surface exposed water ice on the Moon. The distribution and formation of ice are also discussed.

9:40 a.m. Raut U. * Karnes P. L. Retherford K. D. Czajka E. Poston M. J. Davis M. W. Liu Y. Patrick E. L. Gladstone G. R. Greathouse T. K. Hendrix A. R. Mokashi P.
Investigating Far-ultraviolet hydration signatures in the Southwest Ultraviolet Reflectance Chamber (SwURC) in support of LRO-LAMP observations **[#5037]**
We will present results from our laboratory investigations on far-ultraviolet reflectance measurements of dry and water vapor-exposed Apollo soils made in support of LRO-LAMP observations.

10:00 a.m. *Coffee Break*

PANEL DISCUSSION ON DISTRIBUTION OF VOLATILES
10:30 a.m. Bldg. 200, Room E-100

Moderator: Norbert Schorghofer

Panel Members: Elizabeth Fisher
Shuai Li
Matt Seigler

11:30 a.m. *Lunch*

Wednesday, August 8, 2018
TRANSPORT OF VOLATILES AT THE POLES AND PROCESSES THAT INFLUENCE DISTRIBUTION: I
1:00 p.m. Bldg. 200, Room E-100

Chair: Debra Needham

1:00 p.m. Hendrix A. R. *
A Review of Diurnally-Varying Lunar Hydration Signatures **[#5046]**
We summarize what is currently understood about the results of the last 1–2 decades and their implications for the lunar water cycle.

1:20 p.m. Hurley D. M. * Prem P. Farrell W. M. Benna M. Hendrix A. R.
Exospheric Transport Processes of Lunar Volatiles **[#5013]**
Examination of exospheric transport processes for lunar volatiles — comparing data to models.

1:40 p.m. Poston M. J. *
Cold Trapping Processes on the Moon **[#5025]**
When small quantities are involved, it's not just vapor pressure. Strength of interaction with the substrate is key.

2:00 p.m. Farrell W. M. * Hurley D. M. Poston M. J. Hayne P. O. McLain J. L.
Cold Trapping of Lunar Polar Crater Volatiles: A Model of Desorption from Frosty Grains **[#5002]**
We present an embodiment of the thin water layer covering a lunar grain in a PSR and consider desorption of these water molecules from the exposed regolith. Water is found to stick for T > 110K at sites with large desorption activation energy.

2:20 p.m. *Coffee Break*

2:50 p.m. Honniball C. I. * Lucey P. G. Kaluna H. M. Li S. Sun L. Costello E.
Groundbased Observations of the Lunar Surface at 3 Microns: Implications for the Presence of Mobile Water for Polar Ice Supply **[#5019]**
Groundbased observations of the lunar surface may indicate the presence of molecular water at some locations, enabling potential supply of water to the lunar poles.

3:10 p.m. Plescia J. B. *
Lunar Regolith — Properties/Implications for Volatile Storage **[#5043]**
The lunar regolith is a complex storage medium for volatiles.

3:30 p.m. Rubanenko L. * Venkatraman J. Paige D. A.
The Depth of Small Craters and the Shadows they Cast: Evidence for Buried Ice on the Moon and Mercury **[#5023]**
Craters on the Moon and Mercury become shallower in latitudes where ice should accumulate on their floors. By comparing the deposits' thickness to their maximum possible thickness given by the permanent shadow limit, we estimate their age and origin.

PANEL DISCUSSION ON TRANSPORT AND PROCESSES: I
3:50 p.m. Bldg. 200, Room E-100

Moderator: Parvathy Prem

Panel Members: Casey Honniball
Michael Poston
Bill Farrell
Amanda Hendrix

Wednesday, August 8, 2018
POSTER SESSION: LUNAR POLAR VOLATILES WORKSHOP
5:30 p.m. Bldg. 200, Room E-100

Byron B. D. Retherford K. D.
Far-Ultraviolet Observations and Analysis of Potential South Pole Landing Sites Using LRO-LAMP **[#5049]**
Amundsen crater is a potential landing site for future lunar missions due to the unique properties nearby and within its PSRs. We present LRO-LAMP observations of the crater and characterize the volatile content of the regolith inside the PSRs.

Magaña L. O. Retherford K. D.
An Ultraviolet Spectroscopic Investigation of Exposed Frost in Lunar Permanently Shadowed Regions from the Lunar Reconnaissance Orbiter **[#5050]**
We report initial results of far ultraviolet investigation of craters, Faustini, Shoemaker, and Haworth within the lunar south pole, using Lyman Alpha Mapping Project spectral data from the start of the mission, 2009, to 2016.

Czajka E. A. Retherford K. D. Raut U. Karnes P. L. Wyrick D.
Lunar Simulant Far-Ultraviolet Reflectance Comparisons with Apollo Soils Measured with the Southwest Ultraviolet Reflectance Chamber (SwURC) **[#5051]**
Dry reflected far-ultraviolet spectra of the JSC-1A will be presented and compare to reflectance spectra of Apollo lunar soils. Preliminary results for the far-UV reflectance spectra of ice coated lunar simulant will also be discussed.

Slank R. A. Port S. T. Chevrier V. F.
Locating Lunar Polar Volatiles Using Thermal Inertia and Temperature Maximum to Minimum Ratios **[#5005]**
A new way to find water ice using thermal inertia and T_{max} to T_{min} ratios.

Klem S. M. Robinson M. S. Manheim M. R. LROC Science Team
Extrapolating from Meter to Sub-Meter Block Populations to Constrain Polar Ice Estimates **[#5026]**
Blocks of similar diameter to radar wavelengths can cause backscattering signals similar to those of volatiles. Understanding how meter and sub-meter block populations change and are related will help constrain polar ice estimates.

Roush T. L. Teodoro L. F. A. Colaprete A. Cook A. Elphic R.
Sublimation Behavior of Water-Doped Lunar Simulant at Cryogenic Temperatures **[#5030]**
Ice sublimation from cryogenically cooled water-doped lunar simulant was observed at short-wave infrared wavelengths. After controlled percussions, ice band depths decay to background levels in ~60–90 seconds consistent with ~180 K soil temperature.

Grava C. Chaufray J.-Y. Mazarico E. Siegler M. A. Benna M.
The Effect of Topography on the Transport of Volatiles at the Lunar Poles: Application to Neon **[#5033]**
What is the effect of lunar topography in the transport of volatiles? We address this by including a topographic relief from LRO's altimeter LOLA into our Monte Carlo exospheric code.

O'Brien P. Byrne S. Hayne P. O.
Investigating Sub-Resolution Cold Traps with a Landscape Evolution Model **[#5029]**
We present surface roughness analysis results which calibrate a model of landscape evolution on airless bodies. This model generates realistic synthetic surfaces which can be used to study permanently shadowed regions on the Moon at any scale.

Honniball C. I. Lucey P. G. Li S. Hibbitts K.
Measurement Requirements and Instrument Performance for Remote Measurements of Lunar Surface Water Abundance and Variation Using the 6 Microns Water Absorption **[#5020]**
Spectroscopic observations of the Moon at 6 microns offers a powerful and unambiguous view of water on the lunar surface enabling testing of the hypothesis that water may be mobile on the lunar surface.

Neumann G. A. Mazarico E. Sun X. Deutsch A. N. Lucey P. G.
Precision Laser Sensing of Lunar Polar Volatiles **[#5036]**
A powerful laser altimeter being developed with a sensitive 3 μm-capable detector will unambiguously map hydrogen-bearing deposits using multiple water (hydroxyl) and ice wavelengths and provide precise geolocation for future landed operations.

Qiao L. Ling Z. Head J. W. Ivanov M.
1064 nm Albedo and Impact Cratering Record Analysis of the Permanently Shadowed Regions in the Flat Floors of Lunar Polar Craters: Implications for Surface Water Ice and Future In-Situ Explorations **[#5027]**
Permanently shadowed regions in lunar polar crater floors are symmetrically more reflective at 1064 nm, which can be best explained by surface water ice, other than other factors including solar illumination and surface temperature.

Storm M. Albert M.
Rover Mast Laser Surface Reflection Spectrometer for Volatile Science and Prospecting and 3-Dimensional Terrain Mapping up to 10 km **[#5024]**
A rover-based Compact Lidar Spectrometer (CLS) to enable long-range, up to 10 km, detection of water ice and other surface substances. Can measure high resolution spectrums for mapping into deep dark craters and for 3-dimensional terrain mapping?

Gruener J. E. Bussey D. B. Lawrence S. J. Mason L. S.
Polar Volatiles Exploration in Peary Crater Enabled by NASA's Kilopower Project **[#5042]**
This abstract describes a mission concept involving the exploration of lunar polar volatiles in permanently shadowed regions (PSRs) of Peary Crater. Extended PSR exploration is enabled by NASA's Kilopower space fission power system.

Blewett D. T. Hurley D. M. Halekas J. S. Denevi B. W. Greenhagen B. T.
Understanding the Lunar Water Cycle by In-Situ Assessment of Regolith Hydration in Areas of Varying Solar-Wind Exposure **[#5006]**
A rover mission to a lunar magnetic anomaly could assess regolith hydration in areas of greater and lesser solar-wind exposure, thus helping to define the role that the solar wind has in producing water through interaction with the regolith.

Shirley M. H. Elphic R. C. Colaprete A. Andrews D. R. Miller S. T. **CANCELED**
Applicability of Planning Tools Developed by Resource Prospector to a Broader Class of Lunar Polar Missions **[#5045]**
The goal of this paper is to improve understanding within the research community of the practical constraints on missions, whether sponsored by NASA, ESA, or commercial interests by showing tradeoffs. People can then evaluate options for themselves.

Sarantos M. Janches D. Pokorny P.
Exospheric Water Production from Meteoroids: Sporadics Versus Meteor Showers **[#5016]**
We estimate the expected difference in source rates of water group vapor during sporadics and Geminids and simulate the transport of its constituents to the poles.

RetherfordK. D. Greathouse T. K. Byron B. D. Magaña L. O. Grava C. Egan A. F.
Raut U. Czajka E. Hurley D. M. Cahill J. T. S. Hendrix A. R. Mandt K. E. Liu Y.
Wyrick D. Gladstone G. R.
LRO Lyman Alpha Mapping Project (LAMP)'s Polar Volatile Studies Overview and Future Steps **[#5048]**
The Lunar Reconnaissance Orbiter (LRO) Lyman Alpha Mapping Project (LAMP) investigation has made numerous discoveries and contributions to our understanding of lunar polar volatiles and we'll discuss next steps for far-UV reflectance studies.

Thursday, August 9, 2018
TRANSPORT OF VOLATILES AT THE POLES AND PROCESSES
THAT INFLUENCE DISTRIBUTION: II
9:00 a.m. Bldg. 200, Room E-100

Chair: Andrew Jordan

9:00 a.m. Szalay J. R. * Pokorny P. Horanyi M. Poppe A. R. Janches D. Sarantos M.
Meteoroid Environment and Impact Gardening in the Lunar Polar Regions. **[#5035]**
In this presentation, we extend equatorial measurements of impact ejecta to the lunar polar regions using models of meteoroid impactors at the Moon to constrain the associated impact gardening rates.

9:20 a.m. Deutsch A. N. * Head J. W. Neumann G. A.
Patchy Distribution of Ancient, Lunar Ice Contrasts with Young, Coherent Ice Deposits on Mercury **[#5021]**
We consider how differences in purity and extent of surface water-ice deposits at the poles of the Moon and Mercury may be tied to the age of the ice deposits.

9:40 a.m. Costello E. S. * Ghent R. R. Lucey P. G.
Gardening Ice at the Poles of the Moon and Mercury **[#5031]**
We model the vertical overturn of regolith on the Moon and Mercury due to impact gardening and find after 1 Gyr extensive ice deposits would still be present on Mercury but would be obliterated on the Moon.

10:00 a.m. *Coffee Break*

PANEL DISCUSSION ON TRANSPORT AND PROCESSES: II
10:15 a.m. Bldg. 200, Room E-100

Moderator: Gregory Neumann

Panel Members: Jamey Szalay
Menelaos Sarantos
Emily Costello
Ariel Deutsch

Thursday, August 9, 2018
COMPOSITION OF LUNAR POLAR VOLATILES: IT'S MORE THAN JUST WATER!
10:45 a.m. Bldg. 200, Room E-100

Chair: Lizeth Magana

10:45 a.m. Colaprete A. * Elphic R. C. Shirley M. Heldmann J. Goldstein D.
LCROSS: A Four Minute Mission **[#5032]**
This presentation summarizes the primary observations and findings of the LCROSS mission, including the most recent analysis and modeling efforts, and presents a model for the distribution of volatiles at the impacts site.

11:05 a.m. Luspay-Kuti A. * Mandt K. E.
Comets: A Possible Source of Lunar Volatiles in Light of Rosetta **[#5034]**
We provide a general overview of cometary volatiles with special focus on results from Rosetta, and compare them to LCROSS.

11:25 a.m. Hibbitts C. A. *
Volatile Retention In and Near Lunar PSRs Through Molecular Adsorption **[#5040]**
Water, CO_2, and possibly other volatiles should be thermally stable at significantly higher temperatures than their ice would be. They also have spectral signatures distinct from their ices enabling their detection on the surface of the Moon.

PANEL DISCUSSION FOR COMPOSITION OF LUNAR POLAR VOLATILES:
IT'S MORE THAN JUST WATER!
11:45 a.m. Bldg. 200, Room E-100

Moderator: Elizabeth Fisher

Panel Members: Adrienn Luspay-Kuti
Karl Hibbits
Anthony Colaprete

12:15 p.m. *Lunch*

Thursday, August 9, 2018
FUTURE STEPS
1:20 p.m. Bldg. 200, Room E-100

Chair: William Farrell

1:20 p.m. Petro N. E. *
The Lunar Reconnaissance Orbiter (LRO) Next Steps in Constraining Lunar Polar Volatiles **[#5047]**
With over nine years of observations of the lunar surface and the environment around the Moon, the Lunar Reconnaissance Orbiter (LRO) has generated an unparalleled dataset for investigating the lunar poles.

1:35 p.m. Lucey P. G. * Hurley D. Farrell W. Petro N. E. Cable M. Hibbitts K. Honniball C. I. Li S.
The Lunar Poles: What Remains to be Done **[#5018]**
Gaps in measurements and understanding limit progress, but measurements providing definitive answers to key questions are available for future missions.

1:55 p.m. Elphic R. C. * Colaprete A. Shirley M. H. Siegler M. A. Andrews D.
Next Steps in Evaluating Lunar Polar Volatiles: Land, Prospect, Sample, Assay **[#5044]**
A resource prospecting mission, with mobility, real-time prospecting measurements, sub-surface sample acquisition, and analysis is still needed to address SCEM goals 4a, 4b, and 4c.

2:15 p.m. Mitchell J. L. * Gruener J. E. Lawrence S. J. Fries M. D. Zeigler R. A. McCubbin F. M. Edmunson J. E.
Temperature Constraints on the Storage and Curation of Volatile-Rich Samples from the Lunar Poles **[#5014]**
Future lunar exploration efforts will require the collection and return of samples from the lunar poles. Storage temperatures will have a significant impact on their preservation; these conditions are being quantified by the JSC Curation Office.

2:35 p.m. *Coffee Break*

3:15 p.m. Robinson M. S. Denevi B. * ShadowCam Team
ShadowCam: Seeing in the Shadows **[#5028]**
ShadowCam is a high heritage camera (based on LROC NAC) that will provide critical information about the distribution and accessibility of volatiles in PSRs, and will fly on the Korea Pathfinder Lunar Orbiter (KPLO) slated for launch December 2020.

3:35 p.m. Prem P. * Hurley D. M. Patterson G. W.
Perspectives on Modeling the Transport of Volatiles and Their Distribution at the Lunar Poles **[#5022]**
We present a series of recent investigations aimed at understanding volatile transport and distribution, and discuss the role of numerical models in addressing outstanding questions regarding the origin and distribution of polar water.

Thursday, August 9, 2018
PANEL DISCUSSION ON FUTURE STEPS
4:00 p.m. Bldg. 200, Room E-100

Moderator: Michael Poston

Panel Members: Paul Lucey
Parvathy Prem
Julie Mitchell
Richard Elphic

4:00 p.m. Mandt K.
Workshop Summary

5:15 p.m. Meeting Adjourns

Notes

CONTENTS

UNDERSTANDING THE LUNAR WATER CYCLE BY IN-SITU ASSESSMENT OF REGOLITH HYDRATION IN AREAS OF VARYING SOLAR-WIND EXPOSURE. David T. Blewett[1,*], Dana M. Hurley[1], Jasper S. Halekas[2], Brett W. Denevi[1], and Benjamin T. Greenhagen[1]. [1]Planetary Exploration Group, Johns Hopkins University Applied Physics Laboratory, Laurel, MD 20723 USA; [2]Dept. of Physics and Astronomy, University of Iowa, Iowa City, IA 52242 USA. (*correspondence author: david.blewett@jhuapl.edu)

Introduction: Volatile compounds cold-trapped in the polar regions of airless bodies in the inner Solar System are valuable repositories for both scientific and practical exploration exploitation. The reason for the marked differences between the polar deposits on the Moon and those on Mercury is an outstanding question in planetary science. In order to understand the origin of the polar water ice on the Moon, it is necessary to determine the relative contributions of exogenic sources (impact delivery of icy or hydrated material), production (OH or H_2O generated in the regolith from implanted solar-wind protons), and endogenic sources (release of magmatic volatiles internal to the Moon). Fortunately, the Moon has provided natural laboratories in which the process of hydration can be studied. Areas of crustal magnetism, known as magnetic anomalies [e.g., 1], provide partial shielding of the surface from exposure to solar-wind ions. A rover mission to a magnetic anomaly could assess regolith hydration by measuring the strength of the OH/H_2O absorptions near 3-μm wavelength in areas of greater and lesser solar-wind exposure that are conveniently located at relatively close geographic proximity. Microscopic examination of the regolith would reveal the specific soil constituents (minerals, glass) that are most susceptible to H implantation.

Magnetic Anomalies: The Moon does not at present have a global, internally generated magnetic field. However, the lunar crust does contain areas of magnetized rocks. The crustal magnetic anomalies are correlated with unusual, high-visible-reflectance markings referred to as lunar swirls [e.g., 1–7]. The local magnetic fields produce disturbances in the Moon's interaction with the solar wind [e.g., 8, 9]. Described as "mini-magnetospheres", the disturbances have been detected through analysis of the flux of neutral atoms [10], electrons [11], and solar-wind protons [12]. It is known from orbital remote-sensing data that the high-reflectance parts of swirls exhibit weaker hydroxyl absorptions at 2.82 μm than do the background [13, 14], consistent with a lower flux of solar-wind protons reaching the surface, or a difference in retention. Figure 1 shows a 2.8 μm band-depth map for the Airy swirl and magnetic anomaly.

Lunar Hydroxyl: A major point of debate is whether the hydration observed globally on the surface of the Moon is available to migrate through the lunar exosphere to the polar regions. Before humans ever stepped foot on the Moon, Zeller and colleagues [15] predicted that the bombardment of regolith with solar-wind protons would induce the formation of hydroxyl on the lunar surface. This prediction has been confirmed with remote sensing observations of the Moon in the 3-μm region where OH and H_2O produce absorption bands [16, 17]. However, the distribution of hydration in latitude and local time is debated according to the manner in which phase functions and correction for thermal emission are applied to the data [18–20]. One interpretation is that there is a diurnal variation of the amount of hydroxyl in the regolith, which implies that the hydroxyl is transient in the lunar regolith.

With the benefit of lunar samples returned by the *Apollo* program, Arnold [21] proposed that the observed reduction of Fe^{2+} in regolith silicates by implanted protons may have produced ~1×10^{17} g of water in the gas phase over the last 2×10^9 yr. This water, upon release from the regolith, has the potential to migrate to cold traps in the lunar polar regions, where it could accumulate as ice. Migration models [22] predict that 0.04% of incident protons are ultimately delivered to the lunar polar regions as water molecules. This corresponds to the delivery of an equivalent water-ice layer 40 cm thick spread across the permanently shadowed regions in the last 2×10^9 yr. Clearly, the Moon lacks such a coherent ice layer now. But the question remains as to where the pipeline is interrupted: in the release of H_2O from the surface, in the delivery to the cold traps, or in the retention at the cold traps after delivery.

In-Situ Study: Exploration of a lunar magnetic anomaly by a landed spacecraft offers a wealth of scientific opportunity [23, 24]. A rover payload [25] could address major planetary science questions including the origin of the magnetic anomalies, the nature of solar-wind interactions that lead to the formation of the mini-magnetosphere stand-off regions, the relative importance of ion and micrometeoroid bombardment in the space weathering of silicate surface materials, and the origin of lunar swirls. In addition, the rover could examine key issues about the formation and retention of OH in the regolith by taking advantage of the variations in solar-wind flux that reach the surface within and around a magnetically shielded area. This will better define the role that the solar wind has in producing water

through interaction with the lunar regolith, and thus, the potential importance of the solar wind as a source of water being fed to lunar cold traps.

References: [1] L.L. Hood and G. Schubert (1980), *Science 208*, 49–51. [2] F. El-Baz (1972), *Apollo 16 PSR*, NASA SP-315, 29-93–29-97. [3] P.H. Schultz and L.J. Srnka (1980), *Nature 284*, 22–26. [4] L.L. Hood and C.R. Williams (1989), *Proc. Lunar Planet. Sci. Conf. 19th*, 99-113. [5] D.T. Blewett et al. (2011), *J. Geophys. Res. 116*, E02002. [6] B.W. Denevi et al. (2016), *Icarus 273*, 53–67. [7] A.R. Hendrix et al. (2016), *Icarus 273*, 68–74. [8] C.T. Russell and B.R. Lichtenstein (1975), *J. Geophys. Res. 80*, 4700–4711. [9] C. Lue et al. (2011), *Geophys. Res. Lett. 38*, L03202. [10] M. Wieser et al. (2010), *Geophys. Res. Lett. 37*, L05103. [11] J.S. Halekas et al. (2008), *Planet. Space Sci. 56*, 941–946. [12] Y. Saito et al. (2010), *Space Sci. Rev. 154*, 265–303. [13] G.Y. Kramer et al. (2011), *J. Geophys. Res. 116*, E00G18. [14] C.M. Pieters and I. Garrick-Bethell (2015), *Lunar Planet. Sci. 46*, abstr. no. 2120. [15] E.J. Zeller et al. (1966), *JGR 71*, 4855-4860. [16] C.M. Pieters et al. (2009), *Science 326*, 568–572. [17] J.M. Sunshine et al. (2009), *Science 326*, 565–568. [18] R.N. Clark et al. (2011), *JGR 116*, E00G16. [19] S. Li and R.E. Milliken (2017), *Sci. Adv. 3*, e1701471. [20] J.L. Bandfield et al. (2018), *Nat. Geosci. 11*, 173–177. [21] J. Arnold (1979) *JGR 84*, 5659-5668. [22] D.H. Crider and R.R. Vondrak (2002), *Adv. Space Res. 30*, 1869–1874. [23] D.T. Blewett et al. (2017a), *Low-Cost Planetary Missions Conf.* [24] D.T. Blewett et al. (2018), *Lunar Science for Landed Missions Workshop*. [25] D.T. Blewett et al. (2017b), *Lunar Planet. Sci. 48*, abstr. no. 1251.

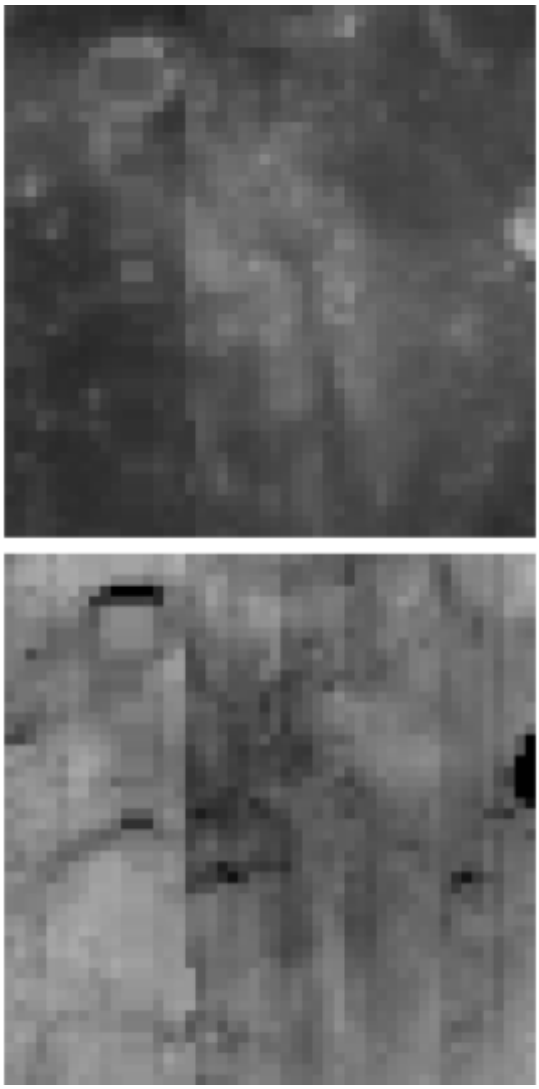

Figure 1. *Top*: Moon Mineralogy Mapper (M3) reflectance image at 750 nm of the area of the Airy swirl and magnetic anomaly, located near 3° E, 18° S. *Bottom*: M3 image of band depth at 2850 nm for the same area as the top reflectance image. Darker tones in the bottom band-depth map correspond to weaker OH absorption. The high-reflectance portion of the swirl has weaker OH absorption than does the background. Width of scene ~7.5 km.

Far-Ultraviolet Observations and Analysis of Potential South Pole Landing Sites Using LRO-LAMP. B. D. Byron[1,2] and K. D. Retherford[2,1], [1]Department of Physics and Astronomy, University of Texas at San Antonio, One UTSA Circle, San Antonio, TX 78249 (ben.byron@swri.org) [2]Space Science and Engineering Department, Southwest Research Institute, 6220 Culebra Rd, San Antonio, TX 78238 (kurt.retherford@swri.org)

Introduction: Lunar South Pole crater Amundsen possesses a number of unique thermal properties, including Permanently Shaded Regions (PSRs) directly adjacent to regions which receive extended periods of sunlight. These contrasting environments exhibit large temperature differentials in relatively close proximities. Furthermore, the floor of Amundsen directly beside its largest PSR is relatively flat and suitable for landing, and receives multiple periods of uninterrupted solar illumination lasting from 2.5-4 days [1]. High circular polarization ratios (CPR) detected by the Mini-RF instrument on LRO also suggest the presence of large amounts of buried water ice within the upper 2 meters of regolith inside the PSRs [2]. For these reasons, Amundsen has been recommended as a potential landing site for future manned or robotic missions with the potential for high scientific return in the study of lunar volatiles [1, 3].

The Lyman Alpha Mapping Project (LAMP) is a far-UV spectrograph onboard the Lunar Reconnaissance Orbiter (LRO) which uses the all-sky Lyman-α skyglow and UV-bright stars as an illumination source for the lunar nightside and within PSRs [4]. This innovative technique enables precise measurements of surface reflectance within the uppermost ~100 nm of the lunar regolith inside cold polar PSRs, regions where exposed volatiles are most likely to exist. LAMP is ideally suited to detecting water ice in these regions due to the "absorption edge" that exists in the water ice reflectance spectrum at 165 nm.

New LAMP Observations of Amundsen Crater: We present the latest LAMP nighttime observations of Amundsen Crater, using all existing pre-Failsafe Door Open (FDO) mode data (October 2009-October 2016) and implementing LAMP's new background subtraction algorithm. A preliminary LAMP nighttime Lyman-α albedo map for Amundsen is shown in Figure 1 (top). To create this map (and other albedo maps) we use a tool called the LAMP Spectral Mapper to make monthly maps in the form of spectral data cubes. We then combine all of these monthly maps, thereby increasing total coverage area and signal-to-noise ratio (SNR). By summing monthly maps from October 2009 to October 2016, the total integration time is raised by a factor of more than 50, leading to a much improved SNR at the On Band (130-155 nm) and Off Band (155-190 nm) wavelengths.

Analysis and Implications for Water Ice: Amundsen's largest PSRs have a lower Lyman-α albedo than the rest of the crater, as seen in Figure 1 (top). A preliminary comparison of this albedo map with a Diviner Lunar Radiometer (Diviner) maximum temperature map (Figure 1 bottom) shows a possible correlation between albedo and temperature. Cold traps inside of Amundsen's PSRs may harbor water frost, therefore we analyze the spectral properties of these regions at Lyman-α and at longer far-UV wavelengths where signatures of water frost occur.

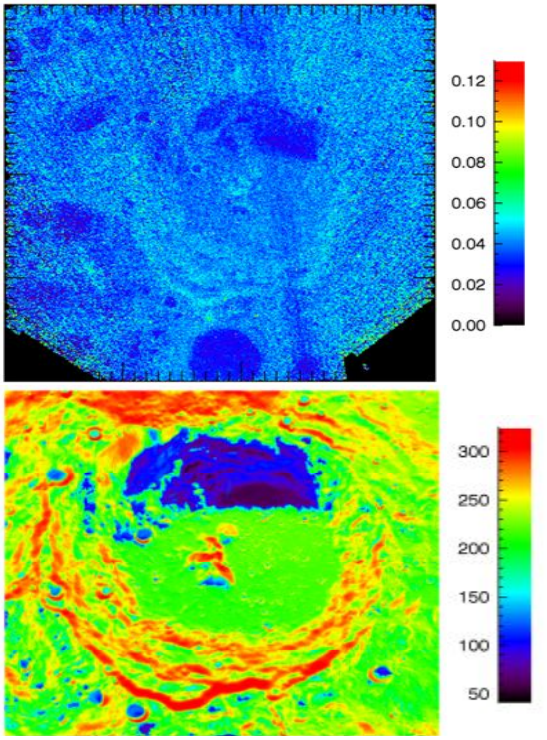

Figure 1: LAMP Lyman-α albedo map (top) and Diviner maximum temperature map (bottom) of Amundsen crater. The cold PSRs inside of Amundsen display low Lyman-α albedos compared to sunlit regions of the crater.

In order to estimate the amount of water ice mixed with the upper layer of regolith inside Amundsen's PSRs, we analyze Off Band/On Band albedo ratio maps and identify regions where this ratio is anomalously high. Previous studies of South Pole PSRs show Off/On ratios >1.2, indicating the presence of 1-2% water frost [5]. The accumulation of integration time over the course of the mission has led to im-

proved SNR at these wavelengths, enabling increased precision for our ratio maps.

We also analyze the far-UV spectral slopes inside of Amundsen's largest PSR and compare with maximum temperature to provide further evidence of water ice inside of the cold traps. These spectral slopes are determined by making linear fits to the water-band (164–173 nm) and off-band regions (175–190 nm) of the albedo spectrum for each spatial pixel inside the PSRs, following the method in Hendrix et al. 2012. A positive (or "red") slope may be consistent with surficial water ice. We analyze spectral slopes both inside of Amundsen's PSRs and at different sunlit regions of the crater in order to characterize the volatile content throughout the crater.

References:

[1] Lemelin et al. (2014) *Planetary and Space Science,* 101, 149-161. [2] Spudis et al. (2013) *JGR: Planets 118.10, 2016-2029.* [3] Sonsalla et al. (2014) *Proceedings of the 12th International Symposium on Artificial Intelligence, Robotics and Automation in Space-i-Sairas.* [4] Gladstone et al. (2010) *Space Sci. Rev., 150, 161-181.* [5] Gladstone et al. (2012) *JGR: Planets* 117.E12

LCROSS: A Four Minute Mission. A. Colaprete[1], R. C. Elphic[1], M. Shirley[1], J. Heldmann[1], D. Goldstein[2], [1]NASA Ames Research Center, Moffett Field, Mountain View, CA, anthony.colaprete-1@nasa.gov, [2]University of Texas, Austin, TX 78712.

Introduction: Using the spent Centaur booster as an impactor, the Lunar Crater Observation and Sensing Satellite (LCROSS) mission sampled one spot within the South Pole crater Cabeus by lifting material from shadow and into sunlight. The LCROSS Shepherding Spacecraft (SSC) flew four minutes behind the impacting Centaur making measurements of the impact, debris clouds, and resulting crater [1]. At the same time, measurements were made by instruments onboard the Lunar Reconnaissance Orbiter (LRO), including the Lyman Alpha Mapping Project (LAMP) spectrometer at impact and the Diviner Lunar Radiometer (DLR) approximately 90 seconds after impact [2,3]. These various observation platforms provided a number of unique and complimentary measurements of the impact. This paper presents an attempt to piece together the conglomerate of observations into a single model for the surface conditions at the LCROSS impact site. In particular, the model addresses the distribution and form of the various volatiles, including water, observed in the LCROSS impact event.

LCROSS Impact Location: The LCROSS Centaur impacted into an area in the crater Cabeus which has been in permanent shadow for the more than one Gyr4]. The impact site was selected based on a variety of criteria, including the presence of hydrogen, temperatures, height to sun illumination, and slopes. Leading up to the final impact target selection, LRO data was used to understand these parameters with nearly continuous updates coming from the LRO instrument teams. The two most important criteria were hydrogen concentrations and height to sun illumination.

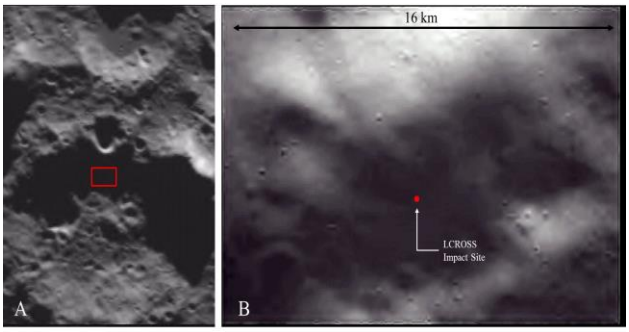

Figure 1. Images taken from a NIR Camera #2 on the LCROSS Shepherding Spacraft at an altitude of approximately 145 km (panel A) and 43 km (panel B) above the surface of Cabeus. The area is in permanent shadow and illumination is the result of light reflected/scattered off adjacent terrain (sun is to the upper left, while the inner walls of small craters in panel B indicate illumination from the bottom of the image).

The LCROSS impact site, imaged by the LCROSS NIR camera and registered to LOLA DEMs [5, 6], was in a depression that would have provided extra shadowing from secondary scattering from surround terrain. It is in these "double-shadowed" areas that temperatures are theoretically coldest (Figure 1).

Characteristics of the Impact and Impact Site: The impact resulted in a two-component ejecta curtain: a high angle plume which has been associated with the low density of the impactor, and the canonical "low angle" curtain, which, while similar to traditional natural impacts, was also modulated by the density of the impactor [5]. Based on the nature of the NIR and visible impact flashes the impact site appears to be relatively low density (porosities >70%) [5]. While the impact generated relatively cool and localized debris (T~1000-1200 K), a variety of vapors were released at impact (including CO and H_2) [2]. Other vapor components (e.g., Na) appear only after the first dust is seen via scattering of sunlight, suggesting some of the volatile components were intimately entrained in the soil/ice mixture [5]. Water ice grains were observed in the ejecta at early times (Impact +20 sec), and again at later times (Impact+230 sec). This observation suggests that these grains were at least part of the high angle ejecta cloud and most likely also in the nominal angle ejecta component [1,7,8]. Increases in water vapor with time after impact suggest exposed water at the impact site. The cold temperatures within the Centaur crater (as observed by the NIR and as observed by Diviner) indicate a possible ice rich soil [1, 3]. Combined, these observations help constrain the types and distribution of volatiles at the LCROSS impact site. This paper will present a summary of the observations and an evaluation of various models for the distribution and form of volatiles at the LCROSS impact site.

[1] Colaprete et al., (2010), *Science*, **330**, 463-468. [2] Gladstone et al., (2010), *Science*, **330**, 472-476. [3] Hayne et al., (2010), *Science*, **330**, 477-479. [4] Paige et al., (2010) *Science*, **330**, 479-482. [5] Schultz et al., (2010), Science, 330, 468-472. [6] Marshall et al., (2011), *PSS*, In Press. [7] Colaprete et al, 2011, 42nd LPSC , abs# 2037. [8] Hermalyn et al.(2011), Wet vs. Dry Moon Workshop, LPI.

Gardening Ice at the Poles of the Moon and Mercury E. S. Costello[1,2], R. R. Ghent[3,4], P. G. Lucey[1] [1]Hawaii Institute of Geophysics and Planetology, University of Hawaii, Honolulu, HI, USA, ecostello@higp.hawaii.edu; [2]Dept. of Geology and Geophysics, University of Hawaii, Honolulu, HI, USA; [3]University of Toronto Dept. of Earth Science, Toronto, ON, Canada; [4]PSI, Tucson, AZ, USA.

Introduction: The Moon and Mercury have polar regions in permanent shadow that provide hospitable conditions for volatiles [1, 2, 3, 4]. While radar observations of the poles of Mercury present strong evidence for the existence of pure water ice deposits that are meters thick in permanently shadowed regions [e.g. 5, 6, 7], ice on the Moon has been less conspicuous. Workers have found traces of water or hydroxyl [e.g. 8, 9, 10, 11, 12, 13] but the Moon does not have unambiguous and extensive Mercury-like surface or shallow buried ice deposits. Mystery remains with respect to cause of the discrepancy in abundance of surface and near-surface ice between the Moon and Mercury.

To investigate this discrepancy we examine the hypothesis that the difference is due to a difference in impact flux affecting the overturn rate. Marchi et al (2005) [14] present a robust model of the meteoroid flux onto the surface of Mercury, and show that the modern flux of impactors of diameters 1 cm - 100 m is about ten times lower on Mercury than it is on the Moon. We use an analytic model to describe the rate and magnitude of impact gardening as a function of time on both bodies. The model is based on the pioneering Apollo-era lunar regolith mixing model presented by Gault et al. (1974) [15], with updated input parameters and an expanded parameter space that allows for exploration of the rate of impact gardening as it is driven by a variety of impactor types into a variety of target materials. We take advantage of the expanded parameter space in this work, as we broaden the scope of the model beyond the Moon to calculate the rate of impact gardening on Mercury.

The model describes the maximum depth influenced by impact gardening as a function of time. Much as Gault et al. (1974) [15] did, we assume the following: 1) the cumulative flux of objects onto the surface is a power-law, and 2) the production of craters follows a Poisson distribution, and 3) the size and shape of craters follow efficiency laws based on target material properties. We update the cratering efficiency laws and implement those presented by Holsapple (1993) [16].

Another important update to the Gault model is the inclusion of secondary cratering, which has been shown to have a significant impact on the rate of gardening on the Moon [17, 18]. In our treatment of both the Moon and Mercury we implement the same treatment of secondary impacts, where secondary impactors follow a size distribution based on the McEwen et al. (2005) study of Zunil crater [19, 20].

The Moon: Our calculations suggest that secondary impacts thoroughly garden regolith to depths that are consistent with the thorough reworking of the top 3 cm of regolith calculated from the homogenous distribution of Al^{26} in Apollo cores [21] and calculated from size frequency distributions of splotches in LROC temporal pairs [22]. Gardening due to secondaries is also generally consistent with the rate at which anomalous surface features such as cold spots [23] and rays [24] are reworked into background regolith. Our calculations with secondaries included are also in better agreement than those of Gault et al. (1974) with the meter and shallower reworking of surface-correlated space weathering products (Is/FeO and cosmic ray tracks) to depth vs. isotope dating compiled from Apollo cores [25, 26].

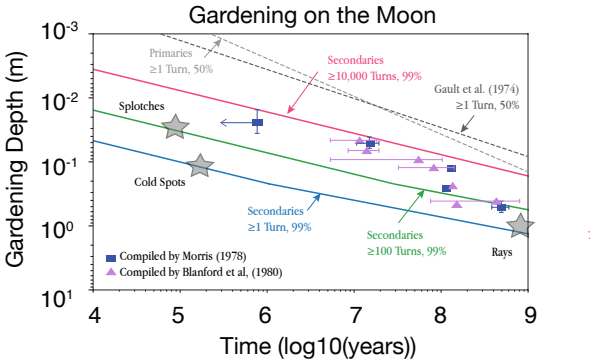

Figure 1: In comparison to the gardening rate due to primary impacts only, the secondary-dirven rate is in much better agreement with the rates calculated from Apollo cores and with the residence time of surface features such as splotches, cold spots and rays.

Mercury: Using the Marchi et al (2005) [14] flux, in Figure 2 we show our gardening calculations for overturn driven by these 1 cm - 100 m meteorites and their secondaries using the modern Mercurial flux, gravity, and average impact velocity and compare to the gardening rate on the Moon as it is driven by the modern lunar impact flux, gravity, and average impact velocity. For this version of the model we assume that target material properties are the same for Mercury and the Moon.

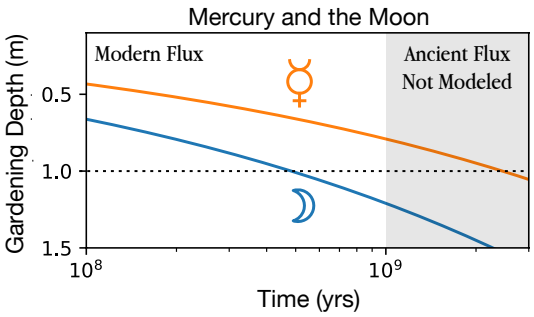

Figure 2: The gardening rate on Mercury and the Moon. Material above the contours has been gardened at least once with 99% certainty by secondary impacts.

Discussion: The model describes the depth reached by impact gardening under exposure to the modern impact flux and consequent secondaries. On Mercury it would take between 2 and 3 Gyr to garden to 1 m depth. On the Moon, gardening reaches 1 m depth in about 500 Myr. Assuming that ice is not replenished and assuming that one gardening event obliterates all ice to the modeled depth, a 1 m thick ice deposit on Mercury would be depleted but still be present after 1 Gyr. The same 1 m ice deposit on the Moon would be erased by impacts in 500 Myr. The model suggests that if the Moon ever had a Mercury-like deposit, it may have succumbed to impact gardening.

Future work: On Mercury, micrometeoroid bombardment is thought to be a dominant surface process [28], and Cintala (1992) [29] predict that unlike the lower flux at larger impactor sizes, the flux of micrometeoroids onto Mercury is approximately 5.5 times greater than the flux onto to the Moon. In future work, we will explore the influence of micrometeorite bombardment at the micron to millimeter scale on the Moon and Mercury. Such work could help to describe the evolution of low albedo lag deposits formed by sublimation and accumulation of dark refractory material that terminate shallower than the penetration depth of radar [7] and tie into the story of thermal shielding of underlying ice.

As noted in the section on Mercury, we do not include a treatment of the flux before 1 Gyr. Such a treatment is possible using the robust crater production functions developed for the inner solar system by the unified productions function for the inner solar system by Neukum et al. (2001) [30]. By modeling gardening due to the ancient flux we may be able to better constrain the depositional age of the Mercury ice deposits and, working backwards, a potential rate of replenishment.

Secondary cratering is crucial for each of these cases and any future application of the model. Our relatively simple assumptions about secondary cratering may vary from planet to planet and even between terrains on the same planet. On Mercury, relatively high gravity and impact velocity may result in a higher number of secondary craters produced by a primary impact. The volume of material ejected by impacts is 10 to 100 times greater for ice targets than crystalline rocks [31]. Inputing a more realistic size and velocity distribution for secondary impactors that is tailored to each planetary case is an important component of ongoing work.

References: [1] Watson, K. et al. (1962). *Icarus*, 1(1-6), 317-327. [2] Vasavada, A.R. et al. (1999). *Icarus*, 141(2), 179-193. [3] Paige, D.A. et al. (2010). *Science*, 479-482. [4] Paige, D.A. et al. (2013). *Science*, 300–303. [5] Slade, M.A. et al. (1992). *Science*. 635-641. [6] Harmon, J.K., et al. (1994): *Nature*. 213-215. [7] Lawrence, D. J. et al. (2013). *Science*, 292-296. [8] Nozette, S., et al. (1996). The Clementine bistatic radar experiment. [9] Colaprete, A. et al. (2010). *Science*, 463-468. [10] Zuber, M. T. et al. (2012). *Nature*, 378-381. [11] Milliken, R. E., & Li, S. (2017). *Nature Geoscience*, 10(8), 561.1 [12] Li, S. et al. (2017). *LPI Contributions*, 2041. [13] Hayne, P. O. et al. (2015). *Icarus*, 255, 58–69. [14] Marchi, S. et al. (2005). *Astronomy & Astrophysics*, 431(3), 1123-1127. [15] Gault, D. E., et al. (1974) *LPS V*, 2365-2386. [16] Holsapple, K. A. (1993) *Annu. Rev. Earth Planet. Sci*. 21:333-73. [17] Costello, E.S. et al. (2017) *LPSC XLVIII*, #1672. [18] Costello, E.S. et al. (2018) *Icarus*, (Accepted). [19] McEwen, A. et al. (2005). *Icarus*, 176(2), 351–381. [20] H. Melosh, *Icarus* 59 (2) (1984) 234-260. [21] Fruchter, J S. et al. (1977). *LPS VIII* 3595-3605. [22] Speyerer, E.J. et al. (2016). *Nature*, 215-218. [23] Bandfield, J.L., et al. (2014). *Icarus*, 231, 221-231. [24] Hawke, B.R., et al. (2004). *Icarus*, 170(1), 1–16. [25] Morris, R.V. (1978). *LPS IX* 1801-1811. [26] Blanford, G. (1980). *LPS XI* 1357-1368. [27] Hurley, D. M. et al. (2012). *Geophysical Research Letters*, *39*(9). [28] Hapke, B. (2001). *Journal of Geophysical Research: Planet*s, 106(E5), 10039-10073. [29] Cintala, M. J. (1992). *Journal of Geophysical Research: Planets*, 97(E1), 947-973. [30] Neukum, G, B A Ivanov, and W K Hartmann. (2001). *Space Science Reviews* 96 (1-4). [31] Lange, M. A., & Ahrens, T. J. (1987). *Icarus*, 69(3), 506-518.

Lunar Simulant Far-Ultraviolet Reflectance Comparisons with Apollo Soils Measured with the Southwest Ultraviolet Reflectance Chamber (SwURC). E.A. Czajka[1,2], K. D. Retherford[2,1], U. Raut[2], P.L. Karnes[2], D. Wyrick[2]. Department of Physics and Astronomy, University of Texas at San Antonio, San Antonio TX 78249, [2] Southwest Research Institute, San Antonio, TX 78238. (elizabeth.czajka@swri.org)

Introduction: Since the Lyman Alpha Mapping Project (LAMP onboard the Lunar Reconnaissance Orbiter (LRO) has found evidence of water frost inside permanently shaded regions (PSR's) of craters on the Moon [1], there has been an increased interest in harnessing water as a resource for future manned missions. Understanding lunar simulants and how they adsorb water ice will be extremely useful for scientists planning the next phase of NASA's lunar missions. There is no one "perfect" lunar simulant, often simulants can closely mirror the soil in elemental abundance but will be significantly different spectrally [2]. JSC-1A remains one of the most popular lunar mare simulants, which was modeled after the Apollo 14 soil sample, 14163 [3]. However, it has been suggested that the JSC-1A may not be geologically similar to the Apollo lunar soils based on the JSC-1A's lack of np-Fe, and differences in grain size distributions, (Figure 1)[4].

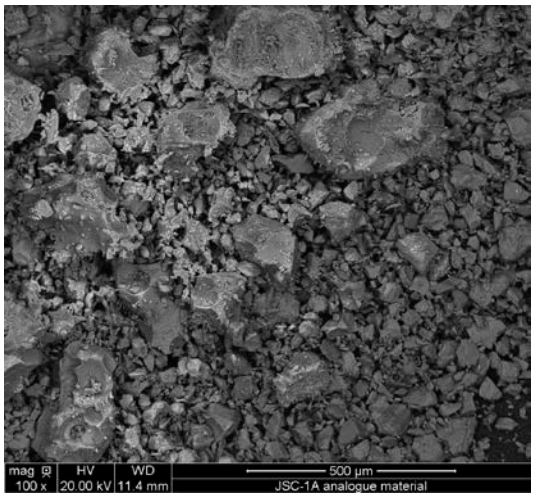

Figure 1: SEM Image of JSC-1A lunar simulant (Photo credit D. Wyrick at SwRI)

These geological differences could indicate a difference in surface area/activation sites for water ice adsorption onto the lunar grains. We will investigate the dry reflected far-ultraviolet spectra of the JSC-1A and compare to the reflectance spectra of the Apollo lunar soils 10084 and 15041 [5]. Preliminary results for the far-UV reflectance spectra of ice coated lunar simulant will also be discussed.

Far-UV Measurements: Far-UV Reflectance spectra of the samples are taken in the Southwest Ultraviolet Reflectance Chamber (SwURC). Before samples can be tested in the SwURC chamber, they are first baked out in a separate chamber at ~100 C for at least 24 hrs to drive off any surface moisture from being open to air. Samples are then placed inside the main vacuum chamber which maintains a base pressure of ~10^{9} Torr. Powdered samples are systematically poured into a sample tray which is then mounted to a horizontal retractable stage, while a CsI-coated channeltron CEM detector rotates around the tray in a circular path. This allows for reflectance measurements to be taken over several phase angles. The UV light source is a 30 W deuterium lamp, mounted to a monochromator which is capable of isolating wavelengths of 115-200 nm with a resolution of 0.5 nm. In order to coat samples with a thin layer of ice, a new microcapillary doser is being added to the chamber. The concentration of water vapor will be monitored by an absolute capacitance manometer. The final reflectance spectra will be calculated using methods described in Raut et al. 2018 [5]. We will present our latest results.

References:

[1] Gladstone, G.R. et al., Far Ultraviolet Reflectance Properties of the Moon's Permanently Shadowed Regions (2012) JGR, 117, E004H04

[2] Taylor, L.A, et al., Evaluations of Lunar Regolith Simulants (2016) Planetary and Space Science, http://dx.doi.org/10.1016/j.pss.2016.04.05

[3]McKay, D.S. et al., JSC-1A: A New Lunar Soil Simulant (1994), American Society of Civil Engineers, Engineering, Construction, and Operations in Space, IV, 857-866

[4]Liu, Y., Taylor, L.A., Characterization of Lunar Dust and a Synopsis of Available Lunar Simulants (2011) Planetary and Space Science, 59, 1769-1783.

[5] Raut, U., Karnes, P.L., Retherford, K.D., Davis, M.W. , Liu, Y., Gladstone, G.R., et al., Far-Ultraviolet Photometric Response of Apollo Soil 10084 (2018) JGR: Planets, 123. https://doi.org/10.1029/2018JE005567

Acknowledgement: Special thanks to the UTSA-SwRI joint Ph.D. program, and to Southwest Research Institute SwURC facility.

PATCHY DISTRIBUTION OF ANCIENT, LUNAR ICE CONTRASTS WITH YOUNG, COHERENT ICE DEPOSITS ON MERCURY. Ariel N. Deutsch[1], James W. Head[1], and Gregory A. Neumann[2], [1]Department of Earth, Environmental and Planetary Sciences, Brown University, Providence, RI 02912 (ariel_deutsch@brown.edu), [2]NASA Goddard Space Flight Center, Greenbelt, MD 20771, USA.

Introduction: The poles of Mercury and the Moon both show evidence for water ice, but the deposits on Mercury have a greater areal distribution [1] and a more pure concentration [2]. Earth-based radar observations revealed an estimated ~25,000 m^2 of ice at Mercury's poles [1] that was modeled to be ~95 wt. % pure [2]. Images [3] and reflectance measurements [4] acquired by the MErcury Surface, Space ENvironment, GEochemistry, and Ranging (MESSENGER) spacecraft showed that these deposits are spatially homogeneous within permanently shadowed regions (PSRs).

In contrast to the relatively pure water-ice deposits on Mercury [2], volatile deposits on the Moon are rather heterogeneous. For instance, multiple volatiles species were detected in the ejecta plume of the LCROSS experiment that impacted into Cabeus at the Moon's south pole, suggesting that the deposits are not pure water ice [5–6]. Additionally, mapping of UV albedo spectra and surface temperature revealed a highly spatially heterogeneous distribution of water frost within PSRs [7].

Impact gardening and space weathering [8] can produce spatial heterogeneities because these processes cause loss and redistribution of volatiles through time. Impacts introduce heterogeneity into the system because they remove volatiles via vaporization, and also preserve volatiles through the emplacement of ejecta, with a net effect of breaking up and burying the ice through time [9]. Because these processes take time, the degree of heterogeneity is inherently related to the age of the ice.

Here, we explore how the differences in purity and spatial heterogeneity of surface ice at Mercury and the Moon may be related to the ages of the ice.

Methodology: *Age estimates of water-ice deposits on Mercury.* Using images acquired by the Wide-Angle Camera during MESSENGER's low-altitude campaign [10], we identify small craters in the PSRs that are correlated with high reflectance, suggestive of excavated material. While the majority of craters observed in the PSRs may be pre-existing topography emplaced before the deposition of the ice [e.g., 11], the anomalous small craters associated with high-reflectance material may have formed after the emplacement of the ice. If so, then these small craters superposing the ice deposit can be used to date the ice surface itself. Here, we estimate the absolute ages of specific mercurian ice deposits (Fig. 1) using small, superposed craters associated with high-reflectance rings. Absolute ages of Laxness, Bechet, and Ensor craters are estimated using CraterstatsII [12] and chronology and production systems from [13].

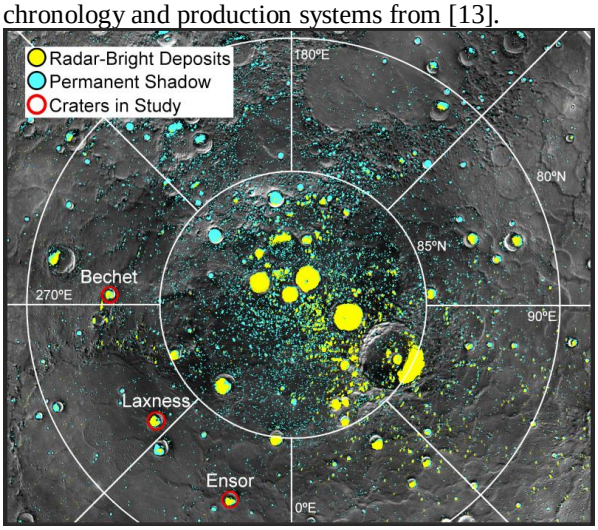

Fig. 1. *Distribution of water ice at the north polar region of Mercury, from 80°–90°N [14]. Regions of permanent shadow [14] are shown in blue and radar-bright materials [1] are shown in yellow. Craters analyzed in this study are outlined in red. Map is a MDIS mosaic in polar stereographic projection [14].*

Spatial heterogeneity measurements for ice deposits on the Moon. We explore the relationship between the spatial heterogeneity of ice and the age of host craters at the lunar poles in order to discuss the timing of volatile delivery to the Moon (Fig. 2). The spatial heterogeneity of a polar deposit is quantified as the percent of the cold trap occupied by ice. We define cold traps as regions with maximum surface temperatures ≤ 110 K, as measured by the Diviner Lunar Radiometer Experiment [15]. To determine what percent of cold traps are occupied, we use maps of surface water-ice detections derived from 1.4, 1.9, and 2.0 μm water absorptions measured by the Moon Mineralogy Mapper (M3) [16]. The ages of host craters are estimated by crater counting techniques [17].

Results: *Age estimates of water-ice deposits on Mercury.* The estimated derived ages for the ice surfaces within Laxness, Bechet, and Ensor craters are 38 ± 10 Myr, 65 ± 30 Myr, and 210 ± 60 Myr, respectively. These ages are slightly higher than, but within the error range of, the 50 Myr age that is predicted for the ice deposits by regolith gardening models [18]. The ages estimated here are also consistent

with the sharp albedo boundaries of ice deposits on Mercury, which suggest that the ice was deposited relatively recently or that a regularly refreshing mechanism exists [3, 10]. Additionally, these ages are consistent with the ice being delivered by a single, young impactor, such as the Hokusai impactor [19].

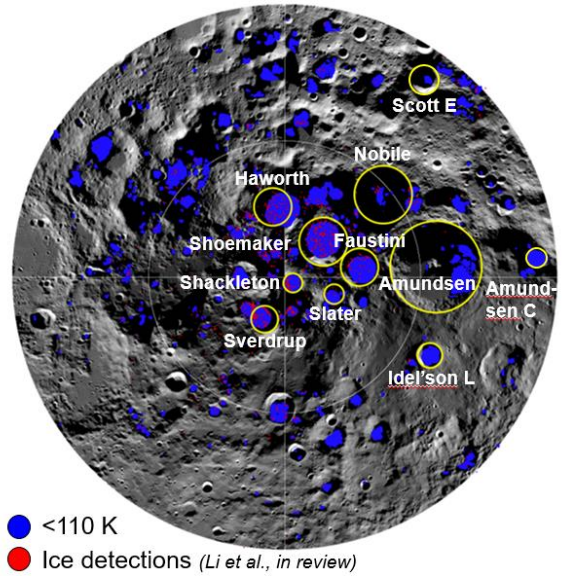

Fig. 2. *Distribution of surface water ice is shown in red for the south polar region of the Moon, from 80°–90°S [16]. Present-day cold traps are mapped in blue from Diviner maximum surface temperatures [14]. Craters analyzed in this study are outlined in yellow. Map is a LRO mosaic in polar stereographic projection.*

Spatial heterogeneity measurements for ice deposits on the Moon. We find that the degree of patchiness of lunar surface ice within a given PSR may be affected by the age of the cold traps. Specifically, we find three major populations of ice distribution: (1) Population 1 consists of ancient craters (>3.8 Ga) that tend to host the most patchy surface ice deposits, (2) Population 2 consists of middle-aged craters (between 2.9 and 3.8 Ga) that tend to host the most spatially coherent surface ice deposits, and (3) Population 3 consists of the youngest craters (<2.5 Ga), which do not show evidence for surface water-ice deposits [16].

Our results suggest that older ice deposits may have undergone higher rates of impact bombardment [8–9], contributing to a more patchy distribution of surface ice. Population 1 is consistent with relatively high impact rates [20], which is suggestive of not only high ice delivery rates, but also high impact destruction rates, where ice deposits are expected to be broken up and buried with time. Population 2 is consistent with a drop-off in impact delivery [20], where ice is still being delivered to the poles, but the ice also experiences relatively less impact destruction. Finally, Population 3 suggests that surface ice was not delivered at high rates after 2.5 Ga.

We also find that there are some ancient craters that are present-day cold traps, but do not host surface ice deposits. It is possible that this is an artefact of lunar true polar wander (TPW), or a physical reorientation of the spin axis relative to the Moon's present-day poles [e.g., 21]. Maps of the lunar poles when the Moon was on its paleo-axis [21] suggest that the specific craters that lack surface ice [16] may not have been stable cold traps for surface ice during the Moon's early history. Thus, our results suggest that surface ice patchiness observed at the lunar poles today may be controlled by ice supply rate, impact destruction rate, and TPW.

Implications: The same impact bombardment and space weathering processes operate on Mercury and the Moon, and Mercury's regolith may be overturned even more frequently than the lunar regolith [22]. The lack of apparent degradation of Mercury's ice deposits further suggests that the ice deposits on Mercury may be relatively young. As with the Moon, impact delivery rates on Mercury were higher during the planet's early history. Thus, it is possible that relatively ancient, degraded ice deposits exist in Pre-Tolstojan, Tolstojan, and Calorian craters (4.0–1.9 Gyr) below the coherent, pure deposits observed on Mercury's surface today.

In conclusion, we suggest that the spatial heterogeneity and purity of the Moon's polar deposits within a given PSR may be explained by relatively ancient deposition of ice, in comparison to relatively recent delivery of ice to Mercury's polar cold traps.

References: [1] Harmon J.K. et al. (2011) *Icarus, 211,* 37–50. [2] Butler B.J. et al. (1993) *JGR, 98,* 15003–15023. [3] Chabot N.L. et al. (2014) *Geology, 42,* 1051–1054. [4] Neumann G.A. et al. (2013) *Science, 339,* 296–300. [5] Colaprete A. et al. (2010) *Science, 330,* 463–468. [6] Schultz P.H. et al. (2010) *Science, 330,* 468–472. [7] Hayne P.O. et al. (2015) *Icarus, 225,* 58–69. [8] Pieters C.M. and Noble S.K. (2016) *JGRP, 121,* 2016JE005128. [9] Hurley D.M. et al. (2012) G*RL, 39,* L09203. [10] Chabot N.L. et al. (2016) *GRL, 43,* 9461–9468. [11] Deutsch A.N. et al. (2018) *Icarus, 305,* 139–148. [12] Michael G.G. and Neukum G. (2010) *EPSL, 294,* 223–229. [13] Neukum G. et al. (2001), *PSS, 49,* 1507–1521. [14] Deutsch A.N. et al. (2016), *Icarus, 280,* 158–171. [15] Paige D.A. et al. (2010) *SSR, 150,* 125–160. [16] Li et al. (2017) *ESF,* Abstract #NESF2017-135. [17] Tye A.R. et al. (2015) *Icarus, 255,* 70–77. [18] Crider D. and Killen R.M. (2005), *GRL, 32,* L12201. [19] Ernst C.M. et al. (2016) *LPS, XLVII,* Abstract #1374. [20] Nesvorný, D. et al. (2017) *Astron. J., 153,* 103. [21] Siegler, M.A. et al. (2016), *Nature, 531,* 480–484. [22] Domingue D.L. et al. (2014) *SSR, 181,* 121–214.

Next Steps in Evaluating Lunar Polar Volatiles: Land, Prospect, Sample, Assay. R. C. Elphic[1], A. Colaprete[1], M. H. Shirley[1], M. A. Siegler[2], D. Andrews[1], [1]NASA Ames Research Center, Moffett Field, CA, Planetary Science Institute, Tucson, AZ

Introduction: The LEAG "Advancing Science of the Moon" Specific Action Team recently evaluated progress toward addressing the lunar polar volatile goals identified in the "Scientific Context of the Exploration of the Moon (2007)." The team concluded that, while progress had been made thanks to the LCROSS impactor, the LRO, SELENE, and Chandrayaan-1 orbital missions, understanding of Goal 4a, compositional state and distribution (lateral and vertical) of lunar polar volatiles, is "far from complete." They pointed out that very little progress has been made in understanding sources (Goal 4b) and transport, retention, alteration, and loss of volatiles (Goal 4c), despite these missions. Likewise, regarding understanding the physical properties of the cold, possibly volatile rich polar regolith, or what it reveals about the ancient solar environment (Goals 4d and 4e, respectively), progress has been minimal at best. In all cases, missions to the surface are called for to address the gaping holes in our understanding of the lunar polar volatile inventory, which appears to be so different from that of Mercury. In particular for in situ resource utilization, there are specific requirements that must be addressed in order to gauge the strategic and economic accessibility and value of such resources.

Composition and Physical State: A variety of measurements addressing both composition and physical state are possible, but a key requirement is a landed, mobile mission. LCROSS demonstrated that there are indeed volatile chemical compounds present at one very cold, permanently-shadowed location. But the physical form of water (massive ice in slabs vs. finely disseminated grains in the regolith) and other compounds remains poorly constrained; in situ investigations are necessary. Further, single-point measurements from a stationary lander are of limited use in characterizing the global resource potential. Mobility is required. Prospecting by its nature requires a continuous characterization of a potential resource over a potential recovery area. We do not understand the sources, physical processes and resulting scales governing the current distribution of, for example, water ice. Equally frigid, equally dark cold traps appear to have retained very different amounts of hydrogen-bearing species. Assaying volatile composition and physical form of subsurface samples acquired during a traverse over scales of 100s of meters to kilometers will greatly improve understanding of the compounds, and their physical forms, that are sequestered in different thermodynamic and geologic settings. These subsurface sample measurements will be tied to surface instrument data acquired continuously during the traverse, and will be the first steps to creating an economic mineral model for commercial use.

Abundance: It is often said by ISRU community experts that a water-equivalent abundance of 0.5 – 1 wt% is the minimum economically viable concentration. While the break-even value must depend on the physical form, composition, details of lateral and vertical distribution, and especially the recovery technology, it is a useful lower limit for instruments and missions to target. In the end, a mineral model that describes lunar polar volatiles for potential ISRU must include abundance for the same economic reasons as conventional mineral ores in terrestrial mining.

Lateral and Vertical Distribution: Absolutely key to successful future ISRU is understanding the lateral and vertical distribution of potential volatile resources. A viable "ore" or "reserve" must have sufficient abundance within a sufficiently manageable potential production area for economic recovery. For example, the recovery of sufficient water for separation into 10,000 kg of oxygen for yearly crew habitat use requires sufficient abundance (>0.5 wt%) in a workable production area (~50 x 50 m), with a sufficiently shallow depth distribution (≥ 0.5 m depth) due to the cost/difficulty of overburden removal. Characterization of such a "reserve", and the geologic and physical processes that shaped it, requires mobility and the combination of surface prospecting and sample acquisition/analysis instrumentation. Again, the combination of composition, form and distribution are key in formulating a mineral model.

Studies in support of Resource Prospector mission traverse planning have shown that some minimum amount of mobile exploration within a potential production area is required to determine the likely mean and variability in spatial scales of the resource. For a 50 x 50 m area, traversing ~200 m within it will provide a characteristic deposit size scale and variability with uncertainties of around 20%.

Water ice cannot be stable for long times where temperatures are much above 110K. Therefore it is helpful in developing requirements to consider ice stability depth, as most recently reported by Siegler et al., *Nature,* [2016]. This work considered the depth at which the regolith temperature is low enough annually to limit ice sublimation/diffusion losses to 1 mm/Ga,

using regolith thermal conductivity and soil density profiles.

A map of ice stability depth reveals the scales that must be explored to develop a mineral model using in situ measurements on the lunar surface. Figure 1 shows two renditions of modeled ice stability depth, based on LOLA gridded topography products from PDS and solar illumination variations over 100 years. The color coding refers to surface ice stability (red: within PSRs, for example), shallow ice stability (green: 0-50 cm depth), deep ice stability (yellow: 50-100 cm), and "dry" as gray. The left panel is a 240-m resolution product, and the right a 20-m resolution map of the same area to the west of Hermite-A (20-km diameter crater centered on 308.98E, 87.94N). While clearly similar on the largest scales, much more local variability in stability depth can be seen in the 20-m map than the 240-m map. Such variability simply reflects the fact that topography controls surface and subsurface temperature at all scales. This means that exploration of the potential resource area must extend from 10-m (and probably smaller, 1-m) scales up to several kilometers.

Future Mission Design: Successful characterization of lunar polar volatiles, whether as a scientific target or a potential resource, requires (1) the ability to identify promising sequestration sites for sample acquisition and analysis, both before and during the mission; (2) the ability to acquire surface/subsurface samples to enable chemical composition, physical state and isotopic analysis, and to ground-truth the prospecting instrument data; (3) the ability to maneuver over 1-1000's meters scales while measuring volatile abundance (i.e., prospecting) within time-space corridors having sun and communications access, having trafficable slopes and hazard densities; (4) the ability to respond in real time to unexpected results for volatile abundance, composition or distribution, and to replan quickly according to those discoveries.

One implication of these requirements is that stationary lander missions are not sufficient to characterize anything beyond the reach of an arm or drill. To fully characterize a potential volatile resource area at the scales needed for use, or to understand volatile emplacement, evolution and loss processes, a score or more of landers would be necessary, and even then would likely not meet a spatial Nyquist sampling criterion. Mobility lays this issue to rest.

A resource prospecting mission, with mobility, real-time prospecting measurements, sub-surface sample acquisition and analysis is called for. A Resource Prospector is the next step.

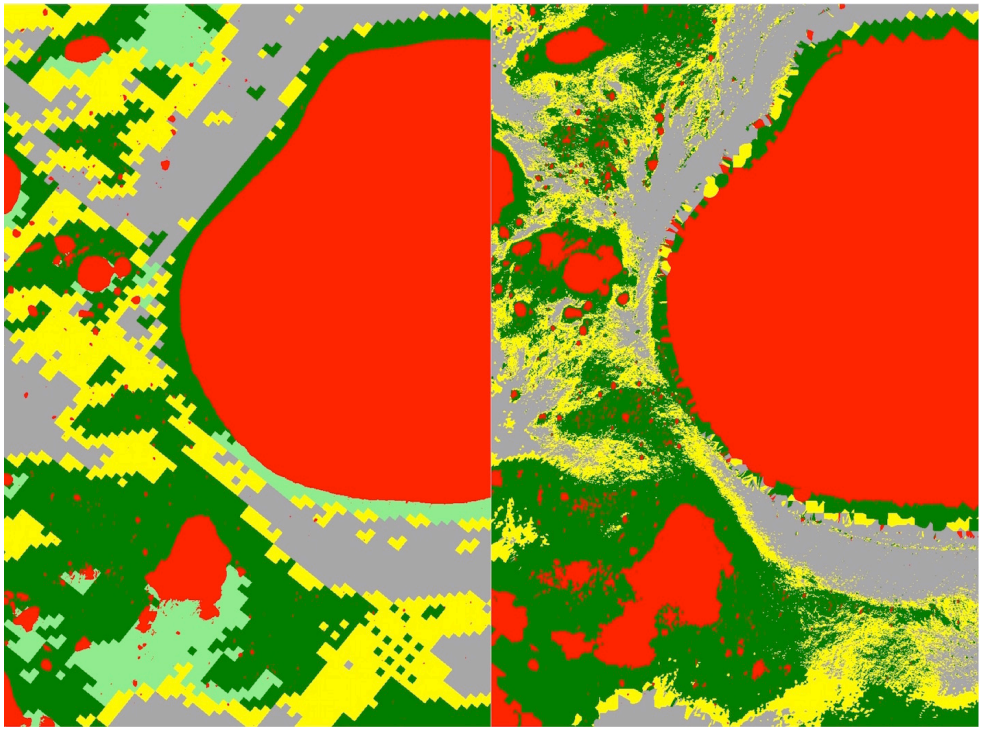

Fig. 1. (Left) 240-m resolution ice stability depth map for western half of Hermite-A area; (Right) 20-m resolution map. Red: surface ice stability; green: 0-50 cm depth; yellow: 50-100 cm depth, gray: >100 cm or not stable at any depth. (Light green denotes shallow ice stability during the paleo-pole epoch as well.)

COLD TRAPPING OF LUNAR POLAR CRATER VOLATILES: A MODEL OF DESORPTION FROM FROSTY GRAINS. W. M. Farrell[1], D. M. Hurley[2], M. J. Poston[3], P. O. Hayne[4], J. L. McLain[5], 1. NASA/Goddard Space Flight Center, Greenbelt MD, 2. Johns Hopkins University/Applied Physics Laboratory, Laurel, MD, 3. Southwest Research Institute, San Antonio, TX, 4. University of Colorado, Boulder, CO, 5. University of Maryland, College Park, MD (William.M.Farrell@nasa.gov)

Introduction: In the Lunar Reconnaissance Orbiter (LRO) era, there is now substantial evidence that cold trapping is indeed occurring and possibly may even be of a dynamic nature within lunar polar craters.

LRO's Diviner IR instrument derived annual average temperatures < 100K at the floor of the larger shadowed south polar craters, and these temperatures are cold enough to allow volatiles like water to stay trapped on surfaces for billions of years [1]. Using LRO's Lyman–α Mapping Project (LAMP), [2] reported on a detectable increase in the FUV water-related reflectance above 160 nm in some of the south polar craters, consistent with an water-regolith mix at the surface of about 2% in areal coverage within Shackleton, 1% in Hayworth, 0.3% in Shoemaker and 0.8% in Faustini craters (although the exact spatial distribution to account for the spectral increase in water is not uniquely known).

An increase in the reflected signal from LRO's Lunar Orbiter Laser Altimeter (LOLA) signal at 1064 nm has also been reported from many of the same south polar crater floors, which has been interpreted to be due to the presence of icy-regolith [3, 4]. The LOLA reflectance increase is substantial along the floor and walls of Shackleton crater and has been interpreted to possibly be related to icy-regolith (at ~20% mixture) or newly-exposed surfaces associated with downslope movement along crater wall [5]. The presence of the UV-bright anorthite in Shackleton crater was also suggested to explain the enhanced LOLA signal returns [6]. Fisher et al [4] specifically pointed out that the correlation of volatile signatures and temperature at the lunar poles is generally poor in comparison to ice at Mercury's poles, suggesting other controlling processes.

Hayne et al. [7] combined LRO Diviner and LAMP data over LOLA topography and demonstrated a correlation of maximum temperature and UV water-related reflectance. Their Figure 15 shows the trend of increasing crater-average reflectance with decreasing crater-average temperature as one might expect in the water cold trapping process. They defined the reflectance via an 'Off-On band' ratio: the reflectance in a band centered near 176 nm (high water reflectance) divided by the reflectance in a band centered near 143 nm (low water reflectance), with ratio values between 1.2 and 10 indicative 1 and 7% water-regolith concentration mix, respectively (see their Figure 3b).

Hayne et al. [7] reported there are many locations with temperatures above 110K with Off/On ratios greater than 1, suggesting surface water molecules are present even above its nominal volatility temperature (T > 110K, Off/On > 1).

The Frosty Grain. For lunar grains with a surface area of 0.1 m^2/g [8], a 1% wt of surface water corresponds to an average water layer of thickness near ~90 nm covering the grain's surface. However, given the complex irregular shape of lunar grains, its very likely that this layer thickness represents an average coverage. We might then expect water ice condensation to be 'pooled' in relative minima, like fissures and indentations on the grains. We also might anticipate quasi-dry exposed regions of regolith substrate at relative maxima. We thus consider the substrate at the microscopic grain scales as a heterogeneous water frost on a grain.

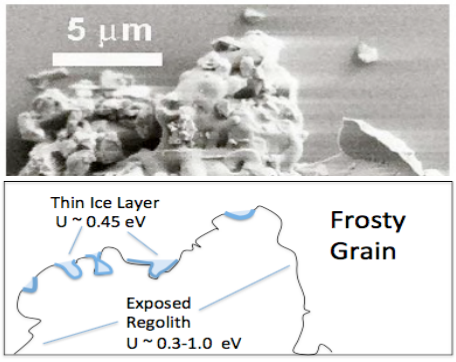

Figure 1. The frosty grain with a complex structure of water trapping energies.

The analog might be the porous activated surfaces found in cryo-pumps [9] that are not yet fully immersed in the condensate, having a sorbent substrate protrude from very thin regions (~100's of nanometers) where the vapor condensate is present. **Figure 1** represents our model 'frosty grain' with any inflowing water molecule having to interact with either an icy or regolith surface.

This frosty-grain model is consistent (but not unique) with the descriptions of intimate water mixtures and water coverage described in Gladstone et al. [2] and Hayne et al. [7]. Also, laboratory work by Poston et al. [8] found that the water activation energies for desorption on grain substrates vary widely at the small (grain) scales. We thus apply the intimate mixture assumption at the smallest grain-level scale, since that is where we have some direct knowledge,

and assume that this mixture is consistent when integrated across the surface to larger kilometers scales within lunar polar craters. Admittedly, we do not have complete knowledge of the patchiness of ice at the meter or kilometer scales in PSRs [10, 11] and thus assume the microscopic model of the frost (Figure 1) integrates across larger scale sizes consistent with the 5 km^2 LAMP observations used by Hayne et al. [7].

Desorption and Sublimation from the Frosty Grain. Figure 2 shows fraction of water retained over 1 billion years from a Monte Carlo surface water sorption model. Specifically, 240000 simulated water molecules are placed on a simulated surface and the desorption activation energy, U, is defined for each water binding site. We do not use a singe U value, but instead the activation energy at each specific water sorption site is selected by a random weighting from a Gaussian distribution in activation energy having initially a distribution center at 0.45 eV and a distribution width of 0.1 eV – similar to that of a water molecule binding to an icy surface. The retention time of each of these water molecules is $t = 10^{-13}\exp(U/T)$ seconds and the number retained for t > 1 By is counted as a function of increasing temperature.

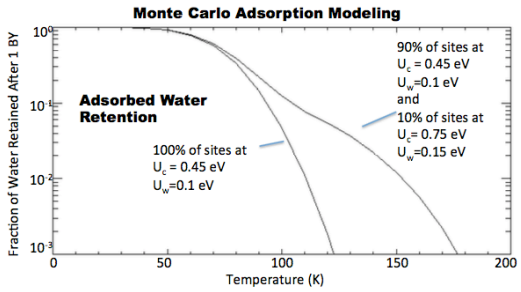

Figure 2. Monte Carlo simulation of water retention after 1 billion years as a function of temperature for sites with a distribution of activation energy centered around 0.45 eV and a Gaussian distribution width of 0.1 eV. Also shown is the effect on water sticking when 10% of the sites have higher activation energy of 0.75 eV.

For the ice-like case having U_c = 0.45 eV and width of U_w = 0.1 eV (the left hand curve in Figure 2) we find that the fraction of water molecules residing on the sorption surface for 1 By drops below 1% at T = 110K. This case is similar to sublimation from an ice-covered surface [12, 13]

However, if we include a population of water sorption sites with higher activation energy like that found by Poston et al. [8], with 10% of the sites having U_c = 0.75 eV and U_w =0.15 eV (and 90% at U_c = 0.45 eV and U_w = 0.1 eV), then there is substantially greater water retention with 1% of the sites retaining trapped water even at T > 150K. This case includes an ice-like surface but also the added effect of the exposed regolith substrate having higher activation energies (deeper water trapping sites).

Thus, if the polar crater floor has a distribution of activation energy similar in nature to the anorthite-rich lunar sample examined by Poston et al. [8], we would expect sorbed water to be retained to relatively high temperatures above 110K.

Comparison to Observations. Figure 3 shows the LAMP-derived Off/On ratios as a function of temperature in Haworth crater (from the data set used by Hayne et al. [7]). Figure 3b shows the Off/On ratio values > 1.2, those indicative of water frost, as a function of temperature. While the peak in the distribution in Figure 3b is below 80K, we note that there is still a population of 'frost' values even above 120K.

We thus present the non-unique possibility that the grains in these locations are 'frosty' having exposed regolith substrate regions on grain surfaces having activation energy > 0.6 eV. At these locations water can be bound to the surface for > 1 By even at temperatures near 150K (see Figure 2). We suggest the controlling variable is thus U/T and not T alone.

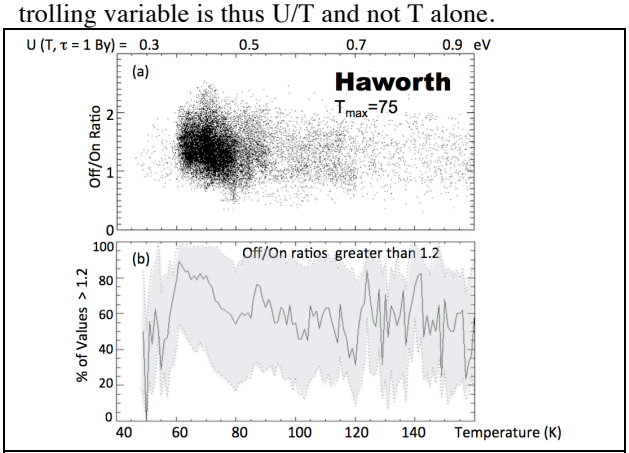

Figure 3: (a) The LAMP Off/On ratios as a function of temperature in Haworth crater. (b) The number of measurement values greater than 1.2 as a function of temperature.

References: [1] Paige, D. A., et al. (2010), Science, 330, 479–482.[2] Gladstone, G. R., et al. (2012), J. Geophys. Res., 117, E00H04, doi:10.1029/2011JE003913. [3] Lucey, P. G., et al. (2014), J. Geophys. Res. Planets, 119, 1665–1679, doi:10.1002/2013JE004592. [4] Fisher, E. A., P. G. Lucey, M. Lemelin et al. (2017), Icarus, 292, 74-85. [5] Zuber, M.T. et al., (2012), Nature 486 (7403), 378–381. [6] Haruyama, J., S. et al.,(2013), Geophys. Res. Lett., 40, 3814–3818, doi:10.1002/grl.50753. [7] Hayne, P.O., et al., (2015), Icarus 255, 58–69. doi:10.1016/j. icarus.2015.03.032. [8] Poston, M. J., et al. (2015), Icarus, 255, 24–29.[9] Day, C. (2007), Basics and applications of cryo-pumps, CAS-CERN Accelerator School, Vacuum in accelerators, p.241-274. [10] Rubanenko, L, and O. Aharonson, (2107), Icarus, in press. [11] Deutsch, A. N., et al. (2017), Geophys. Res. Lett., 44, 9233-9241. [12] Watson, K., B. C. Murray, and H. Brown (1961), J. Geophys. Res., 66, 3033–3041. [13] Zhang, J.A., Paige, D.A., (2009), Geophys. Res. Lett. 36 (16). doi:10. 1029/2009GL038614.

EVIDENCE FOR SURFACE WATER ICE IN THE LUNAR POLAR REGIONS USING REFLECTANCE MEASUREMENTS FROM THE LUNAR ORBITER LASER ALTIMETER AND TEMPERATURE MEASUREMENTS FROM THE DIVINER LUNAR RADIOMETER EXPERIMENT. E. A. Fisher[1], P.G. Lucey[2], M. Lemelin[3], B. T. Greenhagen[4], M. A. Siegler[5,6], E. Mazarico[7], O. Aharonson[8], J. Williams[9], P. O. Hayne[10], G. A. Neumann[7], D. A. Paige[9], D. E. Smith[11], M. T. Zuber[11], Elizabeth_Fisher1@brown.edu, [1]Brown University, Department of Earth, Environmental & Planetary Sciences, Providence, RI, [2]Hawaii Institute of Geophysics and Planetology, University of Hawaii at Manoa, Honolulu HI, [3]Department of Earth & Space Science & Engineering, York University, Toronto, Canada , [4]Johns Hopkins University Applied Physics Laboratory, Laurel, MD, [5]Planetary Science Institute, Tucson, Arizona, [6]Southern Methodist University, Dallas, Texas, [7]NASA Goddard Space Flight Center, Greenbelt, MD, [8] Weizmann Institute of Science, Department of Earth and Planetary Sciences, Rehovot, Israel, [9]Earth, Planetary, and Space Sciences, University of California, Los Angeles, CA 90095, [10]Astrophysical & Planetary Sciences, University of Colorado Boulder, Boulder, CO, [11]Department of Earth, Atmospheric and Planetary Sciences, MIT, Cambridge, MA

Introduction: The concept of volatiles accumulating on the surfaces of airless bodies via 'cold trapping', where volatile molecules are deposited and preserved on cold, permanently shadowed surfaces over geologic timescales, has been recognized for many years [e.g. 1]. Thermally driven sublimation strongly constrains where a volatile may plausibly survive on a planet's surface for extended time periods, because of the exponential relationship between temperature and sublimation rate in a vacuum; e.g. water ice cannot be preserved on surfaces that experience temperatures above ~100K due to rapid sublimation loss [2,3,4]. Water ice was identified on Mercury's surface by correlating surface material with high 1.064 μm reflectance, detected using the Mercury Laser Altimeter, with model biannual maximum temperatures that allow surface ice to be stable for billions of years (<100K) [4,5]. The Lunar Orbiter Laser Altimeter (LOLA) also measures 1.064 μm surface reflectance in the lunar polar regions [6,7,8,9], while the Diviner Lunar Radiometer Experiment measures surface temperature [10,11]. This study, published by Fisher et al., 2017 [12], assesses the behavior of LOLA reflectance as a function of Diviner derived maximum temperature, with the goal of determining if the lunar poles exhibit reflectance increases associated with maximum temperature thresholds (~110K) consistent with the presence of surface water frost.

Methods: Data used in this study includes recalibrated 1.064 μm LOLA derived normal albedo [9,13], and the Diviner derived maximum temperature experienced by each of the LOLA reflectance measurements' locations over the course of the LRO mission [14]. Supporting data includes surface slope (computed with Generic Mapping Tools' grdgradient program [15]) and illumination conditions (calculated using the numerical modeling tools of [16]). Data were spatially resampled to 500×500 m resolution to prevent biases introduced by increased sampling density at the poles.

Analysis. Study data were constrained to latitudes at or within 20° of each pole. The LOLA reflectance data set is affected by instrument challenges over cold surfaces [8], therefore comparisons among terrains were conducted statistically. We analyzed the average of albedo plotted as a function of maximum temperature, to visualize the relationship between 1.064 μm reflectance and maximum surface temperature. The Moon's reflectance is correlated with slope [8], due to mass wasting removing darkened space weathered material from steep slopes. To prevent this effect from biasing our analysis, we separated the data into low-slope (<10 degrees: little mass wasting), and high-slope (>20 degrees: strong control on reflectance by mass wasting) sets, and analyzed them separately. We also compared the reflectance distribution of PSRs (defined as 0% average incident solar flux) with maximum surface temperatures too warm to support stable surface water frost (>125K), with the reflectance distribution of PSR terrain cold enough to support surface water frost over geologic timescales (<~110K), to see if surfaces with the ability to retain frost are brighter than ice-free PSRs.

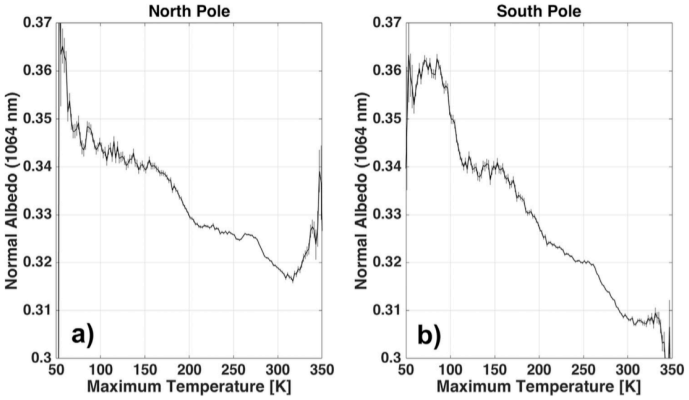

Fig.1. Average reflectance plotted as functions of maximum temperature for the **(a)** North and **(b)** South poles. Maximum temperature bin width = 1 K. Average reflectance curves are plotted with 2σ standard error of the mean [12].

Results: Fig.1 shows reflectance as a function of maximum temperature for the North (Fig.1a) and South (Fig.1b). In both polar regions, average reflectance generally increases with decreasing maximum temperature, and we observe breaks in trend at ~200K and ~300K (Fig,1a, 1b). At ~110K, South polar reflectance abruptly increases (Fig. 1b), accompanied by an upward shift (brightening) of the entire reflectance distribution [12]. High reflectance outliers such as Shackleton crater contribute little to this observed rise in reflectance [12]. No such abrupt increase occurs in the North polar region within that temperature range (Fig. 1a). Low-slope South-polar surfaces free of mass wasting bias also display an abrupt increase in average reflectance below ~110K, nearly identical to the ~110K reflectance peak observed in slope unconstrained data [12]. We also find the temperature-reflectance behavior of polar terrain varies significantly with proximity to the pole [12]. Within 5° of the South Pole, the reflectance of surfaces rapidly increases below maximum temperatures of 110 K; this 110 K feature is not observed at lower polar latitudes in the South polar region and is not observed at any latitude in the North polar region [12].

Discussion: The rapid reflectance increase observed at <110K maximum temperatures in the immediate South-polar region (−85°−90°) is consistent with the presence of surface water ice [Fig.1b;12]. This behavior mirrors observations made by [17], who showed that the ratio of UV wavelengths

Fig. 2.

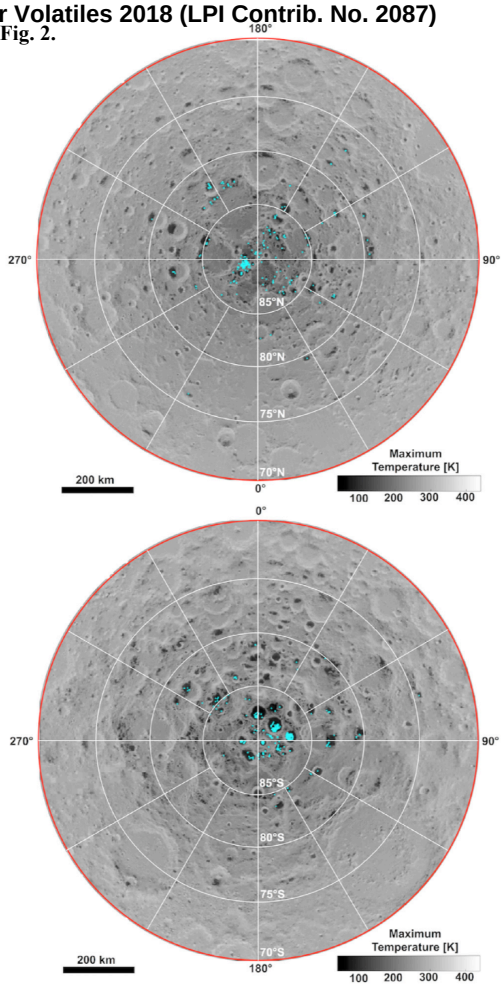

within and adjacent to a water absorption feature, abruptly increases at maximum temperatures ~110K in the South pole, indicating the presence of surface water ice [12]. The North polar region does not show this behavior, nor do South polar surfaces at latitudes more than 5° from the pole. Reflectance-temperature behavior observed within South-polar PSRs is also consistent with the presence of surface water ice; PSRs surfaces capable of maintaining stable surface water frost typically show substantially higher reflectance than those incapable of sustaining stable surface water frost [12]. This difference is not noted in the North. Statistical modeling where reflective ice was randomly added to the South-polar high-temperature PSR reflectance distribution (an ice free surface), shows that 'ice-brightened' material heterogeneously distributed (some ice-free pixels) on a sub-pixel scale best reproduces the reflectance distribution of cold PSRs [12]. This agrees with findings of [17] which suggest that up to 10% of the surface they observe may host surface ice on a 250 m (sub-pixel) scale, and that the distribution of this ice within low-temperature areas is highly heterogeneous. We attribute the general trend of increasing reflectance with decreasing maximum temperature in the North and South to a temperature or illumination-dependent space weathering effect [e.g. 18, 19]. The pattern of 'trend breaks', superimposed on this general trend, which initiate at ~200K and ~300K in the North and South, is reminiscent of reflectance behavior near ~110K attributed to surface water frost (Fig. 1a, 1b); such features may result from deposition of additional volatile species. Candidate species with stability thresholds near ~200K include aromatic hydrocarbons, linear amides, carboxylic acids, and elemental sulfur [3]. Volatile species with stability thresholds near ~300K include complex polycyclic aromatic hydrocarbons such as coronene [20].

We identified areas that are so reflective that they are unlikely to be members of the background variation in reflectance due to ordinary lunar geologic processes. Assuming that the correlation between reflectance and temperature in areas with maximum temperatures greater than 125K is unrelated to processes involving surface water frost, we fit the reflectance-temperature data of ice free (>125K) areas at each pole with a linear trend, and remove that trend from the entire reflectance distribution of each pole. We then computed the statistics of the reflectance distribution of polar areas with maximum temperatures too warm to support the presence of surface ice (125-175K). Areas with maximum temperatures <110K that were 2-sigma more reflective than the mean reflectance of the ice-free distribution at each pole, and with surface slopes <10°, are mapped as potentially hosting surface water frost (Fig. 2);

Conclusions: We find that the reflectance of the lunar surface within 5° of latitude of the South Pole increases rapidly with decreasing temperature near ~110 K, behavior consistent with the presence of surface water ice. This distinction is not observed at the North Pole. The North polar region does not show this behavior, nor do South polar surfaces at latitudes >5° from the pole. South polar regions of permanent shadow show anomalous reflectance when their annual maximum surface temperatures are low enough to preserve water ice, also consistent with surface water frost. We note additional increases in reflectance with decreasing temperature at ~200K and ~300K, which may indicate the presence of additional volatile species. We identified and mapped surfaces with reflectances so high as to be unlikely to be part of an ice-free population (Fig. 2), and in the South we find a similar distribution to that found by [17] based on UV properties. Finally, unlike the North pole of Mercury, where all surfaces below about 100K exhibit reflectance anomalies [5], on the Moon not all surfaces cold enough to host surface ice show increased reflectance. This imperfect correlation between volatile signatures and temperature at the lunar poles stands in contrast with Mercury, where temperature accurately predicts ice distribution. Why this difference exists remains an important question in lunar science.

References: [1]Watson K. et al.(1961)J. Geophys.Res. 66, 3033–3045[2]Schorghofer,N.&Taylor,G.(2007)J. Geophys.Res. 112 (E2), E02010. [3]Zhang, J.A. & Paige, D.A.(2009, 2010 corr.)Geophys. Res.Lett. 36(16). [4]Paige, D.A. et al.(2013)Science 339 (6117), 300–303.[5]Neumann,G.A. et al.(2013)Science 339 (6117), 296–300.[6]Smith,D.E. et al.(2010)Space Sci.Rev.150 (1), 209–241.[7]Zuber,M.T. et al.(2012)Nature 486 (7403), 378–381.[8]Lucey, P.G. et al.(2014)J.Geophys.Res.Planets 119(7), 1665–1679.[9]Lemelin,M. et al.(2016)Icarus 273, 315–328.[10]Paige,D. et al.(2010a)Science 330(6003), 479–482.[11]Paige,D. et al.(2010b)Space Sci. Rev. 150(1-4), 125–160.[12]Fisher,E.A. et al.(2017)Icarus 292: 74-85.[13]Smith, D.(2015)LRO-L-LOLA-3-RADR-V1.0, NASA PDS .[14]Williams, J-P. et al.(2017)Icarus 283: 300-325.[15]Wessel,P. & Smith,W.(1991)EOS Trans. AGU 72, 441.[16]Mazarico,E. et al.(2011)Icarus 211(2), 1066–1081.[17]Hayne,P. et al.(2015)Icarus 255, 58–69.[18]Hemingway, D. et al.(2015)Icarus 261, 66–79.[19]Corley,L. et al.(2016)Lunar Planet.Sci.Conf.,XLVII abs. no. 2692.[20]Chickos, J.S. et al.(2002)J. Chem.Thermodyn. 34(8), 1195–1206.

THE EFFECT OF TOPOGRAPHY ON THE TRANSPORT OF VOLATILES AT THE LUNAR POLES: APPLICATION TO NEON. C. Grava[1*], J.-Y. Chaufray[2], E. Mazarico[3], M. A. Siegler[4], and M. Benna[5], [1]Southwest Research Institute, San Antonio, TX, USA, [2]LATMOS/IPSL, Guyancourt, France, [3]NASA Goddard Space Flight Center, Greenbelt, MD, USA, [4]Planetary Science Institute, Dallas, TX, USA, [5]University of Maryland Baltimore County, Baltimore, MD, USA. [*]cesare.grava@swri.edu

Introduction: Due to the ~1.5° tilt of the Moon's rotation axis with respect to the ecliptic, there exist Permanently Shaded Regions (PSRs) at the Lunar Poles that are never illuminated by direct sunlight, particular in the interior of craters at latitudes greater than ~75°. The idea that such sites might have accumulated water and other volatiles for eons was proposed well before the first lunar missions [1]. An estimated ~10^{17} g of water could have been potentially delivered to such PSRs in the last 2 billion years [2]. Obviously, these deposits play a pivotal role in future lunar exploration.

A key factor in exploitation of resources is the spatial distribution of such volatile deposits. Several instruments onboard the Lunar Reconnaissance Orbiter (LRO) [3] have shown a marked heterogeneity of volatiles distributions with depth: there are craters (such as Shoemaker) where water-equivalent-hydrogen (WEH), measured by the Lunar Exploration Neutron Detector (LEND) [4] or the Lunar Prospector Neutron Spectrometer [5], is enhanced at depths of ~1 meter, but water frost at the top monolayer (hundreds of nm) of the surface, as measured by the Lyman-Alpha Mapping Project (LAMP) [6], is minimal [7,78]. And there are craters (such as Faustini) where LAMP-derived surface frost abundance is relatively high, but LEND-derived WEH at depth is relatively low. Moreover, there is heterogeneity in the lateral surface distribution of volatiles: not all the PSRs have extensive volatile deposits. LAMP showed that water frost is present in nearly the whole PSR at Haworth, but in very little of the Shoemaker PSR [9]. Such patchy distribution of polar volatiles has also implications for the development of the lunar surface-bounded exosphere, since such deposits are bombarded by micrometeroids, Lyman-alpha photons from the interplanetary medium, and solar wind plasma.

We investigate the role of topography in the surface distribution of polar deposits and in the structure of the lunar exosphere. We are modifying our Monte Carlo code of the lunar argon exosphere [10] to include the topography from the LRO's Lunar Orbiter Laser Altimeter (LOLA) [11] and surface temperature as a function of local time from LRO's Diviner radiometer [12]. Parameters of interest are the actual elevation and the slope. One of the hypotheses we want to test is whether volatiles ejected from a wall of a crater have a greater chance to re-impact on another wall of the same crater. This might especially hold for steep and deep polar craters such as Cabeus. In the present work we study the effect of topography on the lunar exosphere by using a non-condensable gas, neon, which is of solar wind origin. Neon density was measured by LADEE's Neutral Mass Spectrometer [13,14] and is used here to constrain the model. Future model runs will use a condensable gas, argon, to study the effect of topography on the surface distribution of lunar volatiles.

References: [1] Watson K. et al. (1961) *J. of Geophys. Res., 66*, 3033-3045, 1961. [2] Arnold J. R. (1979) *J. of Geophys. Res., 84*, 5659-5668. [3] Chin G. et al. (2007) *Sp. Sci Rev., 129(4)*, 391-419. [4] Mitrofanov I. G. et al. (2010) *Sp. Sci Rev., 150*, 183-207. [5] Feldman W. C. et al. (1998) *Science, 281 (5382)*, 1496. [6] Gladstone G. R. et al. (2010) *Sp. Sci. Rev., 150*, 161-181. [7] Sanin A. B. (2017) *Icarus, 283*, 20-30. [8] Hayne, P. O. et al. (2015) *Icarus, 255*, 58-69. [9] Gladstone G. R. et al. (2012) *J. of Geophys. Res., 117*, E00H04. [10] Grava C. et al. (2015) *Icarus, 255*, 135-147. [11] Smith D. E. et al. (2010) *Sp. Sci. Rev., 150*, 209-241. [12] Paige D. A. et al. (2010) *Sp. Sci. Rev., 150*, 125-160. [13] Mahaffy, P. R. et al. (2014) *Sp. Sci Rev., 185*, 27-61. [14] Benna M. et al. (2015), *Geophys. Res. Letters, 42 (10)*, 3723-3729.

POLAR VOLATILES EXPLORATION IN PEARY CRATER ENABLED BY NASA'S KILOPOWER PROJECT. J. E. Gruener[1], D. B. Bussey[2], S. J. Lawrence[1], and L. S. Mason[3],[1]NASA Johnson Space Center (2101 E. NASA Parkway, Houston, TX, 77058) for first author, [2]NASA Headquarters (300 E. St SW, Washington, DC, 20546), [3]NASA Glenn Research Center (21000 Brookpark Rd, Cleveland, OH, 44135).

Introduction: For more than 50 years, scientists have discussed the possibility of the existence of water ice and other frozen volatiles at the lunar poles [1]. However, it was not until the 1990s when the polar orbiting spacecraft Clementine and Lunar Prospector collected data supporting these hypotheses [2]. Subsequent missions, including the Lunar Reconnaissance Orbiter (LRO) mission [3], and the Lunar Crater Observation and Sensing Satellite (LCROSS) mission [4], provided further evidence that supports the existence of water ice deposits at the lunar poles.

During NASA's Constellation Program, several areas at both lunar poles polar were included in 50 Regions of Interest (ROI) for intensive study by the Lunar Reconnaissance Orbiter Camera (LROC) [5]. These polar ROI focused on peaks and craters rims that received high amounts of solar illumination, assuming initial missions back to the lunar surface would utilize solar arrays to generate electricity.

Recently, the successful demonstration of NASA's Kilopower Project at the National Nuclear Security Administration (NNSA) Nevada National Security Site makes it possible to consider lunar polar missions at locations other than highly illuminated regions. The Kilopower Project was initiated in 2015 to demonstrate subsystem-level technology readiness of a small space fission power system [6]. This abstract describes the science objectives and operations for a mission concept developed at NASA Glenn Research Center's COMPASS Concurrent Engineering Team for a 1-year exploration of Peary Crater focused on prospecting for lunar polar volatiles.

Peary Crater: Peary Crater (diameter 73 km), located near the lunar north pole, has high potential for containing lunar polar volatiles on its crater floor. While parts of the crater floor receive up to 45-60 % illumination during a lunar day in summer [7], smaller craters within Peary remain permanently shadowed [8]. It is these permanently shadowed regions (PSRs) that are of interest for lunar volatiles prospecting, with a proposed landing site of approximately 88.3° N, 36° E (figure 1).

Science Objectives: Based on NASA's Strategic Knowledge Gaps (SKGs) for lunar polar regions [9], and the Lunar Exploration Analysis Group (LEAG) Lunar Exploration Roadmap and recent specific action team reports [10], the primary science objectives for this mission concept are: determine the form and species of the volatile compounds within Peary Crater; determine the lateral and vertical distribution and concentration of the volatile deposits; determine the volatile flux in the near-surface exosphere; and determine any secondary alteration mineralogy of the local regolith. Most of these objectives could be met by a robotic rover with science instruments, subsurface drill, and mobility capabilities similar to NASA's Resource Prospector Advanced Exploration Systems (AES) Project [11]. Understanding the volatile flux could be accomplished at a stationary science station near the lander.

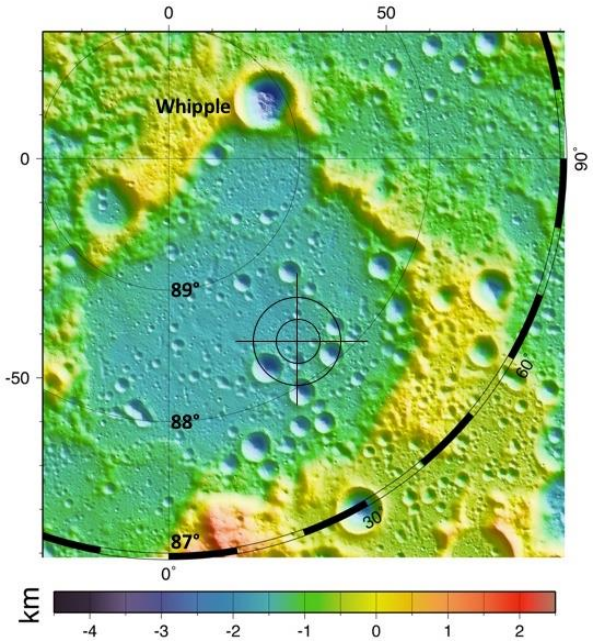

Figure 1 Lunar Orbiter Laser Altimeter (LOLA) topographic map of Peary Crater. Landing site, with inner ring radius of 5 km and outer ring radius of 10 km. From https://lola.gsfc.nasa.gov/feature20110228.html.

Because of the long-lived nature of the Kilopower fission power system, additional primary science objectives based on the National Research Council (NRC) Planetary Science Decadal Survey [12], include the geophysical investigations of seismometry, heat flow, and surface magnetization. These measurements would be made at a stationary science station near the lander.

Science Operations: To address the science objectives, the mission concept involves a long-distance mobile robotic explorer/prospector, and a tethered science station that is deployed 30-m from the lander and connected to the 1-kW Kilopower system that remains on the lander. Once deployed, the fixed science station would include a long-lived geophysical station, volatile flux instrument(s) and an additional communications node located at a distance sufficient to mitigate the radiation environment of the Kilopower system. The mobile robotic rover would explore out to a radius of 5-10 km from the lander, allowing for the assessment of several PSRs and the prospecting for water ice and other volatiles (figure 2). The mobile rover can recharge itself during sunlit conditions using an on-board solar array. During the night, the mobile rover returns to the tethered science station for night power via an inductive charging node. The Kilopower charging station also allows the potential for the mobile rover to perform shorter-duration battery-powered night excursions. A laser-based power beaming technology demonstration is planned, hosted on the tethered service station, that would permit remote charging of the mobile rover within line-of-sight.

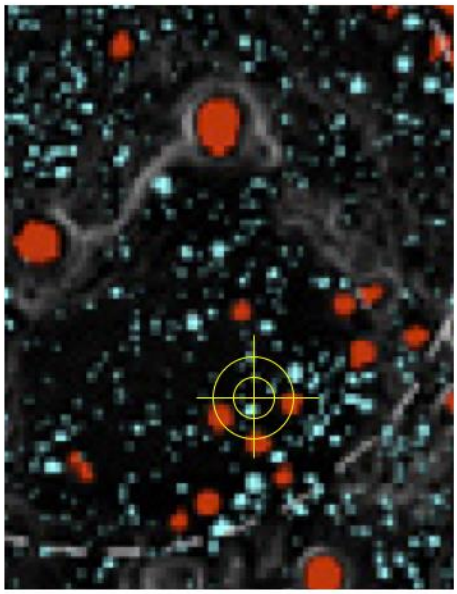

Figure 2 Permanently shadowed regions (PSRs) in Peary Crater. Larger PSRs are shown in red, while smaller PSRs are shown in cyan. Landing site, with inner ring radius of 5 km and outer ring radius of 10 km. From Mazarico et al. (2011).

References:

[1] Watson K. et al. (1961) *JGR*, 66, 1598-1600. [2] Feldmann W. C. et al. (2001) *JGR*, 106, 23231-23525. [3] Sanin A. B. et al. (2017) *Icarus*, 283, 20-30. [4] Colaprete A. et al. (2010) *Science*, 330, 463-467. [5] Gruener J. E. and Joosten B. K. (2009) Lunar Reconnaissance Orbiter Science Targeting Meeting, Abstract #6036. [6] Palac D. T. et al. (2018) ANS NETS 2018, Nuclear and Emerging technologies for Space. [7] Bussey D. B. et al. (2005) Nature, 434, 842. [8] Mazarico E. et al. (2011) *Icarus*, *211*, 1066-1081. [9] https://www.nasa.gov/exploration/library/skg.html. [10] https://www.lpi.usra.edu/leag/ [11] Andrews D. et al. (2014) AIAA SPACE Forum. [12] National Research Council (2011) National Academies Press.

LUNAR POLAR VOLATILES: CURRENT UNDERSTANDING, RECENT DISCOVERIES, AND FUTURE EXPLORATION. P. O. Hayne[1], [1]University of Colorado Boulder (Astrophysical & Planetary Sciences Department and Laboratory for Atmospheric & Space Physics; Paul.Hayne@Colorado.edu).

Introduction: Volatiles are fundamental tracers of a planetary body's origin, evolution, and interaction with its space environment. Water is especially important, because of its myriad effects on the planet's geophysical and geochemical evolution, its relevance to life and habitability, and its potential as a resource for future space exploration. The observed abundance and chemical inventory of condensed volatiles may also reveal a history of dynamical exchange among different regions of the Solar System.

Near the poles of the Moon, large areas of perennial (or "permanent") shadow create cold traps, where volatiles would be thermally stable for billions of years. Permanently shadowed regions (PSRs) may therefore hold a record of volatile delivery, transport, sequestration, and loss through geologic time. Here, I summarize the current state of knowledge of volatiles at the Moon's poles, highlighting some recent discoveries and unresolved questions. I also suggest some possible directions for addressing these questions through further exploration, measurement, and modeling.

Background: Early theoretical work recognized the likely existence of PSRs at the Moon's poles, their low temperatures, and potential for cold-trapping water and other volatiles [1,2]. Atoms and molecules in the extremely tenuous lunar atmosphere rarely encounter one another [3], and "hop" on ballistic trajectories from surface to surface, until they are photolyzed, escape the Moon's gravity, or become cold-trapped.

Prior to direct observation, models predicted PSRs with temperatures < 100 K covering ~0.5% of the lunar surface, where water would be stable on Gyr timescales [4]. Potential sources of volatiles on the Moon include:

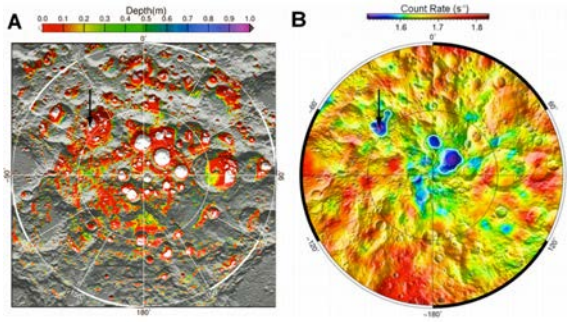

Figure 1: (A) Expected distribution of surface and ground ice in the lunar south polar region based on Diviner measurements [17], compared to (B) the hydrogen abundance inferred from epithermal neutron measurements [19]. The LCROSS impact site is indicated by the arrow.

(1) comet and asteroid impacts, (2) solar wind protons, and (3) outgassing from the lunar interior. Although uncertain, these combined sources could supply enough hydrogen to support ~1-10% H_2O by mass in the upper few meters of regolith in the PSRs. However, if destruction by solar wind sputtering and UV photolysis outpace the supply and/or burial rate, ice may be prevented from accumulating [5]. Due to their very distinct compositions, a chemical inventory of lunar polar volatiles should reveal which of the above sources is dominant.

Data on Lunar Volatiles: In the modern era of spacecraft remote sensing, polar volatiles have become a high-priority target for lunar science and exploration [6]. The Clementine orbiter provided a new view of the polar regions, including the PSRs, and also provided a tantalizing radar signal consistent with cold-trapped ice at the south pole [7]. Shortly thereafter, NASA's Lunar Prospector mission used neutron spectroscopy to measure hydrogen with average concentrations [H] = 1700 ±900 ppm over the region >70° latitude at both poles, corresponding to ~1% H_2O by mass if the hydrogen is in the form of water [8].

Renewed Interest in Water on the Moon. Three separate spacecraft provided detections of water and/or hydroxyl (OH) on the lunar day side using near-IR spectroscopy [9,10,11]. Though its abundance is uncertain, latitudinal trends indicate higher H_2O/OH concentrations in the polar regions. Diurnal variations in the strength of the H_2O/OH absorption feature at 2.8-3.0 μm could indicate a cycle of molecular adsorption and desorption [11], providing a potential source of water to the polar cold traps. However, it remains challenging to quantify these variations and to reconcile them with the low abundances of water and OH ions in the lunar exosphere [12].

LCROSS. The Lunar CRater Observation and Sensing Satellite (LCROSS) mission provided the first direct detections of volatiles at the poles of the Moon [13], through the controlled impact excavation and heating of materials in the south polar PSR within Cabeus crater [14,15]. Spectroscopic measurements from this experiment revealed 5-7 wt% of H_2O, among a comet-like array of volatiles, including (abundance relative to H_2O in parentheses): H_2S (16.8%), NH_3 (6.0%), SO_2 (3.2%), C_2H_4 (3.1%), CO_2 (2.2%), CH_3OH (1.6%), CH_4 (0.7%), OH (0.03%). Additionally, observations of the LCROSS impact plume by the Lunar Reconnaissance Orbiter's (LRO) LAMP instrument [16] revealed molecular H_2 originating in the lunar regolith of the cold, shadowed impact site.

Recent Discoveries. LRO has provided a wealth of new data on the Moon's polar regions, including further evidence for condensed volatiles. Temperature is the controlling factor for volatile stability, and LRO's Diviner instrument has mapped temperatures at ~250-m scale over both polar regions covering the complete diurnal and seasonal variations [17,18]. Epithermal neutron fluxes measured by the LEND instrument show that some, but not all PSRs contain enhanced [H] indicative of condensed water [19]. Spectroscopic and albedo measurements from the LAMP and LOLA instruments show surface reflectance properties consistent with water frost at concentrations ranging from ~0.1 up to ~10 wt% in the south polar PSRs, with a patchy distribution indicating similar source/concentration and loss/diffusion timescales [20,21]. However, the distribution of apparent water frost at the surface does not match the [H] distribution in the uppermost ~1 m determined from neutron spectroscopy. In fact, the patterns of [H] and surface frost do not follow temperature (Fig. 1), as would be expected for a supply-dominated system in equilibrium.

Modeling. Recent modeling efforts have made substantial progress towards understanding the behavior of volatiles on the Moon and other airless bodies. Direct Monte-Carlo simulations of ballistic transport and sequestration of water in the PSRs show that detectable asymmetries may exist in the distribution of water and other volatiles in the exosphere and on the surface [22,23]. Models have also made progress in understanding the sources of lunar volatiles, including the solar wind, micrometeoroids, and larger impacts by comets and asteroids [24,25]. Reorientation of the Moon's spin axis may have altered the distribution of cold traps, with a potentially detectable signature in deeply buried ice deposits [26].

Outstanding Questions and Future Opportunities: Despite recent and ongoing progress in understanding lunar volatiles, many questions remain, including: 1) What are the concentrations of lunar volatiles at the poles, especially water? 2) What are the forms of lunar water? 3) Are the cometary volatile abundances at the LCROSS impact site representative of most PSRs? 4) Why is the apparent distribution of volatiles patchy and inconsistent among different datasets (contrasting with the more coherent distribution observed on Mercury)?

Future investigations will address the above questions through remote sensing and *in situ* measurements in the polar regions. New and innovative approaches are already advancing. For example, bistatic radar measurements of PSRs using the LRO spacecraft's Mini-RF instrument as a receiver have shown near-subsurface backscattering consistent with coherent water ice particles larger than ~1 cm [27]. Pixon reconstruction methods have shown promise for improving spatial resolution and localization of [H] maps from neutron spectroscopy [28]. Scattered sunlight in the PSRs may provide sufficient signal to detect volatiles spectroscopically [29], or failing that, an active illumination approach may be used [30]. It is increasingly clear, however, that order to confidently interpret the remote sensing data and map the distribution and abundance of lunar polar volatiles, ground truth must be obtained by landed missions or rovers.

References: [1] Urey, H. C. (1952), *The Planets, Their Origin and Development*, pp. 17-18. [2] Watson, K., Murray, B. C., & Brown, H. (1961), *JGR*, *66*(9), 3033-3045. [3] Öpik, E. J., and Singer, S. F. (1960), *JGR*, *65*, 3065-3070. [4] Arnold, J. R. (1979), *JGR*, *84*, 5659-5668. [5] Morgan, T. H., & Shemansky, D. E. (1991), *JGR*, *96*, 1351-1367. [6] National Research Council, *Vision and Voyages for Planetary Science in the Decade 2013-2022*. [7] Nozette, S., et al. (1996) Science, 274. [8] Feldman, W. C. (2001), *JGR*, *106*, 23231-23251. [9] Pieters, C. M., et al. (2009), *Science, 326*(5952), 568-572. [10] Clark, R. N. (2009), *Science, 326*(5952), 562-564. [11] Sunshine, J. M., et al. (2009) *Science, 326*(5952), 565-568. [12] Stern, S. A. (1999), *Rev. Geophys.*, *47*, 453. [13] Colaprete, A., et al. (2009), *Science, 330*(6003), 463-468. [14] Schultz, P. H., et al. (2009), *Science, 330*(6003), 468-472. [15] Hayne, P. O., et al. (2009), *Science, 330*(6003), 477-479. [16] Gladstone, G. R., et al. (2009), *330*(6003), 472-476. [17] Paige, D. A., et al. (2009) *Science, 330*(6003), 479-482. [18] Williams, J.-P., et al. (2017), *Icarus*, 283, 300-325. [19] Sanin, A. B., et al. (2017), *Icarus, 283*, 20-30. [20] Hayne, P. O., et al. (2015), *Icarus, 255*, 58-69. [21] Fisher, E. A., et al. (2017), *Icarus, 292*, 74-85. [22] Moores, J. E. (2016), *JGR*, *121*(1), 46-60. [23] Schörghofer, N., et al. (2017), *Icarus, 298*, 111-116. [24] Hurley, D. M., et al. (2017), *Icarus, 283*, 31-37. [25] Prem, P., et al. (2015), *Icarus, 255*, 148-158. [26] Siegler, M. A., et al. (2016), *Nature*, *531*(7595), 480-484. [27] Patterson, G. W., et al. (2017), *Icarus, 283*, 2-19. [28] Teodoro, L. F. A. (2014), *JGR*, *119*(3), 574-593. [29] Li, S., et al. (2017), *LPSC*, 48. [30] Cohen, B. A., et al. (2015), *LEAG Ann. Mtg.*, 1863, p. 2008.

Acknowledgment: This work was supported by the Lunar Reconnaissance Orbiter Project, and the Solar System Exploration Virtual Institute (SSERVI). The author is a member of SSERVI's Volatiles, Regolith and Thermal Investigations Consortium for Exploration and Science (VORTICES) team, led by the Johns Hopkins University's Applied Physics Laboratory.

A REVIEW OF DIURNALLY-VARYING LUNAR HYDRATION SIGNATURES. Amanda R. Hendrix[1], [1]Planetary Science Institute, Tucson, AZ; arh@psi.edu.

Introduction & Background: Since the initial detections of surficial non-polar lunar hydration [1, 2, 3, 4], several sets of observations indicate a diurnally-varying nature to the hydration. In this review, I summarize what is currently understood about these results and their implications for the lunar water cycle.

Several datasets in the last 1-2 decades point to water and hydrated species on the Moon. Galileo Solid State Imager (SSI) broad band spectra [1, 5] first suggested the presence of water-bearing minerals (indicated by the presence of the broad 0.7 μm charge transfer band in oxidized iron) near the lunar South Pole. The Moon Mineralogy Mapper (M3) on Chandrayaan-1 [2] measured the spectral signatures of adsorbed water (near 3 μm) and hydroxyl (near 2.8 μm), finding them to be strongest at high latitudes and at several fresh craters. Initially, thermal emission precluded the detection of OH/H_2O at low latitudes; a re-processing of the M3 data [6] showed that the water-related absorptions appear also at lower latitudes and may vary with time of day [7]. The M3 detections were verified using Cassini Visual and Infrared Mapping Spectrometer (VIMS) data [4] and Deep Impact data [3], which showed the OH and H_2O absorptions to vary with temperature (related to time of day).

A likely scenario for the production of surficial lunar hydration [e.g. 16, 17, 5] is that solar wind protons interact with the lunar regolith, reacting with iron oxide (FeO) to form H_2O and/or OH. Studies with lunar samples [e.g. 18] indicate that activation energy of lunar regolith grain sites is important in allowing the adsorption of OH, and the activation energy may be related to the amount of weathering experienced by the surface.

Since these initial results, newer analyses have been performed, though a consensus on extent of diurnal effect, as well as hydration abundance, type and depth has yet to be reached.

More Recent Analyses: *Moon Mineralogy Mapper (M3):* The M3 data have been further studied, applying new versions of thermal corrections, with varying results regarding diurnal effects. OH and H_2O abundances have been shown to increase with latitude [8], with water abundance varying by ~200 ppm over a lunar day. In contrast, use of a different thermal correction [9] results in the indication of widespread OH/H_2O across the surface with no diurnal effect.

Lunar Reconnaissance Orbiter (LRO) Lyman Alpha Mapping Project (LAMP): Besides the OH/H_2O features near 3 μm, the far-ultraviolet (FUV) hosts a strong H_2O absorption edge near 165 nm, which could be observed at the Moon if H_2O (and possibly OH) were mixed with (or perhaps bound to) lunar regolith grains [10], in the top layer of the regolith, due to the shallow sensing depths of the FUV. Observing in the 165 nm region, LRO LAMP data have been reported to indicate a diurnally-varying effect [10, 11]; this remains under investigation.

LRO Lunar Exploration Neutron Detector (LEND): The LEND instrument measures epithermal neutrons and has detected suppressions associated with permanently shadowed regions near the South Pole, indicating elevated hydrogenation in the regolith down to ~50 cm and below. Such suppressions have also been observed, consistent with the presence of diurnally varying hydrogen in the regolith near the equator [19]; the signature could also be related to variations in regolith temperature.

LRO Cosmic Ray Telescope for the Effects of Radiation (CRaTER): CRaTER data have been used to relate the yield of energetic proton radiation ("albedo") coming from the lunar regolith due to bombardment by galactic cosmic rays (GCRs) to hydrogenation of the lunar regolith. Initial studies [12] indicate increased amounts of hydrogenation (in the upper 1-10 cm of the regolith) at high latitudes. More recent work [13] may indicate a diurnal component to the signature, by observing toward the horizon as compared with the nadir direction. A potential enhancement in proton albedo is seen toward the morning terminator as compared with the evening terminator, consistent with models [14].

Transport to the Polar Regions: The diurnally-varying signatures discussed above occur largely at lower latitudes – but the apparent movement of the OH/H_2O (through the regolith and/or through the exosphere [15]) allows for hydrating species to eventually wind up in the polar regions where they are more stable due to the lower temperatures.

References: [1] Vilas, F., D. L. Domingue, E. A. Jensen, L. A. McFadden, C. R. Coombs, and W. W. Mendell (1999), *Proc. Lunar Planet. Sci. Conf., 30th*, 1343. [2] Pieters, C. M., L. A. Taylor, S. K. Noble, L. P. Keller, B. Hapke, R. V. Morris, C. C. Allen, D. S. McKay, and S. Wentworth (2000), *Meteorit. Planet. Sci., 35,* 1101–1107. [3] Sunshine, J. M., T. L. Farnham, L. M. Feaga, O. Groussin, F. Merlin, R. E. Milliken, and M. F. A'Hearn (2009), *Science, 326*, 565–568. [4] Clark, R. N. (2009), *Science, 326*, 562–564. [5] Vilas, F., E. A. Jensen, D. L. Domingue, L. A. McFadden, C. J. Runyon, and W. W. Mendell (2008), *Earth Planets Space, 60,* 67–74. [6] Clark, R. N., et al. (2010), Proc. Lunar Planet. Sci. Conf., 41st, 2302. [7] McCord, T. B., L. A. Taylor, J.-P. Combe, G. Kramer, C. M. Pieters, J. M. Sunshine, and R. N. Clark (2011),

J. Geophys. Res., 116, E00G05 [8] Li, S. & R. Milliken (2017) *Sci. Adv., 3*: e1701471 [9] Bandfield, J. et al. (2018) *Nat. Geosci.* [10] Hendrix, A. R. et al. (2012) *JGR, 117,* E12001 [11] Hendrix, A. R., D. M. Hurley, W. M. Farrell, K. D. Retherford, T. K. Greathouse, K. E. Mandt, G. R. Gladstone D. E. Kaufman , F. Vilas (2017) *LPSC, XLVIII*. **[12]** Schwadron, N. et al. (2016) *Icarus, 273*, p. 25-35 **[13]** Schwadron, N., J. K. Wilson, A. Jordan, M. D. Looper, C. J. Zeitlin, L. Townsend, H. E. Spence, W. M. Farrell, N. E. Petro, T. J. Stubbs, C. M. Pieters (2017) *American Geophysical Union, Fall Meeting, abstract #P41A-2828*. [14] Schorghofer, N. (2014) *Geophys. Res. Lett., 41,* 4888–4893 [15] Hurley, D. M. et al. (2018) *this meeting.* [16] Housley, R. M., R. W. Grant, and N. E. Paton (1973), *Proc. Lunar Sci. Conf., 4th*, 2737–2749. [17] Housley, R. M., E. H. Cirlin, N. E. Paton, and I. B. Goldberg (1974), *Proc. Lunar Sci. Conf., 5th*, 2623–2642. [18] Poston, M. J. G. A. Grieves, A. B. Alexandrov, C. A. Hibbitts, M. Darby Dyar and T. M. Orlando (2015). *Icarus.* Doi. 10.1016/j.icarus.2014.09.049. [19] Livengood, T. et al. (2015) *Icarus 255*, 100–115.

Volatile retention in and near lunar PSRs through molecular adsorption. C. A. Hibbitts, Johns Hopkins University Applied Physics Laboratory, Laurel, Md., 20723; karl.hibbitts@jhuapl.edu.

Background: Volatiles including H_2O exist in at least some Permanent Shadowed Regions (PSRs) on the Moon as shown through the spectral analyses of surface material ejected into sunlight through the LCROSS impactor experiment[1,2]. Surficial water ice has also now been proven to exist in some PSRs through the analyses of IR reflectance spectroscopy leveraging reflected Earth-shine [3]. Additionally, molecular water, probably adsorbed in lieu of ice, has been tentatively identified in cool polar but sun illuminated terrain through space-based IR spectroscopy [4]. On this and warmer solar illuminated lunar terrain, a ubiquitous infrared absorption feature points to hydroxyl resulting from the interaction of implanted solar wind protons with the silicate oxygen ions [5,6,7]; an absorption feature that varies with time of day, trends with latitude, and which may also have a compositional dependence [e.g. 8]. The temporal, or diurnal, variation in its IR signature may be indicative of a cycle of periodic loss through various channels including H, H_2, and/or H_2O and subsequent rejuvenation [e.g. 9, 10]; a potential continual source of molecular water for trapping in cold terrains.

Discussion: Adsorption onto a refractory substrate such as lunar grains can enable molecular water to exist on surfaces under vacuum and at temperatures higher than that at which ice would sublime. The same principle holds for other volatile molecules also discovered on the Moon or hypothesize to have been delivered to the Moon via cometary accretion such as carbon dioxide, methanol, formaldehyde as some of the more abundant cometary volatiles [11]. Even weak electronic attraction between a volatile molecule and grain can serve to greatly increase its thermal stability. A modest increase in activation energy for desorption, such as has been measured in the laboratory for some lunar samples and analogs while insufficient to significantly increase the residence time on a single grain [12], would potentially greatly lengthen the migration time of a water molecule within the upper regolith [13] and Figure 1.

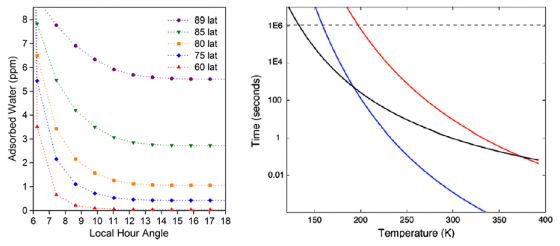

Figure 1. Thermal stability of H_2O on a single grain is extremely short, even at high latitudes leading to very low abundances if only a single grain is considered (left; [12]). However, the effective stability (time it takes for a water molecule to migrate through the approximate optical depth of 3-micron illumination over a lunation) is exponentially increased because of the multiple hops that must occur (right [13]) .

The role of surface area and defects on adsorption: Surface area, both grain size and internal pore space, greatly affect how many molecules may adsorb (e.g.14). Clays can have surface areas that exceed 100m^2/g because of their complex structures, while nominally anhydrous minerals, and specifically lunar soils, have a large but more modest values of 1 to a few m^2/gram. Because of the grains' small size and very complex surface morphology the surface area of lunar soils are sufficiently large that only a monolayer of H_2O can represent a concentration on the order of a part per thousand by mass [14].

The attractiveness of surface for adsorption sites is affected by the local charge environment. And here, the tortured history of the lunar surface makes the grains exceptionally attractive to water and other molecules. Molecular lattice disruptions, atomic sputtering, and grain fracturing due to micrometeorite bombardment creates local charge defects that are high reactive; likely accounting for the gunpowder-like smell ascribed to the dust by Apollo astronauts [e.g. 15] and suggesting a very reactive surface prime for adsorption of water or other molecules. Because of the lunar grain's reactive potential, neutral water that happens to contact the surface is expected to adsorb and disassociate to hydroxyl and subsequently be stable under lunar thermal conditions with the desorption of molecular water on the Moon probably driven by non-thermal processes except at high latitudes [16]. At these cooler, higher latitudes, significant adsorbed H_2O may exist thermally stable. Similarly, other cometary volatiles, such as CO_2, which is a linear molecule with no dipole moment and only a weak quadrupole moment, while more volatile, should be expected to exist adsorbed onto refractory surfaces at temperatures above that which their ices would not be thermally stable. CO_2 is shown to adsorb onto carbonaceous chondritic material under vacuum at the cryogenic temperature of ~ 150K, warmer than the sublimation temperature for its ice ~ 80K [17]. This affinity is scribed largely to the presence of iron-bearing fine grained clay minerals with significant microporosity and local charge asymmetries. Thus, adsorbed cometary

volatiles other than water ice may exist thermally stable in some of the warmer PSRs.

The spectral signatures of adsorbed volatiles: The presence of adsorbed molecules can potentially be determined through remote spectral observations because the physical state of the volatile affects its spectral

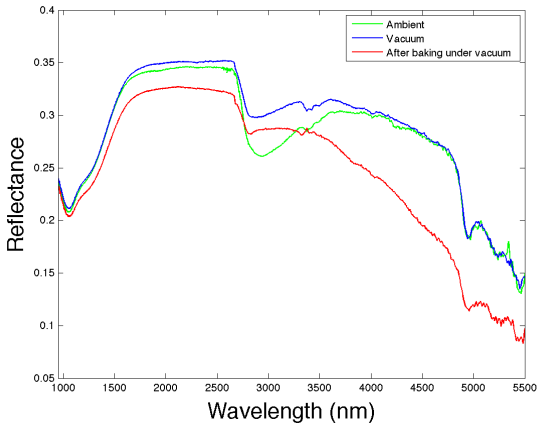

Figure 2. The ν_3 asymmetric stretch absorption band due to adsorbed H_2O is centered near 2.95 μm (2950 nm) for some nominally anhydrous minerals shifts as the sample desiccates under vacuum and water-mineral bonding becomes more significant.

nature. Water has a characteristic combination of wags and bends of the H-O-H and O-H bonds that allow $H_2O_{(l,g,s)}$ to all be distinguished. A spectral signature at 2.95 μm for a sample under vacuum is indicative of adsorbed H_2O or other form of molecular H_2O. Additionally, the asymmetric stretch vibration of H_2O near 2.95 μm can shift few nm depending on the local charge environment, such as bonding to different elements or other water molecules (Figure 2). Additional measurement at ~ 6 μm would be confirmation of the 2.95-μm identification of water. The 6-μm ν_2 vibration is present only in H_2O and there is no nearby similar absorption by OH, as is the case for the 3-μm region.

The physical nature of other cometary volatiles can also potentially be inferred from the infrared signatures. For instance, the position of the ν_3 vibration in CO_2 near 4.25 microns has been observed to be dependent on the precise cation composition of the material onto which it is adsorbed, whether under ambient conditions or cryogenic under vacuum [e.g. 17, 18] and Figure 3. The larger the electric fileld potential of the charge compensating cation, the shorter the wavelengths of the ν_3 absorption.

Conclusions: Water, CO_2 and possibly other volatiles should adsorb and be thermally stable at significantly higher temperatures than their ice would be.

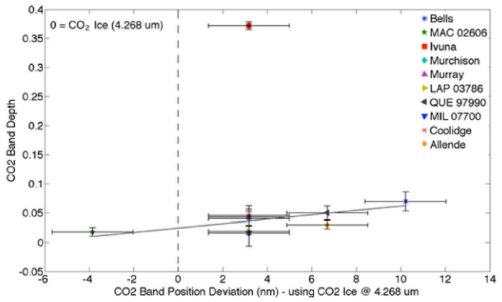

Figure 3. The spectral position of adsorbed CO_2 various by more than 10 nm between various carbonaceous meteorites at cryogenic temperatures and ~ 1e-7 torr [17]

These materials also have spectral signatures distinct from their ices enabling their detection on the surface of the Moon.

References:

[1] Colaprete et al., Science, 330, 463, 2010; [2]Schultz, P.H. et al., Science, 330, 468, 2010; [3] Li et al., 2018 (submitted); [4] Protopapa et al., NASA ESF, 2017; [5] Pieters et al., Science, 10.1126/science.1178658, 2009; [6] Sunshine et al., Science, 10.1126/science1179788, 2009; [7] Clark, R.N. Science, 10.1126/science.1178105, 2009; [8] McCord et al., JGR, 116, doi:10.1029/2010JE003711, 2011. [9] Farrell, et al., Icarus, 255, 116-126, 2015; [10] Jones et al., JGR (submitted), 2018; [11] Crovisier and Encrenaz, Comet Science, 2000; [12] Poston et al., JGR, 118, doi: 10.1029/2012JE042832013; [13] Hibbitts et al., Icarus, 213, 2011; [14] Dyar et al., Icarus, 208, 2010; [15] NASA blog, 1/30/2006; [16] Hodges, JGR, 107, E2, 2002; [17] Berlanga et al., Icarus, 280, 2016; [18] Hibbitts and Szanyi, Icarus, 191, 2007.

Acknowledgments: I would like to acknowledge the support of the JHUAPL SSERVI node, VORTICES, NNA14AB02A.

GROUNDBASED OBSERVATIONS OF THE LUNAR SURFACE AT 3 MICRONS: IMPLICATIONS FOR THE PRESENCE OF MOBILE WATER FOR POLAR ICE SUPPLY. C. I. Honniball[1], P. G. Lucey[1], H. M. Kaluna[2], S. Li[1], L. Sun[1], and E. Costello[1], [1]University of Hawaii at Manoa, Department of Geology and Geophysics, 1680 East-West Rd, Honolulu, HI 96822, cih@higp.hawaii.edu, [2]University of Hawaii at Hilo Department of Physics and Astronomy, 200 W Kawili St, Hilo, HI 96720.

Introduction: In the present epoch, the supply of water to the lunar poles almost certainly requires the presence of molecular water. Hydroxyl, in both its charged state and in the form of the neutral radical, is highly reactive and unlikely to be mobile on the lunar surface. Therefore, hydroxyl is unlikely to be a source of hydrogen to the lunar poles.

While it has been suggested that molecular water can be created from solar wind hydrogen as a consequence of space weathering processes [1], this is not known to occur. Observed variations in the strength of the 3 micron absorption band with lunar time of day, latitude and temperature are indisputable [2,3,4], but whether this variation is due to varying OH/H_2O abundances or thermal contamination remains controversial [4,5,6]. In all cases, the presence of molecular water is pivotal to a solar wind source of hydrogen to the poles [7].

The main spectral differences between hydroxyl and water lie beyond the spectral reach of M^3; measurements from 3-4 microns are required. Groundbased telescopic spectroscopy from the NASA InfraRed Telescope Facility (IRTF) at Mauna Kea Observatory offers access to the entire earth facing hemisphere at 1-2 km resolution with full coverage of the 3 µm feature excepting a small window from 2.5-2.9 µm due to telluric absorptions. The spectral range of the IRTF allows for possible separation of hydroxyl and water.

We used the SpeX infrared cross-dispersed spectrograph [8] at the IRTF to obtain data from 1.5 to 4 µm of small targets on the lunar surface. Our goals were: 1) to verify that lunar 3 µm absorptions could be detected using terrestrial observatories, 2) to collect data similar to previous spacecraft observations to both verify those measurements and validate our technique; and 3) to derive estimates of water/hydroxyl abundances independent of M^3 measurements.

This project combines the wavelength reach of Deep Impact and Cassini measurements needed for confident thermal correction and mineralogic analysis, with access to the entire nearside hemisphere at resolution high enough to resolve small geologic features.

Data: On February 19th, July 15th and November 9th and 10th 2017, observations of the lunar western hemisphere were obtained under photometric conditions, at phase angles 100, 75, 74, and 87 degrees, respectively. Data from February were collected along the equator with varying longitude and lunar time of day similar to the Deep Impact equatorial profile [9]. July data were acquired along the morning terminator with varying latitude in approximately 10 degree increments from the equator towards the north pole to seek latitude variations in water abundances. Lastly, data collected in November were of small geologic sites that show anomalous enhancements of water above background abundances in M^3 data [10,11].

Methods: Astronomical observations are corrected for absorption by water in the terrestrial atmosphere. This calibration uses observations of spectrally solar-like stars at similar atmospheric path lengths as our lunar observations. Lunar observations are ratioed to the solar analog stars to correct for telluric absorptions. Data were processed with the SPEXTOOL software [12].

Data in this spectral region contain very significant thermal contamination that must be accounted for in spectral analysis. Thermal excess of the lunar spectra was modeled and removed using the methodology

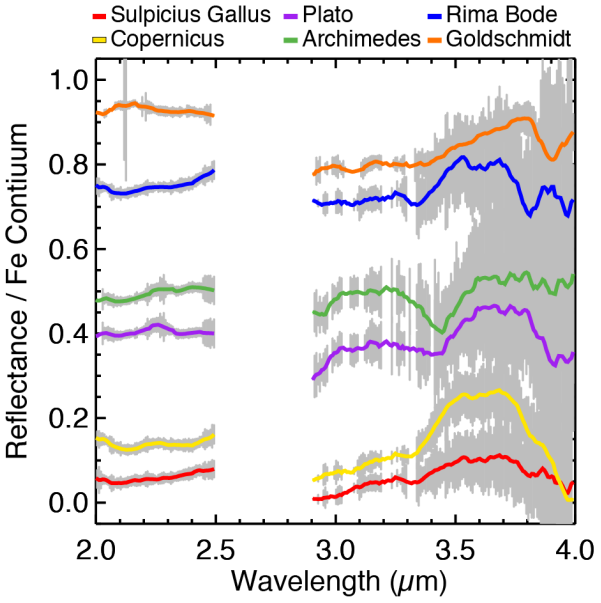

Figure 1: Strong water absorptions at small geologic sites reported as anomalous in M^3 data. Goldschmidt [13], Sulpicius Gallus, Rima Bode, Plato and Archimedes pyroclastic deposits, and Copernicus central peaks [10].

described by [14, 15, 16]. Thermally corrected data were then converted to reflectance by application of appropriate photometric normalizations, and scaling to reflectance factor data from Kaguya Multiband Imager data [17]. Temperatures for each location used the assumption of radiative equilibrium of a rough surface with RMS slope of 20 degrees per [4]. The final data are in the units of reflectance with thermal component removed. Water/hydroxyl abundances were estimated using the methods of [5] assuming a grain size of 60 μm.

Results: Figure 1 shows examples of some of the strongest 3 μm bands with depths on the order of 10 percent or more, confirming that groundbased telescopic observations can detect lunar water at high spatial resolution.

Data acquired along the equator (not shown) represent multiple lunar times of day from 6 am (near the terminator) to 10 am approaching the subsolar point. The equatorial scan shows no absorption at 3 microns or variation from local morning to local noon.

In our latitude scan obtained near the dawn terminator to limit thermal contamination, water abundances were found to rise sharply and non-linearly with increasing latitude, with over 200 ppm detected in Goldschmidt crater at 75N (Fig. 1&2). The small geologic targets called out by [10,11] that we were able to observe all show strong water bands (Fig. 1). Water abundances similar to those reported by [10] are found.

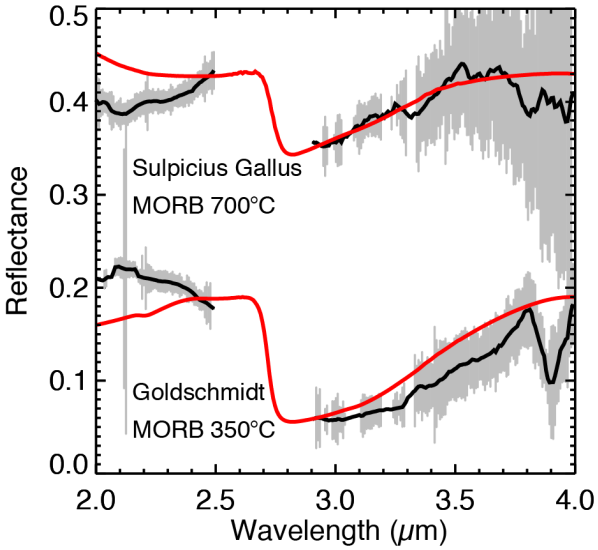

Figure 2: Comparison of Sulpicius Gallus pyroclastic deposit and Goldschmidt crater to water-bearing MORB glasses heated from 350°C to 700°C. At 350°C the glass contains both hydroxyl and molecular water, while heated to 700°C the glass contains only hydroxyl.

When comparing the spectra to water-bearing Mid Ocean Ridge Basalt (MORB) glasses we find that Sulpicius Gallus (Fig. 1&2) and Copernicus (Fig. 1) have similar 3 micron absorption shapes as MORB glass that has been heated to 700°C to drive off all molecular water leaving the glass dominated by hydroxyl. Rima Bode (Fig. 1) and Goldschmidt crater (Fig. 1&2), however, shows spectral shapes similar to MORB glasses with minimal heating and broad 3 micron absorption features, possibly indicating the presence of molecular water. Plato and Archimedes do not have spectral shapes similar to MORB glasses.

Conclusions: Groundbased observations of the lunar surface offers access to the entire lunar nearside with spatial resolutions adequate to resolve many geologic features, and a spectral range and resolution capable of accurate spectral characterization and thermal correction. Our observations showed latitude and time of day systematics consistent with measurements by Cassini VIMS [4] and Deep Impact [3]. Observations of localized 3 μm anomalies identified using M^3 data [10,11] confirmed the presence of a 3 μm band using our greater wavelength coverage, and in the case of the pyroclastic deposits, we derived similar water/hydroxyl abundances using entire independent observations and thermal corrections. Our data may indicate the presence of molecular water at some locations, enabling potential supply of water to the lunar poles.

References: [1] R. M. Housley R.M. et al. (1972), LSC, 2729-2735. [2] Pieters C.M. et al. (2009), Science, 326, 568. [3] Sunshine J.M. et al. (2009), Science, 326,565. [4] Clark R.N. (2009), Science, 326, 562. [4] Bandfield J.L. et al. (2015), Icarus, 10.1016/j.icarus.2014.11.009. [5] Li, S. and Milliken, R.E. (2017) Science advances, 3(9), p.e1701471. [6] C. Wöhler, C., et al. (2017), Science Advances, vol. 3, no. 9, p. e1701286. [7] Hurley D. and Vondrak, R.R. (2000), *J. Geophys. Res.*, vol. 105, no. 11, pp. 26773–26782. [8] Rayner D.W. et al. (2003), PASP, 115, 362. [9] Sunshine et al. (2017), LPSC, 48. [10] Milliken, R.E. and Li, S., 2017. Nature Geoscience, 10(8), p.561. [11] Klima R.L. and Petro N.E. (2017), Phil. Trans. R. Soc. A, 375(2094), p.20150391. [12] Vacca W.D. et al. (2003), PASP, 115, 389. [13] Cheek, L.C., (2011) JGR: Planets, 116(E6). [14] Rivkin, A. et al. (2005) Icarus, vol. 175, no.1, pp. 175-180. [15] Reddy, V. et al. (2009) Meteor. Planet. Sci. 44, 1917–1927. [16] Takir, D. and Emery, J.P. (2012) Icarus, vol 219, no.2, pp. 641-654. [17] Ohtake M. et al. (2013), Icarus, 226(1), 364, 374.

MEASUREMENT REQUIREMENTS AND INSTRUMENT PERFORMANCE FOR REMOTE MEASUREMENTS OF LUNAR SURFACE WATER ABUNDANCE AND VARIATION USING THE 6 MICRONS WATER ABSORPTION. C. I. Honniball[1] P. G. Lucey[1] , S. Li[1], K. Hibbitts[2], [1]Hawaii Institute of Geophysics and Planetology, University of Hawaii at Manoa, 1680 East-West Rd, Honolulu, HI 96822,cih@higp.hawaii.edu, [2]JHU APL, Laurel, MD 20723.

Introduction: Water on the lunar surface was dramatically discovered in data collected by three spacecraft [1,2,3], and was manifest in reflectance spectra of the lunar surface as a strong absorption near 3 microns. The three micron region is a very sensitive spectral region for deteetion and characterization of water in its several molecular forms (see the voluminous FTIR literature) and the Chandryaan-1 Moon Mineralogy Mapper provides wide surface coverage of an important portion of the spectral region.

However, these data are inherently limited by the nature of spectral measurements of the Moon near 3 microns. The three micron absorption region is due to a combination of hydroxyl and water. The processes that give rise to the remotely sensed lunar surface water are still only partly understood [e.g. 4] and uncertainties in the remote sensing results limit the ability to apply constraints. Data in the 3 µm region also suffers from thermal contamination. In this wavelength region the spectral signal is a mixture of reflected light and thermal emission and these terms require very accurate thermal models to separate, if they can be separated at all. Beyond the startling detection of water, the variation in the depth of the water band is a crucial observation, interpreted to be due to diurnal variation in the amount of surface water [3]. But this variation may be entirely due to the competing effects of thermal emission and reflectance [5].

The 3 µm region expresses only two of the water molecule's three fundamental features. The third, the H-O-H bend, occurs at 6.07 microns. This absorption is about half the strength of the combined OH features near 3 microns, but is a strong and narrow feature (Figure 1), well suited for detection of the water molecule, and has no influence from hydroxyl. At 6 microns there is essentially no reflected contamination of the signal, whereas near 3 microns the solar and reflected signal are of similar values, with the reflected signal slightly larger. At 6 microns the ratio of thermal to reflected signal is 1000 times greater than at 3 microns.

The relatively weak spectral signal at 6 microns presents challenges in instrument design. In this work we define a point design for a multiband 6 micron imager as a simple step filter camera/spectrometer with transmission optics optimized for that wavelength. We will define a signal to noise requirement and determine at what lunar latitudes and temperatures this point design can meet the requirement.

The 6 micron feature in minerals and lunar samples: Salisbury et al. 1997 [6] noted the prominent 3 micron absorption feature in their diffuse thermal infrared reflectance spectra of lunar soils from several Apollo landing sites, and attributed that to water probably from terrestrial contamination. They also pointed out the 6 micron feature present in all the spectra and also attributed this to water (Figure 2). We have examined another 17 lunar soils measured at RELAB and each also features a prominent feature at 6 microns.

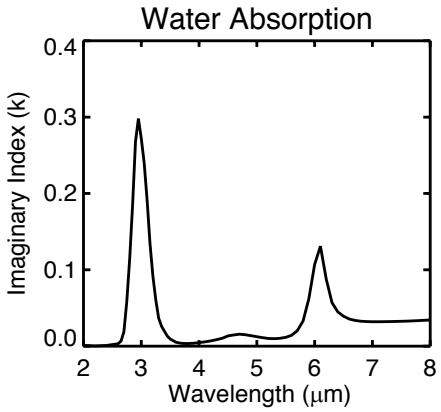

Figure 1: Imaginary index (that controls absorp-tion) of water showing strong peaks at 3 and 6 microns [7].

Li (2016)[8] measured the spectra of a MORB glass in a step-wise heating experiment and these data illustrate the effect of water abundance on the 3 and 6 µm bands. In these samples the 6 µm band depth is strongly correlated with the depth of the 3 µm band supporting its use for remote water detection.

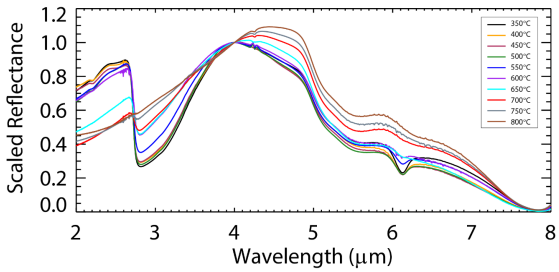

Figure 2: Infrared reflectance spectra of a MORB glass during step-wise heating experiments (Li, 2016) showing prominent, variable 3 and 6 micron bands.

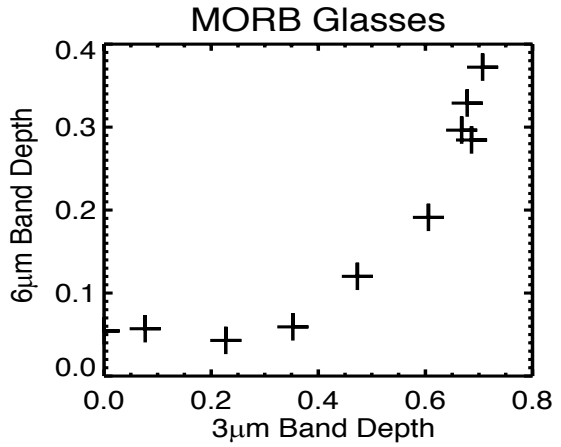

Figure 3: Correlation of 3 and 6 micron bands depths from data in Figure 2 (Li). Note 6 micron depth flattens below a 3um depth of 0.2 owing to loss of molecular water, but retention of hydroxyl.

Utility for lunar surface water studies: Paramount among questions raised by the 3 micron observations is whether the detected time of day spectral variations reflect a variation in water abundance. The observed spectral variations, if entirely attributed to abundance variations, imply a significant diurnal supply of water to the lunar atmosphere, an abundance not observed by LADEE [9]. A secondary question is whether the absorption is due to hydroxyl or water.

At six microns spectral variations cannot be due to mixing of the reflected and thermal signal because the reflected signal is negligible. Furthermore, an observed 6 micron feature must be due to water as hydroxyl contains no vibrational features at this long wavelength. This suggests that observations of the strength of the 6 micron feature during the lunar day will be a powerful test of the hypothesis that water abundance on the lunar surface varies during the diurnal cycle, and answer the question whether water or hydroxyl dominates the H-bearing species on the lunar surface.

Requirements: We found that 100 ppmw water gives rise to an emission feature just under 1% in strength, requiring an SNR of 115 for detection.The sensitivity requirement was derived by adding the k (imaginary index of refraction) of water from [7], proportional to its abundance to a model silicate k that results in a reflectance of 25%, a typical reflectance of lunar soil at 6 microns. Hapke theory is then used to compute the reflectance of the model soil, which is in turn converted to emissivity via Kirchoff's law.

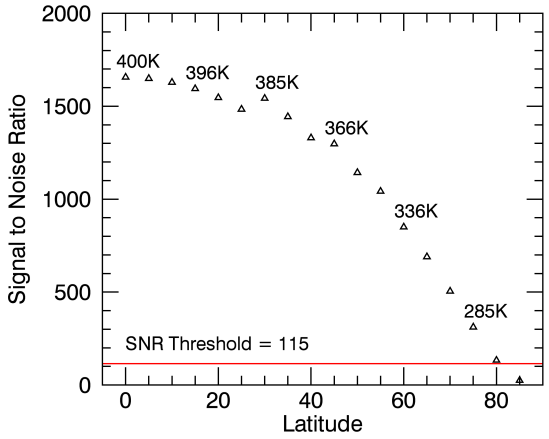

We then computed the signal to noise ratio of the point design as a function of latitude assuming: 1) telescope optics are at ambient temperature of the spacecraft, taken as 0 Celsius; 2) dark current of 800Me/s, equivalent to $2x10^{-5}$ amps/cm^2 3) detector quantum efficiency of 25%; 4) read noise is 100 electrons; 5) surface temperature computed to be equal to 400K times cos(incidence angle)$^{1/4}$ [10]; 6) surface emissivity is 0.75.

Results: Figure 4 shows the signal to noise ratio of the point design vs. latitude, and the SNR requirement is met within 85 degrees of latitude from the equator (at beta = 0), provided the dark current is limited to be less than 20 microamps/cm^2.

Conclusions. Spectroscopic observations of the Moon at 6 microns offers a powerful and unambiguous view of water on the lunar surface enabling testing of the hypothesis that water may be mobile on the lunar surface, and determining the phase of water responsible for the 3 micron absorption feature. First order calculations show that the measurement is feasible with a simple multiband IR camera suitable for Discovery class mission and can cover essentially all illuminated surfaces.

References: [1] Pieters, C. M., et al. science 326.5952 (2009): 568-572. [2] Sunshine, J. M., et al. Science 326.5952 (2009): 565-568. [3] Clark, R. N. Science 326.5952 (2009): 562-564. [4] Hibbitts, C. A., et al. Icarus 213.1 (2011): 64-72. [5] McCord, T. B. et al. Journal of Geophysical Research: Planets 116.E6 (2011). [6] Salisbury, J.W., Basu, A. and Fischer, E.M., 1997. Icarus, 130(1), pp.125-139. [7] Hale, G. M., and M R. Querry. Applied optics 12.3 (1973): 555-563. [8] Li S, PhD Dissertation, Brown University, Providence RI, 2016 [9] Benna, M., Hurley, D.M., Stubbs, T.J., Mahaffy, P.R. and Elphic, R.C., 2015. LPI Contributions, 1863, p.2059. [10] Lawson, S.L., Jakosky, B.M., Park, H.S. and Mellon, M.T., 2000. Journal of Geophysical Research: Planets, 105(E2), pp.4273-4290.

EXOSPHERIC TRANSPORT PROCESSES OF LUNAR VOLATILES. D. M. Hurley[1] P. Prem[1], W. M. Farrell[2], M. Benna[2], A. R. Hendrix[3], [1]Johns Hopkins Applied Physics Laboratory, Laurel, MD 20723, USA (Dana.Hurley@jhuapl.edu), [2]NASA Goddard Space Flight Center, Greenbelt MD 20771 USA, [3]Planetary Science Institute, Boulder, CO

Introduction: Spectroscopic evidence of surface hydration on the Moon exists for two spectral regions: 3 μm and 165 nm. However, there have been multiple reduction methods applied to the data that yield different results regarding the variability of the surface hydration [1-3]. One possibility is that there is a diurnally varying hydration signature.

In order to have a diurnally varying hydration signature on the surface, hydrated species must either move around or have a spatially varying lifetime on the surface. If there is currently a steady state balance between the creation and destruction of hydrated species, the most plentiful potential source of hydrogen is the solar wind. If the solar wind is the source of the observed hydration, then one expects the hydration signature to vary when the Moon is isolated from the solar wind every month as it traverses the Earth's magnetotail. On the other hand, if migration of hydration is involved, then there should be H_2O/OH in the Moon's exosphere at all times. We explore these scenarios and determine measurable quantities for each.

Model: We perform simulations of water sources and migration through the lunar exosphere to compare to the observed hydration cycle. Two scenarios are examined. One looks at the thermal diffusion of implanted solar wind H as a function of temperature [4,5]. These simulations include spatial variations in the solar wind as a source, and include the temporal effects of passing through the Earth's magnetotail on solar wind fluence and the hydration budget. The other scenario examines the migration of water released from the surface by meteoroid impacts [6,7].

The model tracks sample particles as they travel through the lunar exosphere and interact with the surface. An input flux and spatial distribution is assigned as appropriate for the source: solar UV radiation for photon-stimulated desorption, solar particle flux for ion sputtering, and micrometeoritic or meteoritic flux for impact vaporization. At the Moon, the solar wind flux dies off with increasing solar zenith angle due to the curvature of the Moon. Micrometeorite release, in contrast, is enhanced on the morning hemisphere.

The ejected products are assigned an initial velocity drawn from the distribution function appropriate to the release mechanism. When the particle comes back into contact with the surface, there are a variety of processes that can occur, introducing an array of interesting physics questions. These are investigated in the simulations presented here. When the particle reencounters the planet, it may stick to the surface. It may adsorb to the surface long enough to partially or fully thermalize to the local surface temperature and then be re-emitted. Or it may rebound on contact retaining all or most of its incident energy.

When the particle encounters the surface, the code determines whether the particle will stick or be re-emitted depending on the sticking functions assigned to the simulation. In these simulations, sticking is applied as activation energy of a binding site. Each time the particle comes into contact with the surface an activation energy is assigned. The local surface temperature is queried to calculate a residence time for the given activation energy and temperature. The code can immediately consider the later reemission of a stuck particle by rotating it in longitude and requerying the surface temperature. This way, one can determine the material that should be stuck to the surface as a function of time of day.

The probability of photoionization or photodissociation during a given hop is based on the photoionization time and the time of flight in sunlight. The particle escapes the simulation when it crosses a predetermined boundary. Here, we use the Hill sphere (35 R_{Moon}) as the boundary for escape.

Results: We report our findings regarding the surface-properties that best reproduce the hydration signature observed in the UV and IR on the surface of the Moon. This is used to estimate the amount of material involved in migration and the corresponding amounts tied up on the surface (Figure 1) and mobile in the exosphere (Figure 2). This is compared to observations of exospheric water at the Moon by the NMS onboard LADEE. The relationship to possible sources is presented.

Our simulations of a meteoroid generated exosphere are not consistent with the observations from the LADEE NMS if water particles are allowed to take multiple hops through the exosphere. This suggests that the surface is very sticky for water. Therefore, we also investigate the single-hop limit to exospheric transport to determine the delivery rate to the permanently shadowed regions in that regime. Figure 3 shows the distribution of water on the surface after a single ballistic trajectory for a 1 g release of water. We convolve this with a model meteoroid flux to calculate the surface distribution and the PSR delivery rate.

References: [1] Bandfield JL, Poston MJ, Klima RL, Edwards CS (2018) Nature geoscience 11(3):173. [2] Li S. and R. E. Milliken (2016) J. Geophys. Res. 121, 2081-2107. [3] Hendrix A. R. et al. (2012) J. Geophys. Res. 117, E12001. [4] Farrell. W. M. et al. (2017) J. Geophys. Res. 122, 269-289. [5] Wöhler C. et al. (2017) Icarus 285, 118-136. [6] Crider, D. H., and R. R. Vondrak (2003) J. Geophys. Res. 108, E5079. [7] Hurley D. M. and M. Benna (2017) Planet. Space Sci. https://doi.org/10.1016/j.pss.2017.07.008.

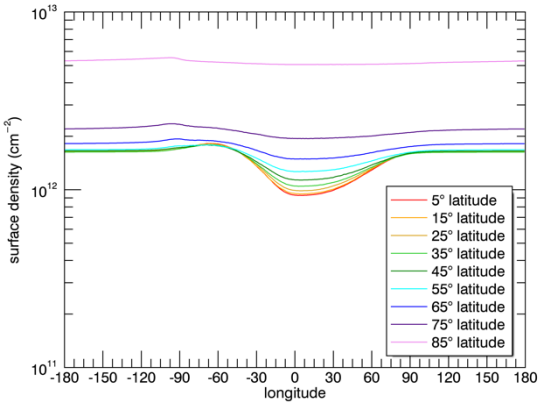

Figure 1. Model results of the surface density of adsorbed water for a solar wind source of water, including migration through the exosphere. Noon local time is at 0° longitude.

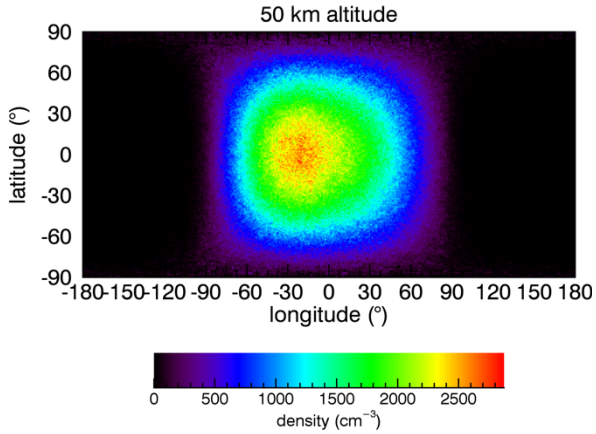

Figure 2. Corresponding exospheric water density at 50 km altitude for the solar wind source of water, when migration through the exosphere is active. Noon local time is at 0° longitude.

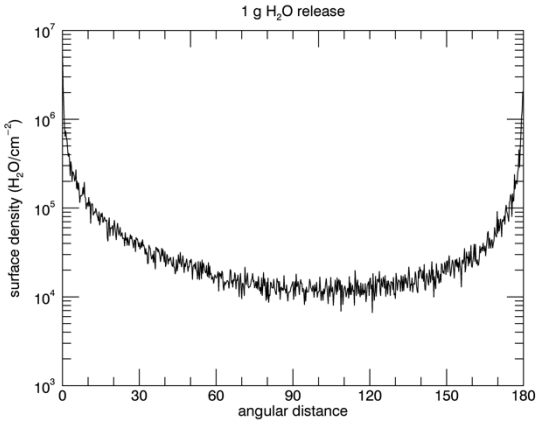

Figure 3. Distribution of water released by a meteoroid impact on the surface after a single ballistic flight is shown for a 1 g release of water at 5000 K. There are concentrations both near the impact site and at the antipode.

A FRAMEWORK TO DETERMINE THE HISTORY OF THE MOON'S POLAR ICE. A. P. Jordan[1,2*], J. K. Wilson[1,2], N. A. Schwadron[1,2], H. E. Spence[1,2], and N. E. Petro[3], [1]EOS Space Science Center, University of New Hampshire, Durham, NH, USA (*email: a.p.jordan@unh.edu), [2]Solar System Exploration Research Virtual Institute, NASA Ames Research Center, Moffett Field, CA, USA, [3]NASA Goddard Space Flight Center, Greenbelt, MD, USA.

Introduction: The history and distribution of water ice on the Moon has been difficult to determine. Differing datasets can have differing interpretations on crater-scales and smaller [e.g., 1]. These differences have often caused larger-scale features to be overlooked, yet such scales are important. For example, by looking at large-scale features in neutron albedo, Siegler et al. [2] found that the data can be explained by two deposits of ice: one ancient (>3.5 Gyr old) and offset from the current poles because it was emplaced when the Moon had a different spin axis, and one more recent and centered on the current poles.

This possible timeline was found by focusing on larger scales, and it shows the insight gained by treating the ice as being in polar "caps." Consequently, we develop a framework for interpreting ice data on large scales. We also show that it is possible to use available data to help constrain the history of lunar ice, because an initial synthesis of surface and subsurface data shows that many of the datasets agree on the large-scale distribution of ice.

Polar ice framework: For the interpretation of data on large scales, our framework focuses on two characteristics of polar ice: its maximum concentration and its extent. The maximum concentration has already been shown to be important in the work mentioned above [2]. In addition to this, the extent, or boundary, of the ice "cap" can also provide critical information about the thermal conditions that have dominated since the ice was deposited.

Two hypothetical examples can show this. First, a recent deposit of ice would be centered on the current pole. It would have a maximum concentration at the pole [e.g., 2], and its boundary would be symmetric about the maximum/pole. In other words, the boundary would follow a line of latitude (Fig. 1, top right).

The second example is a deposit emplaced when the Moon had a different spin axis. In the case, the ice cap would have a maximum at the ancient pole [e.g., 2]. If no ice were added or lost, then the boundary would be symmetric about maximum/palaeopole but not follow a current line of latitude (Fig. 1, top left). In addition to these two scenarios, there could also be admixtures of ancient and recent ice [2], which would superpose these example scenarios (Fig. 1, bottom).

We can modify these basic examples to include the loss of ice. Perhaps, as the spin axis evolved to its present location, some ancient ice would have been lost from one side of the cap. If so, then the maximum of the cap could be at the palaeopole while the boundary would be asymmetric about the maximum. In this case, the boundary of the cap would carry important information about the thermal history of the Moon's poles.

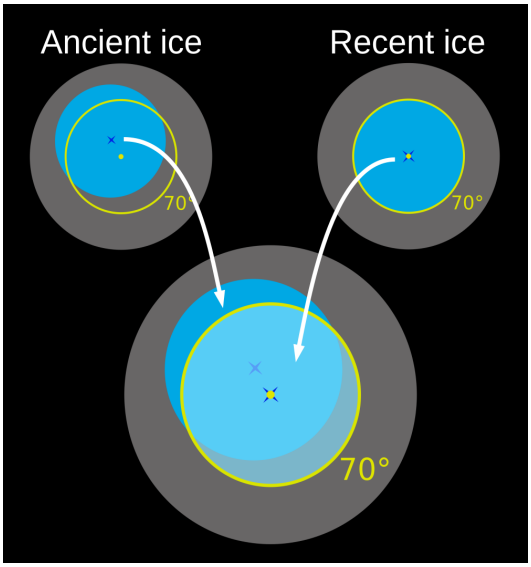

Fig. 1. Top left: Ancient ice deposit (blue) is offset from current pole (yellow dot); boundary is symmetric about maximum ("x"). Top right: Recent ice deposit is symmetric about current pole. Bottom: Admixture of two ice deposits. 70° latitude is predicted to be extent of ice [4].

Polar ice with depth: The above examples focus on deposits at a single depth, but we can use this framework as a function of depth. If surficial ice is recent [e.g., 3], then it is likely symmetric about the current poles, unlike the buried, more ancient ice [2]. In this case, the surface "cap" may not align with the buried "cap."

We show that such analysis, while beyond the scope of this work, is possible by synthesizing observations that probe water ice or hydrogen at a range of depths. At the surface, the Lyman Alpha Mapping Project (LAMP) on the Lunar Reconnaissance Orbiter (LRO) shows a general poleward increase in the southern polar regions that may be due to surface ice. This trend is independent of large permanently shadowed

regions (PSRs) [4], and, if extrapolated, it seems to extend to -75° or -70°. Also at the surface, the Moon Mineralogy Mapper (M3) on Chandrayaan-1 has detected the spectral signatures of ice; all positive detections are found poleward of latitude ±70° [5].

Neutron observations probe to a depth of ~50 cm. The Neutron Spectrometer on Lunar Prospector (LP-NS) and the Lunar Exploration Neutron Detector (LEND) on LRO show a similar latitudinal trend as the surface data, with polar cap boundaries near ±70° [6, 7]. In the LEND data, the trend is independent of large neutron suppression regions [8].

Proton albedo can probe hydrogen at depths of ~1-10 cm, so it provides the link between surface and neutron measurements [9]. Proton albedo measured by the Cosmic Ray Telescope for the Effects of Radiation (CRaTER) on LRO shows that hydrogen increases with increasing latitude [9]. Currently, however, the data cannot show whether this occurs mainly above ±70°, so we have developed new techniques [10] to help us determine whether this boundary appears in the proton albedo. We will report on progress made in this analysis.

Conclusion: Four of the above datasets show that polar ice extends to ~±70°, just as predicted over 50 years ago [11]. Yet while the data confirms this prediction, this synthesis also shows that we have the data in hand to find differences between the datasets as a function of depth. For example, how do the maxima and boundaries change as a function of depth, and are the boundaries symmetric about the maxima? Do the two caps of Siegler et al. [2] extend through mid-range depths (~1-10 cm) and to the surface? If, for instance, surficial ice is indeed more recent than buried ice, proton albedo data will help show whether ice at ~1-10 cm is related more to the surface deposits or to the deeper deposits. With the polar cap framework, we can now begin to answer these questions and constrain the history of lunar ice.

References: [1] Hurley D. M. et al. (2016), white paper,<http://sservi.nasa.gov/wp-content/uploads/2016/02/Volatiles_White_Paper.pdf>. [2] Siegler M. A. et al. (2016), *Nature, 531,* 480-484. [3] Gladstone G. R. (2012), *JGR, 117*, E00H04. [4] Hayne P. O. et al. (2015) *Icarus, 255,* 58–69. [5] Li S. et al. (2017) *SSERVI Exploration Science Forum 2017*, Abstract #NESF2017-135. [6] Feldman W. C. et al. (1998) *Science, 281,* 1496–1500. [7] Litvak M. L. et al. (2012), *JGR, 117*, E00H22. [8] Boynton W. V. et al. (2012), *JGR, 117,* E00H33. [9] Schwadron N. A. et al. (2016), *Icarus, 273*, 25–35. [10] Schwadron N. A. et al. (2017), *Planet. Space Sci., 296,* 99–109. [11] Watson K. et al. (1961), *JGR, 66*, 3033-3045.

Extrapolating from Meter to Sub-meter Block Populations to Constrain Polar Ice Estimates. S.M. Klem[1], M.S. Robinson[1], M. R. Manheim[1], and the LROC Science Team[1]. [1]School of Earth and Space Exploration, Arizona State University, Tempe, AZ, 85251, USA (sklem@ser.asu.edu).

Introduction: Block size-frequency distributions (BSFDs) provide insight to the ejecta and surface roughness in and around craters, and serve as a proxy for the physical state of the substrate [1-4]. This study investigates BSFD (>2.5-m) and how accurately smaller the BSFD can be extrapolated to smaller diameters from orbital imaging.

Block populations were identified from Lunar Orbiter (LO) [2], Surveyor III (SIII) [5], Chang'E-3 (CE-3) [3], and Lunar Reconnaissance Orbiter Camera (LROC) Narrow Angle Camera (NAC) images. Since available pixel scales limits our ability to identify sub-meter scale blocks from orbital imaging, our understanding of block distributions down to the 10-cm scale is incomplete – this size range is critical for the interpretation of Mini-RF radar observations [6].

Mini-RF has two modes, S-band (0.126-m) and X-band (0.42-m) [6]. In the S-band observations, some polar crater interiors have radar backscatter anomalies with high circular polarization ratios (CPRs) and low CPR for their exteriors, these craters are referred to as "anomalous" craters [4, 6-7]. Small blocks with diameters near the wavelength of the radar signal [6] and ice are both potential sources of the high-CPR signals [4]. Accurate estimates of the 0.1-m block population allow testing of the ice or blockiness hypotheses for the high-CPR signals seen in the anomalous craters. Testing these hypotheses is critical for constraining the lunar polar volatile inventory. Currently there are no orbital datasets with the proper pixel scale, so we are stuck with extrapolating from meter-sized blocks visible in orbital images from the NAC (and those to be acquired by ShadowCam in permanently shadowed regions, pixel scale of 1.7-m at an orbit of 100km [8]).

The NAC pixel scale is 0.50-m (from an altitude of 50 km), which allows for confident identification and measurement of blocks >2.5-m in diameter. The goal of this work is to determine the accuracy of extrapolating from >2.5-m diameter block populations down to 0.1-m diameter.

Background: Previous studies, determining block populations for potential landing sites on Mars [9-12], compared block populations and how meter and sub-meter-sized blocks are related. They proposed that larger diameter block populations (>1.5-m) can be accurately extrapolated down to 10-cm scales [11], using an exponential curve fit, but if the counts were limited to >5-m blocks, the extrapolation accuracy diminished [10]. A lower limit for extrapolation for Mars lends some degree of confidence for similar lunar studies.

Cintala and McBride [2] compared LO coverage of several Surveyor landing sites to the work of Shoemaker and Morris [5], finding that for SIII the orbital image counts best matched the lander counts out of all the Surveyor sites studied [2]. Lunar block populations across a broad size range were derived from LO (>2-m diameters) and SIII images (0.001 m to 0.3-m diameters) [2, 5]. Cumulative SFDs of the block counts both had negative slopes, though the LO slope (blocks 2 to 6.3-m) was steeper than the SIII slope (blocks 0.001 m to 0.251-m). The steeper, negative slope for meter-sized blocks overestimates the number of sub-meter blocks. The difference in slope could mean the BSFD is size dependent or one of the counts is incorrect.

More recently, BSFDs from NAC [6, 13] orbital images and CE-3 surface images [3], also showed a roll over as the block size approached the resolution cut.

Block Count Sites: Four sites were selected for this study. Surveyor III and the CE-3 (Fig. 1) landing sites were selected to compare with previous work, which included block counts from surface images, allowing direct comparisons between the sub-meter population and the meter population. Block counts were derived from one NAC pair for each site and three CE-3 LCAM descent images.

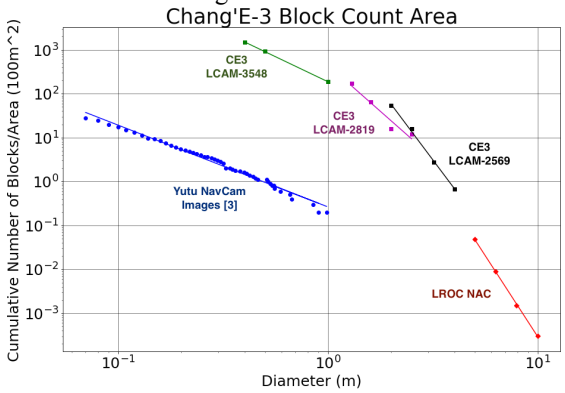

Figure 1. Log-log plot of BSFD for Chang'E-3 landing site with power law fits shown [Table 1].

The two other sites selected were a block field on a low altitude NAC image of the Newton Crater (NC) floor, with pixel dimensions of 0.21 x 0.57-m and processed at 0.2-m pixel scale. This image provided a BSFD with a larger block count area than those of the CE-3 descent images (Fig. 2). A newly formed (October 2012) 70-m impact crater provided an example of the block population around a fresh impact crater.

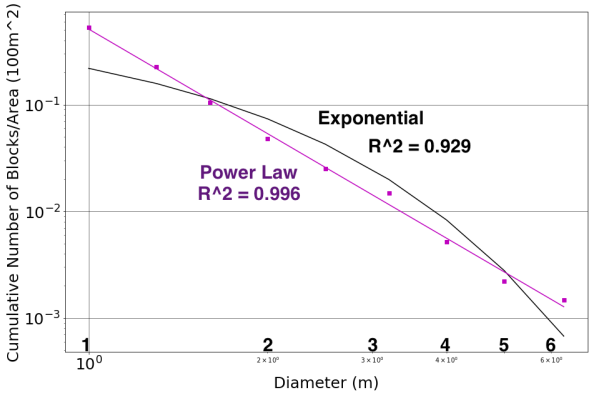

Figure 2. Log-log plot of BSFD for 0.2-m NAC NC image.

Method: The maximum diameter was recorded for the blocks [14], as was done for the LO counts [2]. Block counts from a NAC image covering a similar area used for the LO image for the Surveyor III site [2] for analysis. The cut off for the blocks in the NAC image is 2.5-m, since the pixel scale for the image is 0.5-m. The new block counts were binned to match the data from Cintala and McBride [2]. The counts from the NACs, Chang'E-3 LCAM images, and LO were cut off at 5 times the pixel scale of the images to avoid extending beyond the confidence limit of block diameters.

Results and Discussion: Slope values for the LO [2] and NAC BSFDs are similar, while both differ from the SIII slope (Table 1).

Image/Area	a (Coefficient)	b (Slope)	R^2
SIII [5]	0.049	-2.559	0.899
LO 154H2 [2]	1.154	-5.653	0.960
NAC (SIII)	0.023	-5.039	0.995
NavCam [3]	0.264	-1.863	0.987
LCAM 3548	186.54	-2.282	0.999
LCAM 2819	447.78	-4.218	0.973
LCAM 2569	4752.9	-6.375	0.998
NAC (CE-3)	6880.3	-7.376	0.999
NAC (NC)	0.5115	-3.257	0.996

Table 1: Values derived from the power law: $y = ax^b$

A power law fit to the 0.2-m pixel scale NAC NC image BSFD has lower residuals than an exponential fit (Fig. 2), however the count is cut off at 1-m, and does not cover the transition between the meter and sub-meter populations for this count area.

Overhead block counts for the CE-3 sites (NAC and CE-3 descent camera) were compared to block counts from the Yutu rover NavCam images [3]. The Chang'E-3 descent LCAM 2569, 2819, and 3548 image counts bridge part of the sub-meter to meter range (Fig. 1). Yutu NavCam based BSFD [3] has a different slope possibly due to a small and non-representative area imaged by the rover. The slopes for two of the Chang'E-3 LCAM counts (black and purple markers in Fig. 1) match up with the slope from the NAC CE-3 count indicating that extrapolation from >2.5 m population to sub-meter blocks is possible.

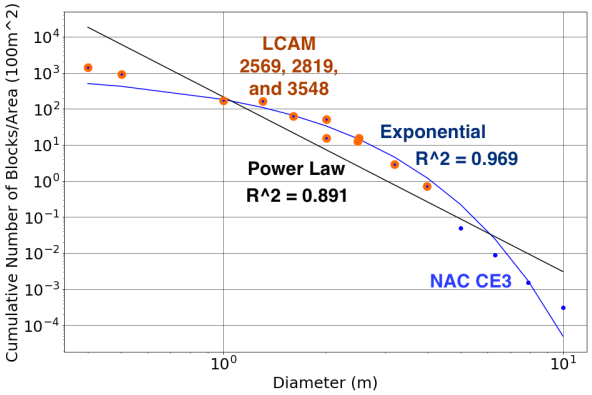

Figure 3. Log-log plot of BSFD of LCAM (2569, 2819, and 3548) and NAC CE-3.

An exponential fit to the NAC and CE-3 LCAM BSFD has lower residuals than a power law fit (Fig. 2) consistent with similar work from Apollo 15 Hasselblad images of Hadley Rille [15]. The BSFD shows a gradual transition occurring between 1 and 3 meters in the CE-3 block counts (Fig. 3).

Conclusion: The BSFD generated by this study shows that there is a change in slope at 1-m. An exponential curve fit accounts for the change in slope (R^2=0.969, Fig. 3), however the power law residuals are unacceptable (R^2=0.891, Fig. 3) unless a piecewise fit is used with a break at 1-m. Therefore, either an exponential or piecewise curve fit is best for representing blocks across the range 0.1-m to 10-m. Allowing for the determination of block populations contributing to the backscatter signal in the Mini-RF S-band.

References: [1] Basilevsky et al. (2013) *PSS*, 89, 118-126. [2] Cintala and McBride (1995) *NASA Tech. Mem*. 104804. [3] Di et al. (2015) *PSS*, 120, 103-112. [4] Ghent et al. (2016) *Icarus*, 273, 182-195. [5] Shoemaker & Morris (1968) *Surv. Proj. Final Rep. Part II*, 86-102. [6] Spudis et al. (2013) *GRL*, 118, 2016-2029. [7] Spudis et al. (2010) *GRL*, 37, L06204. [8] Robinson et al. (2017) *EPSC*, 11. [9] Golombek et al. (1997) *JGR*, 103, 4117-4129. [10] Golombek et al. (2003a) *JGR*, 108, E12. [11] Golombek et al. (2008a) *JGR*, 113, E00A09. [12] Golombek et al. (2012) *Mars J.,* 7, 1-22. [13] Yuan et al. (2017) *PSS*, 1-10. [14] Kneissl et al. (2010) *PSS*, 59, 1243-1254. [15] Manheim et al. (2018) *EPSC*, 996. [16] Hiesinger et al., *JGR*, 105, 29239- 29275.

DIRECT DETECTIONS OF SURFACE EXPOSED WATER ICE IN THE LUNAR POLAR REGIONS. Shuai Li[1], Paul G. Lucey[1], Ralph E. Milliken[2], Paul O. Hayne[3], Elizabeth Fisher[2], Jean P. Williams[4], Dana M. Hurley[5] and Richard C. Elphic[6]. [1]University of Hawaii; [2]Brown University; [3]University of Colorado Boulder; [4]University of California, Los Angeles; [5]Johns Hopkins University Applied Physics Laboratory; [6]Ames Research Center. shuaili@hawaii.edu

Introduction: The low temperature of permanently shaded regions (i.e. < 100 K) on the Moon may allow cold trapping of water that was sourced from solar wind implantation, impact delivery, and the lunar interior [1], and such deposits may preserve a record of the evolution of water in the inner solar system. Knowing the distribution of water ice on the Moon is critical for understanding its origin, stability, processes of deposition, and its viability for *in situ* resource utilization.

There are a number of strong indications of the presence of water ice in similar cold traps at the lunar poles [2-4], but none are unambiguously diagnostic of surface exposed water ice and inferred locations of water ice from different methods are not always correlated. Epithermal neutron counts, for instance, can be used to estimate hydrogen in the upper tens of centimeters of the lunar regolith, but such data cannot discriminate between H_2O, OH or H [4]. Ratios of reflected ultraviolet (UV) radiation measured by the Lyman Alpha Mapping Project (LAMP) instrument onboard the Lunar Reconnaissance Orbiter (LRO) have been interpreted to indicate the presence of H_2O near the lunar south pole [3], but the observed signatures may not be uniquely attributable to water ice because OH may exhibit similar characteristics at UV wavelengths [5]. High reflectance values at 1064 nm wavelength have also been observed near the lunar poles by the Lunar Orbiter Laser Altimeter (LOLA) and may be consistent with water ice, but fine particles and lunar regolith with lower degrees of space weathering may also give rise to higher reflectivity at this wavelength, making this interpretation non-unique [2, 6].

The Moon Mineralogy Mapper (M^3) instrument on the *Chandrayaan-1* spacecraft acquired the highest spatial and spectral resolution NIR data currently available at a global scale, including the polar regions. The wavelength range of M^3 (0.46 – 2.98 μm) is too limited to properly discriminate OH/H_2O species using fundamental vibration modes in the 3 μm region [7, 8], and in this study we focus on the detection of diagnostic overtone and combination mode vibrations for H_2O ice that occur near 1.3, 1.5 and 2.0 μm. Numerical modeling results suggest NIR spectra representing as little as 5 wt.% (intimate mixing) or 2 vol. % (linear areal mixing) water ice are expected to exhibit all three of these absorptions [9].

Methods: We obtained all M^3 images and mosaicked them from 75-90° N/S using a stereographic projection. Only data between 1 μm and 2.5 μm (band 22 – 73 of M^3 data) were applied in this study considering their higher SNR relative to longer wavelengths [10] and all strong ice absorptions are located in this wavelength range [11].

The positions of absorption shoulders and centers of pure water ice reported by Clark [11] were applied as criteria for identifying ice in the lunar polar regions (Table 1). Pixels were marked as ice-bearing if their spectra exhibited three such absorptions centered near 1.3 μm, 1.5 μm, and 2.0 μm, matching all conditions in Table 1. Spectral angles between the spectra of potential ice deposits and the spectrum of pure ice shown in Fig. 1 were also calculated, and a spectral angle less than 30° was empirically applied to further constrain the possible ice deposits.

Table 1. Ice absorptions at 1.0-2.5μm [11]

Absorption (μm)	Shoulder (μm)		Center (μm)	
	Min	Max	Min	Max
1.3	1.130	1.350	1.242	1.323
1.5	1.420	1.740	1.503	1.659
2.0	1.820	2.200	1.945	2.056

Results and Discussion: Several thousand M^3 pixels consistent with the presence of water ice were identified within 15° of the poles. The spectra of all ice bearing pixels were averaged and plotted for the northern and the southern polar regions (Fig. 1). The 1.5 μm absorption appears broader and more asymmetric in the average spectrum for the south compared with that from the north (Fig. 1), which is suggestive of larger grain sizes in the former [11]. Spectral mixing model results suggest that the weak absorption near 1.1 μm and the blue slope of the M^3 spectra may be indicative of 30 wt.% ice or higher if it is mixed intimately with regolith, or over 20 vol.% if ice occurs as patches within otherwise ice-free regolith [9].

Almost all M^3-derived ice locations also exhibited extreme LOLA reflectance and UV

ratio values consistent with the presence of water ice, as well as annual maximum surface temperatures below 110K [9]. The small number of candidate locations with slightly higher surface temperatures (110 – 160 K) or lower LOLA reflectance values may be false detections due to noise in M^3 data. The agreement between these four data sets constitutes a robust detection of water ice at the optical surface in these locations.

The distribution of surface exposed water ice exhibits strong spatial coherence with temperatures less than 110K (Fig. 2), suggesting that temperature is one of the major controlling factors. However, not all regions less than 110K (cold traps) show ice exposures, such as cold traps in craters Amundsen, Hedervari, Idel'son L, and Wiechert near the south pole; the cold trap of Bosch crater near the north pole. The ice stability depth at these locations is coincidentally greater than zero when the Moon is hypothesized on its paleo-axis [13], which indicates that surface ice may only be retained at long timescale cold traps associated with the polar wander, similar to Ceres [14].

The patchy distribution and low abundance of surface exposed water ice in lunar cold traps may reflect a low rate of water supply and a fast rate of ice destruction (i.e. impact gardening) [9].

The absorption minima near 1.5 μm of the M^3 spectra of ice-bearing pixels appear to be shifted ~0.05 μm to longer wavelengths compared with those of pure ice frost (Fig. 1). Such band shifts may reflect the increase of hydrogen bond strength due to bound water [15]. Alternatively, the 0.05 μm shift of the spectra of ice-bearing pixels may suggest that the ice was condensed from vapor phase either due to impacts or migrations through the lunar exosphere [9]. It is also possible that such a shift may reflect higher D/H ratios [9]. However, we cannot rule out the possibility that the 0.05 μm shift of the 1.5 μm absorption is due to the low SNR of the M^3 data.

Conclusions: Unique IR absorptions of ice near 1.3, 1.5, and 2.0 μm were detected using the M^3 data near the lunar polar regions. The detected ice-bearing pixels also exhibited high LOLA albedo and UV ratios as well as annual maximum surface temperatures below 110K. The distribution of ice exposures is dominantly controlled by the temperature, and may also be affected by the water supply rate, ice destruction rate, and thermal environment. The shift of the 1.5 μm absorption may indicate the low-density ice condensed from water vapor that might be associated with impacts and water migrations through the lunar exosphere.

References: [1]. K. Watson *et al.*, *JGR*, (1961). [2]. E. A. Fisher *et al.*, *ICARUS*, (2017). [3]. P. O. Hayne *et al.*, *ICARUS*, (2015). [4]. D. Lawrence *et al.*, *JGR*, (2011). [5]. C. A. Hibbitts *et al.*, in *DPS*. (Provo, Utah, 2017). [6]. M. T. Zuber *et al.*, *Nature*, (2012). [7]. C. M. Pieters *et al.*, *Science*, (2009). [8]. S. Li, R. E. Milliken, *Sci. Adv*, (2017). [9]. S. Li *et al.*, *PNAS*, (Revision Submitted). [10]. R. Green *et al.*, *JGR*, (2011). [11]. R. N. Clark, *JGR*, (1981). [12]. J. P. Williams *et al.*, *ICARUS*, (2017). [13]. M. Siegler *et al.*, *Nature*, (2016). [14]. N. Schorghofer *et al.*, *Astrophys. J*, (2017). [15]. E. Libowitzky, *Chem. Mon.*, (1999).

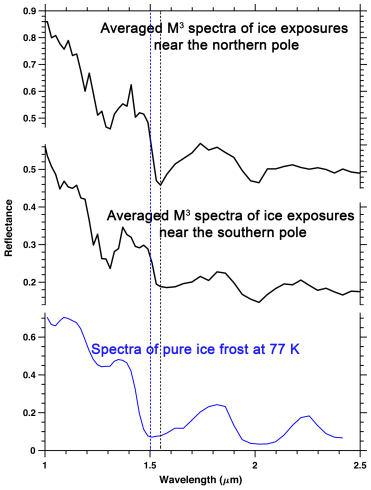

Fig. 1. Averaged M^3 spectra of ice-bearing pixels in the north and south pole, respectively, compared with the spectrum of pure ice frost.

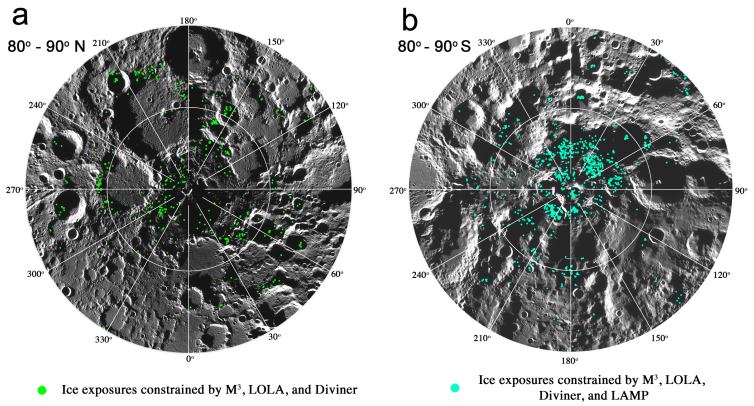

Fig. 2. Locations of ice-bearing pixels seen by the M^3 data and further constrained by the LOLA, Diviner, and LAMP UV band ratio data near the north (a) and south (b) pole, respectively [9]. Each dot represents a M^3 pixel and was enlarged for visualization.

THE LUNAR VOLATILE SYSTEM IN SPACE AND TIME: SUPPLIES TO THE LUNAR POLES. P.G. Lucey[1]; D. Hurley[2]; W. Farrell[3], N. E. Petro[3]; M. Cable[4]; D. Dyar[5]; T. Orlando[6]; M. McCanta[7], E. Fisher[8], K. Hibbitts[2], P. Prem[2]; M. Benna[3]; P. Hayne[9]; R. Green[4]; C. M. Pieters[8], K. Mandt[2], M. Horanyi[9], J. Halekas[10], S. Li[1]. [1]University of Hawaii at Manoa, Honolulu HI (lucey@higp.hawaii.edu), [2]Johns Hopkins University Applied Physics Laboratory, Laurel, MD, [3]Goddard Space Flight Center, Greenbelt, MD, [4]Jet Propulsion Laboratory, Pasadena, CA, [5]Mt. Holyoke College, South Hadley, MA, [6]Georgia Institute of Technology, Atlanta, GA, [7]University of Tennessee, Knoxville, TN, [8]Brown University, Providence, RI, [9]University of Colorado, Boulder, CO, [10]University of Iowa, Iowa City, IA

Introduction: The revolution was not televised, but it was published in *Science*. A series of papers in the years 2008, 2009, and 2010 [1,2,3,4] forced upon the lunar science community a new paradigm, where the Moon changed from an anhydrous, desiccated world, to one where water is an essential part of the conversation.

The revolution invites a rethinking of lunar volatile evolution in time and space, assembling pieces that have been developing over the past decade, of which the poles are a vital part. The lunar volatile system can broadly be divided into three epochs: (1) in the last billion years volatile inputs are dominated by the solar wind and by the steady impact of small meteorites; (2) from one billion years ago to the stabilization of the lunar crust just over four billion years ago volatile inputs from large volcanic eruptions [6] and impacts by large comets and wet asteroids [7] dominate; (3) comprises the formation of the Moon and events shortly thereafter, when the Moon acquired its initial volatile inventory that is seen today in the lunar samples, and driving lunar volcanism throughout its history. Each of these epochs contributed to the lunar polar deposits and were critical inputs to their present conditions.

The Dynamic Now: The solar wind and small meteorites introduce volatiles into the system, and may induce chemical reactions in surface materials that may contribute molecular water and perhaps other mobile species into the lunar atmosphere, potentially available for cold trapping at the lunar poles. The solar wind has been suggested as a source of surface hydrogen 'deposits' for decades, since [8] proposed formation of hydroxyl from reaction of solar wind protons with lunar surface oxygen. Similarly, molecular water was proposed to form in space weathering reactions involving reduction and production of nanophase iron [9]. However, how much hydrogen is converted to mobile species available to the poles is not known. Hydrogen is the largest component of the solar wind in the form of protons with energies around ~1 keV, including intense coronal mass ejections with energies ranging up to 10s of keV. One of the surprising discoveries of Chandrayaan-1 was the presence of promptly reflected high energy neutral hydrogen atoms that constitute a large fraction of the incoming solar wind [10]. The balance of the solar wind may lie in lower energy and thermal energies [11], but this range of reflected solar wind hydrogen remains unmeasured at the Moon. The measurement gap allows that little solar wind is available for surface reactions to supply the poles.

The diurnal, latitude and temperature variation in the strength of the lunar 3 μm band observed by M3 and Deep Impact is suggestive of the presence of mobile water that migrates along temperature gradients, requiring continuous production of molecular water from solar wind [4]. Alternatively, the varying signal maybe be produced from in-place variations in hydroxyl abundance with no mobile compounds. Hydroxyl may be formed from solar wind, then lost to H_2 with increasing temperature [12,13] with no participation by molecular water. Even the variations in abundance suggested by the spectral studies have been called into question as being plausibly attributed to contamination by lunar thermal emission [14]. Therefore the ability of the solar wind to produce molecular water as a source for the poles remains conjecture, and the subject of active research.

The abundance of water in the atmosphere is now tightly constrained by LADEE observations from 50 km. The background level of atmospheric water in thermal equilibrium with the surface is very low, less than 1 molecule per cubic centimeter, and this in turn constrains a continuous source like solar wind production of water, perhaps casting additional doubt on the equating of spectral variation with abundance variation. There is a potential alternative however: production of water may feature interactions of neighboring hydroxyls at the surface, and water formation from this process may produce water that is rotationally hot, but kinetically cold, and so would not rise to altitudes to be sampled by LADEE.

LADEE's neutral mass spectrometer did observe large spikes in water abundance often coincident with meteor showers [15]. This water can be attributed to that borne by the meteorites themselves, or possibly to the impacts providing enough energy to favor water production on the surface from chemical energetic pathways not available to diurnal lunar surface temperatures.

LADEE also may have revealed a lunar carbon cycle with its detection of methane in the atmosphere

[16]. Foreshadowed by Apollo 17 surface mass spectrometer measurements [17], solar wind carbon appears to be interacting with hydrogen in the surface, producing methane. This opens the door to production of other mobile carbon species such as alcohols on the illuminated surface. Significantly, carbon species were detected in the LCROSS plume [18,19] .

The contemporary processes that may contribute volatiles to the poles from locations moonwide are only glimpsed by current measurements. The hydrogen budget is incompletely measured so the magnitude of the potential solar wind contribution is poorly constrained. Directly detected mobile species that may supply polar cold traps are limited only to LADEE's methane and water measurements; other data, such as the varying 3 μm band are suggestive, but not definitive of the presence of mobile water.

The Violent Middle Ages: Looking farther into the past, the impact rate was dramatically higher and impacts of large comets and wet asteroids were common. During impact, the constituent ices of an asteroid or comet nucleus vaporize; a significant part of this vapor remains gravitationally bound to the Moon, possibly transforming the tenuous, collisionless lunar exosphere into a collisionally thick, transient atmosphere [7,19] that may provide very large inputs to the lunar system. The importance of volatile contributions from lunar volcanic eruptions has only recently been recognized [6], with temporary atmospheric pressures estimated to exceed 1% terrestrial and collisional lifetimes in the 10's of millions of years. Reconciling these two potential sources of thick, ferociously reactive water vapor atmospheres with the properties of lunar soil has yet to be done, but the likelihood of large inputs of volatiles into the lunar system seems inescapable.

The implications of such temporary atmospheres has barely been touched. The atmospheric heat transport may drastically increase the temperature of the polar cold traps, and drastically reduce the diurnal surface temperature contrast. Alternatively, the collisional atmosphere may be difficult to develop as from its outset it is subject to collapse upon the entire 100 K night side cold trap, with sunrise subjecting the mass of volatiles piecewise to photochemical loss. Regardless, from a thermophysical standpoint, during these high flux volatile inputs, the Moon would be an utterly different place.

During this era, the vigor of the impact rate also caused the regolith itself to be a significant volatile sink that may interrupt flows to the poles. Even assuming the current abundance of about 100 ppm, the regolith could sequester about 500 km^3 of molecular water, approximately the volume of water ice possibly stored in permanent shadow in the upper meter at 1 wt. % abundance. The impact and volcanic volatile contributions dwindled over time and the formation of the cold traps themselves may have post-dated most of the activity [20]. If there were once thick ice sheets in the PSRs, those have eroded, presumably by impacts [21].

The Beginning of History: Via the volcanic eruption route, the polar cold traps may have been partly supplied by the Moon's internal water. There is some access to the inferences about initial inventory through measurement of the volatile abundance of volcanic glasses, and remote measurements of water contents of deeply derived geologic units.

Conclusion: Throughout lunar history, volatile sources and cycles have provided potential supplies to the lunar poles, but many first order aspects remain unmeasured or only incompletely measured and much remains to be understood.

References: [1] Saal, A. E., E. H. Hauri, M. L. Cascio, J. A. van Orman, M. C. Rutherford, and R. F. Cooper (2008), Nature, 454, 192–195, doi:10.1038/nature07047. [2] Pieters CM, Goswami JN, Clark RN, Annadurai M, Boardman J, Buratti B, Combe JP, Dyar MD, Green R, Head JW, Hibbitts C, science. 23; 326(5952):568-72, 2009. [3] Clark RN. Science. 23;326 (5952):562-4, 2009. [4] Sunshine JM, Farnham TL, Feaga LM, Groussin O, Merlin F, Milliken RE, A'Hearn MF. Science. 23;326(5952):565-8, 2009. [5] Colaprete, A., P. Schultz, J. Heldmann, et al. [2010], Science, 330, 463-468. [6] Needham DH, Kring DA. EPSL. 2017;478:175-8. [7] Berezhnoi, A.A., Klumov, B.A., 2000. Explor. Util. Moon, 175–178. [8] Zeller, E.J. , Ronca, L.B. , Levy, P.W. ,1966. JGR. 71, 4 855–4 860. [9] Housley, R.M., R.W. Grant, and N.E. Paton, Proc. Lunar Sci.Conf., 4th, 2737-2749, 1973. [10] Wieser, M. et al. Planet. Space Sci. 57, 2132-2134, 2009. [11] Hodges, R. R. GRL. VOL. 38, L06201, doi:10.1029/2011GL046688, 2011. [12] Starukhina, L. JGR. 106, 14,70-14,710, 2001. [13] Hurley, D. M. et al. 10.1016 /j.icarus.2016.04.019, Icarus 283, 31-37, 2017. [14] Bandfield JL, Poston MJ, Klima RL, Edwards CS. Nature geoscience. 2018 Mar;11(3):173. [15] Benna M, Hurley DM, Stubbs TJ, Mahaffy PR, Elphic RC, LPI Contributions. 1863:2059, 2015. [16] Hodges RR. GRL. 2016 Jul 16;43(13):6742-8. [17] Hoffman JH, Hodges Jr RR, Johnson FS, Evans DE. In Lunar and Planetary Science Conference Proceedings 1973 (Vol. 4, p. 2865). [18] Gladstone, G. R., et al., Science 330, 472-476, 2010. [19] P. Prem, N.A. Artemieva, D.B. Goldstein P.L. Varghese, L.M. Trafton, Icarus 255 (2015) 148–158. [20] Siegler MA, Bills BG, Paige DA. JGR: Planets. 2011 Mar 1;116(E3). [21] Crider, D. H., and R. R. Vondrak. Adv. Space Res. 31 (11): 2293-2298, 2003.

THE LUNAR POLES: WHAT REMAINS TO BE DONE. P.G. Lucey[1]; D. Hurley[2]; W. Farrell[3], N. E. Petro[3]; M. Cable[4]; K. Hibbitts[2], C. I. Honniball[1], S. Li[1]. [1]University of Hawaii at Manoa, Honolulu HI (lucey@higp.hawaii.edu), [2]Johns Hopkins University Applied Physics Laboratory, Laurel, MD, [3]Goddard Space Flight Center, Greenbelt, MD, [4]Jet Propulsion Laboratory, Pasadena, CA,

Introduction: "Every revolution starts with a man with a vision." [1] In this case, the vision was that of Robert Goddard, who in 1912 teased about the importance of cold trapped volatiles for a lunar polar base [2]. Urey [3] explicitly noted the importance of the small lunar obliquity in creating polar cold traps, and Watson et al. [4] began the scientific study of the poles in earnest. Fast forward to today, where measurements using Clementine, Lunar Prospector, Galileo, Cassini, Chandrayaan-1, Kaguya, MESSENGER, Dawn and LRO as well as groundbased radar and infrared observations have all made major contributions to understanding lunar polar science, either directly or via comparative planetology. But while have have been there, and we have done that (at least something), are we done?

What We Know With Reasonable Certainty: These conclusions are based on strong, relatively uncontroversial and unambiguous evidence:

The poles are cold[5]. Hydrogen is concentrated there [6]. Water ice and other volatiles are present in the shallow lunar subsurface at the LCROSS impact site [7]. The optical surfaces of regions of permanent shadow are physically or compositionally distinct from regions that receive some illumination [8] Water is present in the lunar atmosphere associated with meteorite impacts thus available for transport [9]. Similarly, methane is present in the lunar atmosphere, strongly responding to diurnal temperature variations [10]. Substantial water ice is found in the analogous environment at a pole of Mercury[5], but similar thick ice deposits are not present at the lunar poles[11]. Surface ice is present at the coldest places on Mercury[5]. There is an excellent correlation of temperature and ice distribution on Mercury, and a very poor correlation on the Moon.

What We Know With Reasonable Uncertainty: These conclusions are based on data with significant ambiguities or unknowns, conclusions may rely upon multiple data sets, but there may be contradictory evidence, or methodologies are immature.

Surface ice is present at the lunar poles in permanent shadow[12]. UV, IR multispectral properties and reflectance coupled with temperature properties strongly indicate the presence of patchy surface ice. However, no evidence of ice is found in high signal to noise ratio direct imaging using scattered light[13].

Buried ice is present at Cabeus based on radar properties. Some indications are present, but some data sets are contradictory[14].

A hydrogen-bearing species varies in abundance on the illuminated surface with lunar time of day, temperature and latitude [15]. However, strong arguments are published that argues that the observed spectral variation is an artifact of lunar thermal emission that is also correlated with lunar time of day, temperature and latitude[16].

What We Do Not Know With Any Certainty: The abundance of molecular water on the illuminated surface or the lunar night side. It may be zero.

The fraction of hydrogen in the solar wind that is available for surface chemistry. Thermal hydrogen reflected or emitted from the surface is unmeasured but together with other hydrogen could constitute the entire solar wind input of hydrogen, leaving none or trivial amounts for production of mobile water.

The relative effect of coronal mass ejections and quieter solar wind.

The mineralogical siting of hydrogen bearing compounds in key geologic settings.

The flow of atmospheric species toward the poles, if any.

The chemistry of hydrogen in the lunar surface. Several pathways are possible and accessible to laboratory experiment, but uncertainties about hydrogen inputs, and hydrogen species in the surface provide few constraints on experiment and theory.

The dynamics of the interaction of the solar wind with the surface. The solar wind varies over extremely short timescales. There are important existing measurements, but they are snapshots and rarely coincident.

The isotopic composition of ice at the poles.

The distribution of surface ice at the poles.

What We Would Understand If The Known Unknowns Were Known: The importance of solar wind in supply to the poles; the mass flow of volatiles to the poles; the chemistry of hydrogen in the lunar surface and by extension other planets; the interaction of solar wind with surfaces at short timescales; strong constraints on the sources of polar ice.

How To Get At The Known Unknowns:

Orbital measurements

Ice maps Definitive maps of surface water ice distribution could be obtained using laser spectrometers in key ice absorptions (e.g. Lunar Flashlight [17]) or extremely sensitive passive infrared spectrometers de-

signed to obtain high quality data in scattered light from nearby topographic highs. Laser spectrometers suffer from limited field of view so long mission lengths are required for comprehensive coverage. Passive spectrometers have much greaters fields of view, but the colder polar locations may not feature sufficient illumination for required signal to noise ratios. A combined instrument suite would exploit the advantages of both techniques and mitigate their weaknesses in terms of comprehensive coverage.

Time varying water/hydroxyl abundance. Definitive measurements of global day/night water/hydroxyl abundance can be obtained by a laser spectrometer operating at 3 microns in a few bands. These measurements would be free of thermal contribution, and so pure reflectance data could be obtained at a uniform viewing geometry similar to LOLA or MLA reflectance measurements.

Presence of molecular water. Definitive detection of molecular water can be done with a emission spectrometer operating at 6 μm. The water molecule's H-O-H bend, occurs at 6.07 μm. At 6 μm the ratio of thermal to reflected signal is 1000 times greater than at 3 μm. An observed 6 μm feature must be due to molecular water as hydroxyl contains no vibrational features at this wavelength (except bonded to H). A proof of concept experiment using an high altitude telescope (balloon or aircraft) would be prudent.

Buried water ice. A bistatic radar mission (two radar spacecraft) would be able to map buried, provided LRO experimental issue can be resolved.

Hydrogen Budget. The missing, possibly very large, H component is neutral thermal and slightly energetic hydrogen. This component is susceptible to measurement by UV spectroscopy or imaging (LAMP was not designed to make this measurement, but it was carried out by MESSENGER).

Dynamics of the solar wind and its products. This would use a Maven-like instrument suite that measures in real time the downwelling solar wind, and the upwelling components including hydrogen in its various energy ranges, OH, and water.

Polar exospheric flows. Exospheric instruments placed in polar orbit with sufficient mission lifetime to bin data in latitude and time of day would characterize any movement of volatiles tending toward the polar cold traps.I

Isotopic measurements of polar ice A LADEE-like dust detector, coupled with a mass spectrometer capable of D/H ratio measurements could potentially capture icy grains lofted by impacts into permanent shadow. Count rates would be low owing to the small area of the permanent shadow, but several detections would be expected per year.

LCROSS-like impact experiments

A host of experiments could be carried out with impactors of various sizes as studied by [18]. For example, a microwave spectrometer could plausibly measure oxygen isotope ratios of water vapor release in a targeted impact.

Landed experiments

If the known patchiness of surface ice could be overcome through measurement or other mitigation, landed experiments such as Resource Prospector would address many, but not all science questions. In particular, the role of solar wind would not be solved by a landed package. On the other hand, atmospheric experiments on the edges of polar cold traps over a diurnal cycle would be extremely useful.

Conclusions: Much has been learned about the polar cold traps in the measurement era that began with radar observations of Mercury's poles and continues today with groundbased IR measurements of lunar water, but extremely vexing questions remain, such as the explanation for the stark difference between the poles of the Moon and Mercury.

References: **[1]** Bixby, J. "Mirror Mirror", Star Trek, Paramount Pictures, 1966. [2] Goddard, E.C., Pendray, G.E. (Eds.), 1970. The Papers of Robert H. Goddard. McGraw- Hill, New York, NY. [3] Urey, H. C. (1952), The Planets: Their Origin and Development, 245 pp., Yale Univ. Press, New Haven. [4] Watson, K., H. Brown, and B. Murray (1961a), JGR 66, 1598–1600, doi:10.1029/JZ066i005p01598. [5] Paige DA, et al. science. 2010 Oct 22;330(6003):479-82. [6] Feldman WC et al. Science. 1998 Sep 4;281(5382):1496-500.; Mitrofanov IG, et al. science. 2010 Oct 22;330(6003):483-6. [7] Colaprete, A., P. Schultz, J. Heldmann, et al. [2010], Science, 330, 463-468. [8] Gladstone GR, et al. JGR: Planets. 2012 Dec 1;117(E12).. [9] Benna M, Hurley DM, Stubbs TJ, Mahaffy PR, Elphic RC, LPI. 1863:2059, 2015. [10] Hodges, R. R. GRL. VOL. 38, L06201, doi:10.1029/2011GL046688, 2011. [11] Stacy NJ, Campbell DB, Ford PG. Science. 1997 Jun 6;276(5318):1527-30. [12] Hayne PO, et al. Icarus. 2015 Jul 15;255:58-69. [13] Koeber SD, Robinson MS, Speyerer EJ. In LPSC 2014 Mar (Vol. 45, p. 2811). [14] Patterson GW, et al. Icarus. 2017 283:2-19. [15] Sunshine JM, et al. Science. 23;326(5952):565-8, 2009 [16] Bandfield JL, Poston MJ, Klima RL, Edwards CS. Nature geoscience. 2018 Mar;11(3):173. [17] Cohen BA, et al.. Payload Design for the Lunar Flashlight Mission. [18] Hayne P, Ingersoll A, Paige D. Keck Institute for Space Studies. nd Web. 2017 Apr.

COMETS: A POSSIBLE SOURCE OF LUNAR VOLATILES IN LIGHT OF ROSETTA. A. Luspay-Kuti[1] and K. E. Mandt[2], [1]TBD (aluspaykuti@gmail.com), [2]Johns Hopkins University Applied Physics Laboratory, Laurel, MD 20723

Introduction: The discovery of volatiles in the lunar polar region by recent spacecraft missions has revolutionized our understanding about the evolution of the Moon. The LCROSS impact experiment provided the strongest compositional evidence for water and other volatiles in potentially useful abundances in the permanently shaded regions (PSRs) at Cabeus crater [1]. Also, substantial deposits of volatiles may be present in other PSRs throughout the polar region of the Moon where temperatures are among the coldest in the solar system [2]. However, the origin and sources of these volatiles are currently poorly known.

Comets, on the other hand, are volatile rich, and contain the best-preserved material from the time of before and after planet formation. Interestingly, the same volatiles identified in Cabeus crater by LCROSS have also been detected on a number of comets [3], which may imply that comets are potentially an important source of lunar volatiles. The Earth-Moon system may have received delivery of volatiles by comets during the initial stages of planetary differentiation. Thus, comparative studies of volatiles on comets with lunar volatiles may help understand the composition and origin of volatiles on the Moon.

Method: When it comes to comets, the Rosetta mission of the European Space Agency provides an unprecedented view into the spatial distribution and temporal variation of sublimated volatile ices on a comet. Rosetta orbited comet 67P/Churyumov-Gerasimenko (67P/C-G) for the first time, which provides an unprecedented view into the spatial distribution and temporal variation of sublimated volatile ices on a comet. Orbiting and 'chasing' a comet from farther than 3 au through perihelion and after provided a unique quality of Rosetta that cannot be captured by flybys or ground-based observations. Hence, Rosetta measurements allow for a better characterization of the cometary volatile inventory versus just a snapshot of volatile concentrations at a particular place in the orbit.

The Rosetta Orbiter Spectrometer for Ion and Neutral Analysis (ROSINA) instrument package onboard Rosetta measured the spatial and temporal composition of the coma of 67P/C-G. Even early measurements by ROSINA showed that the abundances of volatile species relative to water can vary over a wide range as a function of longitude and latitude [4, 5, 3]. These variations and changes over time as the comet orbits the Sun provide a more detailed insight into the volatile composition of 67P/C-G, and indicates the complexity when measuring volatile abundances of other comets via flybys and/or remote sensing.

In this work, we will provide an overview of cometary volatiles, the observed temporal and spatial outgassing pattern of volatiles in 67P/C-G. We will compare the volatile abundances relative to water to the LCROSS observations, which may establish a potential link between lunar and cometary volatile species.

References: [1] Colaprete A. et al. (2010) *Science, 330,* 463–468. [2] Paige D. A. et al. (2010) *Science, 330,* 479-482. [3] Le Roy L. et al. (2015) *A&A, 583,* A1. [4] Hässig M. et al. (2015) *Science,* 347. [5] Luspay-Kuti et al. (2015) *A&A, 583,* A4.

AN ULTRAVIOLET SPECTROSCOPIC INVESTIGATION OF EXPOSED FROST IN LUNAR PERMANANTLY SHADOWED REGIONS FROM THE LUNAR RECONNAISSANCE ORBITER. L. O. Magaña[1,2] and K. D. Retherford[2,1], [1]University of Texas at San Antonio, Physics and Astronomy Department, San Antonio, TX 78249 [2]Southwest Research Institute, Space Science and Engineering Division, San Antonio, TX 78238 (lizeth.magana@swri.org)

Introduction: The Lunar Reconnaissance Orbiter's (LRO) Lyman Alpha Mapping Project (LAMP) uses the all-sky Lyman-alpha glow and ultraviolet (UV) bright stars to produce global brightness and albedo maps of the lunar surface. Maps are generated in far UV wavelength range of 57-196 nm including the Lyman-α spectral band (119-125 nm), On-band (130-155 nm), and Off-band (155-190 nm). The "on" and "off" wavelength bands refer to on and off the ~165 nm water absorption band [1,3]. These maps are therefore ideal for constraining the abundance of water frost [2]. LAMP night-side albedo data over South Pole PSRs from the first 18 months indicate a 1-2% water frost abundances [1].

In this work, we accumulate LAMP monthly spectral maps to produce albedo and brightness maps in the Lyman-alpha, On, and Off wavelength bands. We integrate data from the start of the mission, 2009, through 2016. We investigate the spectral properties of South Pole lunar craters Shoemaker, Haworth, and Faustini, and search for water frost absorption signatures. Here we report initial results of far UV investigations of craters, Faustini, Shoemaker, and Haworth using LAMP data from 2009 to 2016.

FUV Investigations of Faustini, Shoemaker, and Haworth: We present Lyman-alpha albedo maps of the lunar south pole and craters Faustini, Shoemaker, and Haworth. We construct Lyman-alpha albedo maps of the lunar south pole, such as the one shown in Figure 1 by summing LAMP data from the start of the mission through October 2016. Similarly, we produce On-band and Off-band maps of the South Pole, Faustini, Shoemaker, and Haworth. We extract spectra from the corresponding albedo maps for each of the specified regions.

We analyze LRO-LAMP ultraviolet albedo spectra for evidence of exposed frosted volatiles within south pole craters Faustini, Shoemaker, and Haworth. Spectral features consistent with the presence of water frost include: decreasing Lyman-alpha albedo, decreasing On-band albedo, and increasing Off-band albedo. In addition, since Off-band refers to regions with strong water absorption (albedo near unity) while On-band refers to regions with low absorption (albedo near zero), we expect to find high Off-band/On-band ratios for regions where water frost exists on the lunar surface [1,3].

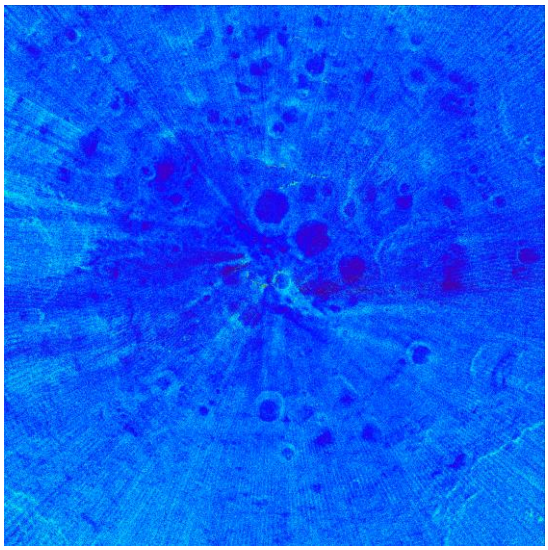

Figure 1- Lyman-alpha albedo map of the lunar south pole produced using LAMP data from 2009 to 2011.

References: [1] Gladstone, G. R. et al. (2012) Far-Ultraviolet Reflectance Properties of the Moon's Permanently Shadowed Regions, *J. Geophys. Res.*, *117*, E00H04. [2] Gladstone, G. R., et al. (2010) LAMP: The Lyman Alpha Mapping Project on NASA's Lunar Reconnaissance Orbiter Mission, *Space Sci. Rev.*, *150*, 161-181. [3] Hayne, P. O. et al. (2015) Evidence for Exposed Water Ice in the Moon's South Polar Regions from Lunar Reconnaissance Orbiter Ultraviolet Albedo and Temperature Measurements, *Icarus*, *255*, 58-69.

COMETS AND METEORITES AS SOURCES OF LUNAR POLAR VOLATILES. K. E. Mandt[1] and A. Luspay-Kuti[2], [1]Johns Hopkins University Applied Physics Laboratory, Laurel, MD 20723 (Kathleen.Mandt@jhuapl.edu), [2]TBD.

Introduction: Lunar polar volatiles have originated from a variety of sources over the history of the Earth-Moon system. One source is comets and meteorites that impact the surface of the Moon and vaporize, releasing volatiles that migrate to the poles. The relative contributions of comets and meteorites compared to other volatile sources has varied over time with the impact rate. This means that the relative amount of volatiles from comets and meteorites delivered in the past was much greater than in the present time. Therefore, the relative source of volatiles in the Lunar polar regions will vary spatially and with depth. Of particular interest to this source of volatiles is the connection between delivery of volatiles to the Moon and to the Earth.

Several studies have compared the volatile composition of the Earth with that of comets and meteorites, and recent studies conclude that CI and CM carbonaceous chondrites are the primary source of Earth's water based on the Hydrogen and Nitrogen isotopes, or D/H and $^{14}N/^{15}N$ [1]. A similar conclusion has been made for the Moon based on analysis of D/H in Lunar volcanic glasses and melt inclusions [2]. Additionally, recent mass balance studies of volatile sources for the Moon using D/H and $^{14}N/^{15}N$ measurements also conclude that chondrites are the main source of water for the bulk water content of the Lunar interior and, by extension for the Earth [3].

Volatiles stored in the cold traps in the Lunar polar regions are of particular value for mapping out a timeline of volatile delivery to the Earth-Moon system. We will review the composition tracers for comets and meteorites that can be used by future missions to the Permanently Shadowed Regions (PSRs) to evaluate the history of volatile delivery to the Moon.

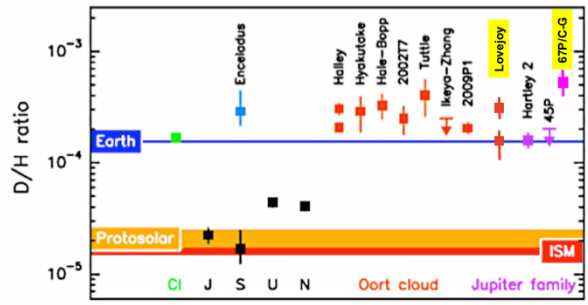

Figure 1: Measurements of D/H throughout the Solar System [adapted from 4]. CI Chondrites and the Earth have similar values, while the most reliable comet observations are enriched in Deuterium.

Composition: The isotopic composition of comets and meteorites provide tracers that could be used by a lander and/or rover in the PSRs to determine the source of volatiles spatially and with depth. Two important tracers are the D/H and $^{14}N/^{15}N$ ratio. In Figs. 1 & 2 we illustrate the D/H and $^{14}N/^{15}N$ ratios measured in comets and CI Chondrites compared to the Earth and other solar system bodies. Measuring the D/H and $^{14}N/^{15}N$ in polar volatiles spatially and with depth can be a valuable method for determining the dominant source of volatiles as a function of time.

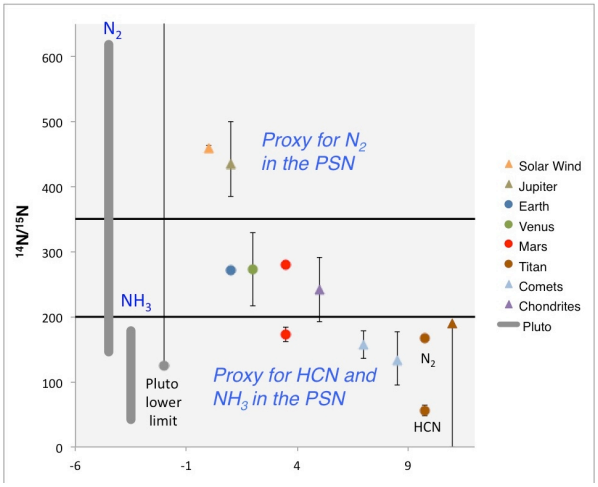

Figure 2: Nitrogen isotope ratios measured throughout the solar system [from 5].

References: [1] Alexander C. M. O'D. (2017) *Phil. Trans. R. Soc. A., 375,* 20150384. [2] Saal A. E. et al. (2013) *Science, 340,* 1317 – 1320. [3] Barnes, J. J. et al. (2016) *Nature Communications, 7*, 11684. [4] Lis D. C. et al. (2013) *ApJL, 774*, L3. [5] Mandt K. E. et al. (2017) *MNRAS, 472,* 118 – 128.

Lunar Regolith Geochemistry Variation May Explain the Polar Wander Observations. T. P. McClanahan[1] (timothy.p.mcclanahan@nasa.gov), I. Mitrofanov[2], W. V. Boynton[3], G. Chin[1], M. Litvak[2], T. Livengood[5], A. Sanin[2], R. D. Starr[4], J. Su[4], D. Hamara[3], K. Harshman[3], A. Parsons[1], [1]NASA Goddard Space Flight Center, Bldg. 34 Room W218, Greenbelt, MD 20771 USA. [2]Institute for Space Research, Moscow, Russia, [3]Lunar Planet. Lab., University of Arizona, Tucson AZ USA, [4]The Catholic University Wash. D.C. USA, [5]University of Maryland, College Park MD USA.

Introduction: In this study we will report preliminary results from our evaluation of the polar wander observation and hypothesis [1]. For the neutron-specific part of the study we will use recently recalibrated observations from the Lunar Reconnaissance Orbiter's Lunar Exploration Neutron Detector (LEND) [2-4]. We will examine these observations in the context of temperature observations from the Lunar Reconnaissance Orbiter's (LRO) Diviner radiometer, altimetry data from LRO's Lunar Observing Laser Altimeter and near-infrared observations from the Moon Mineralogy Mapper onboard Chandraayan-1 [5-7]. In particular, we examine the possibility that regional geochemistry variations provide an alternative explanation for the spatial distribution of the polar epithermal neutron flux and the polar wander observation.

Background: The polar wander hypothesis originates from the identification of antipodal suppressions of the lunar epithermal neutron emission flux, which is thought to indicate the greatest concentrations of hydrogen-bearing volatiles (possibly water ice) near each pole, as detected in Lunar Prospector Neutron Spectrometer (LPNS) observations [1,8]. Theoretical studies suggest that water ice concentrations near the surface are maximized in stable cryogenic temperatures < 110 K, which are conditions found exclusively on the lunar surface in the polar permanently shadowed regions. [9,10]. A suppression in the epithermal neutron emission flux, relative to a region considered to be anhydrous, is consistent with an enhanced concentration of hydrogen-bearing volatiles.

The surprising aspect of the polar wander finding is that the locations of the maximum hydrogen-bearing volatile concentrations at each pole are nearly antipodal, each distant from the pole by approximately 5.5° degrees of latitude, near Cabeus crater in the south and Rozhdestvensky U crater in the north. Furthermore, the polar spatial distribution of the epithermal neutron flux is not strongly consistent with modeled water ice distributions, which indicate that the ice should be concentrated around the poles.

From the antipodal off-polar alignment of the highest-concentration hydrogen deposits it was postulated that at some past time, the poles shifted to their present locations from their paleo-locations at Cabeus and Rozhdestvensky U. Regolith thermal modeling performed for the study [1] indicates that water-ice under the paleo-pole regime became embedded in the regolith and that a remnant of the past water-ice distribution remains, admixed with more recent accumulations of water ice, yielding the present polar spatial distribution of epithermal neutron flux, as detected in the LPNS epithermal neutron flux observations.

A preliminary review of the recalibrated LEND observations is generally consistent with the LPNS findings of the off-pole location of the neutron suppressed regions, though initial review of the LEND results suggests that the magnitude of the neutron suppression at Cabeus may not be as relatively strong in comparison to the other south polar neutron suppressed regions.

Results: From our review of the related studies and our recalibrated LEND observations, we suggest that regolith geochemistry variations may, at least partially, explain the polar wander observations. A key point is that the Moon's neutron emission flux is sensitive not only to hydrogen-bearing volatiles, but also to temperature and geochemistry variation [11,12]. Regolith geochemical variation can cause the energy distribution of the neutron emission flux to vary because the average neutron scattering cross section of the regolith can vary with geochemistry. We suggest that the magnitude of the epithermal neutron flux may be relatively elevated in regions of more mafic geochemistry when compared to the feldspathic highlands geochemistry. Our hypothesis is that near the poles, the expected polar suppression of epithermal neutron flux is being masked by an enhanced neutron emission flux from nearby mafic regions.

For both the north and south poles, the LEND and LPNS observations similarly indicate that the suppression of the epithermal neutron flux is shifted away from the pole and away from regions of more mafic composition. LEND and LPNS polar stereographic thermal neutron maps show consistent flux spatial.

Figure 1 compares the LEND's south polar stereographic maps of A. thermal, B. background subtracted thermal and C. epithermal neutron flux maps against the D. LOLA map of topography [2,6]. Neutron suppressed regions (*dark*) in the epithermal neutron maps may indicate high concentrations of hydrogen

volatiles, which are shifted away from the pole and located towards highland terrain (*blue*). The LEND thermal neutron maps show geochemically distinct regions, which intersect near the south pole and are defined by the low thermal neutron flux in the more mafic South Pole Aitken (SPA) Basin (*blue*) and the higher thermal flux that originates from the Schroedinger crater basin, which is further enhanced towards feldspathic highlands terrain.

North pole results (not shown) indicate a similar relationship. There the suppression of the epithermal neutron flux is shifted away the pole and away from the mafic mare.

Geochemically dependent variations in hydrogen-bearing volatile concentrations may also influence the observation - if the production, migration and regolith storage of hydrogen-bearing volatiles differs for mafic vs feldspathic regions. Studies of near infra-red observations of the mare and the South Pole Aitken basin have indicated that globally, less hydroxyl (detectable by neutron spectrometers), is available in the more mafic regions [13,14]. In this case the lunar emission flux from the more mafic regions is elevated because those regions are relatively anhydrous.

Conclusions: The key point in these studies is that: if regional regolith geochemistry or any other non-hydrogen dependent variations are even partially responsible for the spatial distribution of the epithermal neutron flux near the poles, then key provisions of the polar wander hypothesis may be called into question.

To initiate our study we will review the newly-recalibrated LEND observations and examine the observational evidence for polar wander. Our ongoing work will also consider several factors that are thought to govern the Moon's neutron emission flux. We will also leverage LEND's collimated epithermal neutron sensor results in the study.

References: [1] Seigler *et al., Nat. Geo.* (2016) [2] Su *et al., Sp. Sci. Rev*. (*Submission pending*) (2018) [3] Chin *et al., Sp. Sci. Rev*. (129)-4 (2010) [4] Mitrofanov *et al. Sp. Sci. Rev*. 150(1-4) (2010) [5] Paige *et al., Sp. Sci. Rev* 150(1-4) (2010) [6] Smith *et al., Sp. Sci. Rev*. 150(1-4) (2010) [7] Pieters *et al., Science* DOI: 10.1126/science.1178658 (2009) [8] Feldman *et al., Science* DOI:10.1126/scence.281.5382.1496 (1998) [9] Watson et al, *JGR* 66-9 3033-3045 (1961) [10] Arnold *JGR* DOI: 10.1029/JB084iB10p05659 (1979) [11] Lawrence *et al., JGR* doi:10.1029/2005JE002637 (2006) [12] Little *et al., JGR* 108-E5 (2003) [13] McCord *et al., JGR* doi:10.1029/2010JE003711 (2011) [14] Klima *et al., Phil. Trans. Roy Soc*. DOI:10.1098/rsta.2015.0391 (2017)

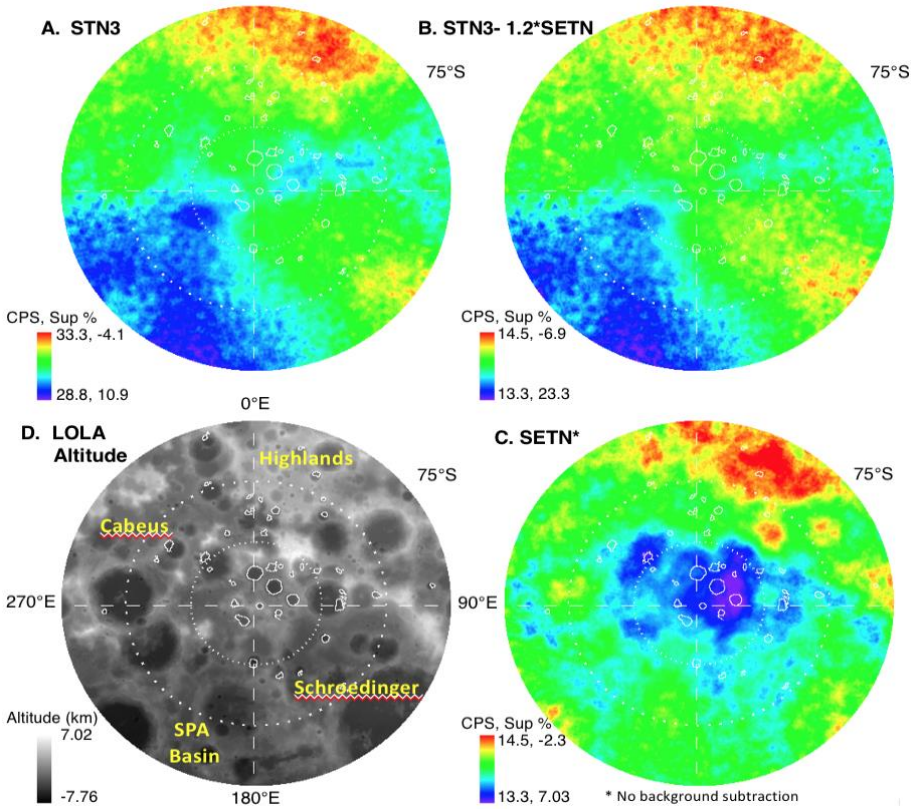

Figure 1: South polar stereographic maps of LEND's uncollimated thermal and epithermal neutron emission flux [2]. Maps A, B show LEND's thermal neutron and thermal background subtracted maps of the regional variation in regolith geochemistry between the more mafic South Pole Aitken Basin and feldspathic highlands terrain. Map C. shows LEND's uncollimated epithermal neutron flux map, showing the shifted neutron flux suppression away from the pole and the South Pole Aitken Basin. Units: counts/sec (CPS), neutron suppression % change from background.

TEMPERATURE CONSTRAINTS ON THE STORAGE AND CURATION OF VOLATILE-RICH SAMPLES FROM THE LUNAR POLES. J. L. Mitchell[1], J. E. Gruener[1], S. J. Lawrence[1], M. D. Fries[1], R. A. Zeigler[1], F. M. McCubbin[1] and J. E. Edmunson[2]. [1]Astromaterials Research and Exploration Science Division, NASA Johnson Space Center, 2101 NASA Pkwy, Houston, Texas 77058 (Julie.L.Mitchell@nasa.gov), [2]Jacobs Technology, Inc./NASA Marshall Space Flight Center.

Introduction: NASA's Lunar Exploration Campaign includes lunar sample return efforts beginning in the mid-2020s and human landed missions in the late 2020s-early 2030s **[1]**. Volatile-rich samples from the lunar poles will be high-priority targets due to their resource potential for human explorers and high science value **[2, 3]**. In order to precisely characterize the nature of these polar volatile materials upon return to Earth, they will need to be transported and curated under conditions that minimize their chemical and physical alteration.

NASA Policy Directive (NPD) 7100.10F mandates the preservation of existing extraterrestrial samples with minimal alteration, extensive and quantitative documentation of alteration that is provided to investigators, and "the development of long-range plans" for samples yet to be acquired **[4]**. This abstract summarizes new efforts by the Astromaterials Acquisition and Curation Office at JSC to assess the optimal storage conditions of lunar polar returned samples.

Background: Permanently Shadowed Regions (PSRs) at the lunar poles reach some of the coldest temperatures in the inner Solar System **[5]**. These cold temperatures are ideal for the accumulation and retention of water ice and other frozen volatiles; previous studies have estimated as much as 10 wt. % water ice at the lunar poles **[6]**. However, remote sensing instruments searching for water ice in the lunar polar regions have produced ambiguous results **[e.g., 7, 8]**.

The Lunar Crater Observation and Sensing Satellite (LCROSS), launched with the Lunar Reconnaissance Orbiter (LRO) in 2009, impacted the crater Cabeus at the Moon's south pole in an effort to assess the abundance of volatiles within that crater's PSR **[6]**. LCROSS and LRO detected numerous volatile species after the impact in Cabeus **[6]**, providing a baseline by which to estimate the composition of lunar polar volatiles (**Table 1**). It is possible that other compounds modeled by Paige et al. (2010) to be stable in PSRs but not detected by LCROSS are also present **[5]**; among these, some highly reactive species could chemically react with other volatiles and/or the lunar regolith at elevated (>50K) temperatures. For example, the reactivity of formaldehyde to produce polyoxymethylenes is catalyzed by small quantities of ammonia (as low as 0.5% relative to formaldehyde) at temperatures as low as 80K **[9]**. Additionally, ammonia and water have been modeled to react with feldspars at temperatures as low as 200K, resulting in alteration of both the volatile compounds and silicate mineral **[10]**. These previous results indicate that storage temperatures <200K may be needed to prevent alteration of the sample immediately after collection, during transit to Earth, and during curation operations on the ground.

Methods: *Lunar Simulant Development*. A lunar polar sample simulant is being developed that includes a range of volatile compositions. A subset of volatiles detected by LCROSS are included (H_2O, NH_3), while the others (H_2S, SO_2, C_2H_4) are excluded from this initial work for safety reasons. These volatiles are substituted by other compounds that fall within the same thermal stability range as the known compounds based on previous modeling efforts (**Figure 1 and Table 1**); in the case of CO_2 and CH_3OH, these were detected by LCROSS, but at low abundance (≤2.5% relative to water). The exact volatile simulant composition is shown in **Table 1**.

Table 1. Volatiles detected by LCROSS and their relative abundances (left) **[5]**; lunar volatile simulant compounds and relative abundances (right).

LCROSS[5,6]		**Simulant**	
Compound	%	Compound	%
H_2O	77.4	H_2O	75
H_2S	13.0	CO_2	15
NH_3	4.7	NH_3	5
SO_2	2.5	CH_2O	2.5
C_2H_4	2.4	CH_3OH	2.5

Remote sensing investigations indicate that volatiles do not exist as clean, distinct layers, but are intimately mixed with lunar regolith **[e.g., 1]**; we replicate this property by preparing the volatile component of the simulant in the presence of an experimental agglutinate-bearing simulant with an OB-1 base, a lunar highlands-type silicate simulant (**Figure 2**) **[12]**. The relative abundances of volatiles in the simulant will be verified by GC-MS.

Storage Tests. Once the volatile/regolith simulant is prepared, aliquots of the simulant will be stored in sealed vials at -20°C and -80°C for one month; this duration is estimated to encompass the time needed for collection, transit, and initial ground characterization of the sample. Silicate-only and silicate-water mixtures

will be prepared using the same procedure and concurrent to the full simulant; these mixtures will serve as control samples for the duration of the test. During the one-month period of time, aliquots will be removed from storage and the volatile composition measured by GC-MS at 0, 1, 5, 10, 15, 20, 25, and 30 days. Particles of the simulant component will be analyzed for compositional and textural changes using FTIR, Raman spectroscopy, SEM, and TEM.

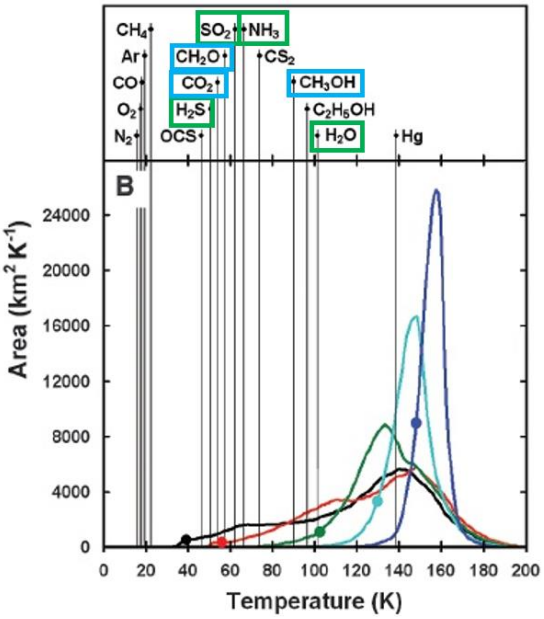

Figure 1. Expected volatiles in lunar PSRs under the temperature range observed by the Diviner instrument (adapted from **[5]**). Green boxes=volatiles detected by LCROSS at >2.5%; blue boxes=additional volatiles included in lunar polar volatile simulant.

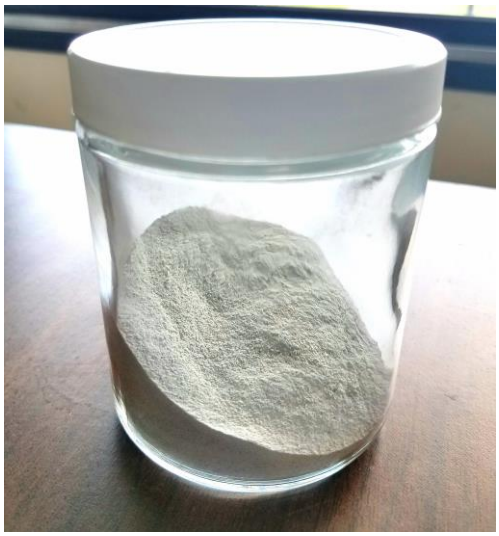

Figure 2. The experimental agglutinate-bearing, OB-1 base lunar highlands-type simulant.

Results and Future Work: Which reaction products are generated, their rates of reaction, and the effect on the silicate fraction of simulant will be quantified. All of these properties will be assessed as a function of temperature. PSRs have significantly lower temperatures than -80°C; therefore, cryogenic temperatures may be needed for future storage tests. However, the technology for pristine, sterile sample handling at cryogenic temperatures does not currently exist; this study will constrain the timescale at which lunar polar volatile samples can be handled in the laboratory at elevated (up to -20°C) temperatures without significant alteration of the sample.

While feasible for ground storage, achieving cryogenic temperatures in flight for a lunar surface sample return system would be cost-prohibitive. This study will therefore provide insights into sample alteration at higher temperatures (up to -20°C) that could be used to drive future spaceflight hardware requirements.

Future studies will incorporate the full suite of LCROSS-detected volatiles, which includes H_2S, SO_2, and C_2H_4. These compounds are highly flammable and/or reactive relative to the other compounds included in this study. Therefore, specific precautions and materials considerations will need to be taken prior to beginning this phase of work.

Once the storage test procedure has been refined and a robust testing protocol developed, future studies will incorporate Apollo lunar regolith instead of simulant to assess the impact of compositional variations between the simulant and lunar highlands regolith (well described in **[12]**). The results of this work will pave the way for accurately assessing volatile resource availability and maximizing the scientific return of future lunar polar sample return missions.

References: [1] Lunar Exploration Campaign, NASA, 2018. [2] Committee on the Scientific Context for Exploration of the Moon (2007). [3] Spudis, P. D. and Lavoie, A. R. (2011) *AIAA, 2011-7185*. [4] McCubbin, F. M., et al. (2016) *LPSC* XLVII, Abst. #2668. [5] Paige, D. A., et al. (2010) *Science, 330, 6003*. [6] Colaprete, A., et al. (2010) *Science, 330, 463*. [7] Sanin, A. B., et al. (2012) *JGR, 117*. [8] Siegler, M. A., et al. (2016), *Nature, 531, 7595, 480-4*. [9] Schutte, W. A., et al. (1993), *Science, 259, 5098, 1143-1145*. [10] Engel, S., Lunine, J. I., and Norton, D. L. (1994) *JGR 99*, E2. [11] Mitchell, J. L., et al. (2017) *PSS*, in press. [12] Battler, M. M. and Spray, J. G. (2009) *PSS* 57, 2128-2131.

A VOLCANIC SOURCE FOR LUNAR POLAR VOLATILES. D. H. Needham[1], D. A. Kring[2], [1]Marshall Space Flight Center (MSFC), 320 Sparkman Drive, Huntsville, AL 35805, debra.m.hurwitz@nasa.gov, [2]Center for Lunar Science and Exploration, Lunar and Planetary Institute, 3600 Bay Area Boulevard, Houston, TX, 77058, kring@lpi.usra.edu.

Introduction: Hydrogen-bearing volatiles trapped in lunar polar Permanently Shadowed Regions (PSRs) are frequently attributed to the accumulation of solar wind and asteroid/comet material delivered to the lunar surface. However, recent work [1] has demonstrated that a substantial mass of volatiles would have been released during the eruption and emplacement of lunar mare basalts. These results require the inclusion of internally derived volatiles in models of sources for the polar volatile deposits in lunar PSRs.

Volcanoes as a Source for Lunar Volatiles: Using mare volume estimates of each basin (Table 1) determined from Lunar Prospector (LP, [2-3]), Clementine [4], Lunar Orbiter Laser Altimeter (LOLA), and Gravity Recovery and Interior Laboratory (GRAIL [5]) data, and using crater size frequency-derived ages of surface mare units [5,6], we determined the volume of mare basalts released as a function of time (Fig. 1). These surface units represent the final stages of mare emplacement and, thus, are interpreted to post-date any underlying mare. We estimate the volume of the underlying mare as the difference between the total mare for a given basin and the volume of the mapped surface flows. Although the ages of these underlying basalts are not known, they are at least as old as the oldest surface unit.

Most mare was emplaced between 3.1 Ga and 3.8 Ga, with the largest volumes emitted ~3.5 Gyrs ago. The largest contributors to the erupted volumes include basalts emplaced within Serenitatis basin (peak at 3.8 Ga), Imbrium, and Oceanus Procellarum basins (peaks at 3.5 Ga).

Estimates of volatile masses released during these eruptions may lead to more accurate volumae approximations of volatiles released during volcanic eruptions ~3.5 Gyrs ago. Volatile abundances in lunar pyroclastic deposits were directly measured in Apollo 15 and 17 volcanic glasses (*e.g.*, [7-9]). Volatiles

Table 1: Volume of mare in lunar basins

Basin	Area (km^2)	Thickness (m)	Volume (km^3)
Crisium [2]	156,103	2,940	458,943
Grimaldi [2]	15,359	3,460	53,142
Humorum [2]	101,554	3,610	366,611
Imbrium [2]	1,010,400	5,240	5,294,497
Nectaris [2]	64,277	840	53,993
Orientale [5]	75,975	88	13,294
Procellarum [3]	1,757,799	325	571,285
Serenitatis [2]	342,716	4,300	1,473,679
Smythii [2]	28,075	1,280	35,937
SPA [4]	206,430	varied	153,240
Tranquillitatis [3]	371,257	350	129,940

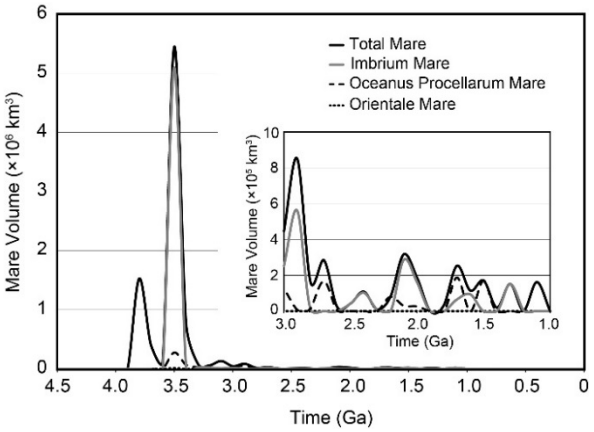

Fig. 1: Volume of erupted mare basalts as a function of time. The inset zooms in on 3–1 Ga to show the continuation of less voluminous lunar eruptions into more recent lunar history. The peak in mare volume at 3.8 Ga is primarily due to eruptions in the Serenitatis basin.

released during mare eruptions have lower concentrations than those released during pyroclastic eruptions: CO (100% liberated from parent magma, 80 – 750 ppm, [10]), H_2 (100% liberated, 0.007 – 45 ppm, [11]), H_2O/OH (85 – 99% liberated, 1.98 – 9.9 ppm, [12]), and S (90% liberated, 90 – 540 ppm, [13]).

We use these mare volatile concentrations to determine the production function of volatiles released over lunar history. Following the recent approach for quantifying volatile production in lunar pyroclastic eruptions [14], the mass of erupted lava was calculated by multiplying the estimated mare volume by the bulk density of typical mare basalt (~3.00 g/cm^3, [15]). This mass was then multiplied by the minimum and maximum contents of each mare volatile species to determine the mass range of each volatile released (Fig. 2). Peak volatile releases coincide with the largest eruption events of 3.8 Ga and 3.5 Ga.

The most prevalent volatile species released are CO ($0.2 – 2.0 \times 10^{19}$ g total) and S ($0.5 – 1.4 \times 10^{19}$ g total); H_2O is the third-most prevalent volatile released ($0.5 – 2.6 \times 10^{17}$ g total). Contents of F and Cl in mare basalts have not yet been explicitly reported and are, therefore, assumed to have been released in amounts smaller than anticipated for pyroclastic deposits (*e.g.*, less than $2 – 9 \times 10^{14}$ g of F and $0 – 4 \times 10^{13}$ g of Cl).

Discussion and Implications: After erupting, the volatiles would have been susceptible to migration towards the poles [16,17], where they would have been cold-trapped in the PSRs. If 0.1% of the total vented

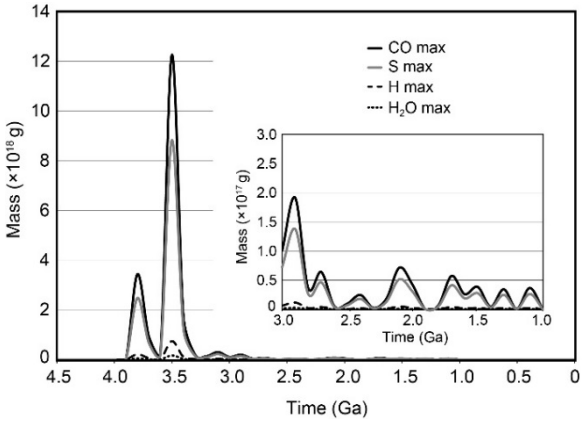

Fig. 2: Volatile mass from all mare eruptions as a function of time. The most prevalent volatile released is CO, followed by S, H, and H_2O.

mare water (calculated above to be ~10^{17} g) is trapped in PSRs, volcanically-derived volatiles could account for all of the water currently observed in lunar PSRs (*e.g.*, 10^{14} g, [18]).

Verifying the Source of Lunar Polar Volatiles: The relative contributions of indigenous and exogenous sources, such as solar wind implantation and asteroid/comet volatile delivery (Fig. 3), are still uncertain, but our results suggest transport models need to account for periods with higher indigenous fluences of volatiles to properly evaluate their contribution to PSR volatile deposits.

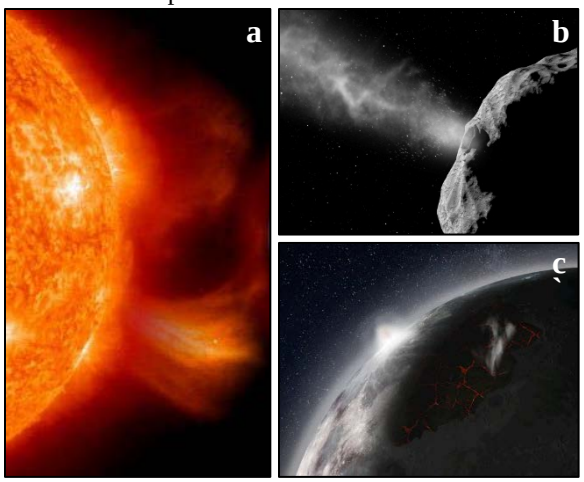

Fig. 3: Sources for lunar polar volatiles include (a) solar wind implantation (NASA), (b) asteroid and comet delivery (ESA), and (c) internal sources (NASA/MSFC).

Volatile distribution in the lunar substrate or at the lunar surface may be correlated with volatile source (Fig. 4). Solar wind implantation, as a continuous process, may result in volatiles being broadly distributed throughout the substrate and adsorbed onto the lunar surface. On the other hand, discrete impact events that delivered volatile material to the lunar

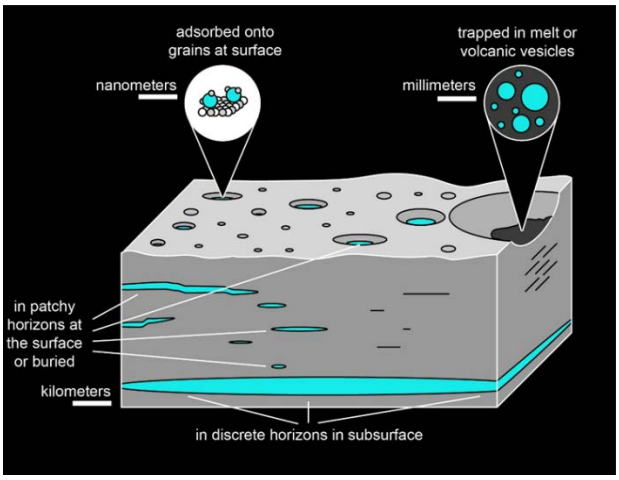

Fig. 4: Volatile distribution on the Moon may be correlated with volatile source. Continuously delivered solar wind-derived volatiles may be located at the surface, discrete impact-delivered volatiles may be concentrated in patchy horizons at or buried beneath the surface, and internally-derived volatiles may form discrete but broader horizons of volatiles in the subsurface. Modified from LPI educational graphic.

surface may generate patchy horizons of volatiles at, or buried beneath, the lunar surface. In contrast, the expected peak eruption(s) of internally-derived volatiles may lead to the formation of discrete but broader horizons of volatiles preserved in the subsurface.

These hypothesized distributions can be tested during future prospecting missions to the lunar surface. In particular, indigenous volatiles will have a distinct isotopic signature [*e.g.*, 19]. Further exploration of PSR volatile deposits, and analyses of their isotopic signatures, will help constrain the sources of lunar polar volatiles and may contribute to improving predictions of where mineable ore deposits of volatiles may exist.

References: [1] Needham, D.H. and Kring, D.A. (2017) *EPSL*, *478*, 175–178. [2] Williams, K.K. and Zuber, M.T. (1998) *Icarus*, 107–122. [3] Hörz, F. (1978) *LPSC*, 3311–3331. [4] Yingst, A.R. and Head, J.W. (1997) *JGR-P*, 10,909–10,932. [5] Whitten, J. et al. (2011) *JGR*, *E00G09*. [6] Hiesinger, H. et al. (2011) *GSA Spec. Papers*, 477, 1–51. [7] Saal, A.E. et al. (2008) *Nature*, 192–195. [8] Rutherford, M.J. and Papale, P. (2009) *Geology*, 219–222. [9] Hauri, E.H. et al. (2011) *Science*, 213–215. [10] Housley, R.M. (1978) *Proc. Ninth LPSC*, 1473–1484. [11] McCubbin, F.M. et al. (2010) *PNAS*, 11,223–11,228. [12] Robinson, K.L. and Taylor, G.J. (2014) *Nature Geosci*. [13] Shearer, C.K. et al. (2006) *Mineral. Geochem.*, 365–518. [14] Kring, D.A. (2014) *LEAG*, #3056. [15] Macke, R.J. et al. (2014) *LPSC*, #1949. [16] Watson, K. et al. (1961) *JGR*, 3033–3045. [17] Arnold, J.R. (1979) *JGR*, 5659–5668. [18] Eke, V.R. et al. (2009) *Icarus*, 12–18; [19] Barnes, J.J. et al. (2016) *Nat. Comm.*, 10.1038/ncomms11684.

PRECISION LASER SENSING OF LUNAR POLAR VOLATILES. G. A. Neumann[1], E. Mazarico[1], X. Sun[1], A. N. Deutsch[2], and P. G. Lucey[3], [1]NASA Goddard Space Flight Center, Greenbelt, MD 20771, USA. (email: gregory.a.neumann@nasa.gov), [2]Department of Earth, Environmental and Planetary Sciences, Brown University, Providence, RI 02912, USA.

Introduction: Resource utilization of hydrogen-bearing deposits will depend on precise knowledge of their abundance, depth of burial, composition, sources and sinks, and their operational accessibility. While it has long been known from neutron spectrometry that hydrogen exists at the poles of airless bodies such as Mercury and the Moon, in the latter case interpretation of radar and optical mapping has been challenging [1–3]. Debate persists as to the hydrogen's origin, mobility and chemical bonding. Sensitive methods to resolve these questions are now reaching technological maturation [4–5]. An in-house development of multi-wavelength lidar at Goddard and U. Hawaii, "Spectroscopic Infra-Red Reflectance Lidar" (SpIRRL) addresses contamination of passive spectroscopy by the competing effects of thermal emission and solar reflectance by means of a highly sensitive active measurement near 3 μm, where water absorbs strongly. Variations in 3 μm water band depth have been interpreted to be due to variation in water abundance. Reflectance measurements near 3 μm and supporting reference wavelengths can definitively answer the question of whether water detected by passive spectrometers moonwide is mobile by comparing day and night band depths which in turn constrains the supply of water to permanently shadowed regions at the poles. The 3-μm region is uniquely sensitive to the presence of all water bearing species and the instrument can characterize the abundance of water ice in permanent shadow down to the lunar background water abundance of about 100 parts per million, far below the abundance accessible to shorter wavelength measurements [5].

Geodetic Information:

The accessibility of volatiles for extraction will require knowledge of their position in relation to the lunar coordinate frame defined by laser retroreflectors and realized by altimetry and optical imaging so as to marshall the considerable assets required to make use of them. To this end, the importance of combining altimetry with spectrometry cannot be overstated. The proposed lidar can provide a global spatial coverage of the Moon every two weeks (half a lunar day) from polar orbits, providing abundant topographic crossover points and tiepoints. As shown for current [6] and previous [7] missions, altimetric ranges can support spacecraft orbit reconstruction accuracy at the 10-20 meter level, even in the absence of radio tracking. The time-of-flight data collected will thus be useful to geolocate the spectrometer data in the established LOLA-based lunar frame (including the data from other instruments onboard). Previous spectrometers such as M-cubed have required painstaking registration with imager mosaics and suffered from undetermined phase geometry (E. Malaret, personal communication).

Detection of sublimation lags overlying radar-bright water ice deposits: While reflectance anomalies are expected in regions of permanent shadow, one of the unknown aspects of lunar volatiles is burial and insulation by a more refractory volatile sublimation blanket composed of complex carbon compounds. If even small cometary impacts have recently carried volatiles to the Moon's cryosphere, they would deposit some amount of impure ice similar to the small-scale deposits inferred from 1064-nm laser reflectance at Mercury [8, 9]. The compounds are typically darker (< 0.05) than even mare regolith, but may be difficult to distinguish from other lithologies without a highly sensitive and optimized active lidar spectrometer. Experiments underway demonstrate the sensitivity of SpIRRL to water and other volatile species in a lunar regolith simulant under <170 K cryogenic conditions.

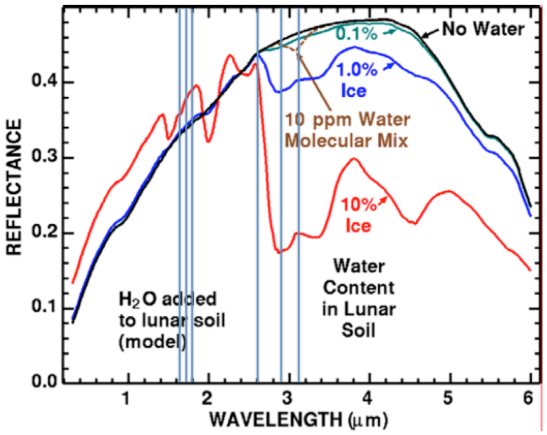

Figure 1. Radiative transfer models of spectral absorption at the 3-μm region which is sensitive to very small amounts of water in several forms [10].

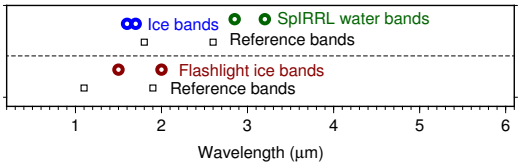

Figure 2. Multiple waveband measurement by SpIRRL as part of a lunar mission [11] suite of instruments vs. the proposed Lunar Flashlight [12].

References: [1] Zuber M. T. et al. (2012) *Nature, 486, 378–381* [2] Spudis P.D. et al. (2013) *JGR, 118,* 2016– 2029. [3] Patterson G. W. et al. (2017) *Icarus, 283,* 2-19. [4] Lucey P. G. et al. (2014) *LPS XLV,* Abstract # 2335. [5] Lucey P. G. et al. (2017) *LEAG,* Abstract #5048. [6] Mazarico E. et al. (2017) *Planet. Space Sci.,* in press. [7] Goossens S. et al. (2018) *LPSC XLIX,* Abstract #1645. [8] Neumann et al. (2013) *Science* 339, 296–300. [9] Deutsch A.N. et al. *GRL 44*, 9233-9241. [10] Clark R.N. (2009) *Science* 326(5952), 562-564. [11] Lucey P. G. et al. (2017) *LEAG,* https://www.hou.usra.edu/meetings/leag2017/presentations/tuesday/lucey.pdf [12] Cohen B.A. et al. (2015) *LEAG,* Abstract #2008.

INVESTIGATING SUB-RESOLUTION COLD TRAPS WITH A LANDSCAPE EVOLUTION MODEL.

P. O'Brien[1], S. Byrne[1], P.O. Hayne[2], [1]Lunar and Planetary Laboratory, University of Arizona, Tucson, AZ 85721 (pob@lpl.arizona.edu), [2]University of Colorado, Boulder, CO 80309

Introduction: The roughness of a planetary surface contains a record of the processes that have shaped that object. For airless bodies like the Moon, the number of processes acting to alter the terrain is relatively small; relief-creation from impact cratering and relief-reduction from diffusive mass-wasting. This permits a detailed study of geologic history from topographic datasets. Quantitative characterization of topographic roughness provides information about the relative effectiveness of the processes that formed and shaped the surface [1,2].

Knowledge of processes that explain surface roughnesses can lead to predictions of surface properties below the resolution of observations. The existence of ice deposits in permanently shadowed regions (PSRs) observed on the Moon, Mercury, and Ceres [3,4] depends heavily on surface roughness in the polar regions [5,6]. Cold traps too small to observe may also exist [7] and could be characterized by a model of landscape evolution calibrated to explain surface roughness at larger scales. High-resolution global topography exists for the Moon [8] and for Ceres, such a study is now possible due to comprehensive stereo coverage from the Dawn Framing Camera's Low Altitude Mapping Orbit [9,10].

Here we demonstrate roughness analysis techniques applied to the dwarf planet Ceres and present global maps of various roughness parameters as well as discuss implications for permanently shadowed regions. We are currently expanding this roughness analysis to the Moon and Mercury, similar to previous studies of roughness from laser altimeter datasets [2,11,12].

Finally, we discuss application of these results to the calibration of a landscape evolution model, which allows us to study lunar-like synthetic surfaces at scales below the resolution limit of spacecraft instruments.

Data: For Ceres, A global shape model has been produced from Dawn Framing Camera images and radiometric tracking data using the stereophotoclinometry method [13,14]. This topography data has a resolution of ~140 m [13] and the resulting 3D shape model [14] has height accuracies of better than 30 m. For our analysis, we sampled the shape model on a global grid of 10000 by 5000 points to generate a DTM. In the polar regions of the Moon, the Lunar Reconnaissance Orbiter's LOLA and LROC datasets permit significantly higher-resolution roughness analysis [15].

Roughness Analysis: The Ceres global DTM was used to produce elevation slope and roughness maps (Figures 1 and 2). Due to sub-optimal lighting conditions near the poles, the data quality in those regions is poor. Therefore, our maps only display latitudes between -80º and +80º. Within this area, roughness statistics were computed for a moving 5ºx5º (~1600 km^2) window. Projection effects were mitigated by reprojecting each rectangular window using an equidistant cylindrical projection, resulting in a resolution of about 300 m/pixel.

For each window, the median bidirectional slope is computed using elevation differentials in both the x- and y-directions (Fig. 1).

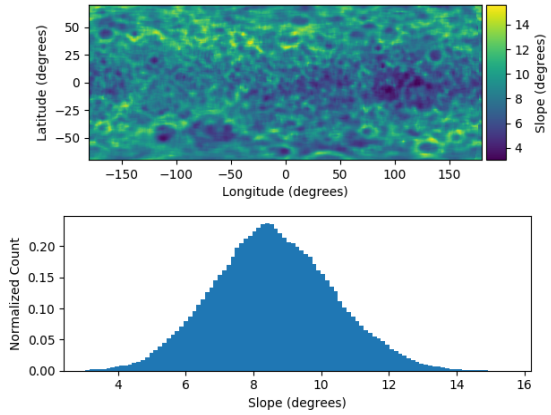

Figure 1. Median global slope map and distribution for Ceres

The heavily cratered nature of Ceres is evident in the small fraction of slopes greater than 12º. These steep slope faces, found often on the walls of impact craters may augment the thermally stable locations for ice deposits in permanently shadowed regions [3,4,5].

The power spectrum of the topography was characterized with a 2D Fourier Transform of the moving window. A line was then fit to the radially-averaged FT in log-log space (Fig. 2).

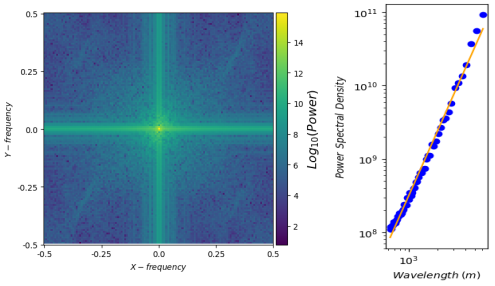

Figure 2. a) 2D Fourier Transform of an elevation grid. b) 1D radial average of a) and linear fit

This fit is performed for each window in the DTM and the slope, β, is used to represent the overall surface roughness for that region. The global map of this parameter is shown in Figure 3. This procedure can also be applied to the Moon to characterize surface roughness at the lunar poles.

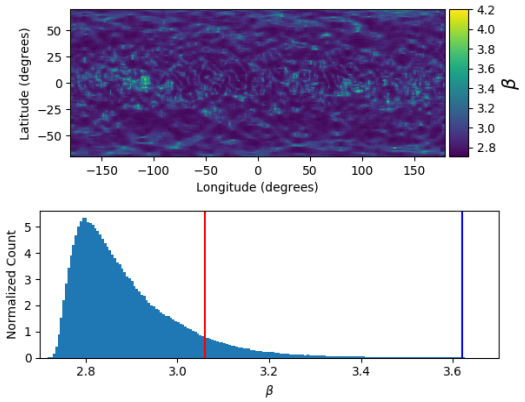

Figure 3. Map and global distribution of roughness parameter, β for Ceres. Vertical lines correspond to the FT slopes of surfaces B & C in Fig. 4

Model Calibration: We are currently performing these surface roughness measurements for the Moon and using the results in the calibration of a landscape evolution model (Fig 4 A-C) that will investigate surface ice deposits in permanently shadowed craters [3,4] as well as space weathering on airless bodies. The two most important processes in this model are relief-creation from impact cratering and relief-reduction from mass wasting (driven by micrometeorite bombardment) [16]. Downslope motion of material is computed via diffusion similar to the method of [17], and we employ accurate impactor population parameters to scale projectiles to final crater dimensions using pi-group scaling techniques [18] and realistic, size-dependent crater shapes [19]. This allows us to vary the source of impacting bodies (e.g. Main Asteroid Belt, near-Earth space, or the Kuiper Belt) and vary target properties such as strength, density and gravity.

Power spectra calculated from 2D Fourier Transforms can measure the roughness of the synthetic and real landscapes. Model landscape diffusivity can be adjusted so that the power spectra of the generated surface resembles that in the polar regions of the Moon. Figure 4D depicts how the power spectral slope differs for varying diffusion rates. Our retrieved diffusivities will be used in higher-resolution model runs over smaller areas to synthesize realistic topography below the resolution limit of current topographic datasets. Solar elevation calculations determine the PSR fraction in our calibrated surfaces (e.g. Fig 4 A-C). We will take a Monte Carlo approach and simulate many landscapes to investigate what PSR fraction is typical and what role sub-resolution cold traps play in the total PSR area. These surfaces could also provide information about the characteristic geometry, e.g. depth-to-diameter ratio, of craters hosting PSRs and could be used to directly model temperatures within realistic synthetic craters.

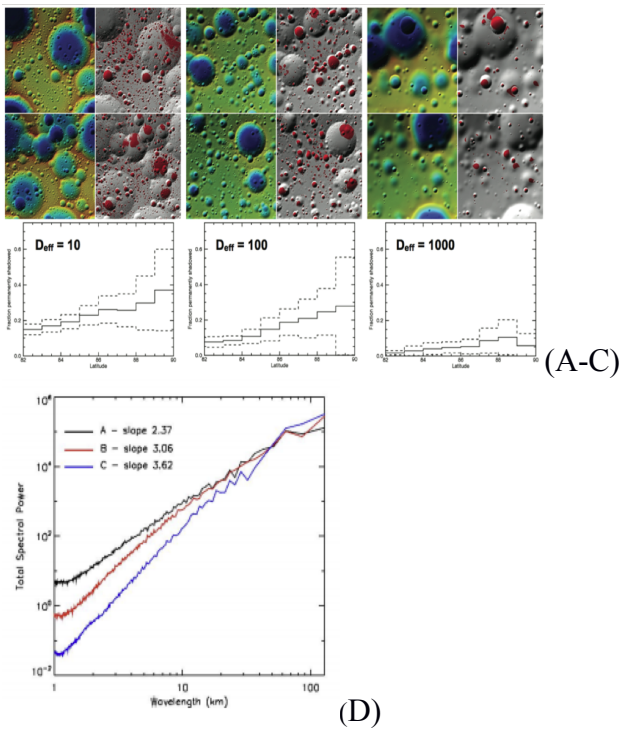

Figure 4. (A-C) Model landscapes centered on Ceres' north pole with increasing diffusivity from left to right. Color represents elevation while red on the shaded maps shows PSRs. Plots show the average and range (over many random landscapes) of the fraction of PSR terrain vs. latitude.
(D) Power spectra of model terrains with different diffusivities have clearly-distinguishable slopes.

Discussion: We present preliminary roughness analysis results for Ceres and the Moon, including global maps of median bidirectional slope and Fourier Transform slope, β. By calibrating our landscape evolution model to the large-scale lunar roughness using these results, we can probe surface conditions below the resolution of spacecraft instruments. We will discuss the application of this model to PSRs on the Moon and present preliminary analysis of calibrated, lunar-like synthetic surfaces.

References: [1] Aharonson et al., *JGR*, 106, 23723-23735 (2001). [2] Smith et al., *Science*, 284, 1495-1503 (1999). [3] Lawrence, D. J., *JGR*, 122, 21-52 (2017). [4] Platz et al., *Nature Astron.*, 1, 0007 (2016). [5] Rubanenko and Aharonson, *Icarus*, 296, 99-109 (2017). [6] Prem et al., *Icarus*, 299, 31-45 (2018). [7] Hayne et al., *JGR*, 120, 1567–1584, (2015). [8]. Scholten et al., JGR, 117, (2012). [9] Raymond et al, *Space Sci. Rev.*, 163, 487–510, (2011). [10] Raymond et al., *LPSC* (2016). [11] Rosenburg et al., *JGR*, 116, (2011). [12] Susorney et al., *JGR*, 122, 1372-1390, (2017). [13] Park et al., *Nature*, 537, 515–517 (2016). [14] Park et al., *EGU*, 3380 (2017). [15] Wagner et al., *LPSC*, 46, #1473 (2015). [16] Fassett, and Thomson, *JGR*, 119, 2255-2271 (2014). [17] Howard, *Geomorphology*, 91, 332-363 (2007). [18] Holsapple, *Annu. Rev. Earth and Planet. Sci*, 21, 333-373 (1993). [19] Richardson, *Icarus*, 204, 697-715 (2009).

A Solar Wind Source of Water in the Polar Regions of the Moon? Thomas M. Orlando[1,2,3], Brant M. Jones[1,3], Alexandr B. Aleksandrov[1], Charles A. Hibbitts[4] and M. Darby Dyar[5], [1]School of Chemistry and Biochemistry, Georgia Institute of Technology, Atlanta, Georgia, [2]School of Physics, Georgia Institute of Technology, Atlanta, Georgia, [3]Center for Space Technology and Research, Georgia Institute of Technology, Atlanta, Georgia, [4]Johns Hopkins University Applied Physics Laboratory, Laurel, Maryland, [5]Mount Holyoke College, Department of Astronomy, South Hadley, Massachusetts

Introduction: Understanding the origin and behavior of water (H_2O) and chemically bound hydroxyl radicals (-OH) on the Moon is necessary and critical for understanding the evolution of our Solar System and for evaluating the overall accessibility of this potential resource in the lunar polar regions. Given the previous work by us and others, we suggest that the solar wind is critical to the formation of water and other hydrogen-containing volatiles on all airless bodies and this can contribute to the slow-build-up of water in the polar regions of the Moon. Solar wind induced formation of water is supported by previous studies [1, 2] of terrestrial minerals bombarded with keV proton, which resulted in the appearance of 2.8 μm absorption associated with chemically bound hydroxyls. These hydroxyl defects will produce gas-phase molecular water at lunar relevant surface temperatures in a process known as recombinative desorption (RD). During RD, neighboring hydroxyl groups are thermally activated and react producing an H_2O molecule while healing the oxygen atom defect created during proton bombardment. We have examined the formation and release of water from lunar samples via this second order thermal process. The derived second order activation energies for mare sample 10084 were as low as 0.8 eV in the high coverage limit extending upward near 1.8 eV at very low coverage. In addition, we have measured the first order desorption activation energies of water molecules chemisorbed on highland and mare Apollo lunar samples. A significant difference in the uptake and abundance of adsorbed water was observed, with mare samples retaining significantly less water (by mass) than the highland samples, likely due to differences in mineralogy and surface exposure age. The coverage dependent first order desorption activation energies were extracted using an inversion method [3]. Generally, the distribution function of water desorption activation energies was similar for both mare and highland samples with a peak binding energy near 0.7 eV and a very small occupancy of sites up to 0.9 eV. Finally, utilizing these available data sets on non-thermal and thermal rates of water formation and desorption from Apollo samples, the 2.8 μm optical signature on the Moon is modeled. Specifically, this band results from formation and loss pathways induced by the solar wind production of chemically bound hydroxyls and subsequent RD. A small fraction of the water formed by RD may migrate or be transported to the polar regions. Any molecular water will trap and adsorb at temperatures less than ~ 160K with clusters and multi-layer ice forming at temperatures below ~140 K. Though water may be trapped at the poles, much of the 2.8 μm optical signature in the polar regions can be interpreted mainly in terms of localized surficial hydroxyl sites that are observable over the penetration depth of the incident IR light.

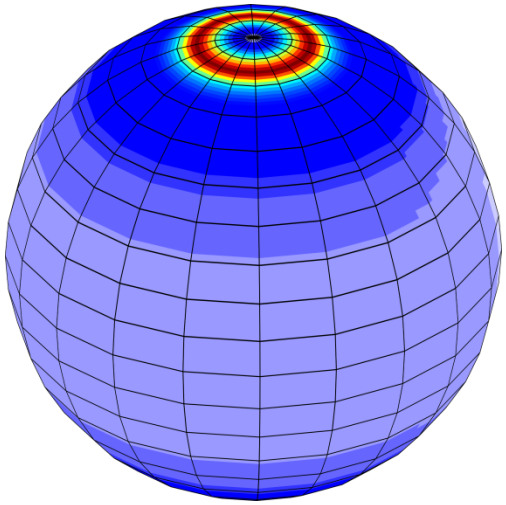

Figure 1: Simulated OH concentration after 1200 lunar days using a chemical kinetics model that centers on proton implantation followed by water formation and release via recombinative desorption. The lowest concentration is at the equator with subsequent build-up near the poles.

References:

[1] Schaible, M.J. and R.A. Baragiola.(2014) J*GR: 119*, 2017-2028.
[2] Bradley, J.P., et al. (2014) *PNAS 111*, 1732-1735.
[3] Tait, S.L., et al. (2005) JCP 122, 164707.

Acknowledgments: This work was carried out as part of REVEALS which was directly supported by the NASA Solar System Exploration Research Virtual Institute cooperative, agreement # NNH16ZDA001N and grant number NNA14AB04A.

THE LUNAR RECONNAISSANCE ORBITER (LRO) NEXT STEPS IN CONSTRAINING LUNAR POLAR VOLATILES. N. E. Petro, Planetary Geology, Geophysics, and Geochemistry Lab, NASA Goddard Space Flight Center, Greenbelt, MD 20771 (Noah.E.Petro@nasa.gov).

Introduction: With over 9 years of observations of the lunar surface and the environment around the Moon, the Lunar Reconnaissance Orbiter (LRO) has generated an unparalleled dataset for investigating the lunar poles [1, 2]. The suite of LRO instruments have provided a rich set of observations at various wavelengths and probing depths of the regolith, which yields a set of constraints on the presence, abundance, and variability of volatiles at and near the poles [3-5]. As LRO prepares to propose for an extended mission (starting in late 2019), we assess where the mission has been (philosophically, and literally) and look to the future for the science focus of the mission.

Science Focus During the Current Extended Mission: The LRO science teams identified three broad science themes, which build on Decadal-relevant science questions: 1) Volatiles and the Space Environment, 2) Volcanism and Interior Processes, and Impacts and 3) Regolith Evolution. A few examples of the science questions we address during the current extended mission are illustrated in Figure 1.

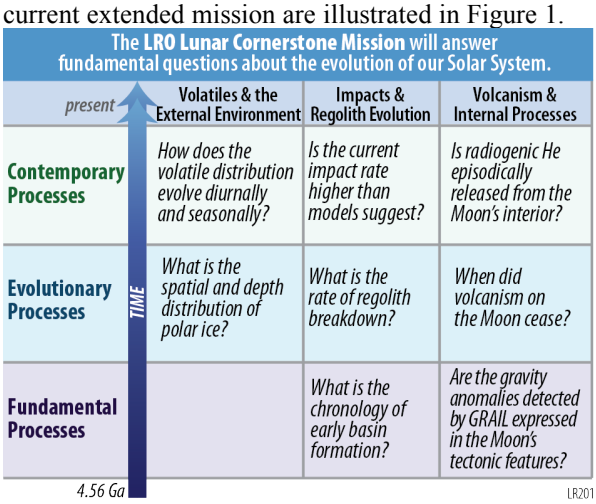

Figure 1. During LRO's CM, the science teams a will address a number of science questions directly related to fundamental Solar System science, which cover processes that have acted over billions of years.

LRO's Orbit Enables Fundamental New Science: LRO has maximized its science return by employing a quasi-stable orbit for more than 6 years, which has minimized fuel consumption. In this configuration, which has LRO with a periapsis over the southern hemisphere (Figure 2), enables focused investigations on the region surrounding the South Pole. Going forward, the LRO mission team is evaluating options for future orbits that will maximize science collection capability for future potential extended missions.

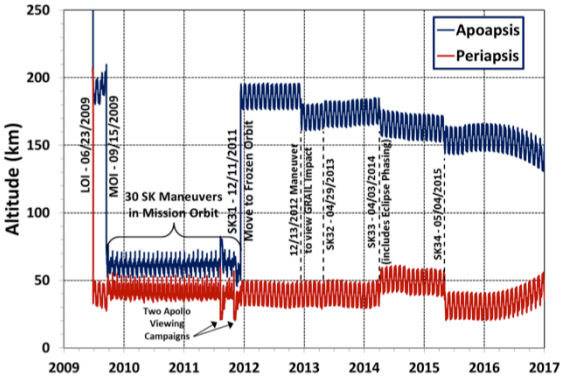

Figure 2. Plot showing the evolution of the LRO orbit since arriving at the Moon in 2009. Since late 2011 LRO has been in a quasi-stable elliptical orbit that allows for a significant reduction in fuel consumption. In this orbit configuration, LRO has made several years' worth of observations over the South Pole.

Future of LRO: The LRO spacecraft has fuel onboard for several more years of observations (~9 additional years), with specific focus of the South Pole. As the LRO orbit evolves, our coverage of the region surrounding the South Pole increases exponentially, allowing for a detailed study of the environment and potential sources/sinks of volatiles there.

References:

[1] Keller, J. W., et al., (2016) *Icarus*, 273, 2-24.
[2] Hayne, P. O., et al., (2015) *Icarus*, 255, 58-69.
[3] Fisher, E. A., et al., (2016) Search for Lunar Volatiles Using the Lunar Orbiter Laser Altimeter and the Diviner Lunar Radiometer, 47, 2574.
[4] Fisher, E. A., et al., (2017) *Icarus*, 292, 74-85.
[5] McClanahan, T. P., et al., (2015) *Icarus*, 255, 88-99.

LUNAR REGOLITH - PROPERTIES / IMPLICATIONS FOR VOLATILE STORAGE. J. B. Plescia, Johns Hopkins University, Applied Physics Laboratory, Laurel MD

Introduction: The regolith is the fragmental layer formed on the surface of the Moon. It is the material that is observed by remote sensing techniques providing information on the bedrock composition and history. The regolith participates in the lunar volatile cycle by serving as a substrate for the productions of H_2O and OH (and other species), as a site for intermediate (diurnal) storage of volatiles on the surface, and as a long-term storage for volatiles. Understanding the properties of the regolith is important to evaluate how the regolith participates in the volatile cycle.

Volatiles are of interest not only for the scientific aspect of their origin and evolution, but also from the perspective of resources. We have begun to recognize that H distribution is not simply a function of latitude and permanent shadow. Regolith H appears to be spatially variable across the surface [1, 2]. Surface volatiles appear to vary as a function of latitude and time of day [3, 4].

Many of the properties of the lunar regolith are understood from a combination of remote sensing and in situ observations. In situ observations and samples are limited to few locations (primarily the Apollo sites). Remote sensing observations provide information on global, but lower resolution basis.

Volatile storage in the regolith can occur in either a physical or chemical basis. Physical storage is meant wherein the regolith simply provides a porous medium in which volatiles can reside. Chemical storage is meant to indicate that the volatile species are bound to the grains. Chemical storage is limited to a few monolayers. Volatiles can also be hosted by individual mineral grains being either juvenile or implanted volatiles.

The regolith can be divided into three layers: (1) The upper few microns that are bombarded by micrometeorites, solar and galactic radiation, and electrostatic forces. (2) The upper ~10 cm influenced by micrometeorites and by the diurnal temperature cycling. and (3) Below about 10 cm, where regolith has approximately uniform temperature and which is shielded from a high frequency of small impact events (but not the lower frequency large events).

Regolith Formation: The regolith is primarily formed by the bombardment of the lunar surface by impacts ranging in size from microns to kilometers [5]. Since the termination of the terminal bombardment, a layer up to 10 m has formed across the highlands and mare. While the initial fragment generation process is bombardment, thermal fatigue is an important process in the long-term disintegration of surface rocks [6-8]. Apollo deep drill cores (extending to depths of 3-4 m) indicate that the regolith has been repeatedly overturned and mixed to at least those depths. The presence of agglutinates, nano-phase iron, cosmogenic nuclides and particle tracks as well as indices of maturity all indicate that all of sampled material had resided within a few mm of the surface at some point in time, despite being presently buried at depths of meters.

Physical Properties: The density of the regolith increases rapidly with depth varying from about 1530 kg m^{-3} at the surface to 1710 at depths >60 cm. Porosity varies from ~85% in the upper few grains to 50-60% at depth. Lunar soil particles have specific surface areas of 0.02 to 0.78 m^2 gm^{-1}, with a typical value of 0.5 m^2 gm^{-1}. Diffusivity estimates are of the order 4-8 cm^2 s^{-1} for He and 1-2 cm^2 s^{-1}. These values suggest that the lunar regolith has the potential to physically store and chemically bind significant quantities of volatiles. In situ physical properties data collected by Apollo shows that the character of the regolith is heterogenous even on scales of meters. Cores and drive tubes taken as close as 50 m apart show little correlation indicating that lateral continuity of stratigraphy is minimal.

Areas within permanent shadow may have regolith properties different from that in areas that experience diurnal variations in sunlight and temperature. The basic impact-generated regolith processes should operate similarly in areas of permanent shadow; however those areas would not experience diurnal temperature variations.

Impact Rate and Regolith Turnover: As a result of micro-macro impact events, the regolith is slowly vertically mixed and matured with time as indicated by the core data. The rate at which turnover and maturation occur have implications for the ability of the regolith to store volatiles. Early model estimates suggested turnover to depth of 10 cm once on the order of 10^7 to 10^9 years [9]. More recently, observations of new formed craters using LROC images suggest overturn rates occurring on timescale about 100x faster previous estimates [10, 11]. These estimates are at odds with some Apollo core data. Core 74001/2 at Shorty Crater shows that only a 5 cm thick gardened layer has formed on the orange soil over the last 10 Ma since the crater formed and exposed the soil [12]. While the upper few cm has solar wind implanted volatiles, virtually no volatiles occur below those

depths. The inconsistently indicates that the timescale and process of regolith overturn is not well understood.

Conclusions: The understanding of the character, formation and evolution of the lunar regolith has substantially changed over the last decade. Heterogeneity is greater, new processes have been considered and rates may be significantly greater than previously recognized. The new insights provide a better understanding of how the regolith forms and evolves. It also has implications for the manner in which the regolith acts as a source, sink and venue for the formation and transport of OH and H_2O.

References: [1] Mitrofanov, I. et al., (2011) Science, 330, 334- [2] Feldman, W. et al. (2000) JGR, 105, 4175-4195. [3] Pieters, C.M. et al. (2009) Science, 326, 568-582, [4] Sunshine, J. et al. (2009) Science, 326, 565-568. [5] Horz, F. and Cintala, M (1997) Met. Planet. Sci., 32, 179-209. [6] Delbo, M. et al. (2014) Nature, 508, 233-236. [7] Molaro J. et al. (2015) JGR, 120, 255-277. [8] El Mir, C. et al. (2016) LEAG, #2073. [9] Gault, D., et al., (1974) Proc. Fifth Lunar Sci. Conf. 2365-2386. [10] Costello, E., et al. (2017) Lunar Planet. Sci. XLVIII, Abstract 1672. [11] Speyerer, E. et al. (2016) Nature, 538, 213-218. [12] Bogard, D. and Hirsch, W.C., (1978) Proc. Lunar Planet. Sci. Conf. 9th, 1981-2000.

Cold Trapping Processes on the Moon. M. J. Poston, Southwest Research Institute, San Antonio, TX.

Introduction: It is common knowledge that lunar polar volatiles are of high interest for possible *in situ* resource utilization (ISRU) by future missions, both robotic and human. Any mass that does not have to be launched from the surface of the Earth, but can instead be harvested from a location with a less pesky gravity to overcome (even physicists agree this is a lot of work!), is a huge savings in launch costs – on the order of 10^4 dollars per kilogram launched to Earth escape! This is even more relevant for resources needed on the surface of the Moon, because landing resources softly at the lunar surface increases the cost per kilogram by an order of magnitude.

Lunar polar volatiles also carry tremendous potential for science. The Moon is already humanity's chronometer for the impact history of the Solar System, but how volatiles ended up in large quantities in the inner Solar System remains a key open question for understanding how it is we are here, and how likely it is there are other organisms having this very same discussion on a lovely habitable world lightyears away from the remote system known as Sol. Cold trapping of volatiles on geological time scales could provide a record of volatile arrival to the Moon-Earth system, which may be a key to understanding the history of volatiles in the Solar System.

(These two purposes for seeking lunar volatiles at the poles are not obviously co-aligned. The former potentially represents millions of dollars in savings, while the latter is priceless, which all too often means it is considered worthless in the present era.)

In order for volatiles to reach the poles, they have to have either been part of the Moon since its formation, or have been delivered from colder regions of the solar system. Deliver seems to be the more common hypothesis, with hundreds of papers on the topic, but a more recent paper has shown the plausibility of large-scale outgassing of volatiles during mare volcanism [1]. To properly interpret the record potentially stored in the dark recesses of the Moon, the dynamics of delivery, migration, and trapping – especially any sampling biases these processes may introduce – must be understood. This presentation will focus on trapping.

Physisorption: The commonly-discussed form of volatile trapping is physisorption. This is the type of trapping Watson, Murray, and Brown [2] considered in their heavily-cited paper about lunar permanently shadowed regions. It is identical to the process by which frost forms on relatively humid (high-latitude) winter days here on Earth. That is, any volatile has a characteristic pressure, known as the "vapor pressure", which thermodynamics demands it maintain in the gas phase. When the partial pressure of the gas exceeds its vapor pressure, condensed phases become stable. If the pressure and temperature are above the "triple point" for the substance, then the condensed phase is liquid, but if either of these are below the triple point, a solid is formed.

The above is a population-level, equilibrium description, and is useful when large quantities of a species are present. When quantities of the species are small, such as at the low pressure understood to exist at the surface of the Moon, it is perhaps more useful to consider the energetics at the interface between the condensed phase and the gas. When talking about cold trapping, this is the true "surface" of the Moon, zoomed in to a scale of 10's of picometers per pixel!

When speaking at the interface level, there are two processes involved in cold trapping: adsorption and desorption. (If the interaction involves molecules going deeper into a substance than the interface itself, this is absorption or possibly implantation.) However, practically speaking, adsorption can be simplified to whether molecules come in physical contact with the surface or not. Desorption is generally the rate-limiting step that defines trapping. In the case of physisorption, desorption follows an Arrhenius equation:

$$d\Theta/dt = \alpha \exp(E_a/RT) \quad (1)$$

where Θ is the surface coverage, α is a prefactor based on the characteristic vibration frequency of the interaction, R is the ideal gas constant, T is temperature, and E_a is the activation energy of desorption. For a slab of solid volatile, it is typically sufficient to assume constant values for α and E_a, and the rate of desorption is then defined by the temperature. However, roughness or porosity at the molecular scale can lead to increased interaction between the molecule and the surface. On a slab of solid volatile, that tends to mean that the most exposed portions of the slab desorb (sublime) more quickly, and the slab surface smooths until roughness is no longer significant. Considering a volatile adsorbed in very thin layers to a less volatile substance (e.g. a silicate mineral), the energetics become more complicated.

Monolayer Buildup and Chemisorption: A volatile interacting with the surface of a grain of dust will interact with energy characteristic of the two materials, as well as the physical molecular topography of the surface. When the energetics are sufficiently weak, the

process is still considered physisorption, but E_a in equation (1) is no longer approximately constant. Instead, the first molecules to adsorb with tend to dwell at the locations on the surface where the interaction is the strongest. As additional molecules adsorb, they do not find strong sites available as often, so their average energy of interaction is lower. Eventually, typically around a full monolayer of coverage, the interaction approaches that of the simple physisorption scenario described above.

If there are specific aspects of the surface that can form a chemical bond with the adsorbed molecule, this is called "chemisorption". This typically occurs at surface defects in the mineral, such as a missing oxygen or extra silicon compared to the ideal arrangement. When considering monolayer buildup or chemisorption, the Arrhenius equation has to be augmented to the Polanyi-Wigner equation:

$$d\Theta/dt = \alpha \exp(E_a/RT)\, \Theta^n \qquad (2)$$

by multiplying the Arrhenius by the instantaneous surface molecular coverage. For simple chemisorption, the order of desorption, *n*, is 1, and *n* can be neglected. However, in cases of very strong interaction, the adsorbed molecule can dissociate, for example, water into OH and H. For such cases the surface state will not technically be the adsorbed molecule, but the species that desorbs will recombine and desorb; in this case *n* will typically be 2, though fractional values are possible in specific situations.

Closing: Despite the name of the presentation, cold trapping does not necessarily have to be all that cold. While traditional lunar trapping of volatiles (physisorption) requires cryogenic temperatures (i.e. below 120K) volatiles can form sub-monolayer quantities of adsorption with interactions that are stable at much higher temperatures. Such interactions with the lunar surface would increase surface lifetimes of migrating volatiles, and increase the possibility of destruction or loss from the Moon by competing surface processes.

References: [1] Needham, D. H. and Kring, D. A. (2017) EPSL, 10.1016/j.epsl.2017.09.002. [2] Watson, K., Murray, B. C., and Brown, H. (1961) JGR, *66*, *9*, 3033.

PERSPECTIVES ON MODELING THE TRANSPORT OF VOLATILES AND THEIR DISTRIBUTION AT THE LUNAR POLES. P. Prem[1]*, D. M. Hurley[1] and G. W. Patterson[1]; [1]Johns Hopkins University Applied Physics Laboratory; 11100 Johns Hopkins Road, Laurel, MD 20723, USA; *parvathy.prem@jhuapl.edu.

Introduction: Over the last several decades, remote sensing observations of lunar polar volatiles have been accompanied by the development of numerical models directed towards both interpreting and guiding observations. Here, we present a series of recent investigations aimed at understanding the transport of volatiles, and their distribution at the lunar poles, through numerical modeling. In discussing these investigations, we focus on (i) the role of numerical modeling in addressing critical outstanding questions regarding the origin and distribution of polar water, and (ii) the assumptions and uncertainties that affect model results, and how these may be addressed.

The models presented here focus on water, as a volatile of interest. This abstract is organized around the following questions: (i) How would a lunar water vapor exosphere behave? (ii) What mechanisms could lead to non-uniform deposition patterns at polar cold traps? (iii) What is the depth distribution and physical form of water at the lunar poles?

I. How would a lunar water vapor exosphere behave? Several suggested source mechanisms (e.g., the solar wind [1], small impacts [2] or the remobilization of cold-trapped volatiles [3]) could give rise to a global water vapor exosphere that could, in turn, deliver water to the lunar poles. Monte Carlo models generally indicate that such an exosphere would be characterized by a dawn-dusk asymmetry and diurnal variations of greater magnitude at higher latitudes [1,4].

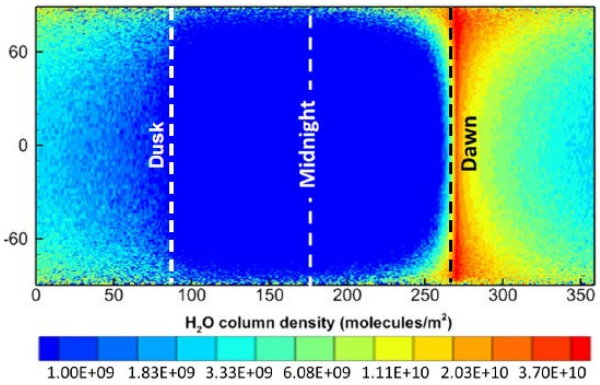

Figure 1. Column density of migrating water molecules (not including molecules adsorbed to the surface) in a representative water vapor exosphere.

Figure 1 shows a representative, quasi-steady state water vapor exosphere (generated arbitrarily by the release, at t = 0, of 100 kg of water vapor, uniformly distributed over the lunar surface), while ***Figure 2*** tracks the fate of this water vapor over time [4]. In particular, Figure 2(b) shows rate coefficients for photodestruction and cold-trapping, which, after the initial transient stage, should be generalizable to other source mechanisms that could generate a collisionless, global water vapor exosphere. The diurnal cycling of the cold-trapping rates illustrates the dependence of transport and deposition rates on local thermal conditions.

Figure 2 also illustrates the influence of small-scale surface temperature variations and shadowing (due to surface roughness), which act to delay the migration of water to the poles and to prolong the lifetime of exospheric molecules (see Figure 2(a)). In this particular model, molecules that encounter the lunar surface are assumed to thermalize fully, and each molecule has a temperature-dependent surface residence time governed by a single desorption activation energy. The effects of surface roughness may be compounded by partial thermalization, and the existence of a distribution of activation energies, as indicated by previous modeling work [5] and laboratory studies [6].

II. What mechanisms could lead to non-uniform deposition patterns at polar cold traps? Several datasets [e.g., 7,8] indicate that the distribution of hydrogen at the lunar poles correlates imperfectly with present-day thermal conditions. This raises a number of intriguing questions: Could presently observed hydrogen have been deposited in a past thermal environment [9]? (Does this provide constraints on the age of polar volatiles [10]?) Or could transport processes, in certain scenarios, distribute volatiles unevenly among cold traps? [e.g., 11,12]. Understanding potential differences between contemporary, continuous source mechanisms (such as the solar wind and micrometeoroid impacts) and ancient, episodic source mechanisms (such as volatile-rich impacts and volcanic eruptions) is a key step towards answering these questions.

The latter mechanisms may temporarily transform the tenuous lunar exosphere into a thicker, collisional atmosphere [e.g., 13,14], calling for different modeling approaches. For instance, modeling of the rarefied gas dynamics of an impact-generated lunar atmosphere indicates that under some conditions, an impact may lead to a non-uniform fallout in cold-traps [11]. The role of impacts in delivering water to the lunar poles is of particular interest due to recent observations of Mercury; Mercury's polar cold-traps too, appear to be unevenly filled [15], and several independent lines of

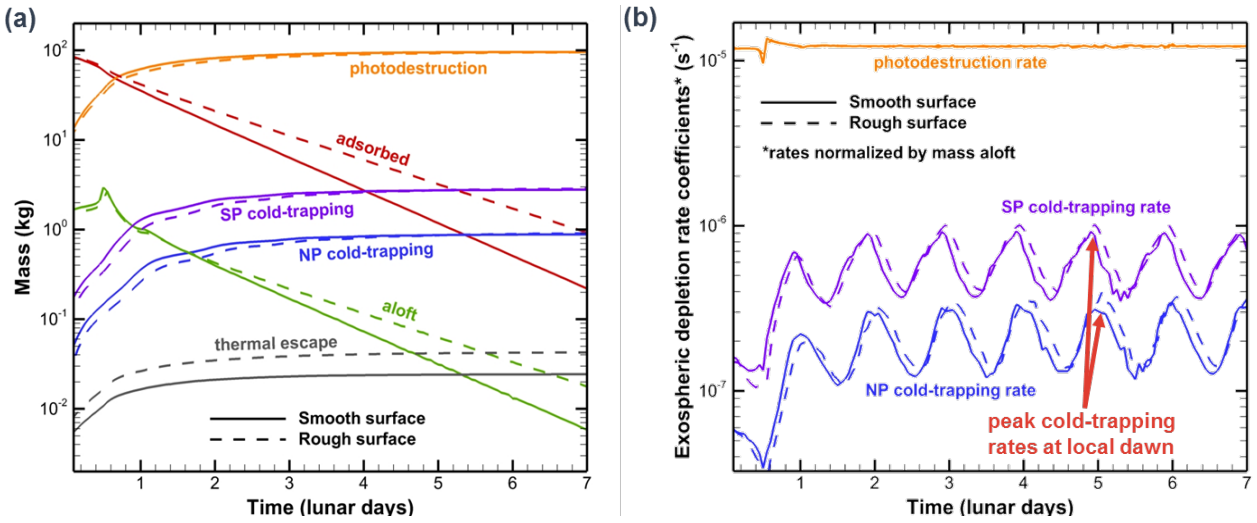

Figure 2. The fate of exospheric water vapor after a global, episodic release, shown in terms of (a) the cumulative mass of water photodestroyed, cold-trapped and lost through thermal escape, as well as the mass of water aloft and adsorbed to the lunar surface, as a function of time; (b) rate coefficients for photodestruction and cold-trapping.

evidence suggest that Mercury's polar ice may have been delivered by a recent impact [16]. Might the lunar poles bear traces of a more ancient impact? How to identify signatures of transient, collisional atmospheres past remains a key question for models to address.

III. What is the depth distribution and physical form of water at the lunar poles? Testing models of the transport and deposition of water against observational data is complicated by the fact that the distribution and physical form of water at the lunar poles remain to be definitively characterized. To close the modeling loop (so as to speak), we conclude with a discussion of ongoing work aimed at interpreting bistatic radar observations of lunar polar craters by the Mini-RF instrument onboard the Lunar Reconnaissance Orbiter (LRO). (Mini-RF is currently acting as a receiver for signals transmitted at S-band (12.6 cm) and X-band (4.2 cm) wavelengths from the Arecibo and Goldstone Observatories, respectively.) Among instruments currently in orbit, Mini-RF shares with LEND and CRaTER (LRO's neutron detector and cosmic ray telescope, respectively) the ability to 'see' below the lunar surface. However, the interpretation of measurements by all three of these instruments necessitates a certain degree of modeling [e.g., 17,18,19].

One particularly interesting recent result from the Mini-RF bistatic campaign has been the detection of a narrow opposition response over the floor of Cabeus crater [20], potentially caused by the presence of buried water ice. We have recently developed a Monte Carlo model for the scattering of electromagnetic radiation by a particulate medium (such as the lunar regolith) [21], with a view to investigating how the nature of the radar opposition response is influenced by incidence angle, regolith composition and structure.

Summary & Outlook. Numerical models may play a key role in addressing outstanding questions regarding the origin and distribution of polar volatiles, whether by illuminating the processes that govern the transport and deposition of volatiles, or by providing tools to better interpret observational data – as represented by the investigations presented here. Ongoing and future observations and laboratory studies may further constrain critical model parameters (such as the specifics of the interaction of migrating molecules with lunar regolith). In addition, almost any future landed lunar mission will release exhaust gases (including water) into the lunar exosphere. This presents both an opportunity to conduct an active volatile release experiment, and a need for models that can predict any resulting contamination of polar reservoirs – with implications for our understanding of past, present and future polar volatiles.

References: [1] Schorghofer et al., 2017, *Icarus*. [2] Schorghofer, 2014, *GRL*. [3] Farrell et al., 2013, *Planet. Space Sci.* [4] Prem et al., 2018, *Icarus.* [5] Hurley et al., 2014, *LPSC*. [6] Poston et al., 2015, *Icarus*. [7] Mitrofanov et al., 2010, *Science*. [8] Hayne et al., 2015, *Icarus*. [9] Siegler et al., 2016, *Nature*. [10] Jordan et al., 2018, *LPSC*. [11] Prem et al., 2015, *Icarus*. [12] Moores, 2016, *JGR*. [13] Stewart et al., 2011, *Icarus*. [14] Needham & Kring, 2017, *EPSL*. [15] Chabot et al., 2018, *JGR*. [16] Lawrence, 2017, *JGR*. [17] Lawrence et al., 2006, *JGR*. [18] de Wet et al., 2018, *LPSC*. [19] Fa et al., 2011, *JGR*. [20] Patterson et al., 2017, *Icarus*. [21] Prem et al., 2018, *LPSC*.

1064 NM ALBEDO AND IMPACT CRATERING RECORD ANALYSIS OF THE PERMANENTLY SHADOWED REGIONS IN THE FLAT FLOORS OF LUNAR POLAR CRATERS: IMPLICATIONS FOR SURFACE WATER ICE AND FUTURE *IN-SITU* EXPLORATIONS.

L. Qiao[1, 2], Z. Ling[1], J. W. Head[2] and M. Ivanov[3], [1]Inst. Space Sci., Shandong Univ., Weihai, 264209, China (LeQiao.GEO@Gmail.com), [2]Dep. Earth, Env. & Planet. Sci., Brown Univ., Providence, RI, 02912, USA, [3]V. I. Vernadsky Inst. Geochem & Anal. Chem, Russian Acad. Sci., 119991 Moscow, Russia.

Introduction: Potential water-ice deposits within the permanently shadowed regions (PSRs) concentrated in lunar polar craters are both scientifically attractive and valuable for future surface *in-situ* explorations [1]. However, the existence and characteristics of these ice deposits still remain controversial after decades of extensive observations covering a wide range of electromagnetic wavelengths [e.g., 2-7]. Previous analyses are usually focused on polar bowl-shaped craters (e.g., Shackleton at the lunar south pole, e.g., [6]), from which the derived conclusions on ice deposits existence are made difficult by the topographic slopes and related surface modification processes (e.g., mass wasting). In addition, these permanently shadowed bowl-shaped craters are also technically challenging for surface *in-situ* explorations.

In this work, we focus on the lunar polar impact craters/basins with flat floors (dominantly <5 °slope), which are partly in PSRs. We analyze the 1064 nm albedo measured by the Lunar Orbiter Laser Altimeter (LOLA), impact cratering records of these PSRs, and compare with the albedo and cratering records of the adjacent non-permanently shadowed regions (non-PSRs).

Data and Method: Lunar Reconnaissance Orbiter LOLA is a laser ranging instrument operating at a wavelength of 1064 nm. From a 50-km altitude spacecraft orbiter, LOLA has an unprecedented vertical ranging precision of ~10 cm [8]. Mazarico et al. [9] has employed high-resolution LOLA topography-derived DEMs to map the illumination conditions in polar regions and the distribution of lunar PSRs, which are used in our work. We also use the LOLA DEM-derived shaded relief maps to study the impact crater frequencies and depths within polar PSRs and the adjacent non-PSRs.

In addition, LOLA is also able to map the reflectivity of the lunar surface (including PSRs) through measuring the backscattered laser energy at the 1064 nm wavelength [10]. We used the normal albedo measured by LOLA to characterize the optical reflectivity of lunar PSRs.

Results: *LOLA 1064 nm albedo*. We analyze the LOLA 1064 nm albedo of each selected PSR and compare it with the albedo of the adjacent non-PSR (a "pair" of regions). This survey is completed for PSRs larger than 10 km^2 in polar regions of latitudes poleward of ±80 °. The selected region pairs are constrained to be within very flat regions (generally slope <~5 °) at polar crater floors, with the considerations of eliminating the slope effect of surface albedo and technical accessibility for surface *in-situ* explorations. Our survey finds 34 pairs of regions in 24 crater/basin floors in the south pole, and 41 pairs of regions in 29 crater/basin floors in the north pole. The 1064 nm albedo of all the selected polar PSRs and their adjacent accompanying non-PSRs are plotted in Fig. 1, with the average values plus one standard derivation (δ). Examination of Fig. 1 shows almost all (71 of 75) of the studied PSRs have higher 1064 nm albedo than their adjacent non-PSRs. The PSRs are on average ~5% (while they can be up to ~12%) brighter than the adjacent non-PSRs; a very small portion (9 of 75) of studied PSR are more than 10% more reflective than their adjacent non-PSRs.

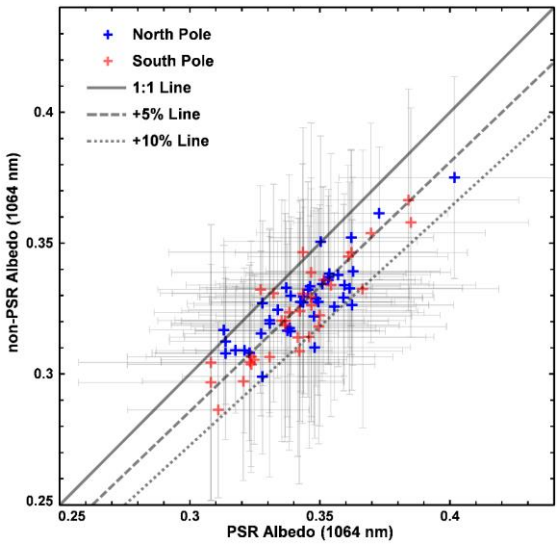

Fig. 1. LOLA 1064 nm albedo average values plus one standard derivation of the selected PSRs (horizontal axis) and comparison with their adjacent non-PSRs (vertical axis).

Impact crater populations and depths. We use LOLA DEM data and the derived shade relief maps to identify and measure the diameters and depths of superposed impact craters in the PSRs at the floor of several representative large craters in both northern and southern polar regions. We also analyze craters within adjacent non-PSR with the same surface area for a comparative crater measurement study. The crater diameter and depth measurements for the PSRs and adjacent non-PSRs within the floor of Nansen F (centered at 84.57 °N, 62.54 °E) are shown in Figs. 2 & 3 as a case demonstration. The

cumulative crater size-frequency distribution of the Nansen F PSR generally overlaps with that of the adjacent non-PSR for the whole diameter range (Fig. 2). Lunar chronology function fitting of craters ⩾1 km in diameter also yields very similar absolute model ages. In addition, Fig. 3 shows that PSR craters in the PSR of Nansen F have comparable d/D ratios with craters in adjacent non-PSRs for variable diameters (0.8–~1.3 km), suggesting the potential water-ice deposits is not thick enough to affect the cratering records.

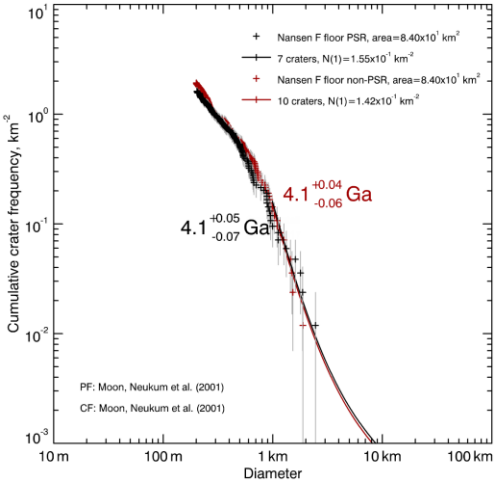

Fig. 2. Cumulative size-frequency distribution of impact craters superposed on the Nansen F floor PSR (black crosses) and adjacent non-PSR.

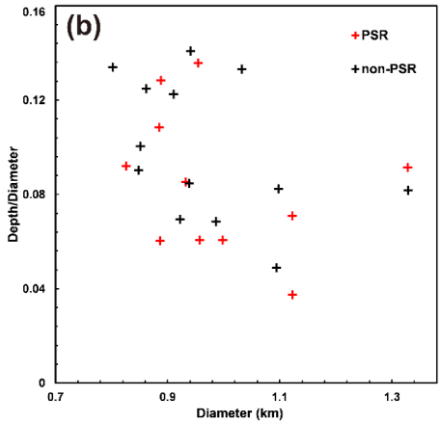

Fig. 3. Variation of depth-to-diameter ratios with respect to diameter of craters in Nansen F floor.

Factor for elevated LOLA 1064 nm albedo: Our LOLA 1064 nm albedo analysis shows unequivocally that the lunar PSRs at both polar regions are prevalently more reflective than their adjacent non-PSRs, consistent with previous analyses [10,11]. Though our albedo analysis of lunar polar PSRs characterized by very flat surfaces (<5 ° slope) has convincingly eliminated brightness effects from steep slopes, a wide range of additional factors may contribute to the observed elevated 1064 nm albedo, including decreased space weathering derived from a lack of solar illumination, surface composition, surface temperature, surface blocky materials, etc.

We quantitatively analyzed the effect of each of these factors on the observed LOLA albedo using a wide range of observational and calculated data sets from solar illumination condition maps [9], Diviner surface annual average bolometric brightness temperature measurements [7], Kaguya MI surface composition mapping [12], long-exposure LROC images [13] and Mini-RF S band radar CPR maps [14]. We find each of these studied factors has no clear or very weak effects on the observed LOLA albedo. Thus, we suggest that the elevated LOLA albedo of the polar PSRs can be best explained by possible presence of ice particles in the regolith of the PSRs.

Characterizations of polar water ice: Our integrated observations of surface 1064 nm albedo and impact crater records also provide insight into the nature of polar surface water ice. LOLA is only able to sample the uppermost micrometer of the surface, and radar experiments do not positively indicate the presence of thick surface water-ice deposits; the interpreted water-ice materials may be in the presence of a surface frost layer or admixture with lunar regolith. This interpretation is also supported by the crater population and depth investigations, which show that the surface water ice in the polar PSRs is not voluminous sufficient to modify the superposed cratering record. The observed very thin nature of these volatiles suggests that the retention of surface water-ice materials at the lunar polar region may be a dynamic process, for instance, volcanically erupted water migrating toward the poles and cold-trapped in PSRs, and then being subject to sublimation due to impact gardening [15,16].

Summary: We find the 1064 nm albedo of the polar PSRs are symmetrically higher than their adjacent non-PSRs. Space weathering, solar illumination, surface temperature-related albedo effect cannot solely explain the observed albedo discrepancy, thus surface water-ice deposits may explain the enhanced albedo. Impact cratering records suggest that the potential surface ice does not have a significant effect on the observed cratering records, indicating lack of massive ice deposits. This work can provide an important reference base for landing site selection and surface operations for future lunar polar ice exploration missions.

References:

[1] Watson et al. (1961) *JGR* 66, 3033-3045. [2] Nozette et al. (1996) *Science* 274, 1495-1498. [3] Feldman et al. (1998) *Science* 281, 1496-1550. [4] Campbell et al. (2006) *Nature* 443, 835-837. [5] Gladstone et al. (2010) *Science* 330, 472-476. [6] Zuber et al. (2012) *Nature* 486, 378-381. [7] Paige et al. (2010) *Science* 330, 479-482. [8] Smith et al. (2010) *SSR* 150, 209-241. [9] Mazarico et al. (2011) *Icarus* 211, 1066-1081. [10] Lucey et al. (2014) *JGR-Planets* 119, 1665-1679. [11] Fisher et al. (2017) *Icarus* 292, 74-85. [12] Haruyama et al. (2008) *EPS* 60, 243 – 255. [13] Cisneros et al. (2017) *LPSC XLVIII*, #2469. [14] Nozette et al. (2010) SSR 150, 285-302. [15] Hayne et al. (2015) *Icarus* 255, 58-69. [16] Needham & Kring (2017) *EPSL* 478, 176-178.

INVESTIGATING FAR-ULTRAVIOLET HYDRATION SIGNATURES IN THE SOUTHWEST ULTRAVIOLET REFLECTANCE CHAMBER (SwURC) IN SUPPORT OF LRO-LAMP OBSERVATIONS.

U. Raut[1], P. L. Karnes[1], K. D. Retherford[1,2], E. Czajka[1,2], M. J. Poston[1], M. W. Davis[1], Y. Liu[3], E. L. Patrick[1]., G. R. Gladstone,[1,2], T. K. Greathouse[1], A. R. Hendrix[4], P. Mokashi[1] [1]Southwest Research Institute, Space Science and Engineering Division, San Antonio, TX 78238, [2]Department of Physics and Astronomy, University of Texas at San Antonio, San Antonio, TX 78249, [3]Lunar and Planetary Institute, Houston, TX 77058, [4]Planetary Science Institute, Tucson, AZ 85719.
(uraut@swri.edu)

Introduction: Far-ultraviolet (FUV) reflectance spectra from the Lyman Alpha Mapping Project (LAMP) spectrograph onboard the Lunar Reconnaissance Orbiter (LRO) shows evidence for surficial water frost in the permanently shadowed regions (PSRs) of the Moon [1]. It also showed the presence of a thin veneer of H_2O and/or hydroxyl species in the lunar regolith with an abundance which varies systematically with latitude and on diurnal timescales [2]. The presence of the hydrated species induces FUV spectral reddening attributed to the strong water ice absorption edge at 165 nm [2].

Deriving accurate estimates of the PSR water content or the spatial abundance and distribution of the water in the lower-latitude lunar regolith from the LAMP FUV observations has proven challenging. Different flavors of radiative transfer theories to model the LAMP spectra require optical constants of endmember species – lunar regolith and water ice. However, these fundamental properties of lunar soils and ice-soil aggregates are largely uncharacterized in the FUV, thereby limiting the accuracy of the hydration estimate. As such, the PSR water abundance is constrained to ~ 1-2% [1], while the dayside abundance constrained to < 1% [2]. Both estimates were obtained by observing and/or modeling the variations in the spectral slope in the 164-173 nm region due to the strong water ice absorption edge at 165 nm.

The surficial water molecules present at lower latitudes can migrate to the lunar poles via ballistic hops [3] and could, therefore, be an important source to the water ice frost in the PSRs cumulated over the geological history of the Moon [4]. Accurate knowledge of the dayside abundance of the lunar hydration could further help constrain the supply rate to the PSRs.

With goals to further refine the LRO-LAMP hydration estimates, we are currently engaged in making bidirectional reflectance and phase curve measurements of dry Apollo soils and especially that of ice-Apollo soil aggregates in the SwURC. We will present robust data on the FUV reflectance of dry Apollo soils (Figure 1), followed by preliminary results on ice-coated and ice-soil aggregates.

Experimental Setup: The bidirectional reflectance measurements of the dry and water vapor-exposed Apollo soils are conducted in the Southwest Ultraviolet Reflectance Chamber (SwURC), which is an ultrahigh vacuum chamber (base pressure ~ 10^{-9} Torr) coupled to a vacuum ultraviolet scanning monochromator that uses a combination of a rotating dispersive grating and a pair of entry/exit slits to select near monochromatic light from a 30 W deuterium lamp source. The monochromatic light is incident on the Apollo soils (mare and highland samples obtained from CAPTEM) assembled on the horizontal sample tray that resides within the high vacuum chamber. The sample tray can be cooled to ~ 85 K using an open-cycle LN_2 flow.

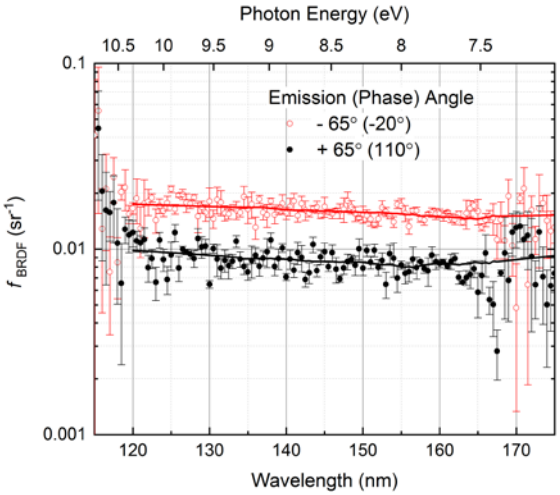

Figure 1- Wavelength dependence of the BRDF function of the canonical Apollo soil 10084 in dry state measured at two different emission angles. We plan to expose the soil to controlled water-vapor flux and study the slope upturn at 165 nm with increasing H_2O content. See Ref. [6] for additional details.

We will also expose the Apollo soils to precisely controlled fluxes of water vapor. Currently, we are completing the installment of a calibrated gas dosing manifold and a micro-capillary array doser on the SwURC. The amount of water vapor leaked into the chamber from the gas manifold will be monitored using absolute MKS-Baratron capacitance manometer gauges. The micro-capillary doser will exude a collimated flux of water directed towards the cooled Apollo soils.

The diffuse light reflected by the dry and wet Apollo soils is received by a sealed CsI-coated channeltron detector which is installed on a rotating mount. The channeltron traces a circular track in the principal plane measuring the intensity of the reflected light over a wide range of emission or phase angles. Our measurements quantify the bidirectional reflectance distribution function f_{BRDF}, which is an invariant sample property for a pair of incidence and emission geometries. The BRDF function for the SwURC geometry simplifies to,

$$f_{BRDF}(g) = \frac{P_r(g)}{[P_i \cos(-45^\circ)]\,\Omega_d}$$

where P_i and P_r are the powers of the incident and reflected flux, g is the phase angle and Ω_d is the projected solid angle. See Ref [5, 6] for more details on the SwURC instrumentation.

Our key objective will be to quantify the relationship between the magnitude of the BRDF slope change with respect to the water content in the wet Apollo soils and apply the laboratory data to obtain refined hydration estimates from LAMP spectral datasets for both PSRs and low-latitude regions.

Acknowledgment: We are thankful to CAPTEM for providing us with Apollo soil samples. The development of the SwURC facility was funded by SwRI Internal Research and Development funds. Measurements in support of LRO-LAMP investigations are funded by NASA.

References: [1] Gladstone, G. R., K. D. Retherford, A. F. Egan, D. E. Kaufmann, P. F. Miles, J. W. Parker, D. Horvath, P. M. Rojas, M. H. Versteeg, and M. W. Davis (2012), Far-ultraviolet reflectance properties of the Moon's permanently shadowed regions, Journal of Geophysical Research: Planets, 117(E12). [2] Hendrix, A. R., et al. (2012), The lunar far-UV albedo: Indicator of hydration and weathering, Journal of Geophysical Research: Planets, 117(E12001), doi:10.1029/2012JE004252. [3] Schörghofer, N. (2014), Migration calculations for water in the exosphere of the Moon: Dusk-dawn asymmetry, heterogeneous trapping, and D/H fractionation, Geophysical Research Letters, 41(14), 4888-4893, doi:10.1002/2014GL060820. [4] Anand, M. (2010), Lunar Water: A Brief Review, Earth, Moon, and Planets, 107(1), 65-73, doi:10.1007/s11038-010-9377-9. [5] Karnes, P. L., et al. (2013), Radiometric calibration of the SwRI ultraviolet reflectance chamber (SwURC) far-ultraviolet reflectometer, paper presented at SPIE Optical Engineering + Applications, SPIE. [6] Raut, U., Karnes, P. L., Retherford, K. D., Davis, M. W., Liu, Y., Gladstone, G. R., et al. (2018). Far-ultraviolet photometric response of Apollo soil 10084. Journal of Geophysical Research: Planets, 123. https://doi.org/10.1029/2018JE005567

LRO Lyman Alpha Mapping Project (LAMP)'s Polar Volatile Studies Overview and Future Steps. K. D. Retherford[1,2], T. K. Greathouse[1], B. D. Byron[2,1], L. O. Magaña[2,1], C. Grava[1], A. F. Egan[3], U. Raut[1,2], E. Czajka[2,1], D. M. Hurley[4], J. T. S. Cahill[4], A. R. Hendrix[5], K. E. Mandt[4], Y. Liu[6], D. Wyrick[1], G. R. Gladstone[1,2]; [1]Southwest Research Institute, San Antonio, TX (kretherford@swri.edu), [2] University of Texas at San Antonio, San Antonio, TX, [3]Southwest Research Institute, Boulder, CO, [4]Johns Hopkins University Applied Physics Laboratory, Laurel, MD, [5]Planetary Sciences Institute, Tucson, AZ, [6]Lunar and Planetary Institute, Houston, TX.

Abstract. Far ultraviolet (FUV) albedo maps obtained using the Lunar Reconnaissance Orbiter (LRO) Lyman Alpha Mapping Project (LAMP)'s innovative nightside observing technique [1,2] have revealed features on the Moon in a new light. Dayside FUV maps are also obtained using the more traditional photometry technique with the Sun as the illumination source, and are very complementary. Together, these LRO-LAMP measurements provide a unique perspective on the lunar "hydrological cycle," connecting the surface abundance of water frost trapped in the Moon's cryosphere to volatile transport processes involving the lunar exosphere. Near the start of the present mission extension phase LAMP's aperture size for dayside observing was greatly expanded to increase data quality of these signals. improving searches for time variable hydration features.

LAMP Instrument and Technique. The LRO-LAMP UV imaging spectrograph is well suited to study how water is formed on the Moon, transported through the lunar exosphere, and deposited in permanently shaded regions (PSRs)[2,3]. LAMP nightside and dayside brightness maps cover wavelength range 57-196 nm. Lyman-α, on-band and off-band albedo maps (i.e., on and off the water frost absorption band at ~165 nm) are useful for constraining the abundance of surficial water frost [1,4,5].

Global dayside FUV albedo maps enable comparisons between the nightside and dayside photometry techniques to help validate the use of Lyman-α and starlight as illumination sources. Analysis of dayside spectra for selected regions complement the nightside maps, and are used to investigate space weathering and other surface signatures [6].

Global nightside and dayside maps are divided (at ±60° latitude) into polar and equatorial regions with stereographic and equirectangular projections, respectively. Additionally, spectral image cube maps have been created for several regions of interest with 2 nm resolution, and are being expanded to cover the full globe.

New Dayside Investigations. LAMP has implemented an exciting new operating mode that enhances the sensitivity of dayside observations by 1-2 orders of magnitude. A one-time opening failsafe door had been included in the design of the LAMP instrument, in case the main aperture door mechanism had somehow failed (stuck shut for example). By opening this failsafe door device a previously blocked component of the telescope's 4 cm by 4 cm aperture would be viewable to space in any event, allowing a 10% throughput of signal compared to the full aperture size [7]. The door itself had been designed with a pinhole aperture for dayside observations at count rates comparable to the nightside signals with a 0.14% throughput. The effective area of dayside observations improved by a factor of 73.6 as a result of this change, allowing better data quality measurements.

New photometric analyses of the far-UV reflectance properties are in hand [8] and compare nicely with laboratory reflectance measurements of Apollo soil sample 10084 [9]. These photometric correction factors are being applied to both the dayside and nightside LAMP mapping and spectral products. The present LRO extended science mission enables more surface reflectance data (60-190 nm) at a variety of incidence and emission angles to improve signal, spectral, and photometric quality and further develop our innovative UV reflectance techniques.

References [1] Gladstone, G. R. et al., Far-Ultraviolet Reflectance Properties of the Moon's Permanently Shadowed Regions, *J. Geophys. Res.*, *117*, E00H04, 2012. [2] Gladstone, G. R., et al., LAMP: The Lyman Alpha Mapping Project on NASA's Lunar Reconnaissance Orbiter Mission, *Space Sci. Rev.*, *150*, 161-181, 2010. [3] Gladstone, G. R. et al., LRO-LAMP Observations of the LCROSS Impact Plume, *Science, 330*, 472-476, 2010. [4] Retherford, K. D., et al., LRO/LAMP Far-UV Albedo Maps, *in preparation*, 2018. [5] Hayne, P. O. et al., Evidence for Exposed Water Ice in the Moon's South Polar Regions from Lunar Reconnaissance Orbiter Ultraviolet Albedo and Temperature Measurements, Icarus (volume 255, pages 58-69, doi:10.1016/j.icarus.2015.03.032). [6] Hendrix, A. R., et al., Lunar Albedo in the Far-UV: Indicator of Hydrated Materials and Space Weathering, *J. Geophys. Res.*, 117, E12001, 2012. [7] Davis, M. W., et al., LRO-LAMP failsafe door-open performance: improving FUV measurements of dayside lunar hydration, SPIE, 2017. [8] Liu, Y., et al., The Far Ultraviolet Wavelength Dependence of the Lunar Phase Curve as seen by LRO LAMP, *J. Geophys. Res. submitted*,2018. [9] Raut, U., et al., Far-Ultraviolet Photometric Response of Apollo Soil 10084, *J. Geophys. Res.*, 123. https://doi.org/10.1029/2018JE005567, 2018.

ShadowCam: Seeing in the Shadows. M. S. Robinson[1] and the ShadowCam Team, [1]School of Earth and Space Exploration, Arizona State University, Tempe AZ, 85287, robinson@ser.asu.edu.

Introduction: Lunar permanently shadowed regions (PSRs) may be the most valuable real estate in the Solar System, with the potential for cold-trapped volatiles, including water ice, which could provide essential resources to enable future exploration of the Moon and beyond. However, the investigation of PSRs in terms of their true resource potential is still in its infancy. Various observations have identified the locations of PSRs [1,2,3,4,5,6] where various volatiles are thermally stable within them [7], detected hydrogen (e.g. [8,9]), water [10], and reflectance variations consistent with surface frost [11, 12]. However, to truly assess the extent, concentration, utility, and accessibility of volatiles contained within PSRs, landed missions are required. Thus, we are building ShadowCam, a focused imaging investigation of PSRs that will provide the necessary information about landforms, traversability, and the spatial and temporal variability of volatiles at spatial scales required for future exploration.

ShadowCam is a focused investigation of lunar PSRs that will provide critical information about the distribution and accessibility of volatiles in PSRs at spatial scales required to both mitigate risks and maximize the results of future exploration activities. ShadowCam was selected to fly on the Korea Aerospace Research Institute (KARI) Korea Pathfinder Lunar Orbiter (KPLO) slated for launch December 2020. ShadowCam is a high-heritage instrument based on the successful Lunar Reconnaissance Orbiter Camera (LROC) Narrow Angle Camera (NAC) with a TDI detector replacing the conventional line scan CCD; the system sensitivity is over 200 times greater than the NAC. ShadowCam will address three of the four NASA strategic knowledge gaps (SKGs) through high-resolution (1.7 m/pixel), high signal-to-noise (S/N >100) imaging of PSRs illuminated only by light reflected off nearby topographic facets, without duplicating measurements from KARI instruments. ShadowCam will saturate while imaging illuminated ground, with no harmful consequences to the shadowed portion of the image.

The ShadowCam investigation has five objectives formulated to achieve a *single overarching goal*: obtain measurements that directly address three of the four lunar volatile strategic knowledge gaps (SKGs) outlined in the KPLO solicitation [13]. The current lack of high-resolution and high S/N PSR images seriously hampers the ability of the science community to make sense of the somewhat contradictory results from a broad range of remote sensing observations. The potential results of the ShadowCam experiment are so compelling that one could justifiably argue that meaningful progress towards understanding polar volatiles in terms of concentration and extent *requires* high-resolution and high S/N PSR imaging. The ShadowCam team will achieve these objectives through unique PSR observations without duplicating measurements from KARI instruments.

Objective 1: Map albedo patterns in PSRs and interpret their nature. *ShadowCam will map albedo variations with high spatial resolution and high S/N to test the competing hypotheses for PSR reflectance to determine whether the surface regolith contains water frost, ice, or lag deposits, or has experienced lower levels of space weathering*

Objective 2: Investigate the origin of anomalous radar signatures associated with some polar craters *ShadowCam will detect blocks as small as 2 m in PSRs to determine whether the interiors of radar anomalous craters contain relatively pure water ice or blocky deposits.*

Objective 3: Document and interpret temporal changes of PSR albedo units. *ShadowCam will monitor albedo in PSRs to search for albedo changes that inform our understanding of the movement and retention of volatiles in PSRs and local regolith properties.*

Objective 4: Map the morphology of PSRs to search for and characterize landforms that may be indicative of permafrost-like processes. *ShadowCam will provide images of PSR geomorphology at pixel scales (<2 m) that enable detailed comparisons with landforms on the Moon, Mars and Earth.*

Objective 5: Provide hazard and trafficability information within PSRs for future landed elements. *ShadowCam will characterize the trafficability of PSRs with morphologic and topographic observations critical for both mitigating risks and maximizing the results of future exploration activities*

References: [1] Shoemaker et al. (1994) *Science*, 266, 1851-1854. [2] Bussey et al. (2003), *GRL*, 30, doi:10.1029/2002GL016180. [3] Bussey et al. (2010) *Icarus*, 208, 558-564. [4] Noda et al. (2008) GRL, 35, doi:10.1029/2008GL035692. [5] Mazarico et al. (2011) Icarus, 211, 1066-1081. [6] Zuber et al. (2012) *Nature*, 486, 378-381. [7] Paige et al. (2010) *Science*, 330, 479-482. [8] Feldman et al. (2000) *JGR*, 105, 4175-4195. [9] Mitrofanov et al. (2010) *Science*, 330, 483-486. [10] Colaprete et al. (2010) *Science*, 330, 463-468. [11] Gladstone et al. (2012) *JGR*, 117, doi:10.1029/2011JE003913. [12] Lucey et al. (2014) *JGR*, 119, 1665-1679. [13] NASA (2016) SALMON-2, NNH12ZDA006O.

SKG	Science Objectives	Scientific Measurement Requirements		Instrument Requirements and Expected Performances			Mission Functional Requirements
		Observable	Measurement	Aspect of Performance	Required Value	Predicted Value	
1. Investigate the spatial and temporal distribution of OH and H2O at high latitudes (KPLO SKG 1)	1.1 Map albedo patterns in PSRs and interpret their nature	Reflectance units with contrast of 5%	Surface reflectance of PSRs from scattered light	GSD	≤2 m (IFOV ≤0.02 μrad)	1.7 m (IFOV 0.017 μrad)	Nominal spacecraft altitude of 100 km
	1.2 Determine the origin of anomalous radar signatures associated with some polar craters by revealing block populations down to 2-m diameter to descriminate between a blocky target and regolith-bound ice	Location, size, shape of landforms	Size–frequency distribution of blocks				Line-of-sight jitter < 8.5 μrad
2. Monitor and model movement of volatiles towards and retention in permanently shadowed regions (KPLO SKG 3)	2.1 Document and interpret temporal changes of PSR albedo units	Imaging during different seasons, times of day	Temporal differences in PSR reflectance	MTF	≥0.2 at Nyquist frequency	≥0.22 at Nyquist frequency	Line-of-sight drift 1.6°/s
				Smear	<2 m (1.26 msec)	1.7 m (1.07 msec)	Alignment <4 mrad
				SNR	SNR >100	SNR >100	Scan rate knowledge 0.4%
				Relative Calibration	2%	1%	Downlink average of 16 gigabits/day
3. Investigate the geomorphology, accessibility, and geotechnical characteristics of cold traps (KPLO SKG 4)	3.1 Map the morphology of PSRs to search for and characterize landforms that may be indicative of permafrost-like processes	Landforms	Location, size, shape of landforms				Polar orbit (90°±0.25°)
	3.2 Provide hazard and trafficability information within PSRs for future landed elements	Landforms	Terrain roughness				Predict SPICE Definitive SPICE
		Stereo imaging	Topography at scales of 6 m				Spacecraft slews for stereo (~20°)

Figure 1. ShadowCam Science Traceability Matrix (from ShadowCam proposal).

Sublimation Behavior of Water-doped Lunar Simulant at Cryogenic Temperatures. Ted L. Roush[1], Luis F. A. Teodoro[2,1], Anthony Colaprete[1], Amanda Cook[3,1], Richard Elphic[1], [1]NASA Ames Research Center, Moffett Field, CA, [2]Bay Area Environmental Research Institute, Moffett Field, CA, [3]Millennium Engineering, Sunnyvale, CA

Introduction: NASA's Resource Prospector (RP) intends to characterize the 3D volatile distribution in lunar polar and permanently shadowed regions [1]. The Near-Infrared Volatile Spectrometer System (NIRVSS, [2]) observes the surface where a drill [3] deposits sub-surface soil.

RP sub-systems tests have occurred in a cryo-vacuum chamber [4-6] that accommodates a tube filled with lunar simulant, NU-LHT-3M, prepared with known abundances of water. During 2016, after the average soil temperature reached ≈180 K, drilling activities commenced and NIRVSS alternated between obtaining spectra and images.

Experimental Data: NIRVSS measures diagnostic signatures of water ice near 2000 and 3000 nm and a band depth (BDs, BD2000 and BD3000) was defined to each to document the ice behavior during drilling [7]. As ice-bearing soils are emplaced onto the surface these BDs increase and then decrease as the ice sublimes (Fig. 1 top). Imaging revealed complex behavior of the drill cuttings piles; including down-slope soil movement, slope failures, and funnel blockage preventing deposition of new soil onto the surface. This dynamic activity discourages using the active drilling observations to assess ice sublimation. On several occasions, the drill, while static, was percussed in an attempt to document the sublimation behavior of exposed ice (Fig. 1, top, orange lines).

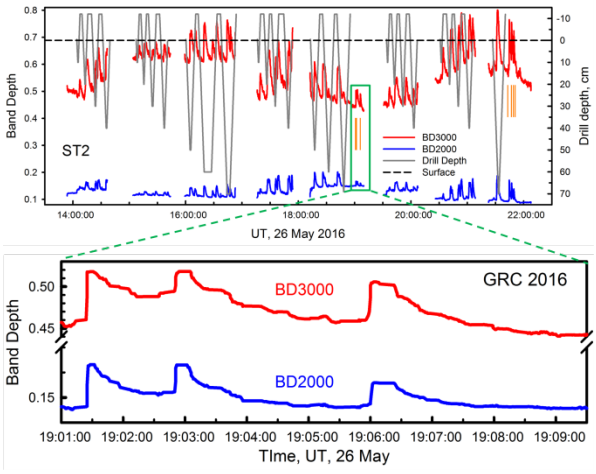

Figure 1. Overview of ice BDs (top) and zoom of percussions (bottom).

Characterizing Sublimation Behavior: Fig. 2 shows BD2000 (blue circles), and BD3000 (red circles) after the final of three one-second percussions shown in the bottom of Fig. 1. Each percussion was fit using a three term exponential decay function of the form: $BD = y_0 + a*e^{(-bx)}$, where x is the elapsed time after the percussion. Example fits are shown as the solid lines in Fig. 2 with residuals at the top for each BD.

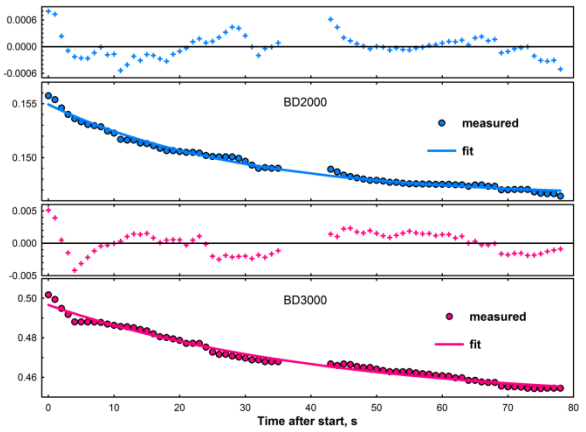

Figure 2. Fits (lines) to BDs (dots) and residuals (above each panel).

Discussion: BDs derived from the NIRVSS spectra document sublimation of exposed water ice during drilling (Fig. 1, top) and after percussion (Fig. 1 bottom). Exponential fits to the BDs after percussions provide an estimate of the sublimation time of the exposed ice (Fig. 2), documenting a decay to background levels in ≈ 60 seconds. Compared to calculations of pure ice [8], this behavior is consistent with relatively fine grained sub-surface ice exposed to temperatures above 150 K, a temperature consistent with the measured average soil temperature (≈180 K). The BD behavior after the percussive events may permit more detailed models of sublimation behavior from the more complex soil-water ice mixture [e.g. 9].

References: **References:** **[1]** Andrews, D., et al., 2014, 52nd AIAA 2014 Space Conf. and Expo., doi: 10.2514/6.2014-4378. **[2]** Roush, T. et al. 2016, AIAA SciTech Forum, doi:10.2514/2016-0228 **[3]** Zacny K., et al., 2015, 46th Lunar Planet. Sci. Conf., abstract 1614. **[4]** Kleinhenz, J. 2014, AIAA SciTech. **[5]** Kleinhenz, J., et al., 2015, AIAA SciTech., doi:10.2514/6/2.2015-1177. **[6]** Kleinhenz, J., et al., 2016, AIAA SciTech 2016. **[7]** Roush, T., et al. 2017, 48th Lunar Planet. Sci. Conf., abstract 1240. **[8]** Andreas, E., 2007, Icarus, 186, 24-30. **[9]** Teodoro, L., et al. 2017, LEAG meeting, abstract 5058.

The Depth of Small Craters and the Shadows they Cast: Evidence for Ice on the Moon and Mercury L. Rubanenko[1], J. Venkatraman[1] and D. A. Paige[1], [1]Department of Earth, Planetary and Space Sciences, UCLA, LA, CA 90095 (liorr@ucla.edu)

Introduction: Topographic depressions near the poles of Mercury and the Moon may trap ice for billions of years inside PSRs [1, 11, 15]. On Mercury, evidence for water ice deposits that are at least a few meters thick was remotely sensed in radar [6]. More recently, data obtained by the MErcury Surface, Space ENvironment, GEochemistry, and Ranging (MESSENGER) revealed bright and dark deposits in areas cold-enough to trap water ice according to a thermal model [3, 8, 10]. Additional evidence for the presence of ice inside individual small craters (~ 1 km) and micro cold-traps ($1-10$ m) was found using data obtained by the Mercury Laser Altimeter (MLA) [4, 12]. In contrast, lunar cold-traps were not observed to contain similar ice quantities. Evidence for a thin layer of ice was found in several lunar craters such as Shackelton [16], but Earth-based radar observations did not detect areas > 1 km^2 with high backscattering [14], indicating that any existing ice must be thinner than a few decimeters or is in the form of distributed grains [2]. Here we show small ($3-15$ km) craters on both Mercury and the Moon become shallower in latitudes where ice is expected to accumulate according to a thermal model. We estimate the thickness of this infill by comparing the depth to diameter ratios (d/D) of craters with the d/D they would have had if they were filled with ice up to the permanent shadow volume (PSV) limit.

Measuring the Ice Depth Inside Small Craters: We begin by identifying small ($3-15$ km), simple craters on the Mercury Dual Imaging System (MDIS) and the Lunar Reconnaissance Orbiter Camera (LROC) global basemaps. We measure craters' elevation along a south-north profile on the gridded Mercury Laser Altimeter polar map (MLA, 250 m/px) and gridded Lunar Orbiter Laser Altimeter (LOLA, 120 m/px), as shown in Figure 1, and use it to calculate their d/D. On Mercury we measured 1003 craters between latitudes $75°-86°$, where the most reliable MLA data is found. On the Moon, we measured 1353 craters in latitudes $74°-90°$, and plan to extend this range to lower latitudes. Next, we model the d/D distribution these craters would have had if they were *filled* with ice up to the permanent shadow limit.

Maximum Possible Infill: Due the exponential dependence of the sublimation rate on temperature, ice can only persist inside permanent shadows. During the day the crater casts transient shadows that add into permanent shadows in high latitudes. We calculate the depth of these transient shadows d_s modeling the craters as hemispherical (bowl-shaped) cavities,

$$\frac{d_s}{d} = 1 - \frac{1}{2\Delta}\cot\theta \qquad (1)$$

where d is the crater's depth, θ is the incidence angle and Δ is the crater d/D ratio. The depth of the permanent shadow volume (PSV) constrains the depth of ice accumulated inside the crater. Therefore, if we subtract the modeled PSV depth from the measured depth in lower latitudes (where only a small amount of ice is expected to persist [11, 13]) we should receive the d/D distribution of craters as if they were *filled with ice* up to the PSV limit. This assumes the d/D does not significantly change with latitude due to some other geologic property.

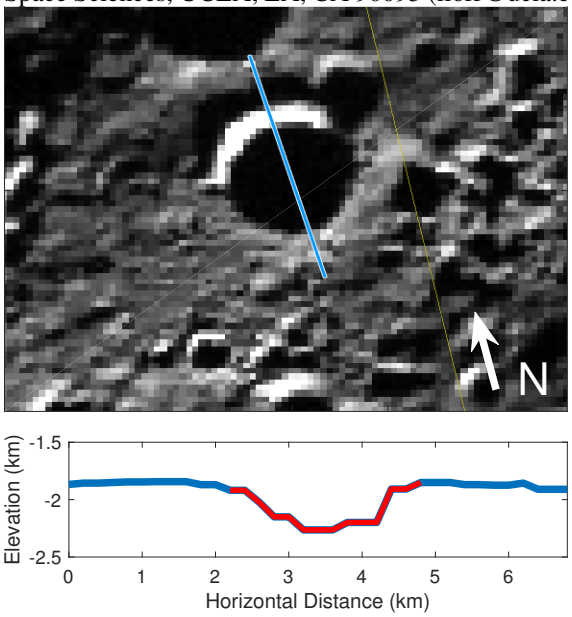

Figure 1: An example showing our method of measurement. The blue line drawn on top of the crater in the top panel marks the the elevation profile shown in blue in the lower panel.

Results: Figure 2 shows the d/D distribution for Mercury (a) and the Moon (b). The mean d/D of craters on Mercury decreases from 0.96 ± 0.0036 in latitudes $75°-78°$ to 0.075 ± 0.0034 in latitudes $83°-86°$. On the Moon we see a similar but less distinct trend; the mean d/D decreases from 0.123 ± 0.0038 in latitudes $75°-78°$ to 0.097 ± 0.0033 in latitudes $87°-90°$. The values above are provided along with the standard error of the mean. As explained above, we model the distribution of craters as if they were filled with ice to the permanent shadow limit (dashed line). We see that on both Mercury and the Moon craters are not filled to the permanent shadow volume limit.

On Mercury, we find craters become shallower with latitude *relative to their maximum potential capacity*. This can be seen in Figure 3(a), where the markers indicating the measured mean d/D are steeper than the maximum potential capacity lines; in latitude $84°$, craters are filled to $\sim 20\%$ of their maximum potential capacity, while in latitude $86°$ craters are filled to $\sim 40\%$ of their maximum potential capacity. This effect is much less prominent on the Moon (Figure 3(b)), where the measured mean d/D trend is almost parallel to the $\sim 20\%$ maximum infill line. We attribute this difference to the age of the ice as near the poles, the lower sublima-

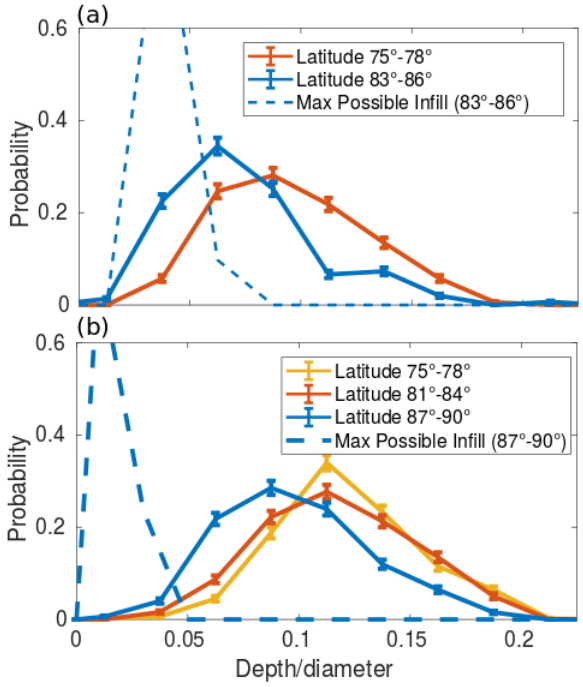

Figure 2: (a) The d/D distribution on Mercury for two latitude rings. Error bars indicate the square root of the sample size. The mean crater depth decreases as deep ($d/D > 0.1$) are replaced by shallow ($d/D < 0.1$) craters. (b) The d/D distribution on the Moon for three latitude rings. On the Moon, craters do not become significantly shallower until near-polar latitudes.

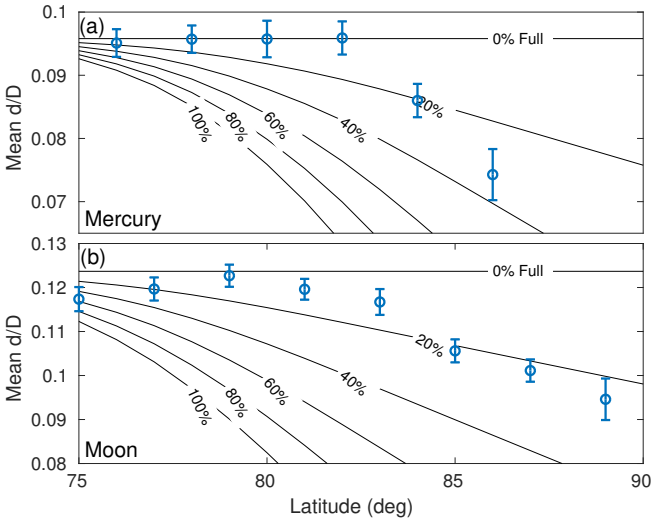

Figure 3: The mean d/D of small crater on Mercury (a) and the Moon (b) decreases with latitude (blue markers). The black lines shows how would the mean d/D decrease if craters were filled with ice up to a fraction of the permanent shadow limit (shown in %). On Mercury, these deposits become thicker with latitude *relative to the PSV limit*, while on the Moon this effect is much less prominent.

tion rate better preserves the ice over long time periods. On Mercury, the near polar ice deposits are layered with younger ice covering older ice. On the Moon, however, ice did not preserve as well as it did on Mercury, and the historic mean ice net accumulation rate is lower.

Discussion: Above we have shown small craters near the poles of Mercury become shallower in latitudes where ice is expected to accumulate on their floors. Similar inspection on the Moon showed craters do not become shallower until near-polar latitudes. Additionally, we find craters on both planetary bodies are not filled to their maximum capacity, which is (to first order) constrained by the depth of the permanent shadow volume. Given the dimensions of the craters we measured, we estimate this infill to be $10 - 100$ m thick. This result is particularly surprising on the Moon, where radar measurements did not show evidence for thick ice deposits. On Mercury, this implies a net delivery rate of a few meters per Ga, in accord with previous theoretical [7, 9] and observational [5] estimates. Additionally, the difference between the mean measured and modeled filled crater distributions indicates the historic net mean volatile accumulation rate is greater on Mercury compared to the Moon. This is also evident by the different thickness of the deposits relative to the maximum potential infill at every latitude, which is greater for Mercury than for the Moon. We attribute this difference to the age of the ice: on Mercury, polar ice has accumulated for a longer time period filling a larger portion of the craters. On the Moon, the historic mean net accumulation rate is probably much closer to zero and the deposits we measured are probably much younger.

References: [1] JR Arnold. *JGR* (1979). [2] BA Campbell et al. *Nature* 426.6963 (2003), 137–138. [3] NL Chabot et al. *Geology* (2014). [4] AN Deutsch et al. *GRL* (2017). [5] AN Deutsch et al. (2017). [6] JK Harmon et al. *Icarus* 149 (2001). [7] JI Moses et al. *Icarus* (1999). [8] GA Neumann et al. *Science* (2013). [9] L Ong et al. *Icarus* (2010). [10] DA Paige et al. *Science* 339 (2013), 300–303. [11] DA Paige et al. *Science* 258 (1992). [12] L Rubanenko et al. *JGR: planets (in review)* (2018). [13] L Rubanenko et al. *Icarus* (2017). [14] NJS Stacy et al. *Science* 276.5318 (1997), 1527–1530. [15] K Watson et al. *JGR* (1961). [16] MT Zuber et al. *Nature* 486.7403 (2012), 378–381.

EXOSPHERIC WATER PRODUCTION FROM METEOROIDS: SPORADICS VERSUS METEOR SHOWERS. M. Sarantos[1](menelaos.sarantos-1@nasa.gov), D. Janches[1], and P. Pokorny[1,2], [1]Heliophysics Science Division, NASA Goddard Space Flight Center, Greenbelt, MD 20771,USA [2]Department of Physics, The Catholic University of America, Washington, DC 20064, USA

Introduction: The Lunar Atmosphere and Dust Environment Explorer (LADEE) measured the lunar atmosphere for a period of five months with two instruments, a Neutral Mass Spectrometer (NMS) and an UltraViolet Spectrometer (UVS). Initial analyses of returned data indicate detections of exospheric water and OH for the first time and enhancements coincident with meteor showers [1]. These observations provide new constraints about the transport of volatiles at the poles, enable us to constrain the physical processes that contribute to the generation of the lunar exosphere, and provide insight about the meteoroid environment around the Moon.

Methods: We will quantify the expected difference in source rates of water and OH during sporadics, the continuously present rain of meteoroids on the Moon, and Geminids if the released water is endogenous to the Moon. For this calculation we utilize a dynamical model of the zodiacal cloud, which includes meteoroids from Jupiter Family, Halley Type and Oort Cloud Comets, and which predict where meteoroids arrive at the Moon [2], with what velocity distribution, with what distribution in latitude and local time, and how this changes with lunar phase. The volume vaporized by a meteoroid is a function of its size and velocity [3]. The Geminids stream consists of bigger particles than the sporadic background, and to capture this effect in our estimates we use constraints from radar measurements. This calculation will provide limits to the relative importance of high-speed meteoroids from long-period comets.

Furthermore, we will present studies of the temporal evolution of water and OH released by impacts during Geminids with a Monte Carlo simulator of the exosphere-surface reservoir. The thermal environment for these transport simulations is provided by 0.5°×0.5° Diviner measurements (Fig 1). The temperature of the released ensemble can be 3000-5000 K (impact vaporization). Given the estimated release profile of water group vapor during Geminids, the simulations seek to quantify the nature (e.g., is there more hydroxyl than water released initially?) and fate of the water group exosphere by testing different sets of microphysical parameters of the soil.

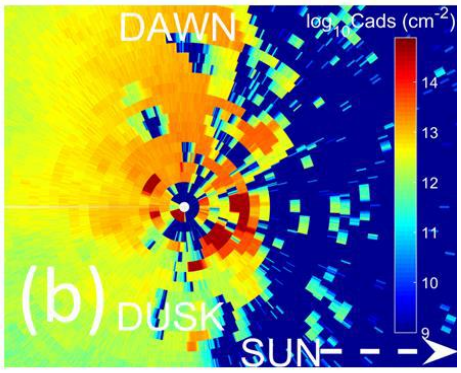

Fig 1: Our simulator provides both gas density as well as surface abundance of an adsorbate. Here the evolution of the water reservoir in the South Pole region was simulated assuming a continuous release from meteoroids for 60 lunar months. If that were true, a monolayer of water frost would quickly accumulate on PSRs grains.

References: [1] Benna, M., et al. 2017, *AGU Fall Meeting Abstracts*. [2] Janches D. et al. 2018, Geophys. Res. Lett., 45, 1713. [3] Cintala, M. J. 1992, *J. Geophys. Res*., 97, 947.

Transport in the Lunar Water Exosphere. Norbert Schörghofer[1,2], [1]Planetary Science Institute, Tucson, AZ and Honolulu, HI, USA, [2]TREX-SSERVI (norbert@psi.edu)

Introduction: The surface-bounded exosphere of the Moon [1, 2] consists of ballistic trajectories, and is governed by its interaction with the surface. A water exosphere can transport molecules to cold traps near the rotational poles where they condense into ice [3].

When a molecule comes in contact with the surface, it thermally accommodates and then leaves in a random direction and with a thermal velocity distribution. A thermal ballistic hop of an H_2O molecule spans on average 200 km and takes 7 min.

Vertical density profile: Exospheres above an atmosphere, such as on Earth and the Sun, have long been investigated theoretically [4–6]. For the simple case of constant gravitational acceleration g, these investigators obtain an exponential density distribution

$$\rho(z) = \frac{\sigma}{H} e^{-z/H} \tag{1}$$

where σ is the column-integrated mass, z the height above the surface (or exobase), and H the scale height $H = k_B T/(mg)$. Here, k_B is the Boltzmann constant, T the surface temperature, and m the mass of the molecule or atom.

These calculations assume a reservoir of molecules at the base. This situation applies for the water exosphere of a fully ice covered body, but on the Moon the number of available molecules is limited. The vertical density distribution for a fixed number of particles is significantly different from (1).

Given a probability distribution of initial velocities, the ensemble average of a quantity per hop/particle is denoted by $\langle . \rangle$. The average of a quantity at a given time, denoted by $\langle\!\langle . \rangle\!\rangle$, has to be weighted by the flight duration. This is the time average of a stationary situation, or, with enough particles, a snapshot. For example, the average maximum height of a ballistic hop is $\langle z_{max} \rangle = H/2$ and $\langle\!\langle z_{max} \rangle\!\rangle = H$.

The vertical density profile of a stationary thermalized surface-bounded exosphere in a uniform gravity field, with a Maxwell distribution for launch velocities is

$$\langle\!\langle \rho \rangle\!\rangle(z) = \frac{\sigma}{2H} e^{-z/2H} K_0\left(\frac{z}{2H}\right) \tag{2}$$

where K_0 is the modified Bessel function of the second kind. Figure 1 shows $\langle\!\langle \rho \rangle\!\rangle$ compared to the barometric formula (1). The density approaches infinity near the surface and decays faster than exponential at great height.

Surface residence times: The constituents of the lunar exosphere can be condensible (e.g. H_2O) or non-condensible (e.g. Ne, He). Basic statistical mechanics

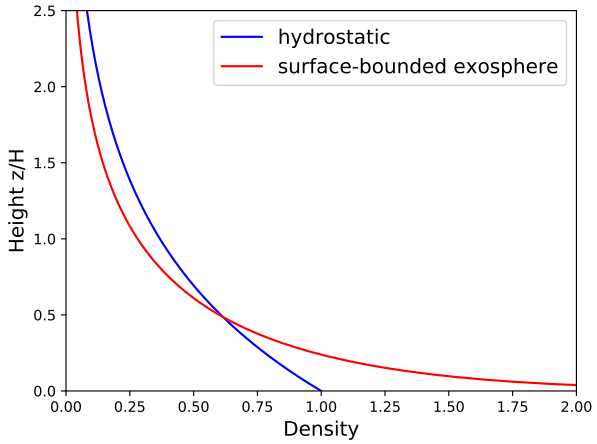

Figure 1: Theoretical vertical density profiles according to eqs. (2) and (1).

provides relations between the saturation vapor pressure p_v, the sublimation rate into vacuum E, and the residence time τ:

$$E = \frac{p_v}{\sqrt{2\pi k_B T m}} \tag{3}$$

$$\frac{1}{\tau} = \frac{\alpha E}{\theta_m} \tag{4}$$

$$p_v \propto \exp\left\{-\frac{1}{k_B}\left[\frac{(\text{Enthalpy})}{T} - (\text{Entropy})\right]\right\} \tag{5}$$

The saturation vapor pressure is defined by a balance between the number of outgoing and incoming molecules. It provides the sublimation rate, even if there are no incoming molecules (3). The average of the inverse of the residence time is the sublimation rate per (exposed) particle (4); θ_m is the number of molecules per area for a monolayer, and α is the condensation coefficent. Knowledge of the (difference in) sublimation/desorption enthalpy alone does not provide the residence time, because the (difference in) entropy is also required (5). On a surface with defects, the entropy differs from that on a perfect crystal.

Although desorption energy measurements have been made for lunar soils and analogues [e.g., 7], extensive measurements of the molecular residence times of water molecules are lacking. Adsorption isotherms [8] can be used to determine the residence time of water molecules adsorbed on the grain surface. Measurements are reproduced in Figure 2 and approximated by an empirical fit. For a reversible isotherm, residence times can be calculated as a function of θ via eqs. (3) and (4).

The surface residence times are relevant for exosphere modeling as well as for near-surface diffusion

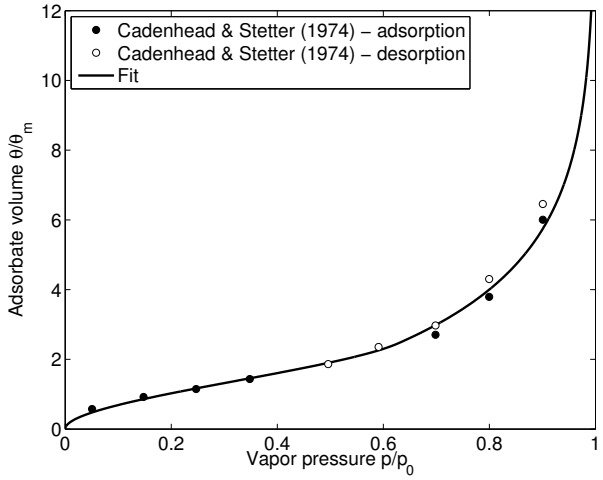

Figure 2: Measured adsorption isotherms for lunar sample 15565,3G at 15°C [8] and an empirical fit. From Ref. [9]

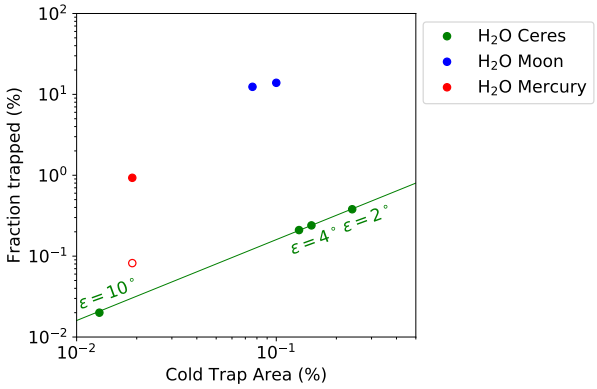

Figure 3: Fraction of water molecules trapped as a function of cold trap area. Solid symbols are for a geographically uniformly distributed source; the empty circle is for a subsolar source. The axis tilt of Ceres oscillates and is denoted by ϵ. Simplified from Ref. [16]

processes. Another thermophysical uncertainty is the distribution of thermal launch velocities, which does not have to be Maxwellian. An Armand distribution has been proposed for argon [10].

Some important numerical results: The ballistic hops in an exosphere can be readily modeled numerically, either by integrating the trajectory numerically or by computing the landing position analytically. There are implementations by Butler, Moore, Kegerreis, Schorghofer [11], Prem, and probably others.

Dusk-dawn asymmetry. For condensible species, such as H_2O, the density of the exosphere and the surface concentration vary greatly with local time. Exosphere-supplied water is concentrated around the morning terminator, but not around the evening terminator, a strong dusk-dawn asymmetry [12, 13].

Capture. Since the hop length is significantly larger than any cold trap, the water exosphere supplies the cold traps uniformly. There is a dependence on the distance from the source,—increasing distance leads to more photo-destruction—, but otherwise deposition is uniform [12]. The "rain shadow" effect is negligible. (The strong latitude dependence found in Ref. [14] is not reproduced by other models.)

Capture rate. The fraction of exospheric water molecules that is trapped depends on the trapping area, which is so far only known in order of magnitude. The total cold trapping area on the Moon is much smaller than the area of permanent shadows, and it depends on the spatial resolution. Modern estimates [15] are significantly lower than the historical estimate of 0.5% of surface area [e.g., 3], which assumed half of all PSRs are cold traps. If the total trapping area is 0.1% of the surface area, about 10% of the available water is trapped before it is lost by photo-destruction at normal solar activity [12]. The trapping fractions on Mercury and Ceres are two orders of magnitude lower than the Moon's (Figure 3), which amplifies the conundrum that the Moon has less exposed water ice than both of these bodies. This would make consistent sense, if the Moon had a much lower supply of water than either of these bodies.

Discussion: Remaining uncertainties in modeling of the lunar exosphere can be readily reduced with additional modeling (including cross-validation), laboratory measurements, and comparisons with observational data.

References

[1] R. M. Killen and W.-H. Ip. *Rev. Geophys.*, 37:361, 1999.
[2] S. A. Stern. *Rev. Geophys.*, 37:453, 1999.
[3] K. Watson, B. C. Murray, and H. Brown. *J. Geophys. Res.*, 66:3033, 1961.
[4] E. J. Öpik and S. F. Singer. *Phys. Fluids*, 4:221, 1961.
[5] C. S. Shen. *J. Atmos. Sci.*, 20:69, 1963.
[6] J. W. Chamberlain. *Planet. Space Sci.*, 11:901, 1963.
[7] M. J. Poston et al. *Icarus*, 255:24, 2015.
[8] D. A. Cadenhead and J. R. Stetter. In *Proc. Fifth Lunar Conf.*, 2301, 1974.
[9] N. Schorghofer and O. Aharonson. *Astrophys. J.*, 788: 169, 2014.
[10] R. R. Hodges and P. R. Mahaffy. *Geophys. Res. Lett.*, 43: 22, 2016.
[11] https://github.com/nschorgh/Planetary-Code-Collection/
[12] N. Schorghofer. *Geophys. Res. Lett.*, 41:4888, 2014.
[13] P. Prem, D. B. Goldstein, P. L. Varghese, and L. M. Trafton. *Icarus*, 299:31, 2018.
[14] J. E. Moores. *J. Geophys. Res.*, 121:46, 2016.
[15] D. A. Paige et al. *Science*, 330:479, 2010.
[16] N. Schorghofer, et al. *Astrophys. J.*, 850:85, 2017.

Applicability of Planning Tools Developed by Resource Prospector to a Broader Class of Lunar Polar Missions. M. Shirley[1], R. Elphic[1], A. Colaprete[1], D. Andrews[1], S. Miller[1], [1]NASA Ames Research Center, Moffett Field, CA 94035 USA, mark.h.shirley@nasa.gov

Introduction: Planning lunar polar missions is more complex than planning similar missions at lower latitudes. There are many operational constraints that combine to limit what can realistically be done. During Resource Prospector's formulation period, the team put a lot of effort into developing and maturing a planning process and supporting tools for these missions. The tools were developed for RP's specific needs, but they apply to a fairly broad class of variations. When describing this work previously, we have shown point solutions (i.e. mission plans) optimized for RP after showing RP's science measurement approach and the rover's design. This presentation uses those tools to step back to look at what features of the rover's design and goals drove these solutions and a few examples of how the solutions would change if the rover or its goals were changed.

Site Selection: The primary criterion for landing site selection is proximity to regions that are scientifically interesting to the specific mission. For RP, this criterion was potential for volatile sequestration, with proxies for that being enhanced levels of hydrogen, permanent shadow, and, in intermittently lit areas, a subsurface temperature history compatible with stable ices [1,2,3]. RP's efforts to pull together and, in some cases, to generate new maps describing these markers have been described elsewhere.

Engineering criteria come second, but are still very important. For rover designs that include both solar power and direct-to-Earth communications, sun and earth elevation during different seasons and their relative phasing can strongly limit the potential duration of mission plans. This applies equally to systems that can survive lunar night but require light and power to perform science tasks.

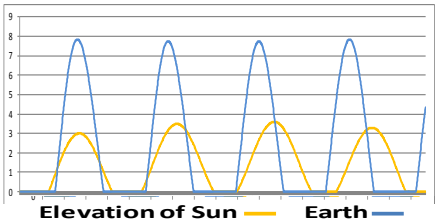

Fig 1: Intersection of favorable sun and DTE-comm varies around local summer

Realistic Activity Dictionary: Many quick-look, rover-oriented mission studies focus on movement as the main activity. There are a few ways this can result in unrealistic mission plans. First, although highly mission-dependent, the time needed for collecting and processing samples is very easily underestimated. Mission plans for RP spent about 40% collecting and processing subsurface samples, 40% of their time driving and 20% on housekeeping tasks. All driving time involved taking data as well, and the driving speed was limited by its impact on data quality. Housekeeping tasks included system maintenance tasks and realistic DSN station handovers and coverage gaps. The current activity dictionary contains just over 100 distinct activities performed by the rover or ops team.

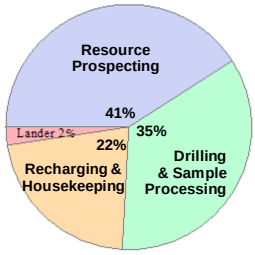

Fig 2: Pie chart shows time allocation over set of 17,000 traverses in one 30 x 30 km study site (many candidate landing sites)

Second, the process of driving a rover remotely is complex and its performance depends on many factors. During development, a process model for driving was developed and evaluated under different technology options (stereo cameras, LIDAR, different levels of onboard autonomy). We will discuss this model and the space of design options it covered. The RP team made choices within this space based on particular cost and risk constraints determined by the project's sponsors.

For instance, RP's planned average driving speed was less than that of Lunokhod 2. This was the result of cost, risk and schedule tradeoffs as is the case in any project. Although how these axies are scaled and their relative importance varies with the organization doing the work, the tradeoffs themselves apply to similar missions. RP looked broadly at design options before focusing on those that fit within the box of allowable solutions necessitated by RP's Class D designation within its sponsoring organization (NASA HEOMD). The structure of these tradeoffs will be described. In particular some of compromises that limited average speed would be very expensive to overcome, while others could be overcome with a small increase in risk.

Mobility Performance Targets: The rover performance targets for RP were set by starting with sci-

ence requirements, planning dozens of traverses by hand and generating many thousands more via automation at various locations and under varying conditions. These targets were validated through tests on existing rovers, prototyping new hardware and evaluation under simulated lunar conditions. The most important performance metric is average driving speed. The RP current average drive speed is 1 cm/sec, which represents a driving efficiency of 10%, i.e., the rover moves at 10 cm/sec for 10% of the time and waits for commands from the ground for 90%. This efficiency is almost exactly Lunokhod's value. Current simulations show speeds somewhat better than this over short operational periods (hours), but the values are dependent on local terrain.

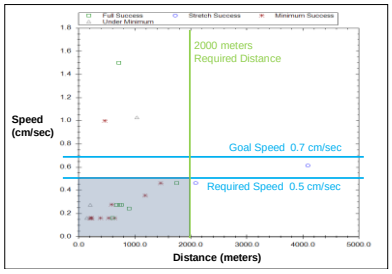

Fig 3: speed x distance scatter plot showing some hand-generated solutions. [speed targets are out-of-date and will be updated in final]

Traverse Planning Tool: Those who operate solar powered rovers must pay attention to how shadows move. The window of sun availability must always be accounted for, but moving shadows impact the placement of traverses within that window, subjectively, in a quarter to a third of cases. This is for realistic driving speeds and science data collection times. We found plans that involve staying in full sun over multiple months to be extremely rare without full autonomy, and that there is a tradeoff between the duration of periods of shadow and the driving speed needed to get to thermally interesting regions.

A custom tool was developed for RP explore these issues and to manage the time-varying sun and DTE-availability maps plus the static maps showing slope limits, block hazards and varying thermal environments. The tool combines these maps to create a single, time-varying, boolean map of locations where the rover can be (a 3D configuration space). While the tool can determine whether any point is reachable from any other, this is not generally useful as the space of possible mission plans involving a realistic activity dictionary is too large. This sort of analysis is very useful if the rover is only driving, but doesn't work well if there are many choices about where to stop to take samples or how long those stops might take, e.g., performing activities conditionally.

Instead, the tool employs two strategies. First, it does reachability analysis incrementally during planning. This handles the hardest part of the problem for human planners … identifying legal corridors of movement from one sampling location to another. Second, it uses planning macros that strongly constrain choices about conditional activities. These macros are tuned for RP's science measurement plan, but creating similar macros for different combinations of instruments and science goals is straightforward.

Finally, the tool simulates candidate traverses (or partial traverses) in order to identify situations where resource usage (e.g., the battery state-of-charge) would prevent the traverse from working. In RP's case, this simulation has been tuned so that it's conservative, it provides enough detail to be useful, and it runs in real-time so that parts of the plan that impact the simulation (e.g., recharge periods, if any) are as quick to update as changing the path the rover will drive. Details will be provided.

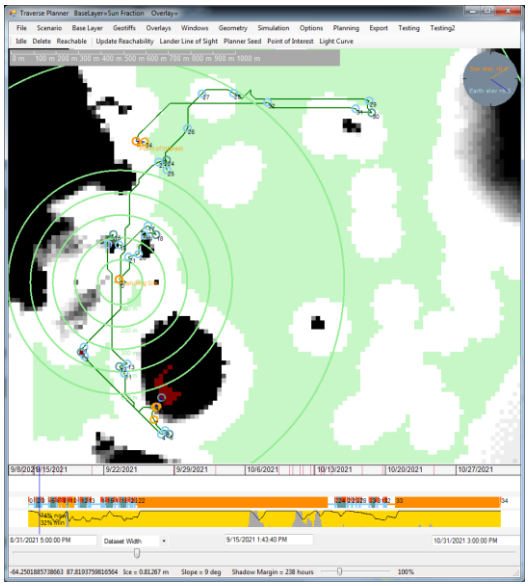

Fig 4: Shows one traverse covering 2 lunar days with a long idle period while Earth is below the horizon. Black, white and gray are sun exposure. Red are PSR locations with Earth comm. Green are candidate landing sites. The center of the bulls-eye is the planned landing site. The outer circle is 1 km from that.

References: [1] Colaprete, A., et al. (2010) *Science* 330.6003: 463-468. [2] Paige, D. A., et al. (2010) *Science* 330.6003: 479-482. [3] Siegler, M. A., et al. (2016) *Nature* 531.7595: 480-484.

SUBSURFACE ICE STABILITY ON THE MOON. M. A. Siegler (Planetary Science Institute, based in Dallas, TX, msiegler@psi.edu), J.T. Keane (California Institute of Technology), David Paige (UCLA)

Introduction: Water ice and other volatiles have now been detected on the Moon by various methods, but the question remains as to how much ice is actually there. This depends on the total volume of subsurface ice reservoirs on the Moon.

Ice will last on the surface of the Moon for about a billion years if it remains at ~100K [1,2,3]. This means that the Moon has about 26,000 km^2 of surface area in the large shadowed regions near the poles cold enough for ice to be stable [4,5]. However, due to the insulating nature of lunar dust, ice buried by as little as 10 cms can survive surface temperatures up to 125 K for billions of years [2]. This means the Moon has 240,000 km^2 of area in the upper meter alone that could harbor subsurface ice (at 1% filling fraction this would be 2.4 km^3, or about 3 times the volume of Haley's comet). Depending on how deep ice could be buried, and how it initially arrived to the Moon, volumes of ice could be much greater.

Near surface ground ice (The upper 1m): As discussed above, the thermal and diffusive protection provided by lunar regolith can vastly increase the stability of ice and other volatiles. In porous material, most heat is transferred via the gasses in pore spaces. Therefore, regolith under vacuum is one of the greatest thermal insulators in the universe, with thermal conductivities below 10^{-3} $Wm^{-1}K^{-1}$. This prevents short periods of maximum heating from reaching depth. Lunar grains are also highly irregular, making a very tortuous path for molecules migrating through the regolith. This leads to water ice stability increasing dramatically with only shallow burial [2,3].

Using data from LRO and recent lunar missions, namely LOLA topography and Diviner infrared data, we have produced accurate models of temperatures within the upper meter of the lunar subsurface [4,5,6]. Temperatures at deeper depths depend on model thermal properties and assumed geothermal heat flux. These can be used to create a prediction of what depth water ice (and other volatiles) would be stable in the upper meter for at least 1 Gyr (assuming no impact gardening or burial). Figure 1 a and b show model predicted ice stability depths within the upper 2.5 m of the lunar surface.

These models show that there is drastically more terrain with ice stable in the shallow subsurface than at the surface (white on these maps), with surface ice stability roughly tracking the predicted 100K contour. As mentioned above, we expect nearly 10 times as much area to have near surface ice that would not be stable at the surface.

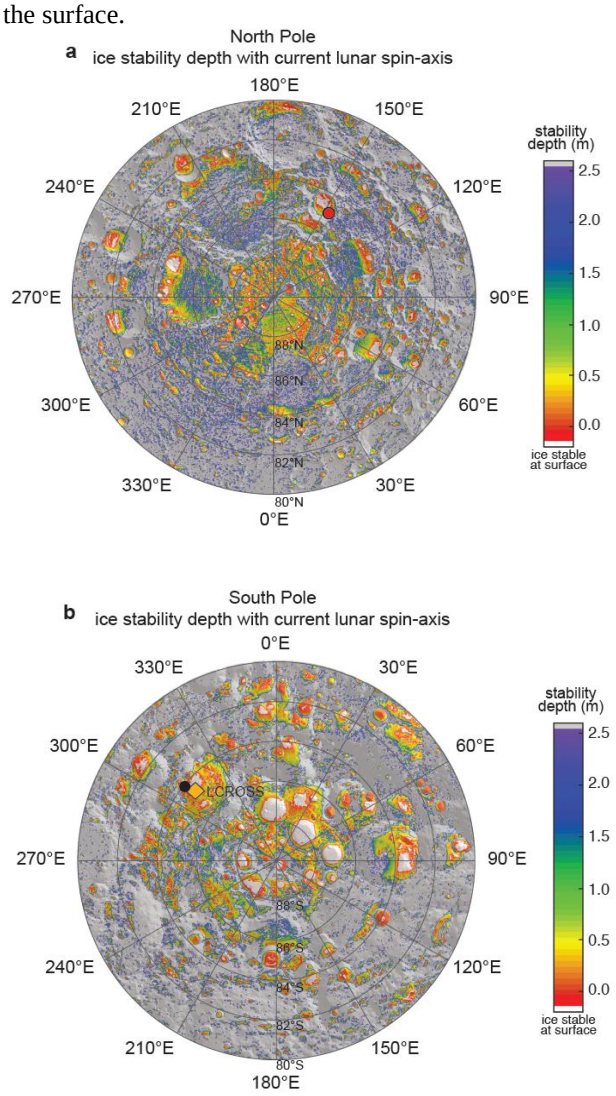

Figure 1: (a) Model results for ice stability depth (where ice could survive for 1Gyr) in the (a North Polar and (b) South Polar region of the Moon.

These models however do not tell us if ice is actually there. In general, these predictions do not correlate well with measurements from epithermal neutron detectors (LPNS [7,8], or LEND [9]), which are sensitive to very small amounts of hydrogen. They also do not correspond well with surface measurements [10,11,12]. This discrepancy is slightly surprising as similar measurements on Mercury seems to show ice in exactly everywhere it is thermally predicted [13]. This has been accredited to many possible causes including [14] low-

er delivery of volatiles to the Moon [15], to impact gardening [16], to obliquity history, [17] to true polar wander.

It could be that the near surface is out of equilibrium due to impact gardening of lack of recent (past billion+ years) volatile delivery, but the deeper subsurface has higher concentrations of ice. We know from several radar measurements [18,19,20,21] that signs of high concentrations (>40% by volume) of ice in the polar regions appear unlikely to exist. Until further measurements are taken or devised, the best information we have of the deeper subsurface comes from the 2009 LCROSS impact [22,23], which found several percent water by volume in the impact plume. The impact was believed to have released volatiles from at least the upper 4 m [22, 24] based on estimations of the crater size. This gives us tantalizing evidence volatile reservoirs of the deeper lunar regolith may be more plentiful than the near surface.

Deep ground ice (upper kms): There is no reason that the deeper subsurface (~5m to 1 km) be should be devoid of water ice and other volatiles that have currently evaded detection. Temperatures in the subsurface can still be cool enough that water ice would be frozen and able to avoid sublimation. Extrapolating the models of [2-6] to deeper depths, we can estimate a complete ice stability volume. This requires an assumption of crustal density and thermal conductivity, geothermal heat production, and a model of lateral heat conduction. Using 3D finite element thermal models with surface temperature conditions derived from [6], we calculate the maximum depth at which water ice would be stable at any given location. Using a density profile roughly consistent with GRAIL measurements [26], GRAIL crustal thickness models [27], and a 15mWm^{-2} geothermal heat flux, we determined the maximum depth to which water ice could be stable on the Moon. Results are shown in Figure 2. Here we see some areas near the South Pole where ice could be stable up to 800m below the lunar surface. This can be considered a map of the South Polar "cryosphere'.

This model makes no assumption as to how ice would get to such depths, be it by deep burial or perhaps outgassing from the lunar interior. It is not unreasonable that some pore space exists to these depths [26], so ice could be driven downward by a past episode of warmer temperatures at high obliquity [3-5], but this is at current only speculation. We performed a brief study of the gravitational signature one might expect from ice filled pores to this depth, but it appears to be within the gravitational noise of even GRAIL data. Such deep ice, if it exists, may require insitu measurements such as a small scale seismic network, deep radar sounding, or other similar instrumentation.

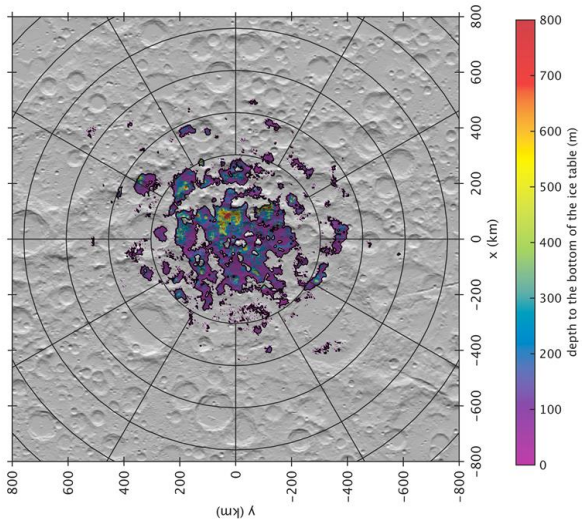

Figure 2: Maximum ice depth as modeled by the authors.

References:

[1] Watson et al., (1961) [2] Schorghofer and Taylor, 2007 [3] Siegler et al. 2011 [4] Paige et al., 2010 [5] Siegler et al, 2014 [6] Siegler et al., 2016 . [7] Feldman et al., 1998 [8] Miller 2014 [9] Mitrofanov et al., 2010 [10] Hayne et al., 2015, [11] Fisher et al., 2017 [12] Li et al, 2017 [13] Paige et al., 2013, [14] Lawrence, 2017 [15] Bruck-Syal, [16] Hurley et al 2012, [17] Siegler et al. 2014, [18] Siegler et al., 2016 [18] Margot, 1999, [19] Campbell et al., 2006, [20] Spudis et al. (2010) GRL *37*(6). [21] Thomson et al. GRL *39*(14). [22] Colaprete et al.2010; [24] Heldmann et al. 2015.[25] Hayne et al., 2010 Science.[26] Bresserer et al., 2016 [27] Weiczorek et al., 2014

LOCATING LUNAR POLAR VOLATILES USING THERMAL INERTIA AND TEMPERATURE MAXIMUM TO MINIMUM RATIOS. R. A. Slank[1], S. T. Port[1], and V. F. Chevrier, Arkansas Center for Space and Planetary Science, University of Arkansas, 332 N. Arkansas Ave., Fayetteville, AR 72701, rslank@uark.edu.

Introduction: Water ice on the Moon has been an area of interest for many decades [1, 2] due to the Moon's small obliquity (~1.5°) and the large variation in topographic relief near the poles. These two factors result in large areas (more than 30,000 km^2 at both poles) [3] that remain in permanent darkness and are thus very cold [4, 5]. Multiple missions have analyzed the lunar poles although the most successful one was the Lunar Reconnaissance Orbiter (LRO), which used the Lunar Exploration Neutron Detector (LEND) to detect water. Maps from LEND were created to indicate areas where water ice may be present [6, 7]. In this abstract we present a new technique to detect water ice at the poles using thermal inertia and temperature maximum and minimum ratios [8]. Thermal inertia was previously used to detected ice in the shallow subsurface of Mars [9] and can detect up to 10 cm into the lunar subsurface [10].

Thermal inertia (P) describes the resistance of a material to changes in temperature [11]. It is defined as:

$$P = \sqrt{K\rho c} \quad (1),$$

where K is the thermal conductivity, ρ is the density, and c is the specific heat. Unfortunately, these parameters cannot be directly measured using remote sensing techniques, so thermal inertia must be either estimated from other directly measured data or modeled. One way to estimate thermal inertia is by calculating the apparent thermal inertia (ATI), which is defined as [11]:

$$ATI = 1-a\ \Delta T \quad (2),$$

where a is the albedo and ΔT is the temperature amplitude over a diurnal cycle.

In order to calculate ΔT, the temperatures at two times of day are required. Although it is best to use the hottest and coolest temperatures experienced during the diurnal cycle to determine ΔT, they are not always obtainable with satellite data. The maximum (T_{max}) and minimum (T_{min}) temperatures can, however, be estimated given temperatures obtained from other parts of the diurnal cycle using [11]:

$$Tmax = T1 + (T1-T2)[\cos(\omega tmax)-\cos(\omega t1)]\ \cos(\omega t1)-\cos(\omega t2) \quad (3),$$

$$Tmin = T2 + (T1-T2)[\cos(\omega tmin)-\cos(\omega t2)]\ \cos(\omega t1)-cos(\omega t2) \quad (4),$$

where ω is the rotational angular frequency of the planet (the Moon in this case), t1 is day satellite overpass time, t2 is night satellite overpass time, T1 is temperature at time t1, and T2 is temperature at time t2. With T_{max} to T_{min}, ΔT can be determined and then ATI can be estimated using Equation (2). The temperature maximum to minimum ratio was calculated by dividing Equation (3) by Equation (4).

Although the ATI is a relative approximation to thermal inertia, it is possible to use the ATI to make a quantitative absolute estimate of the thermal inertia. Xue and Cracknell [12] presented an equation to calculate thermal inertia (P) from ATI:

$$P = ATI(S_0Ct\ \omega)\{A_1[\cos(\omega t_2-\delta_1)-\cos(\omega t1-\delta_1)]\ \sqrt{1+1}\ b+\ 1\ 2b2+\ A_2[\cos(\omega t_2-\delta_2)-\cos(\omega t_1-\delta_2)]\ \sqrt{2}+\sqrt{2}\ b\ +\ 1\ 2b2\} \quad (5),$$

where S_0 is the solar constant (1,366 W/m^2 for the Moon) [13], Ct is the atmospheric transmittance (1 for the Moon), δ1 is solar declination at time t1, δ2 is solar declination at time t2, A1 and A2 are Fourier coefficients, and b is a parameter dependent on the time when T_{max} is attained. The Fourier coefficients A1 and A2 are given by [14]:

$$A1 = 2\ \pi\ sin\delta sin\phi\ +\ 1\ 2\pi\ cos\delta cos\phi[\sin(2\xi)+2\xi] \quad (6),$$

$$A2 = 2sin\delta sin\phi\ 2\pi\ \sin(2\xi)+\ 2cos\sigma cos\phi\ \pi(22-1)\ [2\sin(2\xi)\cos(\xi)-\ \cos(2\xi)\sin(\xi)] \quad (7),$$

where ϕ is latitude and:

$$\xi = \arccos[\tan(\delta)\tan(\phi)] \quad (8).$$

The parameter b is determined using the formula [12]:

$$b = \tan(\omega tmax)\ 1-\tan(\omega tmax) \quad (9).$$

Methods: A MATLAB code was written to calculate the T_{max} to T_{min} ratio, ATI, and thermal inertia. The code first defines the parameters needed for the T_{max}, T_{min}, and thermal inertia calculations: lunar day length (27.321582 Earth days), ω (2.662*10^{-6} radians/second), t_{min} (6.609637×10^5 s), t_{max} (1.227504×10^6 s), S (1.366×10^3 W/m^2), Ct (1), and axial tilt (5.145°). The code then loads the bolometric temperature, local time, Julian date, and visual brightness maps from the PDS using LRO Diviner data. Next it changes all the missing data gap values, set in the PDS to be -32768, to "not a number" (NaN) values. This is to help with statistical analysis, contrast stretching, and to not skew the final results because the missing data value is so small. Then calibration coefficients were applied, each specific to the different data sets given by the label files. After that, the code converted t1 and t2 from lunar hours to Earth seconds, to match the units for t_{max}, t_{min}, and ω. The code than calculates T_{max} to T_{min}, as well as the T_{max} to T_{min} ratio. Once these parameters were calculated the code used equations 5-9 to determine the thermal inertia. The data was then uploaded

into ArcGIS and mapped. These maps were then compared with LEND data to help confirm areas of water ice and look for new areas.

Results and Discussion: Maps were generated in ArcGIS of the Lunar South Pole for both the T_{max} to T_{min} ratio and thermal inertia. A diurnal cycle in 2011 was selected due to the extensive coverage. The night starts on September 13 and the day starts on September 27. For the thermal inertia data, higher thermal inertia values are expected for areas that have water ice. This is because the area would be more resistant to temperature change than the surrounding area. Thermal inertia and the T_{max} to T_{min} ratio are inversely related, in other words areas with water ice would have lower a T_{max} to T_{min} ratio than the surrounding area.

The thermal inertia map (Fig. 1) and the T_{max} to T_{min} ratio map (Fig. 2) are on the same color scale with reds being low values and bright fuchsia being high values. Areas of white are where data is missing. The maps were overlaid on a DEM to verify location. The areas of high thermal inertia values and low T_{max} to T_{min} ratio values were compared with LEND data.

One notable area is Shoemaker crater. Water ice has been identified in the crater by LEND. The crater has high T_{max} to T_{min} ratio values and lower thermal inertia values, compared to the surrounding area. This is indicative of water ice on the surface or very shallow subsurface. Faustini crater is another crater that was analyzed. Again, the crater has high T_{max} to T_{min} ratio values and lower thermal inertia values, compared to the surrounding area.

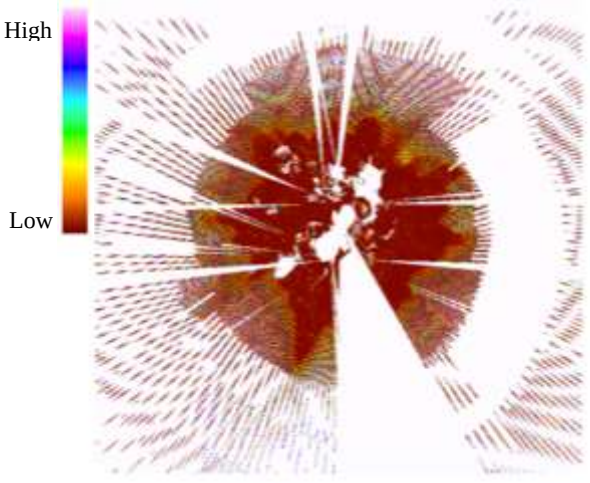

Figure 1: ArcGIS map of thermal inertia for the Lunar South Pole for the diurnal cycle of 9-13-2001 to 9-27-2001. Areas of white are missing data.

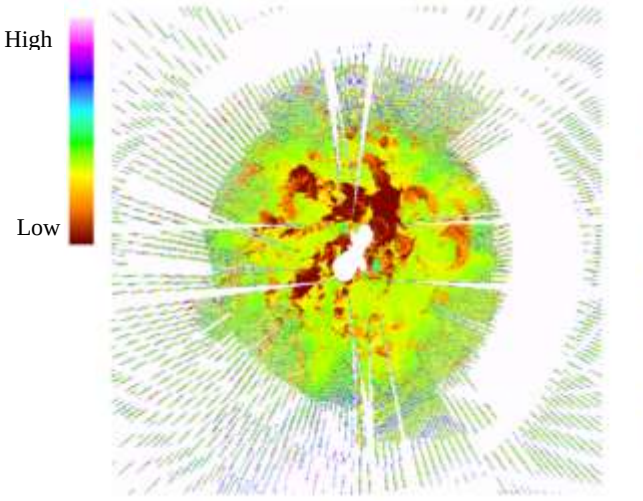

Figure 2: ArcGIS map of the T_{mas} to T_{min} ratio for the Lunar South Pole for the diurnal cycle of 9-13-2001 to 9-27-2001. Areas of white are missing data.

Conclusions: Thermal inertia and T_{max} to T_{min} ratios are a viable technique to detect water ice on the lunar surface. This technique could potentially discover new areas of water ice on the Moon. More diurnal cycles are being analyzed to help create a complete map of water ice on the Moon.

References:

[1] Watson, K., B. Murray, and H. Brown (1961), J. Geophys. Res., 66, 1598–1600. [2] Arnold, J. R. (1979), J. Geophys. Res., 84, 5659–5668 [3] McGovern, J. A.,D., B. J. Bussey, B. T. Greenhagen,,D .A. Paige, ,J. T. S. Cahill, and P. D. Spudis (2013), Icarus, 223, 566 –581. [4] Vasavada, A. R., D. A. Paige, and S. E. Wood (1999), Icarus, 141, 179–193. [5] Paige, D. A., et al. (2010), Science, 330, 479–482. [6] Mitrofanov, I. G., et al. (2010, Science, 330, 483–486. [7] Litvak, M. L., et al. (2012), J. Geophys. Res., 117. [8] Slank, R. A., (2016) UTEP M.S.Thesis. [9] Bandfield, J. L., and W. C. Feldman (2008), J. Geophys. Res., 113. [10] Hayne, P. O., et al., (2017). J. Geophys. [11] Scheidt, S., Ramsey, M., and Lancaster, N., 2010, J. Geophys. Res., vol. 115. [12] Xue, Y. and A.P. Cracknell, (1995), Int. J. Remote Sensing, vol. 3, p. 431-446. [13] Johnson, F.S., (1954), J Atmo. Sci., vol. 11, p. 431- 439. [14] Maltese, A., et al., (2013), Hydrological Sciences Journal, vol. 58, p. 1144-1161.

Rover Mast Laser Surface Reflection Spectrometer for Volatile Science and Prospecting and 3D terrain mapping up to 10 km. M. Storm Author[1] and M Albert[1], [1]Fibertek Inc, 13605 Dulles Technology Drive, Herndon, VA 20171. mstorm@fibertek.com

Introduction: Fibertek proposes to develop a rover-based Compact Lidar Spectrometer (CLS) to enable long-range detection of water ice and other surface substances within the 1.4um to 1.9um and 2.5 um to 4 um wavelength bands. High resolution spectrums can be acquired up to a range of 10,000 m providing the ability to measure deep into dark craters. This CLS can also be used for three-dimensional (3D) terrain mapping across large areas.

The small, compact (~2 kg), low cost package can be mounted on a rover mast accompanying its visible camera and can be directed to areas of interest. The laser spectrometer will provide a 3D terrain map of the location with a spectrum and report on In-Situ Resource Utilization (ISRU) associated with each map location. The proposed ultra-compact rover lidar laser spectrometer is new, innovative and can provide new high value science measurements. The Nd laser based approach uses mature TRL-8 low cost technology and can provide much greater spatial coverage compared to comb laser and other traditional approaches which can provide very high spectral resolution.

Motivation: The ability to identify ISRU materials, such as water, is critical for NASA, and potentially private companies, planning robotic or human exploration of the Moon, Mars, Ceres, Phobos, and Near Earth Objects (NEOs) [1-4]. Evidence of the availability of ISRUs is a key landing site selection criterion. ISRUs such as water, hydrogen, carbon dioxide, and ammonia can be used to sustain habitat, provide life support, and create propulsion fuel.

Innovative Aspects of the Proposed Instrument: The proposed lidar spectrometer is innovative, unique, and compelling in numerous ways:

Increases the rover science utilization, minimizes wear and tear, and maximizes rover lifetime. Large expanses of terrain can be quickly surveyed by the lidar in prospecting for water/ice in daytime or nighttime conditions. By mounting the lidar on a mast with an azimuth/elevation (Az, El) scanning mechanism, 3D terrain maps of surface reflections and spectra are gathered (Figure 1). The lidar will measure the relative percentage of water content in regolith using the reflectance properties between 2.6 um to 3.3 um with ~10 nm resolution similar to the NASA NIRVSS rover instrument that uses a tungsten lamp.

Lidar can see long range as well as inside permanently shadowed craters, which are a prime candidate for water ice, methane ice and ISRU volatiles. Under normal operations, a lidar spectrum can be taken in ~2 seconds for ranges up to 2 km with a typical 5%-10% albedo[5]. For long-range operation, the lidar can be operated up to 10 km for albedos between 5% to 10% with signal averaging (Section 4.12.1.4) and a spectrum collection time of ~ 6.7 minutes. Exhibit 2-1 gives an elevation map of the moon showing ubiquitous craters. Elevation changes of 500-8,000 m are typical. The terrain is diverse enough to provide a rover with a vantage point to look up, across, or down into craters. The range of the lidar is appropriate for the terrain.

Figure 1: Compact Lidar Spectrometer Will Look Similar to Camera Mounted on a Rover (PT Scientists). The CLS can be mounted and coaligned with the camera system.

Faster – increases mission operation productivity and pace. Being able to sample large geographic areas increases the pace of work, enables sampling more locations quickly, and changes the mission planning decision process. A spectral terrain map survey of the locations may be very helpful in planning rover operations to target the richest areas first. It also enables an expanded search area for the mission.

Improve Lunar Missions Success. The ability to survey a large regional area could help optimize the site selection of locations with high surface water content. Lidar can help optimize sites with likely surface water to maximize Rover's limited consumable resources and limited number of core drill opportunities for improved mission success.

Day and night time operations. A rover lidar spectrometer could potentially see cyclic variations in frost deposition and sublimations and potential water–ice state changes in the lidar return spectrum. This could be of scientific interest in addition to ISRU.

Safer – less risk. The rover can be safely positioned to survey and validate potential water locations with a

higher probability of success rather than risking the need for the rover vehicle to traverse questionable terrains, and ascertain potential ice sources.

Provide 3D Terrain mapping The lidar will map the terrain and along with the camera can identify hazardous travel zones and help plan rover routes. The lidar range will be measured and indicate surface roughness. Inclination angles of hill and crater descent information will be available to augment other rover sensor data.

Numerous Science Applications. The spectral data collected is valuable for science of other volatile substances and for mineralogy. The CERES DAWN mission VIRs spectrometer measured numerous minerals and solid forms of ammoniated minerals at 3.06 um, water ice at 2.7 um, and others in the 2.5 to 4 um and near-IR wavelength bands [6]. The albedo of solid methane line are available at 3.3um [7] and Triton/Pluto studies have shown frost can be seen in our wavelength region [8]. Solid methane might be found in the craters near the moons pole for example where very low temperatures occur. Similarly the 1.4um to 1.9um spectral range offers similar scientific opportunity.

Instrument Design Utilizing Space Qual Tech

The tunable laser consists of a Nd pumped OPO using a mature TRL-8 Space Laser that Fibertek qualified and delivered for use in NASA's $750M ICESat-2 Earth Observatory mission. The laser produces 200 uJ/pulse at 10 kHz and is ultra-compact, 2.5" x 1.25" wide. The OPO is a mature, commercially available, periodically poled crystal and provides wavelengths for 2.5 to 4um and 1.4 to 1.95 um as shown in Figure 2. Fibertek has flown TRL-9 OPO technology.

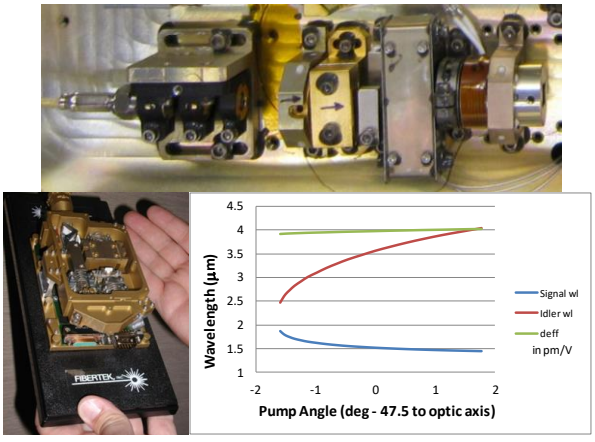

Figure 2: Ultra compact TRL-8 Nd laser developed for $750M ICESat-2 mission. (top). TRL-9 Nd OPO laser (left). Laser wavelengths generated by CLS (bottom). Uses separate detectors for each wavelength band.

Instrument Performance, Measurement Approach and Calibration

Performance: The lidar is expected to operate with signal-to-noise ratio (SNR) >100 for all range measurements. At long range the lidar will average 50-100 or more shots per wavelength to be able to measure down below 0.5% water as defined in Ref 5.

Calibration: the compact lidar spectrometer, tuned across the 1.4 -1.9 um and 2.5-4 um band in 10 nm steps (user defined), measures the outgoing laser energy and reflected return energy, and generates a spectrum. The spectrum will be normalized to outgoing laser energy, solar filter, and detector spectral response curve similar to a spectrometer to produce a high resolution measurement.

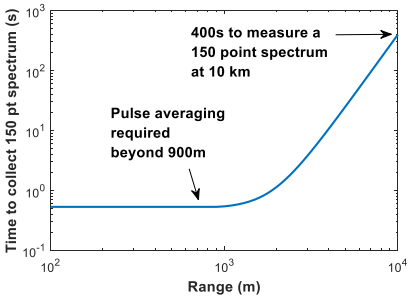

Figure 3: Modeled Instrument Performance Assuming Worst Case Daytime Solar Background. No signal averaging is needed up to 900 meters. Spectral measurements up to 10 km range can be achieved for a 400 second scan.

Summary

Fibertek's proposed, unprecedented, ~2 kg instrument directly serves to identify ISRUs and prospects for lunar volatiles including water and other species within the 1.4-1.9 um and 2.5-4 um spectral bands. The technology being proposed, while aggressive, uses mature technology elements like the Nd pump laser, OPO conversion technology, space heritage detectors, and heritage packaging technology. Our overall program approach is traceable to space and the technology is complimentary with our CubeSat lidar and space laser comm technology.[9]

References:

1. Neumann, G. A. (2013), Science, 339, 296-300.
2. Küppers, M. et al. (2014), Nature, 505, 525-527.
3. Fraeman, Icarus, 229, 196-205
4. Lim, D. S. S. et al., AGU 2015, #P31A- 2031.
5. Izawa, M. E.. EPS Let, 390, 157-164.
6. M.C. De Sanctis, "CERES composition by VIR on DAWN:," 47th LPSC (2016), 1832.
7. K. Adams, GRL, doi:10.1029/2011GL049710, 2012
8. J Spencer, ICARUS, 88, 491-496 (1990).
9. M. Storm, 2017 31st AIAA, Small Sat Conf. Lidar SSC17-S2-03, Optical Communications SSC17-XI-09.

Meteoroid Environment and Impact Gardening in the Lunar Polar Regions. J. R. Szalay[1], P. Pokorny[2,3], M. Horányi[4,5,6], A. R. Poppe[7], D. Janches[2], M. Sarantos[2]. [1]Department of Astrophysical Sciences, Princeton University, [2]Space Weather Lab., GSFC/NASA, [3]Department of Physics, Catholic University of America, [4]Department of Physics, University of Colorado Boulder, [5]Laboratory for Atmospheric and Space Physics, [6]Institute for Modeling Plasma, Atmospheres, and Cosmic Dust, [7]Space Sciences Lab., University of California Berkeley

Introduction: The Moon is continually bombarded by interplanetary meteoroids. While meteoroids turn into shooting stars at Earth due to our thick atmosphere, airless surfaces like the Moon's are completely exposed to meteoroid impacts. The surface of the Moon is covered with a layer of loose rocky material, including fine dust particles. This regolith has been formed, and remains continually reworked, by the intermittent impacts of comets & asteroids, and the continual bombardment by meteoroids. Each meteoroid impact produces orders of magnitude more ejecta mass compared to the primary impactor mass, most of which is bound and returns to reblanket the lunar surface.

Water is thought to be continually delivered to the Moon through geological timescales by water-bearing comets & asteroids and produced continuously in situ by the impacts of solar wind protons of oxygen-rich minerals exposed on the surface. Meteoroids are an unlikely source of water due to their long UV exposure in the inner solar system, but their high-speed impacts can mobilize secondary ejecta dust particles, atoms and molecules. Other surface processes that can lead to mobilization, transport and loss of water molecules and other volatiles include solar heating, photochemical processes, and solar wind sputtering. However, since these drivers are minimized at high latitudes, particularly in Permanently Shadowed Regions (PSRs), dust impacts are an important driver governing the evolution of volatiles in these regions.

The meteoroid environment at the lunar polar regions has been difficult to constrain, given the paucity of available data. However, recent Earth-based observational and modeling efforts have revealed a persistent, high speed and high inclination source of meteoroids at 1 au that continually bombard the lunar polar regions [1]. In-situ ejecta measurements were made at the Moon by the Lunar Dust Experiment (LDEX) onboard the Lunar Atmosphere and Dust Environment Explorer mission. LDEX observations enabled a detailed understanding of the structure of the impact generated, permanently present lunar ejecta cloud and subsequent gardening rates near the lunar equatorial plane [2]. Here, we extend those equatorial measurements to the lunar polar regions using advanced models of meteoroid impactors at the Moon to constrain the associated impact gardening rates.

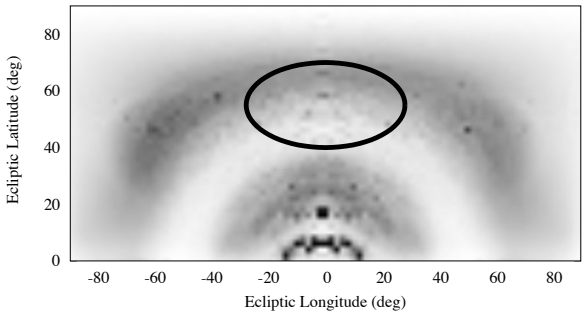

Figure 1. Adapted from Pokorný et al. (2014). Modeled radiant distribution of meteoroids impacting Earth in the northern hemisphere centered on the apex direction. The oval indicates the high latitude population that may be responsible for liberating significant quantities of impact ejecta in the lunar polar regions.

References:

[1] Pokorný, P., Vokrouhlický, D., Nesvorny, D., Campbell-Brown, M., & Brown, P. (2014). ApJ, 789(1), 25. http://doi.org/10.1088/0004-637X/789/1/25

[2] Szalay, J., & Horanyi, M. (2016). *GRL*, *43*(1), 4893–4898. http://doi.org/10.1002/2016GL069148

THE LUNAR INTERIOR AS A SOURCE OF POLAR WATER. G. Jeffrey Taylor[1,2], David A. Kring[2,3], and Debra H. Needham[4]. [1]Hawai'i Inst. of Geophys. and Planetology, U. Hawai'i, Honolulu, HI 96822 (gjtaylor@higp.hawaii.edu), [2]NASA Solar System Exploration Research Virtual Institute, [3]Lunar and Planetary Institute, Houston, TX 77058, [4]NASA/Marshall Space Flight Center, Huntsville, AL 35805.

Introduction: Studies of the sources of water (H, OH, H_2O) in lunar polar deposits have focused on H derived from the solar wind or deposited by hydrous impactors. Since the discovery of water in lunar magmatic products, volcanic eruptions are clearly viable sources for volatiles. Such eruptions deposited substantial volumes of H_2O and other volatiles into the lunar exosphere, possibly leading to the formation of an atmosphere with pressures up to 0.06 kPa [1]. Here we focus on water trapped in the lunar crust that might be released by lunar tectonic and impact processes as a possible long-term source for water to the surface system.

Water Inventory in the Crust: Water was clearly present in lunar magmas producing mare and KREEP basalts, and intrusive igneous rocks (e.g., [2-3]). Using available data and estimates on water concentrations in pre-eruptive magmas, volumes of mare basalts and pyroclastic deposits, crustal thicknesses, and crustal geochemical signatures, we have evaluated the total amount of hydrogen species (expressed as H_2O) in the lunar crust. One uncertainty is the ratio of intrusive to extrusive mare basalt magma. On Earth, the intrusive/extrusive ratio ranges from 1 to 10, with a median of 5:1 [4]. Basaltic shields have ratios of 1:2, whereas ocean ridges have ratios of 5:1. We tentatively assume 2:1 for the Moon, and that mare basalt lavas lost 95% and pyroclastics lost 98% of their initial H_2O concentrations. We also assume that the crust in the PKT was composed entirely of intrusive rocks of the Mg-suite and other KREEP-related magmas, or their impact-melted equivalents (e.g., LKFM), adjusted for the volume of intruded mare basaltic magmas. For the volume of KREEP-related rocks we use the volume of the Procellarum KREEP Terrane as determined by a crustal thickness of 34 km and the Th distribution [5]. From published water measurements (summarized in [2,3]) we estimate that the average mare basaltic magmas contained 100 ppm H_2O, pyroclastic magmas contained 1000 ppm, Mg-suite magmas contained 100 ppm, and that the feldspathic highlands crust contains 0.1 ppm (double the amount measured in FAN rocks). Combined with estimates of the volumes, these order-of-magnitude assumptions result in a total interior mass of H_2O of 5.7×10^{16} kg (Table 1). For comparison, the polar cold traps are estimated to contain ~10^{12} kg of H_2O [6,7].

Water mobility: Theoretical considerations indicate that Ar can be lost by diffusion from the lunar interior [8] and there is some evidence from lunar highland samples for migrating fluid phases in the lunar crust, such as millimeter-sized volatile-rich apatite crystals in granulitic breccia 79215 [9]. On the other hand, precipitation of hydrous minerals provide stable sites for OH, inhibiting further transport. Furthermore, crystallizing magmas at depth are unlikely to lose substantial amounts of water to the surrounding rocks because of the low concentrations and high solubility of H_2O. For example, at a depth of 20 km (middle of the crust), the pressure is about 0.1 GPa (1 kbar) and water has a solubility of 3 wt%, much higher than the concentration in Mg-suite parent magmas (0.01 wt%). Even after 99% crystallization of anhydrous minerals, H_2O concentration would rise to only 1 wt%, still below the saturation level. Moreover, apatite would crystallize after ~90% crystallization, hence decreasing H_2O in the residual magma and, most important, providing a thermodynamically stable site for it as OH. A complicating factor is that a significant percentage of H-species in the magma is H_2 (e.g., [10]), which is likely to be much more mobile than OH or H_2O [11]. However, this would lead to a decrease in H_2O in the interior, with delivery of only molecular hydrogen to the surface. Water transport to the surface is enhanced by early bombardment because of the extensive fracturing of the crust, which led to short diffusion distances before encountering a pore space [8]. Abundant porosity has been proven though analysis of the GRAIL data (e.g., [12]) and has been observed in mid-crustal rocks of large impact basins [13].

A more forceful process than diffusion is required to deliver significant amounts of water to the surface. We consider two here: moonquakes and impacts.

Table 1. Inventory of H_2O in the lunar crust.

	H_2O (kg)
Mare basalt	1.3×10^{14}
Intrusive mare basalt magma	5.2×10^{15}
Pyroclastic deposits	2.1×10^{12}
Intrusions of pyroclastic magma	1.0×10^{14}
Mg-suite and KREEP	3.8×10^{16}
Feldspathic highlands	1.4×10^{16}
Total water in crust	5.7×10^{16}

Water migration triggered by moonquakes: Apollo seismic data and morphological studies indicate that moonquakes are frequent. Many events release argon (summarized in [14]), so it is reasonable to assume that they could also mobilize loosely-bound H_2O from

the porous megaregolith. The most promising are shallow moonquakes confined to the crust, such as those producing some of the lobate scarps and causing boulder falls. These so-called "high-frequency teleseismic (HFT) events" are correlated with releases of ^{40}Ar [15]. We can estimate the amount of H_2O released by these moonquakes in two ways: the correlation of H_2O with ^{40}Ar and from the volume of material affected by stresses in fault zones that encompass the entire thickness of the crust.

Grava et al. [14] reexamined the data from the Lunar Atmosphere Composition Experiment (LACE) deployed during the Apollo 17 mission, estimating that on average 6.7×10^3 kg of ^{40}Ar were released during each HFT event. We can use measurements of the $H_2O/^{40}$Ar ratio due to the HFT moonquakes to estimate the amount of water released by such moonquakes. The LACE experiment indicated $H_2O/^{40}$Ar of 0.07 [16]. In contrast, the Suprathermal Ion Detector Experiment (SIDE) indicated a $H_2O/^{40}$Ar ratio of 2.4. Using these values as upper and lower limits, and a crustal ^{40}Ar content of 2.9×10^{18} kg (from a K concentration of 400 ppm and decay of ^{40}K during 4 Ga), a crustal H_2O content of 5.7×10^{16} kg, and 5 HFT events per year, we estimate that the amount of H_2O released per year is between 4.6×10^2 to 1.6×10^4 kg (see shaded area in Fig. 1).

We estimated water loss during faulting, assuming an H_2O concentration of 10 ppm, a fault plane width of 100 km, fault zone thickness of 10–100 meters, and fault plane length equal to a 30° plane through a crust 34 km thick. Assuming 10–100% water loss, and that each fault has a lifetime of 1 My, this amounts to 10^2–10^4 kg/y, in the range determined from Ar release (Fig. 1).

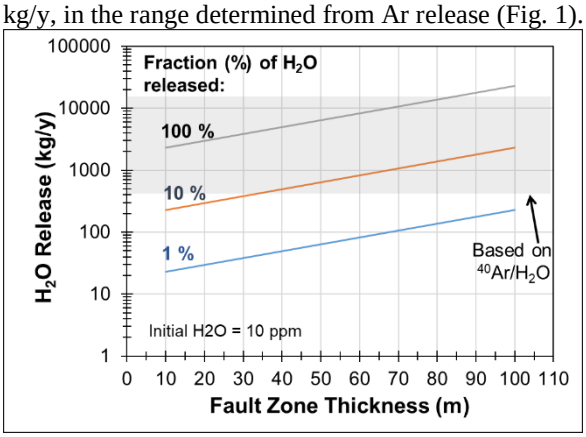

Fig. 1. Water release per year as a function of fault zone thickness and the percentage of water lost over the lifetime of each fault.

Impact Cratering. The Moon is heavily cratered. If moonquakes can cause water to be released from the crust, surely impacts can, too. Assuming an average crustal H_2O concentration of 10 ppm (most of the crust is anorthositic with H_2O of only 0.1 ppm), we calculated the amount lost during impacts over the past 3 Ga, assuming the Hartmann crater production function (equations 5.11 [17]) for craters ranging from 1 to 100 km in diameter, and used the melt production function from Abramov et al. [18], assuming an impact velocity of 14 km/s and an impact angle of 45 degrees. We also made the reasonable assumption that all water is lost from the impact melt, and a less certain assumption that only 10% of the water is lost from the displaced material. The result is that the integrated loss due to impacts in the 1–100 km size range is 2×10^3 kg/y, in the range calculated for release by faulting. Thus, moonquakes and impacts cause the release of similar amounts of water from the interior.

Comparisons with other sources. The amount of water released from the interior due to moonquakes and impact cratering, 10^2–10^4 kg/y is lower than that estimated to be contributed by the solar wind [18] and hydrous asteroids [20], both about 10^7 kg/y. While magmatism would have been a more efficient way to deliver water from the interior to the surface in ancient lunar history, current seismic and impact activity that penetrates beneath the regolith may deliver small abundances of water to the lunar exosphere.

References: [1] Needham. D., and Kring, D. (2017) *EPSL* v. 478, 175-178. [2] Robinson, K.L. and Taylor, G.J. (2014) *Nat. Geosci.* **7,** 401-408; [3] McCubbin, F. et al. (2015) *Am. Mineral.* **100**, 1668-1707. [4] White, S. M. et al. (2006) *G*^{3}, v. 7(3). [5] Taylor, G.J. and Wieczorek, M. (2014) *Phil. Trans. Royal Soc.*, doi:10.1098/rsta.2013.0242. [6] Feldman, W. et al. (1998) *Science* **281**, 1496–1500; [7] Eke, V. R. et al. (2009) *Icarus* **200**, 12–18; [8] Killen, R.M. (2002) *MAPS* v. 37, 1223-1231. [9] Treiman, A. T. et al. (2014) *Am.Mineral.* v. 99, 1860-1870. [10]Hirschmann, M.M. (2012) *EPSL* v. 345, 38-48. [11] Zhang, Y. (2011) *42*nd *LPSC*, #1957. [12] Morgan et al., Science 354, 878-882. [13] Wieczorek, M. et al. (2013) *Science*, doi: 10.1126/science.1231530. [14] Grava, C. et al. (2015) *Icarus* **255**, 135-147. [15] Hodges, R. R. (1977) *Phys. Earth Planet. Int.* v. 144(3), 282-288. [16] Hoffman, J. H. and Hodges, R. R. (1975) *The Moon* v. 14, 159-167. [17] Stöffler et al. (2006) Chapter 5 in *New Views of the Moon*. [18] Abramov, O. et al. (2012) *Icarus* v. 218, 906-916. [19] Crider, D. and Vondrak, R. (2000) *J. Geophys. Res.* v. 105, 26,773-26,782. [20] Syal, M. B. and Schultz, P. H. (2015) *46*th *LPSC*, #1680.

Acknowledgements. We are grateful for support from the Solar System Exploration Research Virtual Institute (through the Center for Lunar Science and Exploration cooperative agreement NNA14AB07A).

Lifetime of a transient atmosphere produced by Lunar Volcanism. O. J. Tucker[1], R. M. Killen[1], P. Saxena[1],R. E. Johnson[2], and [3]P. Prem, [1]NASA/Goddard Space Flight Center, Greenbelt, MD. (Orenthal.J.Tucker@nasa.gov), [2]University of Virginia, Charlottesville, Va., [3]JHU/Applied Physics Laboratory, Laurel MD.

Abstract: The possibility of harvesting volatiles on the Moon to support manned spaceflight missions has revived interest in remnant volatile inventories on the Moon. Our present day Moon possesses a tenuous exosphere primarily composed of the noble gases. The exosphere is primarily derived from the surface and has a surface pressure only ~10^{-15} times that of the Earth. However in the past, outgassing from volcanic activity early in the Moon's history may have produced a significant collisional atmosphere (Needham and Kring, 2017). Needham and Kring (2017) estimated a lifetime of over 70 million years for such atmospheres and found that even a small fraction of the water released could account for the entirety of the hydrogen observed to be trapped in permanently shadowed regions (PSRs) of the lunar poles.

Needham and Kring (2017), herein referred to as NK17, estimated the atmospheric lifetime using the thermal escape rate of ~10^4 g s^{-1} derived in Vondrak et al. (1974). This escape rate was calculated at the lunar surface for an idealized atomic oxygen atmosphere considering rarefied surface pressures e.g., 10^{-17} – 10^{-10} bar. However, the surface pressures in NK17 are more than ~0.01 bar, therefore, the nominal exobase would be at radial distances of ~0.5 – 4.5 R_M above the surface, where R_M represents the Moon's radius. For such atmospheres, the escape rate must be evaluated in the upper atmosphere because the atmosphere is collisional, loosely bound, and possesses a column capable of absorbing solar radiation. Furthermore, atomic oxygen is much lighter than carbon monoxide, the principal atmospheric component considered in NK17. Here, we reconsider the lifetime of such an atmosphere using recent results obtained from gas-kinetic models of thermal escape rates generalized for application to arbitrary planetary bodies and analytical results for escape limited by the absorption of solar energy in the upper atmosphere (e.g., Johnson et al. 2015, 2016).

Recently, gas-kinetic models have been used to demonstrate that thermal escape from the top of an atmosphere is controlled by the efficiency of thermal conduction and adiabatic cooling due to escape (Volkov et al. 2015). For such conditions it has been shown that the escape rate can be estimated as a function of the surface Knudsen number (Kn_0), degree of rarefaction, and surface Jeans gravitational escape parameter (λ_0) (Volkov et al. 2011). Johnson et al. (2015) used these results with combined continuum and kinetic-theory based approach to evaluate the thermal escape rates from KBO atmospheres for a range of surface conditions $Kn_0 \sim 10^{-16} – 10^{-2}$ and $\lambda_0 = 10 – 30$. Here we use this approach to estimate escape from volcanic atmospheres with $Kn_0 = 10^{-8} – 10^{-5}$ and $\lambda_0 \sim 30$. We obtain thermal escape rates more than an order of magnitude lower ~ $10 – 10^3$ g s^{-1}. This finding is problematic because such an atmosphere would have survived over the history of the solar system.

We have calculated the lifetime of an early lunar atmosphere against thermal escape heated by the surface temperature. Contrary to NK17, we find that such an atmosphere would survive the longer than 4.5 Gyr. Our results differ because we evaluated thermal escape using the mass of CO, the principal atmospheric species in NK17, and our estimate includes the effect of adiabatic cooling on the escape rate. In this presentation, we also include estimates of escape induced by solar heating of the upper atmosphere and atmospheric sputtering.

The formation of a volcanically derived atmosphere on an airless body is an intriguing study and applicable to many planetary bodies, e.g. Mercury and Io. Such an atmosphere is likely mitigated by the initial volcanic outflow conditions, temperature and cooling rate of the surface melt, global transport, upper atmospheric heating, the solar wind interaction and meteoroid bombardment. Each of these processes would have varied in importance during different phases of the Moon's evolution. We will discuss these the role of these processes in the loss of an early atmosphere and for consideration of the fraction of remnant volatiles stored in the polar regions.

References: [1] Needham and Kring (2017) *Earth & Planet. Sci., 478*, 175–178. [2] Vondrak et al. (1974) In: Proc. Fifth Lunar Sci. Conf., pp. 2945–2954. [3] Johnson et al. (2015) *Astrophys. J., 271, 809* 43., [4] Johnson et al. (2016) *Icarus, 271,* 202 - 206. [5] Volkov et al. (2015) *ApJ Lett., 812,* L1. [6] Volkov et al. (2011) *ApJ Lett., 729,* L24.